

Modal Analysis of Arbitrarily Damped Three-Dimensional Linear Structures Subjected to Seismic Excitations

by
Yi-Lun Chu, Jianwei Song and George C. Lee

Technical Report MCEER-09-0001

January 31, 2009

NOTICE

This report was prepared by the University at Buffalo, State University of New York as a result of research sponsored by MCEER through a contract from the Federal Highway Administration. Neither MCEER, associates of MCEER, its sponsors, [the University], nor any person acting on their behalf:

- a. makes any warranty, express or implied, with respect to the use of any information, apparatus, method, or process disclosed in this report or that such use may not infringe upon privately owned rights; or
- b. assumes any liabilities of whatsoever kind with respect to the use of, or the damage resulting from the use of, any information, apparatus, method, or process disclosed in this report.

Any opinions, findings, and conclusions or recommendations expressed in this publication are those of the author(s) and do not necessarily reflect the views of MCEER or the Federal Highway Administration.

Modal Analysis of Arbitrarily Damped Three-Dimensional Linear Structures Subjected to Seismic Excitations

by

Yi-Lun Chu,¹ Jianwei Song² and George C. Lee³

Publication Date: January 31, 2009

Submittal Date: January 9, 2009

Technical Report MCEER-09-0001

Task Number 094-D-1.2

FHWA Contract Number DTFH61-98-C-00094

- 1 Ph.D. Student, Department of Civil, Structural and Environmental Engineering, University at Buffalo, State University of New York
- 2 Senior Research Scientist, Department of Civil, Structural and Environmental Engineering, University at Buffalo, State University of New York
- 3 Samuel P. Capen Professor of Engineering, Department of Civil, Structural and Environmental Engineering, University at Buffalo, State University of New York

MCEER

University at Buffalo, State University of New York

Red Jacket Quadrangle, Buffalo, NY 14261

Phone: (716) 645-3391; Fax (716) 645-3399

E-mail: mceer@buffalo.edu; WWW Site: <http://mceer.buffalo.edu>

Preface

The Multidisciplinary Center for Earthquake Engineering Research (MCEER) is a national center of excellence in advanced technology applications that is dedicated to the reduction of earthquake losses nationwide. Headquartered at the University at Buffalo, State University of New York, the Center was originally established by the National Science Foundation in 1986, as the National Center for Earthquake Engineering Research (NCEER).

Comprising a consortium of researchers from numerous disciplines and institutions throughout the United States, the Center's mission is to reduce earthquake losses through research and the application of advanced technologies that improve engineering, pre-earthquake planning and post-earthquake recovery strategies. Toward this end, the Center coordinates a nationwide program of multidisciplinary team research, education and outreach activities.

MCEER's research is conducted under the sponsorship of two major federal agencies, the National Science Foundation (NSF) and the Federal Highway Administration (FHWA), and the State of New York. Significant support is also derived from the Federal Emergency Management Agency (FEMA), other state governments, academic institutions, foreign governments and private industry.

The Center's Highway Project develops improved seismic design, evaluation, and retrofit methodologies and strategies for new and existing bridges and other highway structures, and for assessing the seismic performance of highway systems. The FHWA has sponsored three major contracts with MCEER under the Highway Project, two of which were initiated in 1992 and the third in 1998.

Of the two 1992 studies, one performed a series of tasks intended to improve seismic design practices for new highway bridges, tunnels, and retaining structures (MCEER Project 112). The other study focused on methodologies and approaches for assessing and improving the seismic performance of existing "typical" highway bridges and other highway system components including tunnels, retaining structures, slopes, culverts, and pavements (MCEER Project 106). These studies were conducted to:

- assess the seismic vulnerability of highway systems, structures, and components;
- develop concepts for retrofitting vulnerable highway structures and components;
- develop improved design and analysis methodologies for bridges, tunnels, and retaining structures, which include consideration of soil-structure interaction mechanisms and their influence on structural response; and
- develop, update, and recommend improved seismic design and performance criteria for new highway systems and structures.

The 1998 study, “Seismic Vulnerability of the Highway System” (FHWA Contract DTFH61-98-C-00094; known as MCEER Project 094), was initiated with the objective of performing studies to improve the seismic performance of bridge types not covered under Projects 106 or 112, and to provide extensions to system performance assessments for highway systems. Specific subjects covered under Project 094 include:

- development of formal loss estimation technologies and methodologies for highway systems;
- analysis, design, detailing, and retrofitting technologies for special bridges, including those with flexible superstructures (e.g., trusses), those supported by steel tower substructures, and cable-supported bridges (e.g., suspension and cable-stayed bridges);
- seismic response modification device technologies (e.g., hysteretic dampers, isolation bearings); and
- soil behavior, foundation behavior, and ground motion studies for large bridges.

In addition, Project 094 includes a series of special studies, addressing topics that range from non-destructive assessment of retrofitted bridge components to supporting studies intended to assist in educating the bridge engineering profession on the implementation of new seismic design and retrofitting strategies.

This report presents a theoretical framework for the seismic analysis of arbitrarily damped three dimensional linear structures. A complex 3-D modal analysis-based approach is developed to estimate the seismic responses to multi-directional excitations, accounting for effects of out-of-plane coupled motions and over-damped vibration modes. The procedures developed are suitable for the seismic analysis of structures with complex geometric shapes enhanced with damping devices introducing non-classical damping. A new modal combination rule, based on the theory of stationary random vibration and the existence of principal axes of ground motions, is developed to calculate the peak responses of structures subjected to seismic inputs given in terms of response spectra. The proposed modal combination considers correlations among perpendicular excitation components and between vibration modes. Finally, an over-damped mode response spectrum that accounts for the peak modal response resulting from the over-damped modes is proposed.

ABSTRACT

Modal analysis is a powerful approach that is used to analyze the responses of a structure under dynamic loadings. This approach allows the equation of motion to be decoupled in the modal coordinate space, and subsequently used to evaluate the dynamic response of a structure in the modal coordinate system, which significantly simplifies and accelerates the response calculation. Past research has shown that the modal analysis approach is applicable in earthquake engineering, resulting in its widespread use. For example, the seismic design and analysis of structures with added damping devices is based on the modal analysis concept, in which the motion within a plane and the assumption of classical damping are usually made. However, three-dimensional (3-D) structures with complex geometric shapes enhanced with added damping devices may be highly non-classically damped, possess over-damped modes, and exhibit significant out-of-plane motions. These uncertainties may affect the accuracy of the modal analysis approach in practice.

This report presents a theoretical framework for the seismic analysis of arbitrarily damped 3-D linear structures. First, a complex modal analysis-based approach is developed to analyze seismic responses to multi-directional excitations. This approach is formulated in a 3-D manner and allows the eigenvalues to be real, which correspond to over-damped modes. As a result, the responses resulting from the over-damped modes and the out-of-plane coupled motions can be properly considered. Several useful modal properties are identified and their mathematical proofs are provided. Next, a new modal combination rule is developed to calculate the peak response of arbitrarily damped 3-D linear structures when the seismic inputs are given in terms of response spectra. This modal combination rule is based on the theory of stationary random vibration and the existence of the principal axes of ground motions. In this rule, the correlations among two perpendicular excitation components and between modes are considered. Finally, an over-damped mode response spectrum that accounts for the peak modal response resulting from the over-damped modes is proposed.

ACKNOWLEDGEMENT

Financial support for this research was provided by the Federal Highway Administration (Contract Number: DTFH61-98-C-00094) and National Science Foundation through MCEER (CMS 97-01471). The support is gratefully acknowledged.

TABLE OF CONTENTS

CHAPTER	TITLE	PAGE
1	Introduction	1
1.1	General.....	1
1.2	Literature Review	3
1.2.1	Analysis of Non-classical Damped Structures.....	4
1.2.2	Response Spectrum Methods.....	5
1.2.3	Applications to 3-D Structures under 3-D Excitations	6
1.3	Research Objectives.....	7
1.4	Scope of Work	7
1.5	Organization.....	8
2	Eigenvalue Problem and Modal Properties of Structural Systems	11
2.1	Introduction.....	11
2.2	Equation of Motion.....	11
2.3	Eigenvalue Problem.....	12
2.3.1	Orthogonality of Modes.....	15
2.4	Modal Decomposition and Superposition.....	16
2.5	Structural Residual Matrices.....	17
2.6	Expansion of Inverse of the Mass Matrix \mathbf{M}^{-1}	19
2.7	Expansion of the Inverse of Stiffness Matrix \mathbf{K}^{-1}	20
3	General Modal Response History Analysis.....	21
3.1	Introduction.....	21
3.2	Theoretical Formulation of General Modal Analysis	21
3.2.1	Structural Displacement.....	23
3.2.2	Structural Velocity	30
3.2.3	Structural Absolute Acceleration.....	32
3.2.4	Unified Form for Response Expression	34
3.3	Interpretation of the General Modal Analysis	35
3.4	General Modal Coordinate Transformation Matrix.....	37
3.4.1	Proof of Modal Decoupling	40
3.5	Modal Static Response and Effective Modal Mass	47

TABLE OF CONTENTS (CONT'D)

CHAPTER	TITLE	PAGE
	3.5.1 Effective Modal Mass for Classically Damped Systems w/o Over-Damped Modes.....	48
	3.5.2 Effective Modal Mass for 3-D Arbitrarily Damped Systems	51
	3.6 Reduction to Classically Under-Damped Structures	57
	3.7 Response Expansion in Terms of Seismic Incidence θ	58
4	Development of the Response Spectrum Method	61
4.1	Introduction.....	61
4.2	Current Directional Combination Rules for Multi-component Excitation	62
4.2.1	SRSS Rule.....	62
4.2.2	Percentage Rule	62
4.2.3	CQC3 Rule.....	63
4.3	Ground Motion Model	63
4.4	General Modal Combination Rule for Multi-component Excitation	64
4.4.1	Definition of Vector Operation Symbols.....	65
4.4.2	Modal Response to Stationary Excitation.....	65
4.4.3	Complete Quadratic Combination of Modal Responses.....	73
4.4.4	Identical Horizontal Response Spectra	80
4.4.5	Uniformly Distributed Incident Angle.....	80
4.4.6	GSRSS3	81
4.4.7	Investigation of the Correlation Factors	82
4.4.8	Reduction to Classically Under-Damped Systems	83
4.5	Over-damped Mode Response Spectrum.....	90
4.5.1	The Concept.....	90
4.5.2	Construction of Over-damped Mode Response Spectrum Consistent with 5% Displacement Response Spectrum	92
4.5.3	Validation of the Over-damped Mode Response Spectrum	98
5	Spatially Combined Responses to Multi-Component Seismic Excitations	103
5.1	Introduction.....	103
5.2	Critical Value of Responses Specified in a Given Direction.....	105
5.2.1	Excitation Histories as Inputs	105

TABLE OF CONTENTS (CONT'D)

CHAPTER	TITLE	PAGE
	5.2.2 Response Spectra as Inputs	107
5.3	Critical Value of the Spatially Combined Responses	109
	5.3.1 Response History Approach	109
	5.3.2 Response Spectrum Approach	112
6	Application Example	119
	6.1 Introduction	119
	6.2 Description of the Example Building	120
	6.3 Ground Motion Records	125
	6.4 Modal Response History Analysis	126
	6.4.1 Responses of Each Story	126
	6.4.2 Responses of Each Frame	132
	6.4.3 Discussion	132
	6.5 Response Spectrum Analysis	143
	6.5.1 Responses of Each Story	144
	6.5.2 Responses of Each Fame	144
	6.5.3 Discussion	163
	6.5.4 Effect of Seismic Incidence	163
	6.5.5 Peak Floor Acceleration Bounding Envelope	164
7	Summary, Conclusions and Future Research.....	175
	7.1 Summary	175
	7.2 Conclusions	176
	7.2 Future Research	177
8	REFERENCES.....	179

LIST OF FIGURES

FIGURE	TITLE	PAGE
3.1	3-D MDOF structure subjected to 3-component ground motion.....	23
3.2	Under-damped SDOF system subjected to 3-component ground excitation.....	27
3.3	Basic concept of the general modal response history analysis	36
3.4	Schematic explanation of the modal response history analysis of a 3-D MDOF subjected to 3-component ground excitation.....	37
3.5	A planar N-DOFs multistory frame	50
3.6	Illustration of the static structural response subjected to \mathbf{s}_i	50
4.1	Correlation coefficient ρ_{ij}^{DD} for responses to white noise excitations.....	84
4.2	Correlation coefficient ρ_{ij}^{VV} for responses to white noise excitations.....	85
4.3	Correlation coefficient ρ_{ij}^{VD} for responses to white noise excitations.....	86
4.4	Correlation coefficient ρ_{ij}^{DP} for responses to white noise excitations	87
4.5	Correlation coefficient ρ_{ij}^{PP} for responses to white noise excitations	87
4.6	Generation of over-damped mode response spectrum.....	92
4.7	Variation of η factor for over-damped response	95
4.8	Pseudo-mode response spectrum construction procedures.....	97
4.9	Mean 5% damping displacement response spectrum (a) ensemble A (b) ensemble B	101
4.10	Comparisons of exact and estimated over-damped mode response spectrum (a) ensemble A (b) ensemble B.....	101
5.1	Variation of $r_0(t^*)$ at time instant t^* as θ varies	107
5.2	Concept of spatially combined responses.....	110
5.3	Projection of the two-component spatially combined response	116
5.4	Response elliptical envelope for two-component spatially combined response.....	117
6.1	Planar view of the example six-story steel moment frame building.....	122
6.2	Details of Frame 1 of the example building.....	123
6.3	Details of Frame 2 of the example building.....	123
6.4	Details of Frame 3 of the example building.....	124

LIST OF FIGURES (CONT'D)

FIGURE	TITLE	PAGE
6.5	Details of Frame 4 of the example building.....	124
6.6	Comparisons of story responses along X-axis by response history analysis.....	128
6.7	Comparisons of story responses along Y-axis by response history analysis.....	129
6.8	Comparisons of story responses about Z-axis by response history analysis.....	130
6.9	Estimation errors of the story responses by response history analysis	131
6.10	Comparisons of interstory drifts per frame by response history analysis.....	135
6.11	Comparisons of interstory velocities per frame by response history analysis.....	136
6.12	Comparisons of story shear forces at max. drifts per frame by response history analysis.....	137
6.13	Comparisons of maximum story shear forces per frame by response history analysis.....	138
6.14	Estimation errors of the story drift per frame by response history analysis.....	139
6.15	Estimation errors of the inter story velocity per frame by response history analysis.....	140
6.16	Estimation errors of the story shear force at max. inter story drift per frame by response history analysis	141
6.17	Estimation errors of the maximum story shear force per frame by response history analysis.....	142
6.18	Comparisons of story responses along X-axis by response spectrum method.....	151
6.19	Comparisons of story responses along Y-axis by response spectrum method.....	152
6.20	Comparisons of story responses about Z-axis by response spectrum method.....	153
6.21	Estimation errors of the story responses by response spectrum method	154

LIST OF FIGURES (CONT'D)

FIGURE	TITLE	PAGE
6.22	Comparisons of interstory drifts per frame by response spectrum method.....	155
6.23	Comparisons of interstory velocities per frame by response spectrum method.....	156
6.24	Comparisons of story shear forces at max. drifts per frame by response spectrum method.....	157
6.25	Comparisons of maximum story shear forces per frame by response spectrum method.....	158
6.26	Estimation errors of the story drift per frame by response spectrum method.....	159
6.27	Estimation errors of the inter story velocity per frame by response spectrum method.....	160
6.28	Estimation errors of the story shear force at max. inter story drift per frame by response spectrum method.....	161
6.29	Estimation errors of the maximum story shear force per frame by response spectrum method.....	162
6.30	Story displacement response variation along X-axis with respect to on along X-axis with respect to θ	165
6.31	Story displacement response variation along Y-axis with respect to θ	166
6.32	Story displacement response variation about Z-axis with respect to θ	167
6.33	Story velocity response variation along X-axis with respect to θ	168
6.34	Story velocity response variation along Y-axis with respect to θ	169
6.35	Story velocity response variation about Z-axis with respect to θ	170
6.36	Story total acceleration response variation along X-axis with respect to θ	171
6.37	Story total acceleration response variation along Y-axis with respect to θ	172
6.38	Story total acceleration response variation about Z-axis with respect to θ	173
6.39	Comparison of the response envelopes for the example building.....	174

LIST OF TABLES

TABLE	TITLE	PAGE
3.1	Summary of the expressions of the effective modal mass	56
4.1	Term by term expression of Equation (4.61)	79
4.2	White-noise-determined η factor for over-damped modal response	96
4.3	Far-field ground motions used by Vamvatsikos and Cornell (2004).....	99
4.4	Far-field ground motions used in ATC-58.....	100
6.1	Reactive mass of the example building	121
6.2	Modal periods and damping ratio of the example building	125
6.3	Results of mean peak displacement responses of defined degree-of-freedoms of the example building using ground motion records as inputs	127
6.4	Results of mean peak velocity responses of defined degree-of-freedoms of the example building using ground motion records as inputs	127
6.5	Results of mean peak total acceleration responses of defined degree-of-freedoms of the example building using ground motion records as inputs.....	127
6.6	Results of mean peak responses of frame 1 of the example building using ground motion records as inputs	133
6.7	Results of mean peak responses of frame 2 of the example building using ground motion records as inputs	133
6.8	Results of mean peak responses of frame 3 of the example building using ground motion records as inputs	134
6.9	Results of mean peak responses of frame 4 of the example building using ground motion records as inputs	134
6.10	Results of mean peak displacement responses of defined degree-of-freedoms of the example building using response spectra as inputs	145
6.11	Results of mean peak velocity responses of defined degree-of-freedoms of the example building using response spectra as inputs	145
6.12	Results of mean peak total acceleration responses of defined degree-of-freedoms of the example building using response spectra as inputs	146

LIST OF TABLES (CONT'D)

TABLE	TITLE	PAGE
6.13	Results of mean peak responses of frame 1 of the example building using response spectra as inputs	147
6.14	Results of mean peak responses of frame 2 of the example building using response spectra as inputs	148
6.15	Results of mean peak responses of frame 3 of the example building using response spectra as inputs	149
6.16	Results of mean peak responses of frame 4 of the example building using response spectra as inputs	150

CHAPTER 1

INTRODUCTION

1.1 General

Advancements in modern supplemental damping devices have resulted in their application as a means to protect structures from natural and man-made hazards (Soong and Dargush, 1997; Soong and Spencer, 2002). In the context of earthquake engineering, they have been used to enhance the dynamic performance and resilience of civil infrastructures against seismic loads. Basically, these devices work by increasing the overall damping, stiffness and strength of a given structure, which in turn reduces vibration and alleviates damage in the event of an earthquake. Research and development in their applications has shown a number of advantages, including: (1) control efficiency, (2) cost effectiveness, and (3) reliability. Such advantages have made their use promising in the civil engineering community.

When damping devices are incorporated into structures, the properties of the structure can significantly change. In general, response history analysis with explicit modeling of the damping devices is the most accurate and reliable method used to assess seismic performance. However, professional structural engineers seldom perform response history analysis, mainly due to its prohibitive computational demand and a lack of adequate records to represent the site characteristics. Most engineers prefer not to deal with dynamic analysis and instead use equivalent static loads or, at most, response spectrum analysis. As a result, many static seismic analysis methods of structures with damping devices have been developed (Iwan and Gates, 1979a, b; Tsopelas et al., 1997). These methods have been developed based on a representation of the structural system, including the added damping devices, by an equivalent linear viscously damped SDOF system using the modal analysis concept, in which classical damping conditions are assumed and the frames are limited to a 2-dimensional (2-D) planar frame. These research products have resulted in several design provisions for structures with supplemental damping devices since 2000 in the United States (BSSC, 2003; ASCE, 2006).

However, the classical damping assumption is generally not valid for structures with dampers, because it is difficult to properly size and locate them. In practice, there are only a few specific locations available for their installation. Therefore, structures with added dampers may need to be considered as non-classically damped. In the literature, the treatment of non-classical damping (or non-proportional damping) is well developed by using the state space method. However, the state space method requires manipulation in the complex modal space with doubled dimension and lacks thorough physical explanations; thus, no systematic introduction of the state space method in the earthquake engineering community has been carried out. Furthermore, as the level of the amount of added damping increases, the structure may exhibit considerably high modal damping ratios, from which over-critically damped modes may be present for certain modes. This situation is likely to occur either in the intermediate iteration results or in the final design for optimized damper design. Ignoring such over-critically damped modes can result in notable underestimation of the structural response. However, there is a gap in current modal analysis knowledge about how to handle these uncertainties properly with a theoretical basis. In this study, arbitrarily damped three-dimensional (3-D) structures are used to represent structures with supplemental damping devices, where highly non-classical damping and over-damped modes can be expected.

Currently, when using modal analysis approaches for structures with added damping devices subjected to seismic excitation, it is assumed that there is motion within a plane and that classical damping exists. In other words, traditionally, the 2-D seismic frames with added earthquake protective systems are assumed to be classically damped. With these assumptions, neither orthogonal effects between two perpendicular excitation components, nor the effects of non-classical damping and the over-damped modes are properly considered. For structures with complex geometric shapes enhanced with damping devices, these effects may be significant. Ignoring them in the analysis of arbitrarily damped 3-D structures will result in inadequate designs. In most situations, the responses calculated using the classical damping assumption are much less than the exact solutions that consider 3-D behavior and non-classical damping. In current codes, in order to allow the extra responses resulting from the multiple excitations, a 30% or 40% rule arising from the orthogonal effects is applied. The safety margin of the

percentage rule has not been determined through careful studies. It is used simply because the required computational effort is rather prohibitive and, at the same time, there has been a lack of knowledge necessary to formulate a simple, rational approach. As the complex structural systems become more popular due to advanced innovative technology, it is necessary to design and analyze the structures using a 3-D model together with multiple-component earthquake excitations in order to achieve safe designs. Due to these concerns, the applicability and feasibility of the current classical modal analysis approach may not be adequate and needs to be further examined. Thus, an improved theoretical foundation for the modal analysis approach with a sound scientific basis is desirable. This research is focused on establishing the theoretical base of the modal analysis approach for 3-D arbitrarily damped structures subjected to multiple excitations.

1.2 Literature Review

Modal analysis may be described as a method for decoupling the equations of motion by means of modal coordinate transformation. It is well known that the decoupling coordinate transformation can be determined by the solution of an algebraic eigenvalue problem of the system. In earthquake engineering, the classical modal analysis method is considered as a powerful approach to analyze the seismic responses of classically damped linear structures. In this method, the structure may be treated as a series of independent single-degree-of-freedom (SDOF) systems. Two approaches of this method are: the modal response history analysis, which gives the complete response history of the structures, and the response spectrum analysis. When a given structure satisfies the classical damping criterion proposed by Caughey and O'Kelly (1965), its modes are real-valued and are identical to those of the associated undamped systems. This linear vibrating structure is said to be classically damped and possesses normal modes, and can be decoupled by the same modal transformation that decouples the associated undamped structures. The structures that do not satisfy the Caughey and O'Kelly criterion are said to be non-classically damped; consequently, their equations of motion cannot be decoupled by using the classical modal transformation. In principle, the coupling arises from the damping term due to variation of the energy dissipation rate from different components of

a system. Typical examples include structures with added damping devices, base-isolated structures, and primary-secondary systems.

1.2.1 Analysis of Non-classical Damped Structures

Basically, the responses of non-classically damped structures may be evaluated by using the decoupled method suggested by Foss (1958). However, it is generally believed that, concurrent with the classical damping assumption, the structural responses calculated by the classical modal superposition method are acceptable. For example, current methods for seismic design of structures enhanced with damping devices are developed based on the classical damping assumption (BSSC, 2003). This may not always be true due to the uncertainty of the nature and magnitude of the damping in structures. This phenomenon can be further magnified when the structure is irregularly shaped. There are instances where the structures can be highly non-classically damped (Warburton and Soni, 1977) and, in some cases, develop over-damped modes (Inman and Andry, 1980), which in turn results in the possibility of inaccurate response estimations. For example, Takewaki (2004) demonstrated that the structural energy transfer function and displacement transfer function will be underestimated if the over-damped modes are neglected.

A common approach to analyze non-classically damped structures is to assume that they can be decoupled using classical modal transformation. That is, the off-diagonal terms of the associated transformed damping matrix can be ignored. It is generally believed that this decoupling technique will not produce significant errors if the off-diagonal terms of the transformed damping matrix are small in one order scale compared to the diagonal terms. However, this decoupling approximation may cause substantial errors, depending on the characteristics of the excitation and the analyzed structures. Further, the implications and limitations of this technique are not yet fully understood.

Over the years, in order to advance the application of classical modal analysis to non-classically damped systems, a number of researchers have conducted extensive studies on developing complex modal superposition methods for systems that do not satisfy classical damping conditions. Villaverde and Newmark (1980) developed a deterministic formulation for non-classically damped systems by using complex frequencies and mode

shapes. They showed that the response associated with each complex mode shape can be represented based on the modal relative displacement response and the modal relative velocity response. Igusa et al. (1984) studied the stationary response of multi-degrees-of-freedom (MDOF) non-classically damped linear systems subjected to stationary input excitations. Veletsos and Ventura (1986) presented a critical review of the modal superposition method of evaluating the dynamic response of non-classically damped structures. Singh and Ghafory-Ashtiany (1986) studied the modal time history analysis approach for non-classically damped structures subjected to seismic forces. Yang et al. (1987, 1988) used a real-valued canonical transformation approach to decouple a non-classically damped system from a set of second order differential equations to a set of first order ones, and then performed a time history analysis as well as a response spectrum analysis. Zhou et al. (2004) provided a refined complex mode superposition algorithm to evaluate the seismic responses of non-classically damped systems. All the above are important contributions, but none addressed the over-damped modes or explicitly formulated the analytical solutions in 3-D form to identify the spatial coupling effect.

1.2.2 Response Spectrum Methods

In addition, in earthquake engineering, the response spectrum method is commonly used as an alternative approach to response history analysis for determining the maximum values of the seismic responses of classically damped structures. In this method, the modal peak responses are obtained using the prescribed response spectrum. These modal maxima are then appropriately combined to estimate the peak values of the responses of interest. There are several combination rules proposed by various researchers. Among these, the simplest is the square-root-of-sum-of-squares (SRSS) modal combination rule (Rosenblueth, 1951). This rule ignores the correlations between the vibration modes and provides excellent estimates for structures with well-separated modal frequencies. To further consider the correlations between each vibration mode, Der Kiureghian (1980, 1981) proposed a rational rule, known as the complete quadratic combination (CQC) rule, in which the correlations among modes are connected by correlation coefficients. Both rules deal with classically damped structures.

The conventional response spectrum method is ideal for structures that satisfy classical damping conditions. For structures that are strongly non-classically damped, the accuracy of the SRSS or CQC rule becomes questionable (Clough and Mojtahedi, 1976; Warburton and Soni, 1977; Veletsos and Ventura, 1986). For this reason, several modal combination rules that account for the effects of non-classical damping were developed. Singh and Chu (1976) were among the first to develop an alternative approach based on the stochastic method. Singh (1980) formed a modified conventional SRSS approach where nonproportional damping effects were properly included. Later, Der Kierighian et al. (1983) evaluated the responses of light equipment in structures to stochastic excitations. Igusa et al. (1984) described the responses in terms of spectral moments and provided the formulations of correlation coefficients among modes using a filtered white noise process as inputs. Ventura (1985) stated that the peak modal responses could be obtained by taking the SRSS of the individual modal maxima contributed from the displacement and velocity responses, assuming harmonic excitations. Gupta and Jaw (1986) developed the response spectrum combination rules for non-classically damped systems by using the displacement and velocity response spectrum. Villaverde (1988) improved Rosenblueth's rule (1951) by including the effect of modal velocity responses. Maldonado and Singh (1991) proposed an improved response spectrum method for non-classically damped systems. The method reduces the errors associated with the truncation of the high frequency modes without explicitly using them in the analysis. Zhou et al. (2004) generalized the CQC rule for application to non-classically damped systems.

1.2.3 Applications to 3-D Structures under 3-D Excitations

To address the issue of 3-D structures under 3-D excitations, several research studies have been performed. Lee and Liang (1998) noted the cross effect among directional excitations and modes, implying the necessity of using the CQC rule in a three-dimensional context. To consider the effect among orthogonal excitation components, Semby and Der Kiureghian (1985) further extended the CQC rule to the CQC3 rule, followed by a series of discussions and applications of this rule (Hernandez and Lopez, 2002; Lopez and Torres, 1997). However, none of these combination rules incorporated

over-critically damped modes in the formulation and the response quantities are limited to those that are deformation-related.

To overcome the limitations of these problems, Song et al. (2008) developed a thorough modal analysis approach for structures with non-classical damping and over-damped modes subjected to single directional excitation. This research further advances Song et al. (2008) to include three-dimensional applications.

1.3 Research Objectives

The primary objective of this research is to provide analytical solutions to the potential problems mentioned above by establishing a solid theoretical foundation for design and analysis of 3-D linear MDOF structures with dampers using a modal analysis approach. The specific objectives are:

- (1) Explore the modal properties of the 3-D arbitrarily damped MDOF systems with over-damped modes.
- (2) Establish a more realistic and accurate modal analysis approach for a linear arbitrarily damped MDOF model to best estimate the seismic responses. This modal analysis approach can handle non-classical damping and over-critically damped modes as well as orthogonal effects arising from multi-component earthquake excitations.
- (3) Extend the present response spectrum method to be applicable to non-classically damped systems with over-damped modes.
- (4) Introduce a response spectrum method to predict the peak response of a spatially-combined response vector, which is not a linear combination of the nodal responses.

1.4 Scope of Work

The work has proceeded as follows:

- (1) Examine the theory presently being used for analyzing non-classically damped linear systems.
- (2) Formulate the equation of motion of a 3-D arbitrarily damped MDOF system using the state space method, as well as perform an eigen analysis and explore the modal properties. All the formulations are presented in matrix form.
- (3) Formulate the response history analysis procedure in the manner of modal superposition and offer an interpretation of the physical meaning of the formulation. The main effort focuses on the analytical formulation of the over-damped modes.
- (4) Extend the response history analysis procedure for use by the response spectrum method. Much of this effort focuses on the treatment of over-damped modes.
- (5) Verify that the response spectrum-based approach is applicable to 3-D arbitrarily damped structures to estimate the peak response of a spatially combined response vector.

1.5 Organization

Chapter 2 details the eigen analysis of a 3-D arbitrarily damped MDOF linear structure, concentrating on the treatment of over-damped modes. Several fundamental modal properties are explored and presented.

Chapter 3 presents the formulation of the modal analysis procedures for the 3-D arbitrarily damped linear MDOF structures highlighting the treatment of the over-damped modes. This chapter also presents a unified form suitable for representing any response quantities.

Chapter 4 shows the rigorous formulation of the response spectrum method for the analysis of the 3-D arbitrarily damped linear MDOF structure with over-damped modes. This chapter focuses on the development of a method to handle the over-damped modes when using the site response spectra specified in design codes.

Chapter 5 introduces a response spectrum approach to estimate the peak response of a spatially combined response to multi-component seismic excitation.

Chapter 6 demonstrates the use of the proposed modal analysis method and response spectrum method through a 3-D irregular building arbitrarily installed with linear viscous dampers between floors. The results obtained by using the classical damping assumption and the exact solutions are compared. The effect of the over-damped modes on the peak response estimation is examined and discussed.

Finally, Chapter 7 presents a summary and conclusions, and provides suggestions for future research.

CHAPTER 2

EIGENVALUE PROBLEM AND MODAL PROPERTIES OF STRUCTURAL SYSTEMS

2.1 Introduction

In the real world, structures are continuous systems. However, it is well known that continuous systems can be approximated as lumped-parameter systems by using lumped masses, springs and the concept of equivalent viscous damping. A discrete structure is usually characterized by parameters that do not depend on spatial coordinates and have a finite number of degrees of freedom. This chapter presents the mathematical modeling of a discrete arbitrarily damped linear structure subjected to a set of dynamic loadings. The corresponding eigenvalue problem of an arbitrarily damped structure is established and solutions are presented, including for cases with real-valued eigenvalues. The real-valued eigenvalues represent the presence of over-damped modes, which are usually ignored in practical applications. In addition, the orthogonality of modes is shown. Also, one useful modal property, the sum of the residual matrices, is found and the modal expansion of the mass and stiffness matrices in terms of modal parameters are presented. The results shown in this chapter serve as a solid basis for the analytical formulation presented in the following chapters.

2.2 Equation of Motion

A 3-dimensional (3-D) discrete arbitrarily damped linear structure with N degrees-of-freedom (DOF) subjected to a three-component dynamic loading $\mathbf{f}(t)$ is considered. It has a dimension N and belongs to a real field matrix, i.e., $\mathbf{f}(t) \in \mathbb{R}^N$. The motion of the structure is governed by a matrix ordinary differential equation in the form of

$$\mathbf{M}\ddot{\mathbf{u}}(t) + \mathbf{C}\dot{\mathbf{u}}(t) + \mathbf{K}\mathbf{u}(t) = \mathbf{f}(t) \quad (2.1)$$

in which $\mathbf{M} \in \mathbb{R}^{N \times N}$, $\mathbf{C} \in \mathbb{R}^{N \times N}$ and $\mathbf{K} \in \mathbb{R}^{N \times N}$ are the mass, viscous damping and stiffness matrices with dimension $N \times N$, respectively. \mathbf{M} and \mathbf{K} are positive definite matrices when the structure is completely constrained, while \mathbf{C} is a positive semi-definite

matrix. $\mathbf{u}(t) = [\mathbf{u}_x^T(t) \quad \mathbf{u}_y^T(t) \quad \mathbf{u}_z^T(t) \quad \mathbf{u}_{\theta_x}^T(t) \quad \mathbf{u}_{\theta_y}^T(t) \quad \mathbf{u}_{\theta_z}^T(t)]^T \in \mathbb{R}^N$ is a $N \times 1$ generalized displacement vector representing the translational and rotational DOFs for each node. $\dot{\mathbf{u}}(t) \in \mathbb{R}^N$ and $\ddot{\mathbf{u}}(t) \in \mathbb{R}^N$ are the generalized relative velocity vector and relative acceleration vector, respectively.

2.3 Eigenvalue Problem

When the structure is arbitrarily damped, it cannot be decoupled in the N dimensional physical space; as a result, it is necessary to go through the $2N$ dimensional state space to perform the eigen analysis. Namely, Equation (2.1) can be cast into a set of first-order linear equations as (Veletsos and Ventura, 1986; Yang et al., 1987; Zhou et al., 2004)

$$\mathbf{A}\dot{\mathbf{v}}(t) + \mathbf{B}\mathbf{v}(t) = \mathbf{f}_s(t) \quad (2.2)$$

where

$$\begin{aligned} \mathbf{A} &= \begin{pmatrix} \mathbf{0} & \mathbf{M} \\ \mathbf{M} & \mathbf{C} \end{pmatrix} \in \mathbb{R}^{2N \times 2N}, \quad \mathbf{B} = \begin{pmatrix} -\mathbf{M} & \mathbf{0} \\ \mathbf{0} & \mathbf{K} \end{pmatrix} \in \mathbb{R}^{2N \times 2N} \\ \mathbf{v}(t) &= \begin{Bmatrix} \dot{\mathbf{u}}(t) \\ \mathbf{u}(t) \end{Bmatrix} \in \mathbb{R}^{2N}, \quad \mathbf{f}_s(t) = \begin{Bmatrix} \mathbf{0} \\ \mathbf{f}(t) \end{Bmatrix} \in \mathbb{R}^{2N} \end{aligned} \quad (2.3)$$

The coefficient matrices \mathbf{A} and \mathbf{B} are symmetric but not definite. It can be shown that \mathbf{A} and \mathbf{B} are non-singular matrices; that is, both \mathbf{A}^{-1} and \mathbf{B}^{-1} exist (Song et al., 2008). Let λ be an admissible eigenvalue. Associated with each eigenvalue λ is an admissible eigenvector $\boldsymbol{\psi}$. The associated eigenvalue problem of Equation (2.2) is given by

$$(\lambda\mathbf{A} + \mathbf{B})\boldsymbol{\psi} = \mathbf{0} \quad (2.4)$$

From linear algebra theory, the solution to the above eigenvalue problem leads to a set of $2N$ eigenvalues $\lambda_i \in \mathbb{C}$ (complex field) and $2N$ associated complex eigenvectors $\boldsymbol{\psi}_i \in \mathbb{C}^{2N}$. For a conventional structure or a structure enhanced with passive damping devices, a stable system is expected. In other words, the eigenvalues are either complex-valued with negative real parts or negative real-valued.

When the eigenvalue is complex-valued, the associated eigenvector is also complex-valued, corresponding to an under-damped vibration mode. And, all the eigenvalues and eigenvectors must appear in complex-conjugated pairs, since the eigenvalue problem in Equation (2.4) possesses real-valued coefficients. Assuming that there are N_C pairs of complex eigenvalues, the corresponding eigenvalues and eigenvectors can be expressed as

$$\lambda_i, \lambda_i^* = -\xi_i \omega_i \pm j \omega_{di} \quad (i = 1, 2, 3 \dots N_C) \quad (2.5)$$

$$\Psi_i = \begin{Bmatrix} \lambda_i \Phi_i \\ \Phi_i \end{Bmatrix}, \Psi_i^* = \begin{Bmatrix} \lambda_i^* \Phi_i^* \\ \Phi_i^* \end{Bmatrix} \quad (2.6)$$

where $\Phi_i \in \mathbb{C}^N$ or $\Phi_i^* \in \mathbb{C}^N$ is the i th complex modal shape, $\omega_i \in \mathbb{R}$ and $\xi_i \in \mathbb{R}$ are the i th modal frequency and modal damping ratio, respectively, and $\omega_{di} = \sqrt{1 - \xi_i^2} \omega_i \in \mathbb{R}$ is the i th modal damped frequency. The superscript * in the above equations denotes a conjugate operation. In this situation where Φ_i is complex-valued, it indicates that all components of the structure vibrate synchronously with identical frequency and at an identical decay rate. However, phase difference exists between each component. As a result, the components do not pass through their equilibrium position at the same time instant. For the special case where Φ_i is real-valued and ξ_i does not equal to zero (classical damping case), the components of the structure are either in or out of phase relative to each other and they pass through their equilibrium position at the same time instant.

When the eigenvalues are real-valued, the corresponding modes are over-damped subsystems which are no longer second-order oscillatory subsystems. For the sake of simplicity, all related variables are denoted by superscript or subscript ‘‘P’’ for ‘‘over-damped modes,’’ to differentiate them from the variables associated with complex modes. Mathematically speaking, over-damped modes also appear in pairs. However, based on control theory, each over-damped mode can be considered as an independent basic unit. There are no functional relationships among all over-damped modes, mathematically or physically. Thus, it would not be necessary to group them in pairs in the analytical

formulation process. In this study, all over-damped modes are handled individually. Thus, assuming that there are $N_p [= 2(N - N_C)]$ real and negative eigenvalues:

$$\lambda_i^P = -\omega_i^P \in \mathbb{R} \quad (i = 1, 2, 3 \dots N_p) \quad (2.7)$$

where ω_i^P is larger than zero for a stable system with dimension “rad/sec,” and is defined as the i th over-damped modal natural circular frequency. Each real eigenvalue λ_i^P corresponds to a real-valued eigenvector $\boldsymbol{\psi}_i^P \in \mathbb{R}^{2N}$ ($i = 1, 2 \dots N_p$) and

$$\boldsymbol{\psi}_i^P = \begin{Bmatrix} \lambda_i^P \boldsymbol{\phi}_i^P \\ \boldsymbol{\phi}_i^P \end{Bmatrix} \in \mathbb{R}^{2N} \quad (2.8)$$

where $\boldsymbol{\phi}_i^P \in \mathbb{R}^N$ is the i th “over-damped mode shape.”

The eigenvalue matrix (or spectral matrix), which is the assembly of all eigenvalues, is a diagonal matrix and denoted as

$$\boldsymbol{\Lambda} = \text{diag}(\lambda_1, \lambda_2 \dots \lambda_{N_C}, \lambda_1^*, \lambda_2^* \dots \lambda_{N_C}^*, \lambda_1^P, \lambda_2^P \dots \lambda_{N_p}^P) \in \mathbb{C}^{2N \times 2N} \quad (2.9)$$

The eigenvector matrix, which is the assembly of all eigenvectors, is denoted as

$$\begin{aligned} \boldsymbol{\Psi} &= (\boldsymbol{\psi}_1, \boldsymbol{\psi}_2 \dots \boldsymbol{\psi}_{N_C}, \boldsymbol{\psi}_1^*, \boldsymbol{\psi}_2^* \dots \boldsymbol{\psi}_{N_C}^*, \boldsymbol{\psi}_1^P, \boldsymbol{\psi}_2^P \dots \boldsymbol{\psi}_{N_p}^P) \\ &= \begin{pmatrix} \boldsymbol{\Phi} \boldsymbol{\Lambda} \\ \boldsymbol{\Phi} \end{pmatrix} \in \mathbb{C}^{2N \times 2N} \end{aligned} \quad (2.10)$$

in which $\boldsymbol{\Phi} = (\boldsymbol{\phi}_1, \boldsymbol{\phi}_2 \dots \boldsymbol{\phi}_{N_C}, \boldsymbol{\phi}_1^*, \boldsymbol{\phi}_2^* \dots \boldsymbol{\phi}_{N_C}^*, \boldsymbol{\phi}_1^P, \boldsymbol{\phi}_2^P \dots \boldsymbol{\phi}_{N_p}^P) \in \mathbb{C}^{N \times 2N}$ is the eigenvector matrix associated with the displacement vector and $\boldsymbol{\Phi} \boldsymbol{\Lambda}$ is the eigenvector matrix associated with the velocity vector. Note that for the i th mode shape, $\boldsymbol{\phi}_i$ can be represented as $\boldsymbol{\phi}_i = [\boldsymbol{\phi}_{ix} \quad \boldsymbol{\phi}_{iy} \quad \boldsymbol{\phi}_{iz} \quad \boldsymbol{\phi}_{i\theta_x} \quad \boldsymbol{\phi}_{i\theta_y} \quad \boldsymbol{\phi}_{i\theta_z}]^T$, from which it is observed that the modal motion is not limited to only one global reference direction. This represents the spatial coupling phenomenon in the physical space.

2.3.1 Orthogonality of Modes

The eigenvectors corresponding to different eigenvalues can be shown to be orthogonal to each other with respect to matrices \mathbf{A} and \mathbf{B} , respectively, in which a “no repeated eigenvalues” condition is assumed. That is, when $i \neq j$,

$$\boldsymbol{\psi}_i^T \mathbf{A} \boldsymbol{\psi}_j = 0 \quad \text{and} \quad \boldsymbol{\psi}_i^T \mathbf{B} \boldsymbol{\psi}_j = 0 \quad (2.11)$$

The proof of Equation (2.11) is given as follows. The i th eigenvalue λ_i and its associated eigenvector $\boldsymbol{\psi}_i$ satisfy Equation (2.4); premultiplying it by $\boldsymbol{\psi}_j^T$ gives

$$\lambda_i \boldsymbol{\psi}_j^T \mathbf{A} \boldsymbol{\psi}_i = -\boldsymbol{\psi}_j^T \mathbf{B} \boldsymbol{\psi}_i \quad (2.12)$$

Similarly, the j th eigenvalue λ_j and its associated eigenvector $\boldsymbol{\psi}_j$ satisfy Equation (2.4); premultiplying it by $\boldsymbol{\psi}_i^T$ gives

$$\lambda_j \boldsymbol{\psi}_i^T \mathbf{A} \boldsymbol{\psi}_j = -\boldsymbol{\psi}_i^T \mathbf{B} \boldsymbol{\psi}_j \quad (2.13)$$

Taking transpose of both sides of Equation (2.12) gives

$$\lambda_i \boldsymbol{\psi}_i^T \mathbf{A} \boldsymbol{\psi}_j = -\boldsymbol{\psi}_i^T \mathbf{B} \boldsymbol{\psi}_j \quad (2.14)$$

Comparing Equations (2.13) and (2.14) together with the assumption $\lambda_i \neq \lambda_j$ completes the proof of orthogonality shown in Equation (2.11). Moreover, the orthogonality condition leads to the following two diagonal square matrices:

$$\hat{\mathbf{a}} = \boldsymbol{\Psi}^T \mathbf{A} \boldsymbol{\Psi} = \text{diag} \left(a_1, a_2 \cdots a_{N_c}, a_1^*, a_2^* \cdots a_{N_c}^*, a_1^p, a_2^p \cdots a_{N_p}^p \right) \in \mathbb{C}^{2N \times 2N} \quad (2.15)$$

$$\hat{\mathbf{b}} = \boldsymbol{\Psi}^T \mathbf{B} \boldsymbol{\Psi} = \text{diag} \left(b_1, b_2 \cdots b_{N_c}, b_1^*, b_2^* \cdots b_{N_c}^*, b_1^p, b_2^p \cdots b_{N_p}^p \right) \in \mathbb{C}^{2N \times 2N} \quad (2.16)$$

where

$$a_i = \boldsymbol{\psi}_i^T \mathbf{A} \boldsymbol{\psi}_i = \boldsymbol{\phi}_i^T (2\lambda_i \mathbf{M} + \mathbf{C}) \boldsymbol{\phi}_i \in \mathbb{C} \quad (2.17)$$

$$b_i = \boldsymbol{\psi}_i^T \mathbf{B} \boldsymbol{\psi}_i = \boldsymbol{\phi}_i^T (-\lambda_i^2 \mathbf{M} + \mathbf{K}) \boldsymbol{\phi}_i = -a_i \lambda_i \in \mathbb{C} \quad (2.18)$$

$$a_i^p = (\boldsymbol{\Psi}_i^p)^T \mathbf{A} \boldsymbol{\Psi}_i^p = (\boldsymbol{\Phi}_i^p)^T (2\lambda_i^p \mathbf{M} + \mathbf{C}) \boldsymbol{\Phi}_i^p \in \mathbb{R} \quad (2.19)$$

$$b_i^p = (\boldsymbol{\Psi}_i^p)^T \mathbf{B} \boldsymbol{\Psi}_i^p = (\boldsymbol{\Phi}_i^p)^T [-(\lambda_i^p)^2 \mathbf{M} + \mathbf{K}] \boldsymbol{\Phi}_i^p = -a_i^p \lambda_i^p \in \mathbb{R} \quad (2.20)$$

As shown later, these orthogonality properties are useful in the formulation work presented in Chapter 3.

2.4 Modal Decomposition and Superposition

From the orthogonality of modes, it was determined that Equation (2.2) can be decoupled into a set of uncoupled $2N$ independent modal equations. Let

$$\mathbf{v}(t) = \begin{Bmatrix} \mathbf{u}(t) \\ \dot{\mathbf{u}}(t) \end{Bmatrix} = \boldsymbol{\Psi} \mathbf{w}(t) \quad (2.21)$$

in which

$$\mathbf{w}(t) = [w_1(t), w_2(t), \dots, w_{N_c}(t), w_1^*(t), w_2^*(t), \dots, w_{N_c}^*(t), w_1^p(t), w_2^p(t), \dots, w_{N_p}^p(t)]^T \in \mathbb{C}^{2N} \quad (2.22)$$

is the complex modal coordinate vector in the time domain.

Substituting Equation (2.21) into Equation (2.2) and pre-multiplying $\boldsymbol{\Psi}^T$ to both sides of the resulting equation as well as making use of Equations (2.17) to (2.20), Equation (2.2) can be transformed as (Igusa et al., 1984)

$$\dot{w}_i(t) - \lambda_i w_i(t) = \frac{\boldsymbol{\Phi}_i^T \mathbf{f}(t)}{a_i} \in \mathbb{C} \quad (i = 1, 2, \dots, N_c) \quad (2.23)$$

$$\dot{w}_i^*(t) - \lambda_i^* w_i^*(t) = \frac{\boldsymbol{\Phi}_i^H \mathbf{f}(t)}{a_i^*} \in \mathbb{C} \quad (i = 1, 2, \dots, N_c) \quad (2.24)$$

and

$$\dot{w}_i^p(t) - \lambda_i^p w_i^p(t) = \frac{(\boldsymbol{\Phi}_i^p)^T \mathbf{f}(t)}{a_i^p} \in \mathbb{R} \quad (i = 1, 2, \dots, N_p) \quad (2.25)$$

In Equation (2.24), the superscript ‘‘H’’ denotes Hermitian transpose, which is equivalent to a conjugate and transpose operation. Equations (2.23) to (2.25) are all first-order

differential equations that can be readily solved by using standard digital algorithms. The general solution to Equations (2.23) to (2.25) can be written in the form of (Hart and Wong, 1999)

$$w_i(t) = \int_0^t \frac{\boldsymbol{\Phi}_i^T \mathbf{f}(t)}{a_i} e^{\lambda_i(t-\tau)} d\tau \quad (2.26)$$

$$w_i^*(t) = \int_0^t \frac{\boldsymbol{\Phi}_i^H \mathbf{f}(t)}{a_i^*} e^{\lambda_i^*(t-\tau)} d\tau \quad (2.27)$$

$$w_i^P(t) = \int_0^t \frac{(\boldsymbol{\Phi}_i^P)^T \mathbf{f}(t)}{a_i^P} e^{\lambda_i^P(t-\tau)} d\tau \quad (2.28)$$

After the modal responses $w_i(t)$, $w_i^*(t)$ and $w_i^P(t)$ are solved, the total responses are back-calculated by the superposition of the modal responses. Considering Equation (2.10) in Equation (2.21) gives the following two expressions:

$$\mathbf{u}(t) = \sum_{i=1}^{N_c} [\boldsymbol{\Phi}_i w_i(t) + \boldsymbol{\Phi}_i^* w_i^*(t)] + \sum_{i=1}^{N_p} \boldsymbol{\Phi}_i^P w_i^P(t) \quad (2.29)$$

$$\dot{\mathbf{u}}(t) = \sum_{i=1}^{N_c} [\lambda_i \boldsymbol{\Phi}_i w_i(t) + \lambda_i^* \boldsymbol{\Phi}_i^* w_i^*(t)] + \sum_{i=1}^{N_p} \lambda_i^P \boldsymbol{\Phi}_i^P w_i^P(t) \quad (2.30)$$

Note that the modal responses $w_i(t)$, $w_i^*(t)$ and $w_i^P(t)$ are complex-valued and have no physical interpretations. In addition, the computation efforts for solving Equations (2.23) to (2.25) are demanding since they are presented in complex-valued form. Thus responses expressed by the form shown in Equations (2.29) and (2.30) are not preferred. In the following chapter, a rigorous analytical formulation with all expressions presented in terms of real-valued quantities is developed.

2.5 Structural Residual Matrices

Taking the derivative of Equation (2.29) with respect to time gives

$$\dot{\mathbf{u}}(t) = \sum_{i=1}^{N_c} [\boldsymbol{\Phi}_i \dot{w}_i(t) + \boldsymbol{\Phi}_i^* \dot{w}_i^*(t)] + \sum_{i=1}^{N_p} \boldsymbol{\Phi}_i^P \dot{w}_i^P(t) \quad (2.31)$$

Substituting Equations (2.23) to (2.25) into Equation (2.31) leads to

$$\dot{\mathbf{u}}(t) = \sum_{i=1}^{N_C} \left[\frac{\boldsymbol{\varphi}_i \boldsymbol{\varphi}_i^T \mathbf{f}(t)}{a_i} + \lambda_i \boldsymbol{\varphi}_i w_i(t) + \frac{\boldsymbol{\varphi}_i^* \boldsymbol{\varphi}_i^H \mathbf{f}(t)}{a_i^*} + \lambda_i^* \boldsymbol{\varphi}_i^* w_i^*(t) \right] + \sum_{i=1}^{N_p} \left[\frac{\boldsymbol{\varphi}_i^P (\boldsymbol{\varphi}_i^P)^T \mathbf{f}(t)}{a_i^P} + \lambda_i^P \boldsymbol{\varphi}_i^P w_i^P(t) \right] \quad (2.32)$$

After comparing Equations (2.30) and (2.32),

$$\sum_{i=1}^{N_C} \left[\frac{\boldsymbol{\varphi}_i \boldsymbol{\varphi}_i^T}{a_i} + \frac{\boldsymbol{\varphi}_i^* \boldsymbol{\varphi}_i^H}{a_i^*} \right] \mathbf{f}(t) + \sum_{i=1}^{N_p} \left[\frac{\boldsymbol{\varphi}_i^P (\boldsymbol{\varphi}_i^P)^T}{a_i^P} \right] \mathbf{f}(t) = \mathbf{0}_{N \times N} \in \mathbb{C}^{N \times N} \quad (2.33)$$

As $\mathbf{f}(t)$ is arbitrary, it implies that

$$\sum_{i=1}^{N_C} \left[\frac{\boldsymbol{\varphi}_i \boldsymbol{\varphi}_i^T}{a_i} + \frac{\boldsymbol{\varphi}_i^* \boldsymbol{\varphi}_i^H}{a_i^*} \right] + \sum_{i=1}^{N_p} \left[\frac{\boldsymbol{\varphi}_i^P (\boldsymbol{\varphi}_i^P)^T}{a_i^P} \right] = \mathbf{0}_{N \times N} \in \mathbb{C}^{N \times N} \quad (2.34)$$

which can be assembled in a simple matrix form

$$\boldsymbol{\Phi} \hat{\mathbf{a}}^{-1} \boldsymbol{\Phi}^T = \mathbf{0}_{N \times N} \in \mathbb{C}^{N \times N} \quad (2.35)$$

Further, denoting

$$\mathbf{R}_i = \mathbf{R}_i^R + j \mathbf{R}_i^I = \frac{\boldsymbol{\varphi}_i \boldsymbol{\varphi}_i^T}{a_i} \in \mathbb{C}^{N \times N} \quad (i = 1, 2 \dots N_C) \quad (2.36)$$

$$\mathbf{R}_i^* = \mathbf{R}_i^R - j \mathbf{R}_i^I = \frac{\boldsymbol{\varphi}_i^* \boldsymbol{\varphi}_i^H}{a_i^*} \in \mathbb{C}^{N \times N} \quad (i = 1, 2 \dots N_C) \quad (2.37)$$

$$\mathbf{R}_i^P = \frac{\boldsymbol{\varphi}_i^P (\boldsymbol{\varphi}_i^P)^T}{a_i^P} \in \mathbb{R}^{N \times N} \quad (i = 1, 2 \dots N_p) \quad (2.38)$$

\mathbf{R}_i , \mathbf{R}_i^* and \mathbf{R}_i^P are the structural residual matrices corresponding to the eigenvalues λ_i , λ_i^* and λ_i^P , respectively. Note that all residual matrices only depend on the structural system parameters and are independent of the normalization manner of the modes. Consequently, Equation (2.34) can be represented as

$$2 \sum_{i=1}^{N_c} \mathbf{R}_i^R + \sum_{i=1}^{N_p} \mathbf{R}_i^P = \mathbf{0} \in \mathbb{R}^{N \times N} \quad (2.39)$$

The modal property shown in Equation (2.39) was first found in Ventura (1985); however, the proof was interpreted in a physical manner rather than given in a rigorous mathematical manipulation as shown in this study.

2.6 Expansion of Inverse of the Mass Matrix \mathbf{M}^{-1}

Substituting Equation (2.10) into Equation (2.16) yields

$$\Psi^T \mathbf{B} \Psi = \begin{pmatrix} \Phi \Lambda \\ \Phi \end{pmatrix}^T \begin{pmatrix} -\mathbf{M} & \mathbf{0} \\ \mathbf{0} & \mathbf{K} \end{pmatrix} \begin{pmatrix} \Phi \Lambda \\ \Phi \end{pmatrix} = -\Lambda \Phi^T \mathbf{M} \Phi \Lambda + \Phi^T \mathbf{K} \Phi = \hat{\mathbf{b}} = -\hat{\mathbf{a}} \Lambda \quad (2.40)$$

that is,

$$\Lambda \Phi^T \mathbf{M} \Phi \Lambda - \Phi^T \mathbf{K} \Phi = \hat{\mathbf{a}} \Lambda \quad (2.41)$$

Pre-multiplying $\Phi \hat{\mathbf{a}}^{-1}$ and post-multiplying $\hat{\mathbf{a}}^{-1} \Phi^T$ to both sides of Equation (2.41) leads to

$$\left(\Phi \hat{\mathbf{a}}^{-1} \Lambda \Phi^T \right) \mathbf{M} \left(\Phi \hat{\mathbf{a}}^{-1} \Lambda \Phi^T \right) - \left(\Phi \hat{\mathbf{a}}^{-1} \Phi^T \right) \mathbf{K} \left(\Phi \hat{\mathbf{a}}^{-1} \Phi^T \right) = \left(\Phi \Lambda \hat{\mathbf{a}}^{-1} \Phi^T \right) \quad (2.42)$$

Considering Equation (2.35) in Equation (2.42) becomes

$$\left(\Phi \hat{\mathbf{a}}^{-1} \Lambda \Phi^T \right) \mathbf{M} \left(\Phi \Lambda \hat{\mathbf{a}}^{-1} \Phi^T \right) = \left(\Phi \Lambda \hat{\mathbf{a}}^{-1} \Phi^T \right) \quad (2.43)$$

As a result,

$$\mathbf{M}^{-1} = \Phi \hat{\mathbf{a}}^{-1} \Lambda \Phi^T \quad (2.44)$$

Equation (2.44) can be further expanded as

$$\begin{aligned}
\mathbf{M}^{-1} &= \mathbf{\Phi} \hat{\mathbf{a}}^{-1} \mathbf{\Lambda} \mathbf{\Phi}^T = \sum_{i=1}^{N_c} \left(\frac{\lambda_i \boldsymbol{\varphi}_i \boldsymbol{\varphi}_i^T}{a_i} + \frac{\lambda_i^* \boldsymbol{\varphi}_i^* \boldsymbol{\varphi}_i^H}{a_i^*} \right) + \sum_{i=1}^{N_p} \frac{\lambda_i^p \boldsymbol{\varphi}_i^p (\boldsymbol{\varphi}_i^p)^T}{a_i^p} \\
&= 2 \sum_{i=1}^{N_c} \operatorname{Re} \left(\frac{\lambda_i \boldsymbol{\varphi}_i \boldsymbol{\varphi}_i^T}{a_i} \right) + \sum_{i=1}^{N_p} \frac{\lambda_i^p \boldsymbol{\varphi}_i^p (\boldsymbol{\varphi}_i^p)^T}{a_i^p} \\
&= -2 \sum_{i=1}^{N_c} \left(\xi_i \omega_i \mathbf{R}_i^R + \omega_{di} \mathbf{R}_i^I \right) - \sum_{i=1}^{N_p} \omega_i^p \mathbf{R}_i^P
\end{aligned} \tag{2.45}$$

This modal expansion will be used in the development of a unified form the expression of the nodal velocity shown in Chapter 3.

2.7 Expansion of the Inverse of Stiffness Matrix \mathbf{K}^{-1}

Pre-multiplying $\mathbf{\Phi} \hat{\mathbf{a}}^{-1} \mathbf{\Lambda}^{-1}$ to both sides of Equation (2.41) leads to

$$\left(\mathbf{\Phi} \hat{\mathbf{a}}^{-1} \mathbf{\Lambda}^{-1} \mathbf{\Lambda} \mathbf{\Phi}^T \right) \mathbf{M} \mathbf{\Phi} \mathbf{\Lambda} - \left(\mathbf{\Phi} \hat{\mathbf{a}}^{-1} \mathbf{\Lambda}^{-1} \mathbf{\Phi}^T \right) \mathbf{K} \mathbf{\Phi} = \mathbf{\Phi} \mathbf{\Lambda}^{-1} \hat{\mathbf{a}}^{-1} \hat{\mathbf{a}} \mathbf{\Lambda} \tag{2.46}$$

At the same time, using the structural residual matrices, $\mathbf{\Phi} \hat{\mathbf{a}}^{-1} \mathbf{\Phi}^T = \mathbf{0}$, in Equation (2.46), it becomes

$$-\mathbf{\Phi} \hat{\mathbf{a}}^{-1} \mathbf{\Lambda}^{-1} \mathbf{\Phi}^T \mathbf{K} \mathbf{\Phi} = \mathbf{\Phi} \tag{2.47}$$

Therefore,

$$\mathbf{K}^{-1} = -\mathbf{\Phi} \hat{\mathbf{a}}^{-1} \mathbf{\Lambda}^{-1} \mathbf{\Phi}^T \tag{2.48}$$

Equation (2.48) can be further expanded as

$$\begin{aligned}
\mathbf{K}^{-1} &= -\mathbf{\Phi} \hat{\mathbf{a}}^{-1} \mathbf{\Lambda}^{-1} \mathbf{\Phi}^T = -\sum_{i=1}^{N_c} \left(\frac{\boldsymbol{\varphi}_i \boldsymbol{\varphi}_i^T}{\lambda_i a_i} + \frac{\boldsymbol{\varphi}_i^* \boldsymbol{\varphi}_i^H}{\lambda_i^* a_i^*} \right) - \sum_{i=1}^{N_p} \frac{\boldsymbol{\varphi}_i^p (\boldsymbol{\varphi}_i^p)^T}{\lambda_i^p a_i^p} \\
&= -2 \sum_{i=1}^{N_c} \operatorname{Re} \left(\frac{\boldsymbol{\varphi}_i \boldsymbol{\varphi}_i^T}{\lambda_i a_i} \right) - \sum_{i=1}^{N_p} \frac{\boldsymbol{\varphi}_i^p (\boldsymbol{\varphi}_i^p)^T}{\lambda_i^p a_i^p} \\
&= -\frac{2}{\omega_i^2} \sum_{i=1}^{N_c} \left(-\xi_i \omega_i \mathbf{R}_i^R + \omega_{di} \mathbf{R}_i^I \right) + \sum_{i=1}^{N_p} \frac{\mathbf{R}_i^P}{\omega_i^p}
\end{aligned} \tag{2.49}$$

This modal expansion is used to develop an effective modal mass for arbitrarily damped structures, as described in Chapter 3.

CHAPTER 3

GENERAL MODAL RESPONSE HISTORY ANALYSIS

3.1 Introduction

In Chapter 2, the dynamic response of an arbitrarily damped linear MDOF structure was expressed by means of the superposition of its modal responses. However, it was given in a complex-valued form without physical meaning. An improved general solution, completely expressed in real-valued form, for calculating the seismic response history of an MDOF structure subjected to three orthogonal excitations simultaneously is deduced in this chapter using linear algebra theory. The physical explanations of each of the resulting terms are given. In this formulation, the Laplace transformation approach is employed, by which the original differential equations of the system in the time domain are converted to algebraic equations in the Laplacian domain, to show the intrinsic relationship among the system's parameters. An "over-damped mode" concept is introduced to account for the presence of over-critically damped modes. It is shown that all response quantities, including the relative velocities and absolute accelerations, can be expressed in a unified form, which is a linear combination of modal displacements and modal velocities as well as modal responses resulting from the over-damped modes. This unified form is made possible by several modal properties identified in this chapter. In addition, the expression of the modal static response of an arbitrarily damped structure subjected to inertia forces is given, from which the general effective modal mass is defined. This newly-defined effective modal mass can be a good index to determine the number of modes required in the modal analysis procedure to achieve more reasonable response estimates. Furthermore, a new real-valued modal transformation relationship to decouple the arbitrarily damped structures is identified.

3.2 Theoretical Formulation of General Modal Analysis

When the structure, shown in Figure 3.1, is subjected to a three-component ground motion $\ddot{\mathbf{u}}_g(t)$, Equation (2.1) can be written as

$$\mathbf{M}\ddot{\mathbf{u}}(t) + \mathbf{C}\dot{\mathbf{u}}(t) + \mathbf{K}\mathbf{u}(t) = -\mathbf{M}\mathbf{J}\mathbf{T}\ddot{\mathbf{u}}_g(t) \quad (3.1)$$

$\mathbf{J} = [\mathbf{J}^{(x)} \quad \mathbf{J}^{(y)} \quad \mathbf{J}^{(z)}]$ is the influence matrix with dimension $N \times 3$, which contains three resultant displacement vectors of the mass to a static application of a unit ground displacement along three structure reference axes \mathbf{X} , \mathbf{Y} and \mathbf{Z} , respectively. $\ddot{\mathbf{u}}_g(t) = [\ddot{u}_{g1}(t) \quad \ddot{u}_{g2}(t) \quad \ddot{u}_{g3}(t)]^T$ is the acceleration vector consisting of three orthogonal components along reference axes $\mathbf{1}$, $\mathbf{2}$ and $\mathbf{3}$, respectively. In most practical situations, the direction of the third component $\mathbf{3}$ is assumed to be identical to the vertical structure reference axes \mathbf{Z} . \mathbf{T} is a 3×3 transformation matrix to account for the effect as the horizontal directions of the ground motions, i.e., $\mathbf{1}$ and $\mathbf{2}$, do not coincide with the horizontal structure reference axes, \mathbf{X} and \mathbf{Y} , respectively. Assuming θ to be the angle of rotation between the two sets of horizontal axes as shown in Figure 3.1, the transformation matrix \mathbf{T} can be written as

$$\mathbf{T} = \begin{bmatrix} \cos \theta & -\sin \theta & 0 \\ \sin \theta & \cos \theta & 0 \\ 0 & 0 & 1 \end{bmatrix} \quad (3.2)$$

As a result, the complex modal equations shown in Equations (2.23) to (2.25) can be written as

$$\dot{w}_i(t) - \lambda_i w_i(t) = \frac{-\boldsymbol{\phi}_i^T \mathbf{M}\mathbf{J}\mathbf{T}\ddot{\mathbf{u}}_g(t)}{a_i} \in \mathbb{C} \quad (i=1, 2, \dots, N_C) \quad (3.3)$$

$$\dot{w}_i^*(t) - \lambda_i^* w_i^*(t) = \frac{-\boldsymbol{\phi}_i^H \mathbf{M}\mathbf{J}\mathbf{T}\ddot{\mathbf{u}}_g(t)}{a_i^*} \in \mathbb{C} \quad (i=1, 2, \dots, N_C) \quad (3.4)$$

and
$$\dot{w}_i^p(t) - \lambda_i^p w_i^p(t) = \frac{-(\boldsymbol{\phi}_i^p)^T \mathbf{M}\mathbf{J}\mathbf{T}\ddot{\mathbf{u}}_g(t)}{a_i^p} \in \mathbb{R} \quad (i=1, 2, \dots, N_p) \quad (3.5)$$

To simplify further development, the Laplace transformation is employed to transform the differential equations to linear algebraic equations in the Laplace domain, by which the system response in the Laplace domain can be easily expressed as a linear combination of complete orders of modal subsystems (composed of corresponding modal

parameters). The responses in the time domain for a complete system and its subsystems are easily retrieved through inverse Laplace transform.

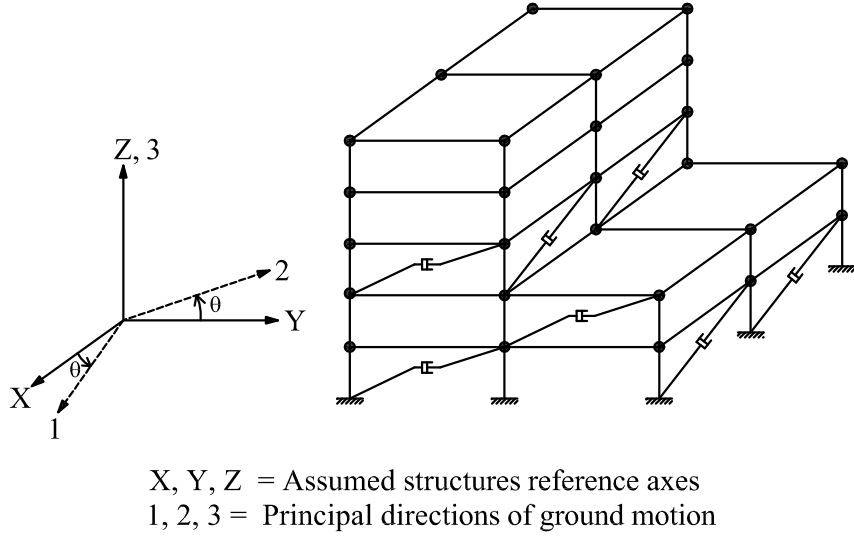


Figure 3.1 3-D MDOF structure subjected to 3-component ground motion

3.2.1 Structural Displacement

Applying the Laplace transform to Equations (2.29) and (3.3) to (3.5), respectively, yields

$$\mathbf{U}(s) = \sum_{i=1}^{N_C} [\boldsymbol{\varphi}_i \mathcal{W}_i(s) + \boldsymbol{\varphi}_i^* \mathcal{W}_i^*(s)] + \sum_{i=1}^{N_P} \boldsymbol{\varphi}_i^P \mathcal{W}_i^P(s) = \boldsymbol{\Phi} \mathbf{W}(s) \quad (3.6)$$

$$(s - \lambda_i) \mathcal{W}_i(s) = -\frac{\boldsymbol{\varphi}_i^T \mathbf{M} \mathbf{J} \mathbf{T} \ddot{\mathbf{U}}_g(s)}{a_i} \in \mathbb{C} \quad (i = 1, 2, \dots, N_C) \quad (3.7)$$

$$(s - \lambda_i^*) \mathcal{W}_i^*(s) = -\frac{\boldsymbol{\varphi}_i^H \mathbf{M} \mathbf{J} \mathbf{T} \ddot{\mathbf{U}}_g(s)}{a_i^*} \in \mathbb{C} \quad (i = 1, 2, \dots, N_C) \quad (3.8)$$

and

$$(s - \lambda_i^P) \mathcal{W}_i^P(s) = -\frac{\boldsymbol{\varphi}_i^P \mathbf{M} \mathbf{J} \mathbf{T} \ddot{\mathbf{U}}_g(s)}{a_i^P} \in \mathbb{C} \quad (i = 1, 2, \dots, N_P) \quad (3.9)$$

respectively, where s is the Laplace parameter and

$$\mathbf{W}(s) = \left[W_1(s), W_2(s) \cdots W_{N_c}(s), W_1^*(s), W_2^*(s) \cdots W_{N_c}^*(s), W_1^P(s), W_2^P(s) \cdots W_{N_p}^P(s) \right]^T \quad (3.10)$$

is the modal coordinates vector expressed in the Laplace domain and $\mathbf{W}(s) \in \mathbb{C}^{2N_c \times 2N}$. $\mathbf{U}(s)$ is the Laplace transformation of the displacement vector $\mathbf{u}(t)$ and $\ddot{\mathbf{U}}_g(s)$ is the Laplace transformation of the excitation vector $\ddot{\mathbf{u}}_g(t)$.

Solving $W_i(s)$, $W_i^*(s)$ and $W_i^P(s)$ from Equations (3.7) to (3.9), respectively, and substituting the resulting solutions into Equation (3.6) obtains

$$\begin{aligned} \mathbf{U}(s) &= - \left\{ \sum_{i=1}^{N_c} \left[\frac{\boldsymbol{\varphi}_i \boldsymbol{\varphi}_i^T}{a_i(s - \lambda_i)} + \frac{\boldsymbol{\varphi}_i^* \boldsymbol{\varphi}_i^H}{a_i^*(s - \lambda_i^*)} \right] + \sum_{i=1}^{N_p} \frac{\boldsymbol{\varphi}_i^P (\boldsymbol{\varphi}_i^P)^T}{a_i^P(s - \lambda_i^P)} \right\} \mathbf{MJT} \ddot{\mathbf{U}}_g(s) \\ &= - \left[\sum_{i=1}^{N_c} \left(\frac{\mathbf{R}_i}{s - \lambda_i} + \frac{\mathbf{R}_i^*}{s - \lambda_i^*} \right) + \sum_{i=1}^{N_p} \frac{\mathbf{R}_i^P}{s - \lambda_i^P} \right] \mathbf{MJT} \ddot{\mathbf{U}}_g(s) \\ &= \sum_{i=1}^{N_c} \mathbf{U}_i(s) + \sum_{i=1}^{N_p} \mathbf{U}_i^P(s) \end{aligned} \quad (3.11)$$

where \mathbf{R}_i , \mathbf{R}_i^* and \mathbf{R}_i^P are the structural residual matrices shown in Section 2.5. Thus,

$$\mathbf{U}_i(s) = - \left(\frac{\mathbf{R}_i}{s - \lambda_i} + \frac{\mathbf{R}_i^*}{s - \lambda_i^*} \right) \mathbf{MJT} \ddot{\mathbf{U}}_g(s) \in \mathbb{C}^N \quad (3.12)$$

Equation (3.12) is the i th complex modal structural response vector represented in Laplace form and

$$\mathbf{U}_i^P(s) = - \frac{\mathbf{R}_i^P}{s - \lambda_i^P} \mathbf{MJT} \ddot{\mathbf{U}}_g(s) \in \mathbb{C}^N \quad (3.13)$$

is the i th over-damped modal structural response vector represented in Laplace form.

Substituting the complex-valued eigenvalues shown in Equation (2.5) and the residual matrices shown in Equations (2.34) and (2.35) into Equation (3.12) gives

$$\begin{aligned}
\mathbf{U}_i(s) &= - \left[\frac{\mathbf{R}_i^R + j\mathbf{R}_i^I}{s - (-\xi_i\omega_i + j\omega_{di})} + \frac{\mathbf{R}_i^R - j\mathbf{R}_i^I}{s - (-\xi_i\omega_i - j\omega_{di})} \right] \mathbf{M}\mathbf{J}\mathbf{T}\ddot{\mathbf{U}}_g(s) \\
&= - \left(\frac{\mathbf{A}_{Di}S}{s^2 + 2\xi_i\omega_i s + \omega_i^2} + \frac{\mathbf{B}_{Di}}{s^2 + 2\xi_i\omega_i s + \omega_i^2} \right) \mathbf{T}\ddot{\mathbf{U}}_g(s) \quad (i=1,2,3\cdots N_C)
\end{aligned} \tag{3.14}$$

where

$$\mathbf{A}_{Di} = 2\mathbf{R}_i^R \mathbf{M}\mathbf{J} \in \mathbb{R}^{N \times 3} \tag{3.15}$$

$$\mathbf{B}_{Di} = 2\omega_i \left(\xi_i \mathbf{R}_i^R - \sqrt{1 - \xi_i^2} \mathbf{R}_i^I \right) \mathbf{M}\mathbf{J} \in \mathbb{R}^{N \times 3} \tag{3.16}$$

Substituting Equations (2.7) and (2.36) into Equation (3.13) yields

$$\mathbf{U}_i^P(s) = - \frac{\mathbf{A}_{Di}^P}{s + \omega_i^P} \mathbf{T}\ddot{\mathbf{U}}_g(s) \quad (i=1,2,3\cdots N_p) \tag{3.17}$$

in which

$$\mathbf{A}_{Di}^P = \mathbf{R}_i^P \mathbf{M}\mathbf{J} \in \mathbb{R}^{N \times 3} \tag{3.18}$$

Moreover, coefficient vectors \mathbf{A}_{Di} , \mathbf{B}_{Di} and \mathbf{A}_{Di}^P shown in Equations (3.15), (3.16) and (3.18), respectively, can also be expressed as

$$\mathbf{A}_{Di} = 2 \operatorname{Re} \left(\frac{\boldsymbol{\varphi}_i \hat{\boldsymbol{\Gamma}}_i}{\lambda_i} \right) = \left[\mathbf{A}_{Di}^{(x)} \quad \mathbf{A}_{Di}^{(y)} \quad \mathbf{A}_{Di}^{(z)} \right] \in \mathbb{R}^{N \times 3} \tag{3.19}$$

$$\mathbf{B}_{Di} = -2 \operatorname{Re} \left(\frac{\boldsymbol{\varphi}_i \hat{\boldsymbol{\Gamma}}_i}{\lambda_i} \lambda_i^* \right) = 2 \left[\omega_i \xi_i \operatorname{Re} \left(\frac{\boldsymbol{\varphi}_i \hat{\boldsymbol{\Gamma}}_i}{\lambda_i} \right) - \omega_{di} \operatorname{Im} \left(\frac{\boldsymbol{\varphi}_i \hat{\boldsymbol{\Gamma}}_i}{\lambda_i} \right) \right] = \left[\mathbf{B}_{Di}^{(x)} \quad \mathbf{B}_{Di}^{(y)} \quad \mathbf{B}_{Di}^{(z)} \right] \in \mathbb{R}^{N \times 3} \tag{3.20}$$

and

$$\mathbf{A}_{Di}^P = \frac{\boldsymbol{\varphi}_i^P \boldsymbol{\Gamma}_i^P}{\lambda_i^P} = \left[\mathbf{A}_{Di}^{P(x)} \quad \mathbf{A}_{Di}^{P(y)} \quad \mathbf{A}_{Di}^{P(z)} \right] \in \mathbb{R}^{N \times 3} \tag{3.21}$$

respectively, where

$$\hat{\boldsymbol{\Gamma}}_i = \frac{\lambda_i \boldsymbol{\varphi}_i^T \mathbf{M}\mathbf{J}}{a_i} = \left[\hat{\boldsymbol{\Gamma}}_i^{(x)} \quad \hat{\boldsymbol{\Gamma}}_i^{(y)} \quad \hat{\boldsymbol{\Gamma}}_i^{(z)} \right] \tag{3.22}$$

in which

$$\hat{\Gamma}_i^{(k)} = \frac{\lambda_i \boldsymbol{\phi}_i^T \mathbf{M} \mathbf{J}^{(k)}}{a_i}, \quad k \in \{\mathbf{x}, \mathbf{y}, \mathbf{z}\} \quad (3.23)$$

Equation (3.22) is the row vector of the complex modal participation factors associated with the three structure reference axes for mode i and

$$\boldsymbol{\Gamma}_i^{\text{P}} = \frac{\lambda_i^{\text{P}} (\boldsymbol{\phi}_i^{\text{P}})^T \mathbf{M} \mathbf{J}}{a_i^{\text{P}}} = \left[\Gamma_i^{\text{P}(\text{x})} \quad \Gamma_i^{\text{P}(\text{y})} \quad \Gamma_i^{\text{P}(\text{z})} \right] \quad (3.24)$$

in which

$$\Gamma_i^{\text{P}(k)} = \frac{\lambda_i^{\text{P}} (\boldsymbol{\phi}_i^{\text{P}})^T \mathbf{M} \mathbf{J}^{(k)}}{a_i^{\text{P}}}, \quad k \in \{\mathbf{x}, \mathbf{y}, \mathbf{z}\} \quad (3.25)$$

Equation (3.24) is the row vector of the over-damped modal participation factors associated with the three structure reference axes for mode i .

Furthermore, denoting

$$\mathbf{Q}_i(s) = H_i(s) \ddot{\mathbf{U}}_g(s) \in \mathbb{C}^3 \quad \text{and} \quad \mathbf{Q}_{V_i}(s) = H_{V_i}(s) \ddot{\mathbf{U}}_g(s) \in \mathbb{C}^3 \quad (3.26)$$

where

$$H_i(s) = -\frac{1}{s^2 + 2\xi_i \omega_i s + \omega_i^2} \in \mathbb{C} \quad (3.27)$$

and

$$H_{V_i}(s) = -\frac{s}{s^2 + 2\xi_i \omega_i s + \omega_i^2} \in \mathbb{C} \quad (3.28)$$

are the displacement and velocity transfer function of an under-damped SDOF system with the i th modal damping ratio ξ_i and the i th modal natural frequency ω_i , respectively.

In fact, Equation (3.26) can be considered as the resulting Laplace transformation of the following differential equation set expressed in the time domain with zero initial conditions

$$\ddot{\mathbf{q}}_i(t) + 2\xi_i \omega_i \dot{\mathbf{q}}_i(t) + \omega_i^2 \mathbf{q}_i(t) = -\ddot{\mathbf{u}}_g(t) \quad (3.29)$$

where

$$\mathbf{q}_i(t) = L^{-1}[\mathbf{Q}_i(s)] = \begin{Bmatrix} q_{1i}(t) \\ q_{2i}(t) \\ q_{3i}(t) \end{Bmatrix} \in \mathbb{R}^3 \quad (3.30)$$

$$\dot{\mathbf{q}}_i(t) = L^{-1}[\mathbf{Q}_{v_i}(s)] = \begin{Bmatrix} \dot{q}_{1i}(t) \\ \dot{q}_{2i}(t) \\ \dot{q}_{3i}(t) \end{Bmatrix} \in \mathbb{R}^3$$

In Equation (3.30), L^{-1} stands for inverse Laplace transformation operator. Equation (3.29) can be further expanded as

$$\begin{cases} \ddot{q}_{1i}(t) + 2\xi_i\omega_i\dot{q}_{1i}(t) + \omega_i^2q_{1i}(t) = -\ddot{u}_{g1}(t) \\ \ddot{q}_{2i}(t) + 2\xi_i\omega_i\dot{q}_{2i}(t) + \omega_i^2q_{2i}(t) = -\ddot{u}_{g2}(t) \\ \ddot{q}_{3i}(t) + 2\xi_i\omega_i\dot{q}_{3i}(t) + \omega_i^2q_{3i}(t) = -\ddot{u}_{g3}(t) \end{cases} \quad (3.31)$$

As a matter of fact, either Equation (3.29) or (3.31) describes the equation of motion of an under-damped SDOF system with i th modal natural frequency ω_i and damping ratio ξ_i subjected to accelerations $\ddot{u}_{g1}(t)$, $\ddot{u}_{g2}(t)$ and $\ddot{u}_{g3}(t)$, respectively. This concept is illustrated schematically in Figure 3.2.

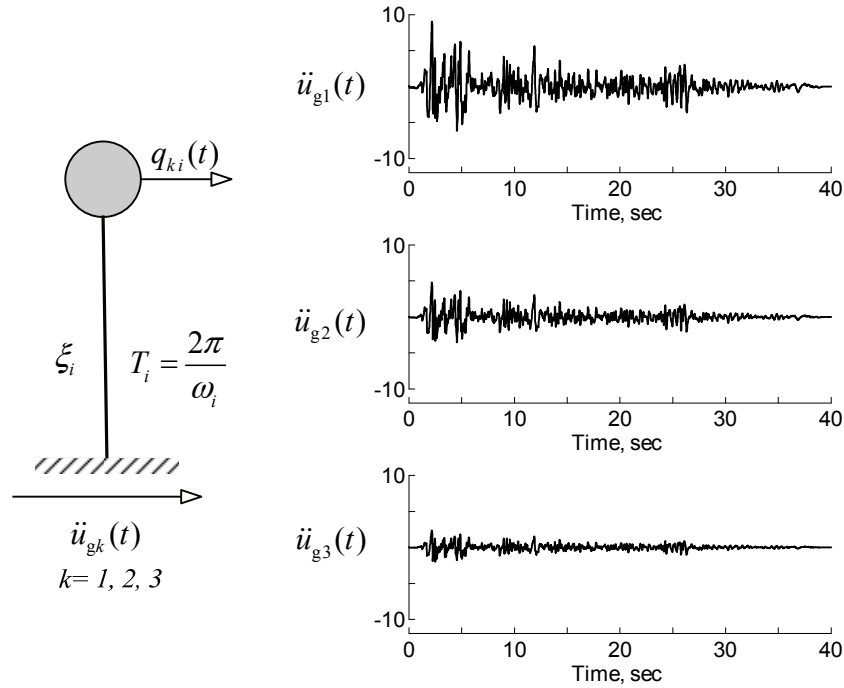


Figure 3.2 Under-damped SDOF system subjected to 3-component ground excitation

Now, the structural responses have been well presented in the Laplace domain through Equation (3.11). To obtain the response in the time domain, the inverse Laplace transformation is employed as follows. Taking the inverse Laplace transform of Equation (3.27) leads to

$$h_i(t) = L^{-1} [H_i(s)] = -\frac{1}{\omega_{di}} e^{-\xi_i \omega_i t} \sin(\omega_{di} t) \in \mathbb{R} \quad (3.32)$$

where $h_i(t)$ is the unit impulse response function of the SDOF system with a natural frequency ω_i and damping ratio ξ_i . Thus, the i th modal displacement response vector $\mathbf{q}_i(t)$ can be written as

$$\begin{aligned} \mathbf{q}_i(t) &= L^{-1} [\mathbf{Q}_i(s)] = L^{-1} [H_i(s) \ddot{\mathbf{U}}_g(s)] = \int_0^t h_i(t-\tau) \ddot{\mathbf{u}}_g(\tau) d\tau \\ &= \frac{-1}{\omega_{di}} \int_0^t e^{-\xi_i \omega_i (t-\tau)} \sin \omega_{di} (t-\tau) \ddot{\mathbf{u}}_g(\tau) d\tau \end{aligned} \quad (3.33)$$

Equation (3.33) is the well-known Duhamel's Integral (Chopra, 2001).

For the case of over-damped modes, denoting

$$\mathbf{Q}_i^p(s) = H_i^p(s) \ddot{\mathbf{U}}_g(s) \in \mathbb{C} \quad (3.34)$$

in which

$$H_i^p(s) = -\frac{1}{s + \omega_i^p} \in \mathbb{C} \quad (3.35)$$

Similar to the transforming procedure of the complex mode case, Equation (3.34) is the Laplace transformation of the following first-order differential equation with a zero initial condition.

$$\dot{\mathbf{q}}_i^p(t) + \omega_i^p \mathbf{q}_i^p(t) = -\ddot{\mathbf{u}}_g(t) \quad (3.36)$$

where

$$\mathbf{q}_i^p(t) = L^{-1} [\mathbf{Q}_i^p(s)] = \begin{Bmatrix} q_{1i}^p(t) \\ q_{2i}^p(t) \\ q_{3i}^p(t) \end{Bmatrix} \in \mathbb{R}^3 \quad (3.37)$$

is the i th over-damped modal response vector. Equation (3.36) can also be expressed as

$$\begin{cases} \dot{q}_{1i}^p(t) + \omega_i^p q_{1i}^p(t) = -\ddot{u}_{g1}(t) \\ \dot{q}_{2i}^p(t) + \omega_i^p q_{2i}^p(t) = -\ddot{u}_{g2}(t) \\ \dot{q}_{3i}^p(t) + \omega_i^p q_{3i}^p(t) = -\ddot{u}_{g3}(t) \end{cases} \quad (3.38)$$

Note that $\mathbf{q}_i^p(t)$ has the dimension of velocity, which is the dimension of $\dot{\mathbf{q}}_i(t)$. The inverse Laplace transformation of $H_i^p(s)$ is given by

$$h_i^p(t) = -e^{-\omega_i^p t} \in \mathbb{R} \quad (3.39)$$

As a result, the over-damped modal response vector can be expressed as

$$\begin{aligned} \mathbf{q}_i^p(t) &= \mathcal{L}^{-1}[\mathbf{Q}_i^p(s)] = \mathcal{L}^{-1}[H_i^p(s)\ddot{\mathbf{U}}_g(s)] = \int_0^t h_i^p(t-\tau)\ddot{\mathbf{u}}_g(\tau) d\tau \\ &= -\int_0^t e^{-\omega_i^p(t-\tau)}\ddot{\mathbf{u}}_g(\tau) d\tau \end{aligned} \quad (3.40)$$

Also, Equations (3.14) and (3.17) can be represented as

$$\mathbf{U}_i(s) = -(\mathbf{A}_{Di}H_{Vi}(s) + \mathbf{B}_{Di}H_i(s))\mathbf{T}\ddot{\mathbf{U}}_g(s) \quad (i = 1, 2, 3 \dots N_c) \quad (3.41)$$

$$\mathbf{U}_i^p(s) = -\mathbf{A}_{Di}^p H_i^p(s)\mathbf{T}\ddot{\mathbf{U}}_g(s) \quad (i = 1, 2, 3 \dots N_p) \quad (3.42)$$

Applying the inverse Laplace transform to Equations (3.41) and (3.42) in conjunction with Equations (3.33), (3.34) and (3.37) gives

$$\mathbf{u}(t, \theta) = \sum_{i=1}^{N_c} [\mathbf{A}_{Di}\mathbf{T}\dot{\mathbf{q}}_i(t) + \mathbf{B}_{Di}\mathbf{T}\mathbf{q}_i(t)] + \sum_{i=1}^{N_p} \mathbf{A}_{Di}^p \mathbf{T}\mathbf{q}_i^p(t) \quad (3.43)$$

The variable θ is included in the expression to reveal that the response vector is also dependent on the seismic incident angle θ considered through the transformation matrix \mathbf{T} . Unlike Equation (2.27), it is observed that the displacement responses are expressed in terms of real-valued quantities. They are a linear combination of the modal displacements and velocities of a set from an SDOF system as well as the over-damped modal responses. In Equation (3.43), the terms associated with the modal displacement

vector $\mathbf{q}_i(t)$ are used to represent the motion of the structure, assuming all DOFs move either in phase or out of phase during the vibration process. This assumption only holds true for classically damped structures. When the structure is not classically damped, all DOFs no longer vibrate in phase or out of phase. Therefore, the terms associated with the modal velocity vector $\dot{\mathbf{q}}_i(t)$ are used to modify the response so that the non-classical damping effect, leading to phase differences between the motions of all DOFs, can be considered. The terms related to the over-damped modal response vector $\mathbf{q}_i^p(t)$ are used to compute the modal responses contributed from the over-damped modes when they are present.

3.2.2 Structural Velocity

Intuitively, the structural velocity response vector can be obtained directly by taking the derivative of Equation (3.43) with respect to time variable t as

$$\dot{\mathbf{u}}(t, \theta) = \sum_{i=1}^{N_c} \left[\mathbf{A}_{D_i} \mathbf{T} \ddot{\mathbf{q}}_i(t) + \mathbf{B}_{D_i} \mathbf{T} \dot{\mathbf{q}}_i(t) \right] + \sum_{i=1}^{N_p} \mathbf{A}_{D_i}^p \mathbf{T} \dot{\mathbf{q}}_i^p(t) \quad (3.44)$$

This approach seems to be simple and has been used by other researchers such as Takewaki (2004). However, this formulation requires the incorporation of two additional modal responses $\ddot{\mathbf{q}}_i(t)$ and $\dot{\mathbf{q}}_i^p(t)$ in the expression. A different approach to derive the expression of the relative velocity vector is given as follows.

First, Equations (3.29) and (3.36), respectively, are rearranged as

$$\ddot{\mathbf{q}}_i(t) = -2\xi_i \omega_i \dot{\mathbf{q}}_i(t) - \omega_i^2 \mathbf{q}_i(t) - \ddot{\mathbf{u}}_g(t) \in \mathbb{R}^{N \times 3} \quad (3.45)$$

$$\dot{\mathbf{q}}_i^p(t) = -\omega_i^p \mathbf{q}_i^p(t) - \ddot{\mathbf{u}}_g(t) \in \mathbb{R}^{N \times 3} \quad (3.46)$$

Upon substitution of Equations (3.45) and (3.46) into Equation (3.44),

$$\begin{aligned} \dot{\mathbf{u}}(t, \theta) = & \sum_{i=1}^{N_C} \left[(\mathbf{B}_{D_i} - 2\xi_i \omega_i \mathbf{A}_{D_i}) \mathbf{T} \dot{\mathbf{q}}_i(t) - \omega_i^2 \mathbf{A}_{D_i} \mathbf{T} \mathbf{q}_i(t) \right] + \sum_{i=1}^{N_P} (-\omega_i^P \mathbf{A}_{D_i}^P) \mathbf{T} \mathbf{q}_i^P(t) \\ & - \left[\sum_{i=1}^{N_C} \mathbf{A}_{D_i} + \sum_{i=1}^{N_P} \mathbf{A}_{D_i}^P \right] \mathbf{T} \ddot{\mathbf{u}}_g \end{aligned} \quad (3.47)$$

in which the last term can be expressed as follows after considering Equations (3.15) and (3.18)

$$\left[\sum_{i=1}^{N_C} \mathbf{A}_{D_i} + \sum_{i=1}^{N_P} \mathbf{A}_{D_i}^P \right] \mathbf{T} \ddot{\mathbf{u}}_g = \left[\sum_{i=1}^{N_C} 2\mathbf{R}_i^R + \sum_{i=1}^{N_P} \mathbf{R}_i^P \right] \mathbf{M} \mathbf{J} \mathbf{T} \ddot{\mathbf{u}}_g \quad (3.48)$$

Furthermore, considering the structural residual matrices shown in Equation (2.39), it is found that

$$\sum_{i=1}^{N_C} \mathbf{A}_{D_i} + \sum_{i=1}^{N_P} \mathbf{A}_{D_i}^P = \mathbf{0} \in \mathbb{R}^{N \times 3} \quad (3.49)$$

Therefore, the velocity vector $\dot{\mathbf{u}}(t, \theta)$ can be expressed as

$$\dot{\mathbf{u}}(t, \theta) = \sum_{i=1}^{N_C} [\mathbf{A}_{V_i} \mathbf{T} \dot{\mathbf{q}}_i(t) + \mathbf{B}_{V_i} \mathbf{T} \mathbf{q}_i(t)] + \sum_{i=1}^{N_P} \mathbf{A}_{V_i}^P \mathbf{T} \mathbf{q}_i^P(t) \quad (3.50)$$

where

$$\begin{aligned} \mathbf{A}_{V_i} &= \mathbf{B}_{D_i} - 2\xi_i \omega_i \mathbf{A}_{D_i} = -2\omega_i \left(\xi_i \mathbf{R}_i^R + \sqrt{1 - \xi_i^2} \mathbf{R}_i^I \right) \mathbf{M} \mathbf{J} \in \mathbb{R}^{N \times 3} \\ \mathbf{B}_{V_i} &= -\omega_i^2 \mathbf{A}_{D_i} = -2\omega_i^2 \mathbf{R}_i^R \mathbf{M} \mathbf{J} \in \mathbb{R}^{N \times 3} \\ \mathbf{A}_{V_i}^P &= -\omega_i^P \mathbf{A}_{D_i}^P = -\omega_i^P \mathbf{R}_i^P \mathbf{M} \mathbf{J} \in \mathbb{R}^{N \times 3} \end{aligned} \quad (3.51)$$

Note that Equations (3.44) and (3.50) are equivalent. However, Equation (3.50) is preferred in this study since the two additional modal responses $\ddot{\mathbf{q}}_i(t)$ and $\dot{\mathbf{q}}_i^P(t)$ do not appear in the expression and is consistent with the displacement vector $\mathbf{u}(t, \theta)$ shown by Equation (3.43).

On the other hand, if the coefficient vectors \mathbf{A}_{Di} , \mathbf{B}_{Di} and \mathbf{A}_{Di}^P shown in Equations (3.19), (3.20) and (3.21) are adopted in Equation (3.51) with a few rearrangements, the result is

$$\begin{aligned}\mathbf{A}_{Vi} &= 2 \operatorname{Re}(\underline{\lambda}_i \frac{\boldsymbol{\Phi}_i \hat{\boldsymbol{\Gamma}}_i}{\lambda_i}) \in \mathbb{R}^{N \times 3} \\ \mathbf{B}_{Vi} &= -2 \operatorname{Re}\left(\underline{\lambda}_i \frac{\boldsymbol{\Phi}_i \hat{\boldsymbol{\Gamma}}_i}{\lambda_i} \lambda_i^*\right) \in \mathbb{R}^{N \times 3} \\ \mathbf{A}_{Vi}^P &= \underline{\lambda}_i^P \frac{\boldsymbol{\Phi}_i^P \boldsymbol{\Gamma}_i^P}{\lambda_i^P} \in \mathbb{R}^{N \times 3}\end{aligned}\tag{3.52}$$

It is found that the coefficient vectors \mathbf{A}_{Vi} , \mathbf{B}_{Vi} and \mathbf{A}_{Vi}^P appearing in the velocity vector $\dot{\mathbf{u}}(t, \theta)$ differ from those in the displacement vector $\mathbf{u}(t, \theta)$ by having an additional multiplier, λ_i or λ_i^P in the corresponding coefficient vectors as indicated by the underscore, which is the associated eigenvalue, in each modal term. This finding can also be observed by comparing the displacement vector and velocity vector shown in Equations (2.27) and (2.28), respectively.

3.2.3 Structural Absolute Acceleration

To derive the absolute acceleration vector, the relative acceleration is used as a starting point, which can be obtained by taking derivative of the velocity vector $\dot{\mathbf{u}}(t, \theta)$ with respect to time. As a result,

$$\ddot{\mathbf{u}}(t, \theta) = \sum_{i=1}^{N_C} [\mathbf{A}_{Vi} \mathbf{T} \ddot{\mathbf{q}}_i(t) + \mathbf{B}_{Vi} \mathbf{T} \dot{\mathbf{q}}_i(t)] + \sum_{i=1}^{N_P} \mathbf{A}_{Vi}^P \mathbf{T} \dot{\mathbf{q}}_i^P(t) \in \mathbb{R}^N\tag{3.53}$$

Substituting Equations (3.45) and (3.46) into Equation (3.53) leads to

$$\ddot{\mathbf{u}}(t, \theta) = \sum_{i=1}^{N_C} [\mathbf{A}_{Ai} \mathbf{T} \dot{\mathbf{q}}_i(t) + \mathbf{B}_{Ai} \mathbf{T} \mathbf{q}_i(t)] + \sum_{i=1}^{N_P} \mathbf{A}_{Ai}^P \mathbf{T} \dot{\mathbf{q}}_i^P(t) - \left[\sum_{i=1}^{N_C} \mathbf{A}_{Vi} + \sum_{i=1}^{N_P} \mathbf{A}_{Vi}^P \right] \mathbf{T} \ddot{\mathbf{u}}_g(t)\tag{3.54}$$

where

$$\begin{aligned}
\mathbf{A}_{Ai} &= \mathbf{B}_{Vi} - 2\xi_i \omega_i \mathbf{A}_{Vi} = 2\omega_i^2 \left[(2\xi_i^2 - 1) \mathbf{R}_i^R + 2\xi_i \sqrt{1 - \xi_i^2} \mathbf{R}_i^I \right] \mathbf{M} \mathbf{J} \in \mathbb{R}^{N \times 3} \\
\mathbf{B}_{Ai} &= -\omega_i^2 \mathbf{A}_{Vi} = 2\omega_i^3 \left(\xi_i \mathbf{R}_i^R + \sqrt{1 - \xi_i^2} \mathbf{R}_i^I \right) \mathbf{M} \mathbf{J} \in \mathbb{R}^{N \times 3} \\
\mathbf{A}_{Ai}^P &= -\omega_i^P \mathbf{A}_{Vi}^P = (\omega_i^P)^2 \mathbf{R}_i^P \mathbf{M} \mathbf{J} \in \mathbb{R}^{N \times 3}
\end{aligned} \tag{3.55}$$

Using the modal expansion of the inverse of the mass \mathbf{M}^{-1} shown by Equation (2.45) in Section 2.6, the last term in Equation (3.54) becomes

$$\begin{aligned}
\left[\sum_{i=1}^{N_c} \mathbf{A}_{Vi} + \sum_{i=1}^{N_p} \mathbf{A}_{Vi}^P \right] \mathbf{T} \ddot{\mathbf{u}}_g(t) &= \left[-2 \sum_{i=1}^{N_c} \left(\xi_i \omega_i \mathbf{R}_i^R + \omega_{di} \mathbf{R}_i^I \right) - \sum_{i=1}^{N_p} \omega_i^P \mathbf{R}_i^P \right] \mathbf{M} \mathbf{J} \mathbf{T} \ddot{\mathbf{u}}_g(t) \\
&= \mathbf{M}^{-1} \mathbf{M} \mathbf{J} \mathbf{T} \ddot{\mathbf{u}}_g(t) \\
&= \mathbf{J} \mathbf{T} \ddot{\mathbf{u}}_g(t)
\end{aligned} \tag{3.56}$$

From Equation (3.56), it can be seen that

$$\sum_{i=1}^{N_c} \mathbf{A}_{Vi} + \sum_{i=1}^{N_p} \mathbf{A}_{Vi}^P = \mathbf{J} \in \mathbb{R}^{N \times 3} \tag{3.57}$$

Substituting Equation (3.56) into Equation (3.54) and denoting the structural absolute acceleration vector as $\ddot{\mathbf{u}}_A(t, \theta) \in \mathbb{R}^N$, which can be expressed as $\ddot{\mathbf{u}}_A(t, \theta) = \ddot{\mathbf{u}}(t, \theta) + \mathbf{J} \mathbf{T} \ddot{\mathbf{u}}_g(t)$, Equation (3.54) becomes

$$\ddot{\mathbf{u}}_A(t, \theta) = \sum_{i=1}^{N_c} \left[\mathbf{A}_{Ai} \mathbf{T} \dot{\mathbf{q}}_i(t) + \mathbf{B}_{Ai} \mathbf{T} \mathbf{q}_i(t) \right] + \sum_{i=1}^{N_p} \mathbf{A}_{Ai}^P \mathbf{T} \mathbf{q}_i^P(t) \tag{3.58}$$

Note that the modal relative acceleration vector $\ddot{\mathbf{q}}_i(t)$ and the ground acceleration vector $\ddot{\mathbf{u}}_g(t)$ are not explicitly involved in the expression of the absolute acceleration vector $\ddot{\mathbf{u}}_A(t, \theta)$.

If Equation (3.52) is adopted in Equation (3.55),

$$\begin{aligned}
\mathbf{A}_{Ai} &= 2 \operatorname{Re}(\underline{\lambda}_i^2 \frac{\boldsymbol{\Phi}_i \hat{\boldsymbol{\Gamma}}_i}{\lambda_i}) \in \mathbb{R}^{N \times 3} \\
\mathbf{B}_{Ai} &= -2 \operatorname{Re}\left(\underline{\lambda}_i^2 \frac{\boldsymbol{\Phi}_i \hat{\boldsymbol{\Gamma}}_i}{\lambda_i} \lambda_i^*\right) \in \mathbb{R}^{N \times 3} \\
\mathbf{A}_{Ai}^p &= (\underline{\lambda}_i^p)^2 \frac{\boldsymbol{\Phi}_i^p \boldsymbol{\Gamma}_i^p}{\lambda_i^p} \in \mathbb{R}^{N \times 3}
\end{aligned} \tag{3.59}$$

Similar to the expression of the relative velocity vector $\dot{\mathbf{u}}(t, \theta)$ shown in Equation (3.50), it is found that the absolute acceleration vector $\ddot{\mathbf{u}}_A(t, \theta)$ differs from the displacement vector $\mathbf{u}(t, \theta)$ by having an additional multiplier as indicated by the underscore in the corresponding coefficient vectors, which is the square of the associated eigenvalue λ_i^2 or $(\lambda_i^p)^2$, in each modal term. Note that the relative displacement, relative velocity and absolute acceleration are related by the associated eigenvalue in each modal term.

3.2.4 Unified Form for Response Expression

Comparing the expressions of relative displacement, relative velocity and absolute acceleration vectors shown in Equations (3.43), (3.50) and (3.58), respectively, it is found that the three response quantities are the linear combination of the modal response $\mathbf{q}_i(t)$, $\dot{\mathbf{q}}_i(t)$ and $\mathbf{q}_i^p(t)$. They only differ in their respective coefficient vectors. Thus, it is convenient to represent the three response vectors in a similar manner as follows.

$$\mathbf{u}_0(t, \theta) = \sum_{i=1}^{N_C} \left[\mathbf{A}_{0i} \mathbf{T} \dot{\mathbf{q}}_i(t) + \mathbf{B}_{0i} \mathbf{T} \mathbf{q}_i(t) \right] + \sum_{i=1}^{N_P} \mathbf{A}_{0i}^p \mathbf{T} \mathbf{q}_i^p(t) \tag{3.60}$$

In Equation (3.60), $\mathbf{u}_0(t, \theta)$ can be $\mathbf{u}(t, \theta)$, $\dot{\mathbf{u}}(t, \theta)$ or $\ddot{\mathbf{u}}_A(t, \theta)$, and \mathbf{A}_{0i} , \mathbf{B}_{0i} and \mathbf{A}_{0i}^p are the coefficient vectors associated with the response quantities of interest.

In general, most response quantities, denoted as $r_0(t, \theta)$, are either deformation-related, such as bending moments, interstory drifts, shear forces, etc.; velocity-related, such as the interstory velocity; or absolute acceleration-related, such as the floor acceleration. As a result, most response quantities within the structure can be expressed by a linear combination of the response vector $\mathbf{u}_0(t, \theta)$ through appropriate transformation. That is,

$$\begin{aligned}
r_0(t, \theta) &= \mathbf{d}^T \mathbf{u}_0(t, \theta) \\
&= \sum_{i=1}^{N_c} \left[\mathbf{d}^T \mathbf{A}_{0i} \mathbf{T} \dot{\mathbf{q}}_i(t) + \mathbf{d}^T \mathbf{B}_{0i} \mathbf{T} \mathbf{q}_i(t) \right] + \sum_{i=1}^{N_p} \mathbf{d}^T \mathbf{A}_{0i}^P \mathbf{T} \mathbf{q}_i^P(t) \\
&= \sum_{i=1}^{N_c} \left[\mathbf{A}'_{0i} \mathbf{T} \dot{\mathbf{q}}_i(t) + \mathbf{B}'_{0i} \mathbf{T} \mathbf{q}_i(t) \right] + \sum_{i=1}^{N_p} \mathbf{A}'_{0i}{}^P \mathbf{T} \mathbf{q}_i^P(t)
\end{aligned} \tag{3.61}$$

where \mathbf{d} is a transformation vector, $\mathbf{A}'_{0i} = \mathbf{d}^T \mathbf{A}_{0i} = [\mathbf{A}_{0i}^{(1)} \quad \mathbf{A}_{0i}^{(2)} \quad \mathbf{A}_{0i}^{(3)}]_{1 \times 3}$, $\mathbf{B}'_{0i} = \mathbf{d}^T \mathbf{B}_{0i} = [\mathbf{B}_{0i}^{(1)} \quad \mathbf{B}_{0i}^{(2)} \quad \mathbf{B}_{0i}^{(3)}]_{1 \times 3}$ and $\mathbf{A}'_{0i}{}^P = \mathbf{d}^T \mathbf{A}_{0i}^P = [\mathbf{A}_{0i}^{P(1)} \quad \mathbf{A}_{0i}^{P(2)} \quad \mathbf{A}_{0i}^{P(3)}]_{1 \times 3}$. This form indicates that any structural response quantities are able to be represented in a consistent form. It is also useful to employ this unified form in the development of a general modal combination rule for the response spectrum method, as presented in Chapter 4.

3.3 Interpretation of the General Modal Analysis

Basically, the dynamic response of a structure is a process that describes how the structure would respond to the excitation forces in the 3-D space domain as time advances. One important feature of the modal analysis is the use of modal coordinate transformation as shown in Equation (2.21), which separates the space domain and the time domain in the solution of the modal response. Modal analysis avoids the manipulation of the coupled equations simultaneously, improves the solution efficiency both analytically and numerically, and provides a clear physical interpretation. The response contributed from each mode can be computed individually; then they are combined together at each time instant to complete the total response history. In the case of multi-component excitations, the response due to each component can be considered independently.

Figure 3.3 explains the basic concept of the modal analysis. To be more specific, the physical interpretation of the formulation of the modal analysis procedure of Equation

Figure 3.4. An N -DOF arbitrarily damped structure is first decoupled into N_c sets of an SDOF system and N_p sets of a first-order linear system. Each set of SDOF system and each first-order linear system is subjected to the three ground accelerations individually as characterized by Equations (3.31) and (3.38). The responses resulting from each

acceleration excitation are superimposed to obtain the contribution of i th mode to the dynamic responses. Combining all the modal responses with consideration of the seismic incidence (i.e., the transformation matrix \mathbf{T} shown in Equation (3.2)) gives the seismic response history of the arbitrarily damped structure.

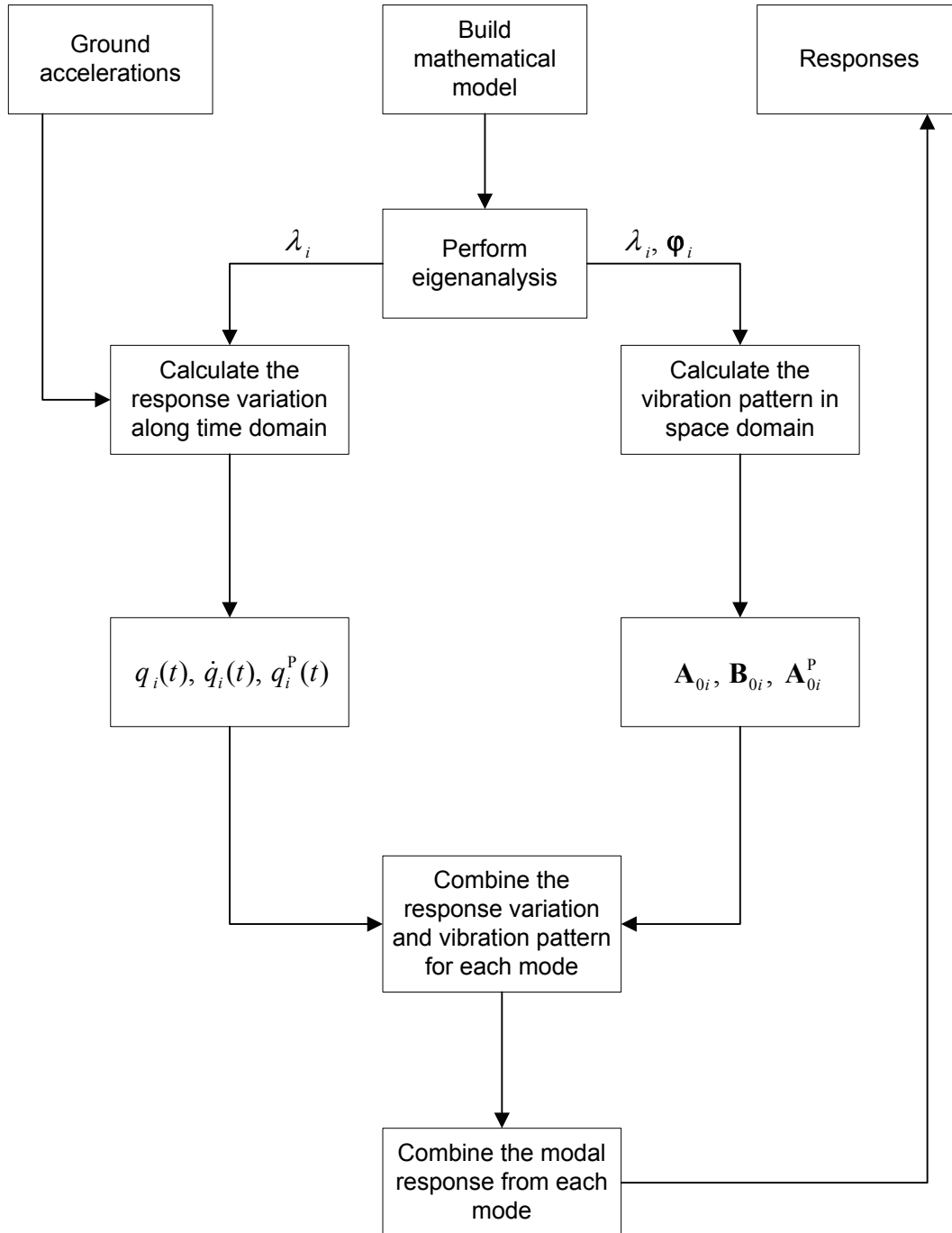
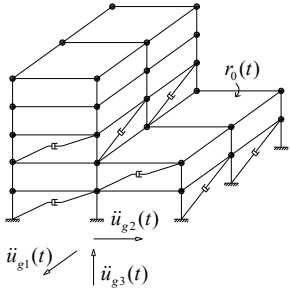


Figure 3.3 Basic concept of the general modal response history analysis



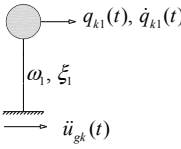
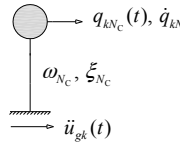
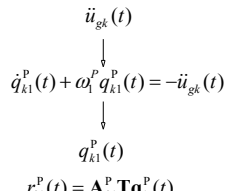
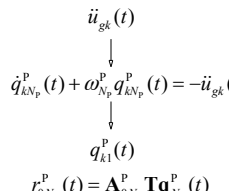
Mode	1	•	•	•	N_c		$k=1, 2, 3$
Complex Mode	 $r_{01}^C(t) = \mathbf{A}_{01} \mathbf{T} \mathbf{q}_1(t) + \mathbf{B}_{01} \mathbf{T} \dot{\mathbf{q}}_1(t)$	•	•	•	 $r_{0Nc}^C(t) = \mathbf{A}_{0Nc} \mathbf{T} \mathbf{q}_{Nc}(t) + \mathbf{B}_{0Nc} \mathbf{T} \dot{\mathbf{q}}_{Nc}(t)$		$r_0^C(t) = \sum_{i=1}^{N_c} r_{0i}^C(t)$
Mode	1	•	•	•	N_p		
Over-damped Mode	 $r_{01}^P(t) = \mathbf{A}_{01}^P \mathbf{T} \mathbf{q}_1^P(t)$	•	•	•	 $r_{0Np}^P(t) = \mathbf{A}_{0Np}^P \mathbf{T} \mathbf{q}_{Np}^P(t)$		$r_0^P(t) = \sum_{i=1}^{N_p} r_{0i}^P(t)$
Complete Response	$r_0(t) = r_0^C(t) + r_0^P(t) = \sum_{i=1}^{N_c} [\mathbf{A}_{0i} \mathbf{T} \mathbf{q}_i(t) + \mathbf{B}_{0i} \mathbf{T} \dot{\mathbf{q}}_i(t)] + \sum_{i=1}^{N_p} \mathbf{A}_{0i}^P \mathbf{T} \mathbf{q}_i^P(t)$						

Figure 3.4 Schematic explanation of the modal response history analysis of a 3-D MDOF subjected to 3-component ground excitation

3.4 General Modal Coordinate Transformation Matrix

Unlike classical modal analysis, the equation of motion of an arbitrarily damped structure cannot be decoupled in terms of the N modal coordinates $\mathbf{q}(t)$ established by the undamped structure using the transformation $\mathbf{u}(t) = \mathbf{\Phi} \mathbf{q}(t)$. However, it is still possible to find another set of modal coordinates in the physical space to decouple the doubled dimension equation of motion in state space. This process is shown below.

From the above formulation, the response state vector $\mathbf{v}(t)$ introduced in Chapter 2 can be expressed as

$$\mathbf{v}(t) = \begin{Bmatrix} \dot{\mathbf{u}}(t) \\ \mathbf{u}(t) \end{Bmatrix} = \mathbf{A}_T \mathbf{T}_G \mathbf{Q}(t) \in \mathbb{R}^{2N} \quad (3.62)$$

where

$$\mathbf{T}_G = \begin{bmatrix} \mathbf{T} & & & \mathbf{0} \\ & \mathbf{T} & & \\ & & \ddots & \\ \mathbf{0} & & & \mathbf{T} \end{bmatrix}_{6N \times 6N} \quad (3.63)$$

is a general transformation matrix composed of $2N$ transformation matrix \mathbf{T} and

$$\mathbf{Q}(t) = \begin{Bmatrix} \dot{\mathbf{q}}(t) \\ \mathbf{q}(t) \\ \mathbf{q}^P(t) \end{Bmatrix} \in \mathbb{R}^{6N} \quad (3.64)$$

is defined as the general modal coordinate vector in which

$$\mathbf{q}(t) = [q_{11}(t), q_{21}(t), q_{31}(t) \cdots q_{1N_c}(t), q_{2N_c}(t), q_{3N_c}(t)]^T \in \mathbb{R}^{3N_c} \quad \text{and}$$

$$\mathbf{q}^P(t) = [q_{11}^P(t), q_{21}^P(t), q_{31}^P(t) \cdots q_{1N_p}^P(t), q_{2N_p}^P(t), q_{3N_p}^P(t)]^T \in \mathbb{R}^{3N_p}, \text{ and}$$

$$\mathbf{A}_T = \begin{pmatrix} \mathbf{A}_V & \mathbf{B}_V & \mathbf{A}_V^P \\ \mathbf{A}_D & \mathbf{B}_D & \mathbf{A}_D^P \end{pmatrix} \in \mathbb{R}^{2N \times 6N} \quad (3.65)$$

Equation (3.64) is termed as the general modal coordinate transformation matrix, in which

$$\begin{aligned} \mathbf{A}_V &= (\mathbf{A}_{V1}, \mathbf{A}_{V2} \cdots \mathbf{A}_{VN_c}) \in \mathbb{R}^{N \times 3N_c} \\ \mathbf{B}_V &= (\mathbf{B}_{V1}, \mathbf{B}_{V2} \cdots \mathbf{B}_{VN_c}) \in \mathbb{R}^{N \times 3N_c} \\ \mathbf{A}_D &= (\mathbf{A}_{D1}, \mathbf{A}_{D2} \cdots \mathbf{A}_{DN_c}) \in \mathbb{R}^{N \times 3N_c} \\ \mathbf{B}_D &= (\mathbf{B}_{D1}, \mathbf{B}_{D2} \cdots \mathbf{B}_{DN_c}) \in \mathbb{R}^{N \times 3N_c} \\ \mathbf{A}_V^P &= (\mathbf{A}_{V1}^P, \mathbf{A}_{V2}^P \cdots \mathbf{A}_{VN_p}^P) \in \mathbb{R}^{N \times 3N_p} \\ \mathbf{A}_D^P &= (\mathbf{A}_{D1}^P, \mathbf{A}_{D2}^P \cdots \mathbf{A}_{DN_p}^P) \in \mathbb{R}^{N \times 3N_p} \end{aligned} \quad (3.66)$$

and

$$\mathbf{A}_{Di} = (\mathbf{R}_i \mathbf{M} \mathbf{J} + \mathbf{R}_i^* \mathbf{M} \mathbf{J}) = \left(\frac{\boldsymbol{\varphi}_i \boldsymbol{\varphi}_i^T}{a_i} + \frac{\boldsymbol{\varphi}_i^* \boldsymbol{\varphi}_i^H}{a_i^*} \right) \mathbf{M} \mathbf{J} \in \mathbb{R}^{N \times 3} \quad (3.67)$$

$$\mathbf{B}_{Di} = -(\lambda_i^* \mathbf{R}_i \mathbf{M} \mathbf{J} + \lambda_i \mathbf{R}_i^* \mathbf{M} \mathbf{J}) = -\left(\frac{\lambda_i^* \boldsymbol{\varphi}_i \boldsymbol{\varphi}_i^T}{a_i} + \frac{\lambda_i \boldsymbol{\varphi}_i^* \boldsymbol{\varphi}_i^H}{a_i^*} \right) \mathbf{M} \mathbf{J} \in \mathbb{R}^{N \times 3} \quad (3.68)$$

$$\mathbf{A}_{Di}^p = \mathbf{R}_i^p \mathbf{D}_i^p = \frac{\boldsymbol{\varphi}_i^p (\boldsymbol{\varphi}_i^p)^T \mathbf{M} \mathbf{J}}{a_i^p} \in \mathbb{R}^{N \times 3} \quad (3.69)$$

$$\mathbf{A}_{Vi} = (\lambda_i \mathbf{R}_i \mathbf{M} \mathbf{J} + \lambda_i^* \mathbf{R}_i^* \mathbf{M} \mathbf{J}) = \left(\frac{\lambda_i \boldsymbol{\varphi}_i \boldsymbol{\varphi}_i^T}{a_i} + \frac{\lambda_i^* \boldsymbol{\varphi}_i^* \boldsymbol{\varphi}_i^H}{a_i^*} \right) \mathbf{M} \mathbf{J} \in \mathbb{R}^{N \times 3} \quad (3.70)$$

$$\mathbf{B}_{Vi} = -\lambda_i \lambda_i^* (\mathbf{R}_i \mathbf{M} \mathbf{J} + \mathbf{R}_i^* \mathbf{M} \mathbf{J}) = -\lambda_i \lambda_i^* \left(\frac{\boldsymbol{\varphi}_i \boldsymbol{\varphi}_i^T}{a_i} + \frac{\boldsymbol{\varphi}_i^* \boldsymbol{\varphi}_i^H}{a_i^*} \right) \mathbf{M} \mathbf{J} \in \mathbb{R}^{N \times 3} \quad (3.71)$$

$$\mathbf{A}_{Vi}^p = \lambda_i^p \mathbf{R}_i^p \mathbf{M} \mathbf{J} = \frac{\lambda_i^p \boldsymbol{\varphi}_i^p (\boldsymbol{\varphi}_i^p)^T \mathbf{M} \mathbf{J}}{a_i^p} \in \mathbb{R}^{N \times 3} \quad (3.72)$$

From Equations (3.66) to (3.72), it can be seen that all elements of \mathbf{A}_T belong to real numbers and are only specified by the structural system's parameters, including modal parameters, mass matrix \mathbf{M} and ground motion influence vector \mathbf{J} ; and are independent from the loading type and the direction of the excitation and how the mode shapes are normalized. \mathbf{J} is a time-invariant vector and is related to the spatial distribution of the excitation load caused by ground motion. When a structural system and the type of external loading are determined, \mathbf{J} is also determined and can be considered as a system parameter vector.

Equation (3.62) gives the modal expansion of the response vector $\mathbf{v}(t)$ in terms of the real-valued modal coordinate vector $\mathbf{Q}(t)$. Intuitively, using Equation (3.62), the coupled equations defined by Equation (2.2) can be transformed into a set of uncoupled equations expressed in terms of real-valued quantities. This hypothesis is proved mathematically in the next section, where some intermediary formulas are used and discussed to expose further characteristics and advantages of the general transformation matrix.

3.4.1 Proof of Modal Decoupling

To simplify the proof of the modal decoupling, the arrangement of the vectors in matrix \mathbf{A}_T and the elements in the modal coordinate vector $\mathbf{Q}(t)$ are reset without interference from the transformation results. Denote

$$\mathbf{v}(t) = \mathbf{A}_{ST} \mathbf{T}_G \mathbf{Q}_S(t) \in \mathbb{R}^{2N} \quad (3.73)$$

where $\mathbf{v}(t) = (\mathbf{u}^T(t), \mathbf{u}^T(t))^T \in \mathbb{R}^{2N}$ remains the same as the definition in Equation (3.62); and

$$\mathbf{A}_{ST} = \begin{pmatrix} \mathbf{A}_{v1} & \mathbf{B}_{v1} & \mathbf{A}_{v2} & \mathbf{B}_{v2} & \cdots & \mathbf{A}_{vN_c} & \mathbf{B}_{vN_c} & \mathbf{A}_{v1}^p & \mathbf{A}_{v2}^p & \cdots & \mathbf{A}_{vN_p}^p \\ \mathbf{A}_{d1} & \mathbf{B}_{d1} & \mathbf{A}_{d2} & \mathbf{B}_{d2} & \cdots & \mathbf{A}_{dN_c} & \mathbf{B}_{dN_c} & \mathbf{A}_{d1}^p & \mathbf{A}_{d2}^p & \cdots & \mathbf{A}_{dN_p}^p \end{pmatrix} \in \mathbb{R}^{2N \times 6N} \quad (3.74)$$

$$\mathbf{Q}_S(t) = [\dot{\mathbf{q}}_1(t), \mathbf{q}_1(t), \dot{\mathbf{q}}_2(t), \mathbf{q}_2(t) \cdots \dot{\mathbf{q}}_{N_c}(t), \mathbf{q}_{N_c}(t), \mathbf{q}_1^p(t), \mathbf{q}_2^p(t) \cdots \mathbf{q}_{N_p}^p(t)]^T \in \mathbb{R}^{6N} \quad (3.75)$$

For each column in Equation (3.74), it can be expanded as

$$\begin{aligned} \begin{Bmatrix} \mathbf{A}_{vi} \\ \mathbf{A}_{di} \end{Bmatrix} &= \begin{Bmatrix} \left(\frac{\lambda_i \boldsymbol{\varphi}_i \boldsymbol{\varphi}_i^T + \lambda_i^* \boldsymbol{\varphi}_i^* \boldsymbol{\varphi}_i^{*H}}{a_i} \right) \mathbf{M} \mathbf{J} \\ \left(\frac{\boldsymbol{\varphi}_i \boldsymbol{\varphi}_i^T + \boldsymbol{\varphi}_i^* \boldsymbol{\varphi}_i^{*H}}{a_i} \right) \mathbf{M} \mathbf{J} \end{Bmatrix} = \begin{Bmatrix} \lambda_i \boldsymbol{\varphi}_i & \lambda_i^* \boldsymbol{\varphi}_i^* \\ \boldsymbol{\varphi}_i & \boldsymbol{\varphi}_i^* \end{Bmatrix} \begin{Bmatrix} \frac{\boldsymbol{\varphi}_i^T \mathbf{M} \mathbf{J}}{a_i} \\ \frac{\boldsymbol{\varphi}_i^H \mathbf{M} \mathbf{J}}{a_i^*} \end{Bmatrix} \\ &= (\boldsymbol{\Psi}_i, \boldsymbol{\Psi}_i^*) \begin{Bmatrix} \frac{\boldsymbol{\varphi}_i^T \mathbf{M} \mathbf{J}}{a_i} \\ \frac{\boldsymbol{\varphi}_i^H \mathbf{M} \mathbf{J}}{a_i^*} \end{Bmatrix} \in \mathbb{R}^{2N \times 3} \end{aligned} \quad (3.76)$$

$$\begin{aligned}
\begin{Bmatrix} \mathbf{B}_{Vi} \\ \mathbf{B}_{Di} \end{Bmatrix} &= - \begin{Bmatrix} \lambda_i \lambda_i^* \left(\frac{\boldsymbol{\varphi}_i \boldsymbol{\varphi}_i^T}{a_i} + \frac{\boldsymbol{\varphi}_i^* \boldsymbol{\varphi}_i^H}{a_i^*} \right) \mathbf{M} \mathbf{J} \\ \left(\frac{\lambda_i^* \boldsymbol{\varphi}_i \boldsymbol{\varphi}_i^T}{a_i} + \frac{\lambda_i \boldsymbol{\varphi}_i^* \boldsymbol{\varphi}_i^H}{a_i^*} \right) \mathbf{M} \mathbf{J} \end{Bmatrix} \\
&= - \begin{pmatrix} \lambda_i \boldsymbol{\varphi}_i & \lambda_i^* \boldsymbol{\varphi}_i^* \\ \boldsymbol{\varphi}_i & \boldsymbol{\varphi}_i^* \end{pmatrix} \begin{Bmatrix} \frac{\lambda_i^* \boldsymbol{\varphi}_i^T \mathbf{M} \mathbf{J}}{a_i} \\ \frac{\lambda_i \boldsymbol{\varphi}_i^H \mathbf{M} \mathbf{J}}{a_i^*} \end{Bmatrix} = - (\boldsymbol{\psi}_i, \boldsymbol{\psi}_i^*) \begin{Bmatrix} \frac{\lambda_i^* \boldsymbol{\varphi}_i^T \mathbf{M} \mathbf{J}}{a_i} \\ \frac{\lambda_i \boldsymbol{\varphi}_i^H \mathbf{M} \mathbf{J}}{a_i^*} \end{Bmatrix} \in \mathbb{R}^{2N \times 3}
\end{aligned} \tag{3.77}$$

$$\begin{aligned}
\begin{Bmatrix} \mathbf{A}_{Vi}^P \\ \mathbf{A}_{Di}^P \end{Bmatrix} &= \begin{Bmatrix} \frac{\lambda_i^P \boldsymbol{\varphi}_i^P (\boldsymbol{\varphi}_i^P)^T \mathbf{M} \mathbf{J}}{a_i^P} \\ \frac{\boldsymbol{\varphi}_i^P (\boldsymbol{\varphi}_i^P)^T \mathbf{M} \mathbf{J}}{a_i^P} \end{Bmatrix} = \begin{Bmatrix} \lambda_i^P \boldsymbol{\varphi}_i^P \\ \boldsymbol{\varphi}_i^P \end{Bmatrix} \begin{Bmatrix} \frac{[(\boldsymbol{\varphi}_i^P)^T \mathbf{M} \mathbf{J}]}{a_i^P} \\ \frac{[(\boldsymbol{\varphi}_i^P)^T \mathbf{M} \mathbf{J}]}{a_i^P} \end{Bmatrix} = \boldsymbol{\psi}_i^P \begin{Bmatrix} \frac{(\boldsymbol{\varphi}_i^P)^T \mathbf{M} \mathbf{J}}{a_i^P} \\ \frac{(\boldsymbol{\varphi}_i^P)^T \mathbf{M} \mathbf{J}}{a_i^P} \end{Bmatrix} \in \mathbb{R}^{2N \times 3}
\end{aligned} \tag{3.78}$$

Thus, \mathbf{A}_{ST} can be rewritten as

$$\mathbf{A}_{ST} = \boldsymbol{\psi}_S \boldsymbol{\Gamma} = \begin{Bmatrix} \boldsymbol{\Phi}_S \boldsymbol{\Lambda}_S \\ \boldsymbol{\Phi}_S \end{Bmatrix} \boldsymbol{\Gamma} \tag{3.79}$$

where

$$\boldsymbol{\Phi}_S = \left(\boldsymbol{\varphi}_1, \boldsymbol{\varphi}_1^*, \boldsymbol{\varphi}_2, \boldsymbol{\varphi}_2^* \cdots \boldsymbol{\varphi}_{N_C}, \boldsymbol{\varphi}_{N_C}^*, \boldsymbol{\varphi}_1^P, \boldsymbol{\varphi}_2^P \cdots \boldsymbol{\varphi}_{N_P}^P \right) \in \mathbb{C}^{N \times 2N} \tag{3.80}$$

$$\boldsymbol{\Lambda}_S = \text{diag} \left(\lambda_1, \lambda_1^*, \lambda_2, \lambda_2^* \cdots \lambda_{N_C}, \lambda_{N_C}^*, \lambda_1^P, \lambda_2^P \cdots \lambda_{N_P}^P \right) \in \mathbb{C}^{2N \times 2N} \tag{3.81}$$

$$\boldsymbol{\psi}_S = \left(\boldsymbol{\psi}_1, \boldsymbol{\psi}_1^*, \boldsymbol{\psi}_2, \boldsymbol{\psi}_2^* \cdots \boldsymbol{\psi}_{N_C}, \boldsymbol{\psi}_{N_C}^*, \boldsymbol{\psi}_1^P, \boldsymbol{\psi}_2^P \cdots \boldsymbol{\psi}_{N_P}^P \right) \in \mathbb{C}^{2N \times 2N} \tag{3.82}$$

$$\boldsymbol{\Gamma} = \begin{pmatrix} \boldsymbol{\Gamma}_{C1} & & & & & \\ & \boldsymbol{\Gamma}_{C2} & & & & \\ & & \ddots & & & \\ & & & \boldsymbol{\Gamma}_{CN_C} & & \\ & & & & \boldsymbol{\Gamma}_1^P & \\ & \mathbf{0} & & & & \ddots \\ & & & & & & \boldsymbol{\Gamma}_{N_P}^P \end{pmatrix} \in \mathbb{C}^{2N \times 6N} \tag{3.83}$$

$$\mathbf{\Gamma}_{Ci} = \begin{pmatrix} \frac{\boldsymbol{\varphi}_i^T \mathbf{M} \mathbf{J}}{a_i} & -\frac{\lambda_i^* \boldsymbol{\varphi}_i^T \mathbf{M} \mathbf{J}}{a_i} \\ \frac{\boldsymbol{\varphi}_i^H \mathbf{M} \mathbf{J}}{a_i^*} & -\frac{\lambda_i \boldsymbol{\varphi}_i^H \mathbf{M} \mathbf{J}}{a_i^*} \end{pmatrix} \in \mathbb{C}^{2 \times 6} \quad (3.84)$$

$$\mathbf{\Gamma}_i^P = \frac{1}{a_i^P} [(\boldsymbol{\varphi}_i^P)^T \mathbf{M} \mathbf{J}] \in \mathbb{R}^{1 \times 3} \quad (3.85)$$

Analogous to the formula defined for classically damped systems (Clough and Penzien, 1993; Chopra, 2001), $\mathbf{\Gamma}_{Ci}$ and $\mathbf{\Gamma}_i^P$ can be termed as the i th modal participation factor matrix for a complex mode i and the over-damped modal participation factor matrix for over-damped mode i , respectively.

According to the orthogonality of the eigen-matrix proven in Chapter 2, Equations (2.15) and (2.16) can be rewritten as

$$\hat{\mathbf{a}}_s = \boldsymbol{\psi}_S^T \mathbf{A} \boldsymbol{\psi}_S = \text{diag}(a_1, a_1^*, a_2, a_2^* \cdots a_{N_c}, a_{N_c}^*, a_1^P, a_2^P \cdots a_{N_p}^P) \in \mathbb{C}^{2N \times 2N} \quad (3.86)$$

$$\hat{\mathbf{b}}_s = \boldsymbol{\psi}_S^T \mathbf{B} \boldsymbol{\psi}_S = \text{diag}(b_1, b_1^*, b_2, b_2^* \cdots b_{N_c}, b_{N_c}^*, b_1^P, b_2^P \cdots b_{N_p}^P) \in \mathbb{C}^{2N \times 2N} \quad (3.87)$$

For simplicity, the equation of motion of the structure represented in the state space form shown in Equation (2.2) is revisited here

$$\mathbf{A} \dot{\mathbf{v}}(t) + \mathbf{B} \mathbf{v}(t) = \mathbf{f}_s(t) \quad (3.88)$$

Substituting Equation (3.73) into Equation (3.88) and pre-multiplying $(\mathbf{A}_{ST} \mathbf{T}_G)^T$ to the resulting equation yields

$$\mathbf{T}_G^T \mathbf{A}_{ST}^T \mathbf{A} \mathbf{A}_{ST} \mathbf{T}_G \dot{\mathbf{Q}}_S(t) + \mathbf{T}_G^T \mathbf{A}_{ST}^T \mathbf{B} \mathbf{A}_{ST} \mathbf{T}_G \mathbf{Q}_S(t) = \mathbf{T}_G^T \mathbf{A}_{ST}^T \mathbf{f}_s(t) \quad (3.89)$$

in which

$$\mathbf{A}_{ST}^T \mathbf{A} \mathbf{A}_{ST} = \mathbf{\Gamma}^T (\boldsymbol{\Psi}_S^T \mathbf{A} \boldsymbol{\Psi}_S) \mathbf{\Gamma} \quad (\in \mathbb{R}^{6N \times 6N})$$

$$= \left(\begin{array}{cccc} \mathbf{\Gamma}_{c1}^T \begin{pmatrix} a_1 & 0 \\ 0 & a_1^* \end{pmatrix} \mathbf{\Gamma}_{c1} & & & \\ & \mathbf{\Gamma}_{c2}^T \begin{pmatrix} a_2 & 0 \\ 0 & a_2^* \end{pmatrix} \mathbf{\Gamma}_{c2} & & \mathbf{0} \\ & & \ddots & \\ & & & \mathbf{\Gamma}_{cN_c}^T \begin{pmatrix} a_{N_c} & 0 \\ 0 & a_{N_c}^* \end{pmatrix} \mathbf{\Gamma}_{cN_c} \\ \mathbf{0} & & & (\mathbf{\Gamma}_1^P)^T a_1^P \mathbf{\Gamma}_1^P \\ & & & \ddots \\ & & & (\mathbf{\Gamma}_{N_r}^P)^T a_{N_r}^P \mathbf{\Gamma}_{N_r}^P \end{array} \right) \quad (3.90)$$

$$\mathbf{A}_{ST}^T \mathbf{B} \mathbf{A}_{ST} = \mathbf{\Gamma}^T (\boldsymbol{\Psi}_S^T \mathbf{B} \boldsymbol{\Psi}_S) \mathbf{\Gamma} \quad (\in \mathbb{R}^{6N \times 6N})$$

$$= \left(\begin{array}{cccc} \mathbf{\Gamma}_{c1}^T \begin{pmatrix} b_1 & 0 \\ 0 & b_1^* \end{pmatrix} \mathbf{\Gamma}_{c1} & & & \\ & \mathbf{\Gamma}_{c2}^T \begin{pmatrix} b_2 & 0 \\ 0 & b_2^* \end{pmatrix} \mathbf{\Gamma}_{c2} & & \mathbf{0} \\ & & \ddots & \\ & & & \mathbf{\Gamma}_{cN_c}^T \begin{pmatrix} b_{N_c} & 0 \\ 0 & b_{N_c}^* \end{pmatrix} \mathbf{\Gamma}_{cN_c} \\ \mathbf{0} & & & (\mathbf{\Gamma}_1^P)^T b_1^P \mathbf{\Gamma}_1^P \\ & & & \ddots \\ & & & (\mathbf{\Gamma}_{N_r}^P)^T b_{N_r}^P \mathbf{\Gamma}_{N_r}^P \end{array} \right) \quad (3.91)$$

and

$$\begin{aligned}
\mathbf{A}_{\text{ST}}^T \mathbf{f}_s(t) &= \left\{ \begin{matrix} \mathbf{0} \\ \mathbf{f}(t) \end{matrix} \right\} = -\mathbf{\Gamma}^T (\mathbf{\Phi}_s^T \mathbf{M} \mathbf{J} \mathbf{T}) \ddot{\mathbf{u}}_g(t) \quad (\in \mathbb{R}^{6N \times 1}) \\
&= \left(\left\{ \begin{matrix} 2 \operatorname{Re} \left[\frac{(\mathbf{J}^T \mathbf{M} \boldsymbol{\varphi}_1)(\boldsymbol{\varphi}_1^T \mathbf{M} \mathbf{J} \mathbf{T})}{a_1} \right] \\ -2 \operatorname{Re} \left[\frac{\lambda_1^* (\mathbf{J}^T \mathbf{M} \boldsymbol{\varphi}_1)(\boldsymbol{\varphi}_1^T \mathbf{M} \mathbf{J} \mathbf{T})}{a_1} \right] \end{matrix} \right\}^T, \left\{ \begin{matrix} 2 \operatorname{Re} \left[\frac{(\mathbf{J}^T \mathbf{M} \boldsymbol{\varphi}_2)(\boldsymbol{\varphi}_2^T \mathbf{M} \mathbf{J} \mathbf{T})}{a_2} \right] \\ -2 \operatorname{Re} \left[\frac{\lambda_2^* (\mathbf{J}^T \mathbf{M} \boldsymbol{\varphi}_2)(\boldsymbol{\varphi}_2^T \mathbf{M} \mathbf{J} \mathbf{T})}{a_2} \right] \end{matrix} \right\}^T, \right. \\
&\quad \left. \left\{ \begin{matrix} 2 \operatorname{Re} \left[\frac{(\mathbf{J}^T \mathbf{M} \boldsymbol{\varphi}_{N_c})(\boldsymbol{\varphi}_{N_c}^T \mathbf{M} \mathbf{J} \mathbf{T})}{a_{N_c}} \right] \\ \dots \\ -2 \operatorname{Re} \left[\frac{\lambda_{N_c}^* (\mathbf{J}^T \mathbf{M} \boldsymbol{\varphi}_{N_c})(\boldsymbol{\varphi}_{N_c}^T \mathbf{M} \mathbf{J} \mathbf{T})}{a_{N_c}} \right] \end{matrix} \right\}^T \right) \\
&\quad \left(\frac{(\mathbf{J}^T \mathbf{M} \boldsymbol{\varphi}_1^p)(\boldsymbol{\varphi}_1^p)^T \mathbf{M} \mathbf{J} \mathbf{T}}{a_1^p}, \frac{(\mathbf{J}^T \mathbf{M} \boldsymbol{\varphi}_2^p)(\boldsymbol{\varphi}_2^p)^T \mathbf{M} \mathbf{J} \mathbf{T}}{a_2^p}, \dots, \frac{(\mathbf{J}^T \mathbf{M} \boldsymbol{\varphi}_{N_p}^p)(\boldsymbol{\varphi}_{N_p}^p)^T \mathbf{M} \mathbf{J} \mathbf{T}}{a_{N_p}^p} \right)^T [-\ddot{\mathbf{u}}_g(t)]
\end{aligned} \tag{3.92}$$

After substituting Equations (3.90) to (3.92) back into Equation (3.89), the corresponding i th block element for the complex mode and the over-damped mode for both sides of the resulting equation can be further manipulated as

$$\begin{aligned}
&\left(\begin{matrix} \mathbf{T}^T & 0 \\ 0 & \mathbf{T}^T \end{matrix} \right) \mathbf{\Gamma}_{c_i}^T \begin{pmatrix} a_i & 0 \\ 0 & a_i^* \end{pmatrix} \mathbf{\Gamma}_{c_i} \begin{pmatrix} \mathbf{T} & 0 \\ 0 & \mathbf{T} \end{pmatrix} \begin{Bmatrix} \ddot{\mathbf{q}}_i \\ \dot{\mathbf{q}}_i \end{Bmatrix} + \left(\begin{matrix} \mathbf{T}^T & 0 \\ 0 & \mathbf{T}^T \end{matrix} \right) \mathbf{\Gamma}_{c_i}^T \begin{pmatrix} b_i & 0 \\ 0 & b_i^* \end{pmatrix} \mathbf{\Gamma}_{c_i} \begin{pmatrix} \mathbf{T} & 0 \\ 0 & \mathbf{T} \end{pmatrix} \begin{Bmatrix} \dot{\mathbf{q}}_i \\ \mathbf{q}_i \end{Bmatrix} \\
&= \left\{ \begin{matrix} 2 \operatorname{Re} \left[\frac{(\mathbf{T}^T \mathbf{J}^T \mathbf{M} \boldsymbol{\varphi}_i)(\boldsymbol{\varphi}_i^T \mathbf{M} \mathbf{J} \mathbf{T})}{a_i} \right] \\ -2 \operatorname{Re} \left[\frac{\lambda_i^* (\mathbf{T}^T \mathbf{J}^T \mathbf{M} \boldsymbol{\varphi}_i)(\boldsymbol{\varphi}_i^T \mathbf{M} \mathbf{J} \mathbf{T})}{a_i} \right] \end{matrix} \right\} [-\ddot{\mathbf{u}}_g(t)]
\end{aligned} \tag{3.93}$$

$(i = 1, 2, \dots, N_c)$

$$\mathbf{T}^T (\mathbf{\Gamma}_i^p)^T a_i^p \mathbf{\Gamma}_i^p \mathbf{T} (\dot{\mathbf{q}}_i^p + \omega_i^p \mathbf{q}_i^p) = \frac{(\mathbf{T}^T \mathbf{J}^T \mathbf{M} \boldsymbol{\varphi}_i^p)(\boldsymbol{\varphi}_i^p)^T \mathbf{M} \mathbf{J} \mathbf{T}}{a_i^p} [-\ddot{\mathbf{u}}_g(t)] \quad (i = 1, 2, \dots, N_p) \tag{3.94}$$

In Equation (3.93),

$$\begin{aligned}
& 2 \left\{ \begin{array}{l} \text{Re} \left[\frac{(\mathbf{T}^T \mathbf{J}^T \mathbf{M} \boldsymbol{\varphi}_i)(\boldsymbol{\varphi}_i^T \mathbf{M} \mathbf{J} \mathbf{T})}{a_i} \right] \\ -\text{Re} \left[\frac{\lambda_i^* (\mathbf{T}^T \mathbf{J}^T \mathbf{M} \boldsymbol{\varphi}_i)(\boldsymbol{\varphi}_i^T \mathbf{M} \mathbf{J} \mathbf{T})}{a_i} \right] \end{array} \right\} \begin{array}{l} \ddot{\mathbf{q}}_i \\ \dot{\mathbf{q}}_i \end{array} \\
& -\text{Re} \left[\frac{\lambda_i^* (\mathbf{T}^T \mathbf{J}^T \mathbf{M} \boldsymbol{\varphi}_i)(\boldsymbol{\varphi}_i^T \mathbf{M} \mathbf{J} \mathbf{T})}{a_i} \right] \ddot{\mathbf{q}}_i + \text{Re} \left[\frac{(\lambda_i^*)^2 (\mathbf{T}^T \mathbf{J}^T \mathbf{M} \boldsymbol{\varphi}_i)(\boldsymbol{\varphi}_i^T \mathbf{M} \mathbf{J} \mathbf{T})}{a_i} \right] \dot{\mathbf{q}}_i \\
& +2 \left\{ \begin{array}{l} -\text{Re} \left[\frac{\lambda_i (\mathbf{T}^T \mathbf{J}^T \mathbf{M} \boldsymbol{\varphi}_i)(\boldsymbol{\varphi}_i^T \mathbf{M} \mathbf{J} \mathbf{T})}{a_i} \right] \\ \text{Re} \left[\frac{\omega_i^2 (\mathbf{T}^T \mathbf{J}^T \mathbf{M} \boldsymbol{\varphi}_i)(\boldsymbol{\varphi}_i^T \mathbf{M} \mathbf{J} \mathbf{T})}{a_i} \right] \end{array} \right\} \begin{array}{l} \dot{\mathbf{q}}_i \\ \mathbf{q}_i \end{array} \\
& + \text{Re} \left[\frac{\omega_i^2 (\mathbf{T}^T \mathbf{J}^T \mathbf{M} \boldsymbol{\varphi}_i)(\boldsymbol{\varphi}_i^T \mathbf{M} \mathbf{J} \mathbf{T})}{a_i} \right] \dot{\mathbf{q}}_i - \text{Re} \left[\frac{\omega_i^2 \lambda_i^* (\mathbf{T}^T \mathbf{J}^T \mathbf{M} \boldsymbol{\varphi}_i)(\boldsymbol{\varphi}_i^T \mathbf{M} \mathbf{J} \mathbf{T})}{a_i} \right] \mathbf{q}_i \\
& = \left\{ \begin{array}{l} 2 \text{Re} \left[\frac{(\mathbf{T}^T \mathbf{J}^T \mathbf{M} \boldsymbol{\varphi}_i)(\boldsymbol{\varphi}_i^T \mathbf{M} \mathbf{J} \mathbf{T})}{a_i} \right] \\ -2 \text{Re} \left[\frac{\lambda_i^* (\mathbf{T}^T \mathbf{J}^T \mathbf{M} \boldsymbol{\varphi}_i)(\boldsymbol{\varphi}_i^T \mathbf{M} \mathbf{J} \mathbf{T})}{a_i} \right] \end{array} \right\} [-\ddot{\mathbf{u}}_g(t)] \in \mathbb{R}^6 \quad (3.97)
\end{aligned}$$

Equation (3.97) corresponds to two equations. The first one is

$$\begin{aligned}
& 2 \text{Re} \left[\frac{(\mathbf{T}^T \mathbf{J}^T \mathbf{M} \boldsymbol{\varphi}_i)(\boldsymbol{\varphi}_i^T \mathbf{M} \mathbf{J} \mathbf{T})}{a_i} \right] \ddot{\mathbf{q}}_i - 2 \text{Re} \left[\frac{\lambda_i^* (\mathbf{T}^T \mathbf{J}^T \mathbf{M} \boldsymbol{\varphi}_i)(\boldsymbol{\varphi}_i^T \mathbf{M} \mathbf{J} \mathbf{T})}{a_i} \right] \dot{\mathbf{q}}_i - 2 \text{Re} \left[\frac{\lambda_i (\mathbf{T}^T \mathbf{J}^T \mathbf{M} \boldsymbol{\varphi}_i)(\boldsymbol{\varphi}_i^T \mathbf{M} \mathbf{J} \mathbf{T})}{a_i} \right] \dot{\mathbf{q}}_i \\
& + 2 \text{Re} \left[\frac{\omega_i^2 (\mathbf{T}^T \mathbf{J}^T \mathbf{M} \boldsymbol{\varphi}_i)(\boldsymbol{\varphi}_i^T \mathbf{M} \mathbf{J} \mathbf{T})}{a_i} \right] \mathbf{q}_i = 2 \text{Re} \left[\frac{(\mathbf{T}^T \mathbf{J}^T \mathbf{M} \boldsymbol{\varphi}_i)(\boldsymbol{\varphi}_i^T \mathbf{M} \mathbf{J} \mathbf{T})}{a_i} \right] [\dot{\mathbf{q}}_i + (-\lambda_i - \lambda_i^*) \dot{\mathbf{q}}_i + \omega_i^2 \mathbf{q}_i] \\
& = 2 \text{Re} \left[\frac{(\mathbf{T}^T \mathbf{J}^T \mathbf{M} \boldsymbol{\varphi}_i)(\boldsymbol{\varphi}_i^T \mathbf{M} \mathbf{J} \mathbf{T})}{a_i} \right] [\ddot{\mathbf{q}}_i + 2 \xi_i \omega_i \dot{\mathbf{q}}_i + \omega_i^2 \mathbf{q}_i] = 2 \text{Re} \left[\frac{(\mathbf{T}^T \mathbf{J}^T \mathbf{M} \boldsymbol{\varphi}_i)(\boldsymbol{\varphi}_i^T \mathbf{M} \mathbf{J} \mathbf{T})}{a_i} \right] [-\ddot{\mathbf{u}}_g(t)] \in \mathbb{R}^3 \quad (3.98)
\end{aligned}$$

while the second one is expressed as

$$\begin{aligned}
& -2 \text{Re} \left[\frac{\lambda_i^* (\mathbf{T}^T \mathbf{J}^T \mathbf{M} \boldsymbol{\varphi}_i)(\boldsymbol{\varphi}_i^T \mathbf{M} \mathbf{J} \mathbf{T})}{a_i} \right] \ddot{\mathbf{q}}_i + 2 \text{Re} \left[\frac{(\lambda_i^*)^2 (\mathbf{T}^T \mathbf{J}^T \mathbf{M} \boldsymbol{\varphi}_i)(\boldsymbol{\varphi}_i^T \mathbf{M} \mathbf{J} \mathbf{T})}{a_i} \right] \dot{\mathbf{q}}_i + 2 \text{Re} \left[\frac{\omega_i^2 (\mathbf{T}^T \mathbf{J}^T \mathbf{M} \boldsymbol{\varphi}_i)(\boldsymbol{\varphi}_i^T \mathbf{M} \mathbf{J} \mathbf{T})}{a_i} \right] \dot{\mathbf{q}}_i \\
& - 2 \text{Re} \left[\frac{\omega_i^2 \lambda_i^* (\mathbf{T}^T \mathbf{J}^T \mathbf{M} \boldsymbol{\varphi}_i)(\boldsymbol{\varphi}_i^T \mathbf{M} \mathbf{J} \mathbf{T})}{a_i} \right] \mathbf{q}_i = -2 \text{Re} \left[\frac{\lambda_i^* (\mathbf{T}^T \mathbf{J}^T \mathbf{M} \boldsymbol{\varphi}_i)(\boldsymbol{\varphi}_i^T \mathbf{M} \mathbf{J} \mathbf{T})}{a_i} \right] [\dot{\mathbf{q}}_i + (-\lambda_i - \lambda_i^*) \dot{\mathbf{q}}_i + \omega_i^2 \mathbf{q}_i] \\
& = -2 \text{Re} \left[\frac{\lambda_i^* (\mathbf{T}^T \mathbf{J}^T \mathbf{M} \boldsymbol{\varphi}_i)(\boldsymbol{\varphi}_i^T \mathbf{M} \mathbf{J} \mathbf{T})}{a_i} \right] [\ddot{\mathbf{q}}_i + 2 \xi_i \omega_i \dot{\mathbf{q}}_i + \omega_i^2 \mathbf{q}_i] = -2 \text{Re} \left[\frac{\lambda_i^* (\mathbf{T}^T \mathbf{J}^T \mathbf{M} \boldsymbol{\varphi}_i)(\boldsymbol{\varphi}_i^T \mathbf{M} \mathbf{J} \mathbf{T})}{a_i} \right] [-\ddot{\mathbf{u}}_g(t)] \in \mathbb{R}^3 \quad (3.99)
\end{aligned}$$

Comparing Equations (3.98) and (3.99), it can be easily found that they are identical whether or not $(\boldsymbol{\varphi}_i^T \mathbf{M} \mathbf{J} \mathbf{T})$ is equal to the zero matrix, which can be simplified as a second order equation of motion for a SDOF system with the i th modal frequency and damping ratio:

$$\ddot{\mathbf{q}}_i + 2\xi_i \omega_i \dot{\mathbf{q}}_i + \omega_i^2 \mathbf{q}_i = -\ddot{\mathbf{u}}_g(t) \quad (3.100)$$

For the over-damped modes, substituting Equation (3.85) into Equation (3.94), results in

$$\frac{(\mathbf{T}^T \mathbf{J}^T \mathbf{M} \boldsymbol{\varphi}_i^P)((\boldsymbol{\varphi}_i^P)^T \mathbf{M} \mathbf{J} \mathbf{T})}{a_i^P} (\dot{\mathbf{q}}_i^P + \omega_i^P \mathbf{q}_i^P) = \frac{(\mathbf{T}^T \mathbf{J}^T \mathbf{M} \boldsymbol{\varphi}_i^P)((\boldsymbol{\varphi}_i^P)^T \mathbf{M} \mathbf{J} \mathbf{T})}{a_i^P} [-\ddot{\mathbf{u}}_g(t)] \quad (3.101)$$

If $[(\boldsymbol{\varphi}_i^P)^T \mathbf{M} \mathbf{J} \mathbf{T}] \neq \mathbf{0}$, Equation (3.101) can be further simplified as a first-order differential equation for an over-damped mode

$$\dot{\mathbf{q}}_i^P + \omega_i^P \mathbf{q}_i^P = -\ddot{\mathbf{u}}_g(t) \quad (3.102)$$

It has now been successfully shown that the general transformation matrix \mathbf{A}_T can decouple the original MDOF structural motion differential equation represented in the state space form.

3.5 Modal Static Response and Effective Modal Mass

When using the modal superposition method, the response contributions of all modes should be included to achieve an exact result. However, experience suggests that a limited amount of modes can usually provide sufficiently accurate results. In general, the participating mass for a certain mode provides a measure of how important the mode is for computing the response to seismic loads in each of the three orthogonal directions. Note that there is no information about the accuracy of the responses subjected to other loads. The number of modes required is well defined for classical damping using the cumulative effective modal mass (Wilson, 2004; Clough and Penzien, 1993). The most common criterion used is the “90% rule for participating mass” specified in many design codes (IBC, 2003). For 3-D arbitrarily damped systems with over-critically damped

modes, similar criteria have not been addressed. This issue is considered in this section. First, the formulation of the effective modal mass and its physical interpretation in classically damped systems is briefly reviewed. Then, a general effective modal mass is formulated in a manner which has a parallel physical interpretation as in the classically damped systems.

3.5.1 Effective Modal Mass for Classically Damped Systems w/o Over-Damped Modes

The definition of the effective modal mass discussed in this section mainly follows the work given in Chopra (2001). It is briefly reviewed to facilitate subsequent formulation of the general effective modal mass. The equation of motion governing the response of a planar N -DOFs multistory frame (as shown in Figure 3.5) due to earthquake induced ground motion, $\ddot{x}_g(t)$, can be written as

$$\mathbf{M}\ddot{\mathbf{x}}(t) + \mathbf{C}\dot{\mathbf{x}}(t) + \mathbf{K}\mathbf{x}(t) = -\mathbf{M}\mathbf{I}\ddot{x}_g(t) \quad (3.103)$$

in which \mathbf{I} is the unit vector with dimension $N \times 1$ and $\mathbf{x}(t)$ is a $N \times 1$ vector representing the translational DOFs for each node. A classically damped system possesses normal modes, which are re-denoted as $\phi_i \in \mathbb{R}^N$ in order to distinguish them from the complex modes $\boldsymbol{\varphi}_i$ in the discussion. The spatial distribution of the effective earthquake force is defined by $\mathbf{s} = \mathbf{M}\mathbf{J}$ and is loosely referred to as a force vector, although it has a unit of mass or can be considered as a force vector produced by unitary ground motion acceleration by letting $\ddot{x}_g(t) = 1$. Further, it can be expanded as a summation of the modal inertia force distribution s_i

$$\mathbf{s} = \mathbf{M}\mathbf{J} = \sum_{i=1}^N \mathbf{s}_i = \sum_{i=1}^N \mathbf{M}\phi_i \Gamma_i \quad (3.104)$$

where

$$\Gamma_i = \frac{\phi_i^T \mathbf{M}\mathbf{J}}{\phi_i^T \mathbf{M}\phi_i} \quad (3.105)$$

is the i th modal participation factor defined for classically damped systems. As a result, the contribution of the i th mode to the nodal displacements $\mathbf{x}(t)$ can be expressed by

$$\mathbf{x}_i(t) = \Gamma_i \boldsymbol{\phi}_i \frac{A_i(t)}{\omega_i^2} \quad (3.106)$$

where $A_i(t)$ is the pseudo acceleration response of an SDOF system with the i th modal damping ratio, ξ_i , and the i th circular frequency, ω_i , subjected to $\ddot{x}_g(t)$. Consequently, the i th modal response contribution $r_i(t)$ to any response quantity $r(t)$ can be determined by the static analysis of the structure combined with the dynamic response, $A_i(t)$, of the corresponding SDOF. That is,

$$r_i(t) = r_i^{\text{st}} A_i(t) \quad (3.107)$$

where r_i^{st} denotes the modal static response due to external force \mathbf{s}_i . This is explained schematically in Figure 3.6. The base shear due to the i th mode, V_{bi} , is obtained by specializing Equation (3.107) for V_{bi} :

$$V_{bi}(t) = V_{bi}^{\text{st}} A_i(t) \quad (3.108)$$

in which V_{bi}^{st} is the base shear force due to the applied force \mathbf{s}_i as shown in Figure 3.6 and can be expressed as

$$V_{bi}^{\text{st}} = \sum_{j=1}^N s_{ji} = \mathbf{J}^T \mathbf{s}_i = \frac{(\boldsymbol{\phi}_i^T \mathbf{M} \mathbf{J})^2}{\boldsymbol{\phi}_i^T \mathbf{M} \boldsymbol{\phi}_i} \quad (3.109)$$

where s_{ji} is the j th component of the i th external force \mathbf{s}_i . Equation (3.109) is also recognized as the base shear effective modal mass for a classically damped system or, for brevity, effective modal mass, which can be re-denoted as

$$m_i^{\text{eff}} = \frac{(\boldsymbol{\phi}_i^T \mathbf{M} \mathbf{J})^2}{\boldsymbol{\phi}_i^T \mathbf{M} \boldsymbol{\phi}_i} \geq 0 \quad \in \mathbb{R} \quad (3.110)$$

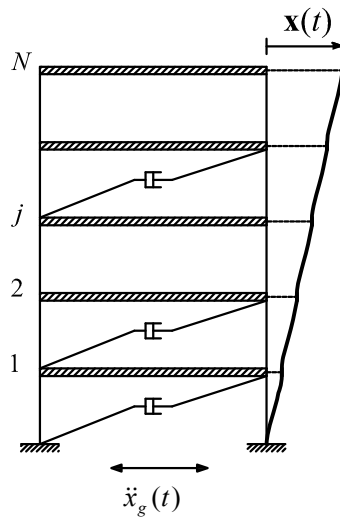


Figure 3.5 A planar N -DOFs multistory frame

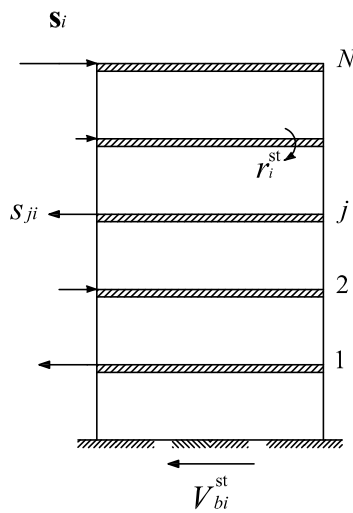


Figure 3.6 Illustration of the static structural response subjected to s_i

It can be proved that the sum of all effective modal masses is equal to the total mass of the system (Chopra, 2001 pp.524; Clough and Penzien, 1993 pp.627).

As a result, Equation (3.108) can be written as

$$V_{bi}(t) = m_i^{\text{eff}} A_i(t) \in \mathbb{R} \quad (3.111)$$

Equation (3.111) indicates that only the portion m_i^{eff} of the total mass of the system is responding to the earthquake in the i th mode. Therefore, the effective modal mass m_i^{eff} is commonly used as a criterion to determine how many modes should be included in the modal superposition, e.g. the 90% rule of the participating mass specified in most seismic design codes. The preceding formulation states that the effective modal mass for mode i is equivalent to the static base shear force due to the external force \mathbf{s}_i . This implies that the 90% rule used to determine the number of modes required in the analysis can only guarantee that the base shear force under static external force has an error of less than 10%. For other response quantities, the error may exceed 10%. In addition, the modal response is also affected by the dynamic response term $A_i(t)$, which means that even if a sufficient number of modes are included to achieve 90% of the total static response, the error in the dynamic response may exceed 10%. Nevertheless, the effective modal mass is still accepted in engineering practice for its simplicity.

3.5.2 Effective Modal Mass for 3-D Arbitrarily Damped Systems

This section presents two methods to define the effective modal mass for a 3-D arbitrarily damped linear system. Method 1 follows a similar concept in the derivation of the effective modal mass in classically damped systems by extending it in a 3-D space. Method 2 is formulated based on the modal expansion pattern of the inverse of the mass matrix given in Section 2.6.

Method 1

In light of the preceding explanation, only the portion of the static response is considered as a way to define the effective modal mass for 3-D arbitrarily damped systems. Thus, the central idea here is to expand the inertia force distribution $\mathbf{s} = \mathbf{M}\mathbf{J} = \mathbf{M} \begin{bmatrix} \mathbf{J}^{(x)} & \mathbf{J}^{(y)} & \mathbf{J}^{(z)} \end{bmatrix}$ in terms of the complex modal shapes possessed by the arbitrarily damped systems for each mode as represented by $\mathbf{s}_i = \begin{bmatrix} \mathbf{s}_i^{(x)} & \mathbf{s}_i^{(y)} & \mathbf{s}_i^{(z)} \end{bmatrix}$. This expanded $\mathbf{s}_i^{(k)}$ is therefore applied to the structure along the k direction and the resulting static base shear force along the k direction is regarded as the effective modal mass of the i th mode along the k direction. To

do so, the static displacement vector, denoted as $\mathbf{u}_0^{(k)}$ in which $k \in \{x, y, z\}$, of the systems subjected to the inertia force distribution $\mathbf{s}^{(k)} = \mathbf{M}\mathbf{J}^{(k)}$ is calculated. Consequently, the static displacement vector $\mathbf{u}_0^{(k)}$ is

$$\mathbf{u}_0^{(k)} = \mathbf{K}^{-1}\mathbf{M}\mathbf{J}^{(k)} \in \mathbb{R}^N \quad (3.112)$$

Substituting the expansion of \mathbf{K}^{-1} shown in Equation (2.48) into Equation (3.112) gives

$$\mathbf{u}_0^{(k)} = -2 \sum_{i=1}^{N_c} \text{Re} \left(\frac{\boldsymbol{\varphi}_i \boldsymbol{\varphi}_i^T \mathbf{M}\mathbf{J}^{(k)}}{\lambda_i a_i} \right) - \sum_{i=1}^{N_p} \frac{\boldsymbol{\varphi}_i^p (\boldsymbol{\varphi}_i^p)^T \mathbf{M}\mathbf{J}^{(k)}}{\lambda_i^p a_i^p} \quad (3.113)$$

Equation (3.113) suggests that the static displacement contributed from the i th complex mode (including its conjugate part), $\mathbf{u}_{0i}^{(k)}$, can be written as

$$\mathbf{u}_{0i}^{(k)} = -2 \text{Re} \left(\frac{\boldsymbol{\varphi}_i \boldsymbol{\varphi}_i^T \mathbf{M}\mathbf{J}^{(k)}}{\lambda_i a_i} \right) \in \mathbb{R}^N \quad (3.114)$$

Also, the static displacement contributed from the i th over-damped mode, $\mathbf{u}_{0i}^{(k)P}$, can be expressed as

$$\mathbf{u}_{0i}^{(k)P} = - \frac{\boldsymbol{\varphi}_i^p (\boldsymbol{\varphi}_i^p)^T \mathbf{M}\mathbf{J}^{(k)}}{\lambda_i^p a_i^p} \in \mathbb{R}^N \quad (3.115)$$

Therefore, the contribution of the i th complex mode to the vector $\mathbf{s}^{(k)} = \mathbf{M}\mathbf{J}^{(k)}$ is

$$\mathbf{s}_i^{(k)} = \mathbf{K}\mathbf{u}_{0i}^{(k)} = -2 \text{Re} \left(\frac{\mathbf{K}\boldsymbol{\varphi}_i \boldsymbol{\varphi}_i^T \mathbf{M}\mathbf{J}^{(k)}}{\lambda_i a_i} \right) \in \mathbb{R}^N \quad (3.116)$$

and the contribution of the i th over-damped mode to the vector $\mathbf{s}^{(k)} = \mathbf{M}\mathbf{J}^{(k)}$ is

$$\mathbf{s}_i^{(k)P} = \mathbf{K}\mathbf{u}_{0i}^{(k)P} = - \frac{\mathbf{K}\boldsymbol{\varphi}_i^p (\boldsymbol{\varphi}_i^p)^T \mathbf{M}\mathbf{J}^{(k)}}{\lambda_i^p a_i^p} \in \mathbb{R}^N \quad (3.117)$$

Summation of Equations (3.116) and (3.117) gives the complete expansion of $\mathbf{s}^{(k)} = \mathbf{M}\mathbf{J}^{(k)}$. As a result, the base shear force due to the static inertia force $\mathbf{s}_i^{(k)}$ along the k direction is

$$\begin{aligned}
V_{bi}^{(k)st} &= \sum_{j=1}^{N_c} s_{ji}^{(k)} = (\mathbf{J}^{(k)})^T \mathbf{s}_i^{(k)} \\
&= -2 \operatorname{Re} \left(\frac{(\mathbf{J}^{(k)})^T \mathbf{K} \boldsymbol{\varphi}_i \boldsymbol{\varphi}_i^T \mathbf{M} \mathbf{J}^{(k)}}{\lambda_i a_i} \right) \\
&= -2 \operatorname{Re} \left(\frac{\boldsymbol{\varphi}_i^T \mathbf{K} \mathbf{J}^{(k)} \boldsymbol{\varphi}_i^T \mathbf{M} \mathbf{J}^{(k)}}{\lambda_i a_i} \right) \in \mathbb{R}
\end{aligned} \tag{3.118}$$

where $s_{ji}^{(k)}$ is the j th component of the i th external force $\mathbf{s}_i^{(k)}$. The resulting base shear force due to the static inertia force $\mathbf{s}_i^{(k)P}$ is

$$\begin{aligned}
V_{bi}^{(k)Pst} &= \sum_{j=1}^{N_p} s_{ji}^{(k)P} = \mathbf{J}^T \mathbf{s}_i^{(k)P} \\
&= - \frac{(\mathbf{J}^{(k)})^T \mathbf{K} \boldsymbol{\varphi}_i^P (\boldsymbol{\varphi}_i^P)^T \mathbf{M} \mathbf{J}^{(k)}}{\lambda_i^P a_i^P} \\
&= - \frac{(\boldsymbol{\varphi}_i^P)^T \mathbf{K} \mathbf{J}^{(k)} (\boldsymbol{\varphi}_i^P)^T \mathbf{M} \mathbf{J}^{(k)}}{\lambda_i^P a_i^P} \in \mathbb{R}
\end{aligned} \tag{3.119}$$

where $s_{ji}^{(k)P}$ is the j th component of the i th external force $\mathbf{s}_i^{(k)P}$. Thus, in parallel to the definition of the effective modal mass given for classically damped systems, Equation (3.118) is then defined as the i th effective modal mass, $\hat{m}_i^{(k)\text{eff}}$, associated with the i th complex mode (including its conjugate counterpart) in the k direction and Equation (3.119) is defined as the i th effective modal mass, $\hat{m}_i^{(k)P\text{eff}}$, in the k direction for the i th over-damped mode. These effective modal masses $\hat{m}_i^{(k)\text{eff}}$ and $\hat{m}_i^{(k)P\text{eff}}$ in the k direction are then sequenced in an ascending order according to the absolute value of their corresponding eigenvalues (λ_i and λ_i^P). The cumulative mass in the k direction based on this sequence is used to determine how many modes will be required to reach the prescribed participation mass ratio (e.g. the 90% rule). In general, the amount of modes that can achieve 90% participating masses in all three orthogonal directions is used.

Similar to the case of classically damped systems, the sum of all general effective modal masses along the k direction is equal to the total unrestrained mass acting in the k direction, $M_{\Sigma}^{(k)} = (\mathbf{J}^{(k)})^T \mathbf{M} \mathbf{J}^{(k)}$. That is,

$$\sum_{i=1}^{N_C} \hat{m}_i^{\text{eff}} + \sum_{i=1}^{N_P} \hat{m}_i^{\text{Peff}} = M_{\Sigma}^{(k)} \in \mathbb{R} \quad (3.120)$$

Equation (3.120) can be proven by recognizing that $\hat{m}_i^{(k)\text{eff}} = (\mathbf{J}^{(k)})^T \mathbf{s}_i^{(k)}$ [Equation (3.118)] and $\hat{m}_i^{(k)\text{Peff}} = (\mathbf{J}^{(k)})^T \mathbf{s}_i^{(k)\text{P}}$ [Equation (3.119)], which implies that the sum of all effective modal mass equals to $(\mathbf{J}^{(k)})^T \left(\sum_{i=1}^{N_C} \mathbf{s}_i^{(k)} + \sum_{i=1}^{N_P} \mathbf{s}_i^{(k)\text{P}} \right) = (\mathbf{J}^{(k)})^T \mathbf{M} \mathbf{J}^{(k)}$.

Method 2

Alternatively, the inertia force distribution $\mathbf{s}^{(k)} = \mathbf{M} \mathbf{J}^{(k)}$ along the k direction can also be expanded in another pattern different from the one derived in method 1. First, the expansion of the inverse of the mass matrix \mathbf{M}^{-1} shown in Equation (2.45) is repeated here.

$$\begin{aligned} \mathbf{M}^{-1} &= \Phi \hat{\mathbf{a}}^{-1} \Lambda \Phi^T \\ &= 2 \sum_{i=1}^{N_C} \text{Re} \left(\frac{\lambda_i \boldsymbol{\varphi}_i \boldsymbol{\varphi}_i^T}{a_i} \right) + \sum_{i=1}^{N_P} \frac{\lambda_i^{\text{P}} \boldsymbol{\varphi}_i^{\text{P}} (\boldsymbol{\varphi}_i^{\text{P}})^T}{a_i^{\text{P}}} \in \mathbb{R}^{N \times N} \end{aligned} \quad (3.121)$$

Post-multiplying by $\mathbf{M} \mathbf{J}^{(k)}$ in Equation (3.121) results in

$$\begin{aligned} \mathbf{J}^{(k)} &= \Phi \hat{\mathbf{a}}^{-1} \Lambda \Phi^T \mathbf{M} \mathbf{J}^{(k)} \\ &= 2 \sum_{i=1}^{N_C} \text{Re} \left(\frac{\lambda_i \boldsymbol{\varphi}_i \boldsymbol{\varphi}_i^T \mathbf{M} \mathbf{J}^{(k)}}{a_i} \right) + \sum_{i=1}^{N_P} \frac{\lambda_i^{\text{P}} \boldsymbol{\varphi}_i^{\text{P}} (\boldsymbol{\varphi}_i^{\text{P}})^T \mathbf{M} \mathbf{J}^{(k)}}{a_i^{\text{P}}} \in \mathbb{R}^N \end{aligned} \quad (3.122)$$

Thus, the inertia force distribution $\mathbf{s}^{(k)} = \mathbf{M} \mathbf{J}^{(k)} \in \mathbb{R}^N$ can be expanded as

$$\mathbf{s}^{(k)} = \mathbf{M} \mathbf{J}^{(k)} = \sum_{i=1}^{N_C} \mathbf{s}_i^{(k)} + \sum_{i=1}^{N_P} \mathbf{s}_i^{(k)\text{P}} = 2 \sum_{i=1}^{N_C} \text{Re} \left(\frac{\lambda_i \mathbf{M} \boldsymbol{\varphi}_i \boldsymbol{\varphi}_i^T \mathbf{M} \mathbf{J}^{(k)}}{a_i} \right) + \sum_{i=1}^{N_P} \frac{\lambda_i^{\text{P}} \mathbf{M} \boldsymbol{\varphi}_i^{\text{P}} (\boldsymbol{\varphi}_i^{\text{P}})^T \mathbf{M} \mathbf{J}^{(k)}}{a_i^{\text{P}}} \quad (3.123)$$

Therefore, the contribution of the i th complex mode to the vector $\mathbf{s}^{(k)} = \mathbf{M}\mathbf{J}^{(k)}$ is

$$\mathbf{s}_i^{(k)} = 2 \operatorname{Re} \left(\frac{\lambda_i \mathbf{M} \boldsymbol{\varphi}_i \boldsymbol{\varphi}_i^T \mathbf{M} \mathbf{J}^{(k)}}{a_i} \right) \in \mathbb{R}^N \quad (3.124)$$

and the contribution of the i th over-damped mode to the vector $\mathbf{s}^{(k)} = \mathbf{M}\mathbf{J}^{(k)}$ is

$$\mathbf{s}_i^{(k)P} = \frac{\lambda_i^P \mathbf{M} \boldsymbol{\varphi}_i^P (\boldsymbol{\varphi}_i^P)^T \mathbf{M} \mathbf{J}^{(k)}}{a_i^P} \in \mathbb{R}^N \quad (3.125)$$

The resulting static base shear force along k direction due to $\mathbf{s}_i^{(k)}$ is defined as the i th effective modal mass, $\hat{m}_i^{(k)\text{eff}}$, associated with the i th complex mode (including its conjugate counterpart). That is,

$$\begin{aligned} V_{bi}^{(k)\text{st}} &= \hat{m}_i^{(k)\text{eff}} \\ &= \sum_{j=1}^N s_{ji}^{(k)} = (\mathbf{J}^{(k)})^T \mathbf{s}_i^{(k)} \\ &= 2 \operatorname{Re} \left(\frac{\lambda_i (\boldsymbol{\varphi}_i^T \mathbf{M} \mathbf{J}^{(k)})^2}{a_i} \right) \in \mathbb{R} \end{aligned} \quad (3.126)$$

Also, the resulting static base shear force along the k direction due to $\mathbf{s}_i^{(k)P}$ is defined as the i th effective modal mass, $\hat{m}_i^{(k)P\text{eff}}$, associated with the i th over-damped mode

$$\begin{aligned} V_{bi}^{(k)P\text{st}} &= \hat{m}_i^{(k)P\text{eff}} \\ &= \sum_{j=1}^N s_{ji}^{(k)P} = (\mathbf{J}^{(k)})^T \mathbf{s}_i^{(k)P} \\ &= \frac{\lambda_i^P [(\boldsymbol{\varphi}_i^P)^T \mathbf{M} \mathbf{J}^{(k)}]^2}{a_i^P} \in \mathbb{R} \end{aligned} \quad (3.127)$$

Similarly, the sum of all general effective modal masses in the k direction is equal to the total unrestrained mass acting in the k direction as

$$M_{\Sigma}^{(k)} = (\mathbf{J}^{(k)})^T \mathbf{M} \mathbf{J}^{(k)} \quad (3.128)$$

Substituting Equation (3.123) into Equation (3.128) gives

$$\begin{aligned}
M_{\Sigma}^{(k)} &= \sum_{i=1}^{N_c} (\mathbf{J}^{(k)})^T \mathbf{s}_i^{(k)} + \sum_{i=1}^{N_p} (\mathbf{J}^{(k)})^T \mathbf{s}_i^{(k)P} \\
&= \sum_{i=1}^{N_c} \hat{m}_i^{(k)\text{eff}} + \sum_{i=1}^{N_p} \hat{m}_i^{(k)\text{Peff}}
\end{aligned} \tag{3.129}$$

The proof is shown. Note that the $\hat{m}_i^{(k)\text{eff}}$ and $\hat{m}_i^{(k)\text{Peff}}$, formulated in methods 1 and 2, may be positive or negative and are independent of how the mode shapes are normalized. This indicates that the summation of the effective modal mass over modes may or may not be monotonic, although the summation contributed from all modes converges to the total mass of the system. In this study, the effective modal mass expressions derived in both methods are considered as indicators to determine the number of modes required in the superposition. The participating mass percentage rule used in classically damped systems still applies in the 3-D arbitrarily damped linear MDOF systems. Table 3.1 gives a summary of the expressions of the effective modal mass acting along the k direction derived by methods 1 and 2, including the special case where classical damping is observed.

Table 3.1 Summary of the expressions of the effective modal mass

Effective Modal Mass	3-D Arbitrarily Damped Systems		Classically Damped Systems
	Method 1	Method 2	
$\hat{m}_i^{(k)\text{eff}}$, under-damped Mode	$-2 \operatorname{Re} \left(\frac{(\boldsymbol{\varphi}_i^T \mathbf{K} \mathbf{J}^{(k)}) (\boldsymbol{\varphi}_i^T \mathbf{M} \mathbf{J}^{(k)})}{\lambda_i a_i} \right)$	$2 \operatorname{Re} \left(\frac{\lambda_i (\boldsymbol{\varphi}_i^T \mathbf{M} \mathbf{J}^{(k)})^2}{a_i} \right)$	$\frac{(\boldsymbol{\varphi}_i^T \mathbf{M} \mathbf{J}^{(k)})^2}{\boldsymbol{\varphi}_i^T \mathbf{M} \boldsymbol{\varphi}_i}$
$\hat{m}_i^{(k)\text{Peff}}$, over-damped Mode	$-\frac{[(\boldsymbol{\varphi}_i^P)^T \mathbf{K} \mathbf{J}^{(k)}][(\boldsymbol{\varphi}_i^P)^T \mathbf{M} \mathbf{J}^{(k)}]}{\lambda_i^P a_i^P}$	$\frac{\lambda_i^P [(\boldsymbol{\varphi}_i^P)^T \mathbf{M} \mathbf{J}^{(k)}]^2}{a_i^P}$	

In parallel with the definition of classically damped systems, the effective modal mass ratios for a 3-D arbitrarily damped system, $R_{m_i}^{(k)}$ and $R_{m_i}^{(k)P}$, are defined as follows

$$\mathbf{R}_{mi}^{(k)} = \hat{m}_i^{(k)\text{eff}} / M_{\Sigma}^{(k)} \quad (3.130)$$

$$\mathbf{R}_{mi}^{(k)P} = \hat{m}_i^{(k)P\text{eff}} / M_{\Sigma}^{(k)} \quad (3.131)$$

Based on Equations (3.120) and (3.129), the following equation can be easily derived

$$\sum_{i=1}^{N_C} \mathbf{R}_{mi}^{(k)} + \sum_{i=1}^{N_P} \mathbf{R}_{mi}^{(k)P} = 1 \quad (3.132)$$

3.6 Reduction to Classically Under-Damped Structures

The formulation above is applicable to all linear systems regardless of the damping distribution. For a structure satisfying the Caughey criterion $\mathbf{C}\mathbf{M}^{-1}\mathbf{K} = \mathbf{K}\mathbf{M}^{-1}\mathbf{C}$ (Caughey and O'Kelly, 1965) with an under-damped assumption (i.e., $N_C = N$ and $N_P = 0$), its mode shapes $\boldsymbol{\varphi}_i$ are real-valued and are consistent with its respective undamped system. Consequently, Equation (2.17) can be reduced to

$$a_i = \boldsymbol{\varphi}_i^T (2\lambda_i \mathbf{M} + \mathbf{C}) \boldsymbol{\varphi}_i = 2m_i (\lambda_i + \xi_i \omega_i) = j2m_i \omega_{di} \quad (3.133)$$

where $m_i = \boldsymbol{\varphi}_i^T \mathbf{M} \boldsymbol{\varphi}_i \in \mathbb{R}$ is the i th modal mass. Revisiting Equation (2.34), the residual matrices become

$$\mathbf{R}_i^R = \text{Re} \left(\frac{\boldsymbol{\varphi}_i \boldsymbol{\varphi}_i^T}{a_i} \right) = \mathbf{0} \in \mathbb{R}^{N \times N} \quad \text{and} \quad \mathbf{R}_i^I = \text{Im} \left(\frac{\boldsymbol{\varphi}_i \boldsymbol{\varphi}_i^T}{a_i} \right) = -\frac{\boldsymbol{\varphi}_i \boldsymbol{\varphi}_i^T}{2m_i \omega_{di}} \in \mathbb{R}^{N \times N} \quad (3.134)$$

Substituting Equation (3.134) into the displacement coefficient vectors as shown in Equations (3.15) and (3.16), respectively, gives

$$\mathbf{A}_{Di} = \mathbf{0} \in \mathbb{R}^{N \times 3} \quad (3.135)$$

$$\mathbf{B}_{Di} = -2\omega_{di} \mathbf{R}_i^I \mathbf{M} \mathbf{J} = \frac{\boldsymbol{\varphi}_i \boldsymbol{\varphi}_i^T \mathbf{M} \mathbf{J}}{m_i} = \boldsymbol{\varphi}_i \boldsymbol{\Gamma}_i \in \mathbb{R}^{N \times 3} \quad (3.136)$$

where $\Gamma_i = \boldsymbol{\varphi}_i^T \mathbf{M} \mathbf{J} / m_i \in \mathbb{R}^{1 \times 3}$ is the i th modal participation factor vector defined for classically damped structures. As a result, the displacement response vector $\mathbf{u}(t, \theta)$ shown in Equation (3.43) reduces to

$$\mathbf{u}(t, \theta) = \sum_{i=1}^N \boldsymbol{\varphi}_i \Gamma_i \mathbf{T} \mathbf{q}_i(t) \quad (3.137)$$

With the same conditions and approaches used for deriving Equation (3.137), the structural velocity $\dot{\mathbf{u}}(t, \theta)$ and absolute acceleration vectors $\ddot{\mathbf{u}}_A(t, \theta)$ can be obtained as

$$\dot{\mathbf{u}}(t, \theta) = \sum_{i=1}^N \boldsymbol{\varphi}_i \Gamma_i \mathbf{T} \dot{\mathbf{q}}_i(t) \quad (3.138)$$

$$\ddot{\mathbf{u}}_A(t, \theta) = \sum_{i=1}^N \boldsymbol{\varphi}_i \Gamma_i \mathbf{T} \left[2\xi_i \omega_i \dot{\mathbf{q}}_i(t) + \omega_i^2 \mathbf{q}_i(t) \right] \quad (3.139)$$

It may be observed from Equation (3.139) that the structural absolute acceleration of a classical under-damped system is the summation of the absolute acceleration response of a series of SDOF systems multiplied with their corresponding modal participation factors and mode shapes.

3.7 Response Expressed in Terms of Seismic Incidence θ

To show the incident angle θ in the expression explicitly, Equation (3.61) is expanded after considering Equations (3.2), (3.30) and (3.37) as

$$\begin{aligned} r_0(t, \theta) = & \sum_{i=1}^{N_C} \left[\mathbf{A}_{0i}^{(1)} \cos \theta \dot{q}_{1i}(t) + \mathbf{A}_{0i}^{(2)} \cos \theta \dot{q}_{2i}(t) - \mathbf{A}_{0i}^{(1)} \sin \theta \dot{q}_{2i}(t) + \mathbf{A}_{0i}^{(2)} \sin \theta \dot{q}_{1i}(t) + \mathbf{A}_{0i}^{(3)} \dot{q}_{3i}(t) \right] \\ & + \sum_{i=1}^{N_C} \left[\mathbf{B}_{0i}^{(1)} \cos \theta q_{1i}(t) + \mathbf{B}_{0i}^{(2)} \cos \theta q_{2i}(t) - \mathbf{B}_{0i}^{(1)} \sin \theta q_{2i}(t) + \mathbf{B}_{0i}^{(2)} \sin \theta q_{1i}(t) + \mathbf{B}_{0i}^{(3)} q_{3i}(t) \right] \\ & + \sum_{i=1}^{N_p} \left[\mathbf{A}_{0i}^{P(1)} \cos \theta q_{1i}^P(t) + \mathbf{A}_{0i}^{P(2)} \cos \theta q_{2i}^P(t) - \mathbf{A}_{0i}^{P(1)} \sin \theta q_{2i}^P(t) + \mathbf{A}_{0i}^{P(2)} \sin \theta q_{1i}^P(t) + \mathbf{A}_{0i}^{P(3)} q_{3i}^P(t) \right] \end{aligned} \quad (3.140)$$

In the following derivation, it is convenient to rewrite Equation (3.140) in the following form.

$$\begin{aligned}
r_0(t, \theta) = & \left\{ \sum_{i=1}^{N_c} [A_{0i}^{(1)} \dot{q}_{1i}(t) + B_{0i}^{(1)} q_{1i}(t)] + \sum_{i=1}^{N_p} [A_{0i}^{P(1)} q_{1i}^P(t)] \right\} \cos \theta \\
& + \left\{ \sum_{i=1}^{N_c} [A_{0i}^{(2)} \dot{q}_{2i}(t) + B_{0i}^{(2)} q_{2i}(t)] + \sum_{i=1}^{N_p} [A_{0i}^{P(2)} q_{2i}^P(t)] \right\} \cos \theta \\
& - \left\{ \sum_{i=1}^{N_c} [A_{0i}^{(1)} \dot{q}_{2i}(t) + B_{0i}^{(1)} q_{2i}(t)] + \sum_{i=1}^{N_p} [A_{0i}^{P(1)} q_{2i}^P(t)] \right\} \sin \theta \\
& + \left\{ \sum_{i=1}^{N_c} [A_{0i}^{(2)} \dot{q}_{1i}(t) + B_{0i}^{(2)} q_{1i}(t)] + \sum_{i=1}^{N_p} [A_{0i}^{P(2)} q_{1i}^P(t)] \right\} \sin \theta \\
& + \left\{ \sum_{i=1}^{N_c} [A_{0i}^{(3)} \dot{q}_{3i}(t) + B_{0i}^{(3)} q_{3i}(t)] + \sum_{i=1}^{N_p} [A_{0i}^{P(3)} q_{3i}^P(t)] \right\}
\end{aligned} \tag{3.141}$$

Further, the first term on the right side of Equation (3.141) is defined as $r_{1x}(t) \cos \theta$. $r_{1x}(t)$ can be interpreted as the response resulting from the ground acceleration $\ddot{u}_{g1}(t)$ applied in the **X**-direction. By analogy, the remaining four terms on the right side of Equation (3.141) can be defined as $r_{2y}(t) \cos \theta$, $r_{2x}(t) \sin \theta$, $r_{1y}(t) \sin \theta$ and $r_{3z}(t)$, respectively. $r_{2y}(t)$ represents the response due to the ground acceleration $\ddot{u}_{g2}(t)$ applied in the **Y**-direction, $r_{2x}(t)$ represents the response due to the ground acceleration $\ddot{u}_{g2}(t)$ applied in the **X**-direction and $r_{1y}(t)$ is the response due to the ground acceleration $\ddot{u}_{g1}(t)$ applied in the **Y**-direction while $r_{3z}(t)$ is the response due to the ground acceleration $\ddot{u}_{g3}(t)$ applied in the **Z**-direction. Hence, Equation (3.141) can also be expressed as

$$r_0(t, \theta) = [r_{1x}(t) + r_{2y}(t)] \cos \theta + [r_{1y}(t) - r_{2x}(t)] \sin \theta + r_{3z}(t) \tag{3.142}$$

As shown in Chapter 5, this expression is convenient for determining the peak response within the entire response history when all possible angle θ are considered (Lopez and Torres, 1997).

CHAPTER 4

DEVELOPMENT OF THE RESPONSE SPECTRUM METHOD

4.1 Introduction

In general, there is no need to know the complete response history of a structure for design purposes. Instead, the peak value of the response parameters is the primary concern. In earthquake engineering, the response spectrum method is commonly used as an alternative approach to response history analysis for determining the maximum values of the seismic responses of classically damped structures. In this method, the modal peak responses are obtained using a prescribed response spectrum. These modal maxima are then appropriately combined to estimate the peak values of the responses of interest. This chapter presents a general modal combination rule for the response spectrum method targeted for 3-D arbitrarily damped linear structures. The derivation is based on the theory of the general modal response history analysis developed in Chapter 3, relying on the fact that the strong phase of the ground motion is approximately stationary and a set of orthogonal axes exist along which the three ground motion components can be considered as mutually uncorrelated. As noted in Chapter 3, over-critically damped modes may develop, such as for a building with added seismic response modification devices. To account for the over-critically damped modes when the seismic inputs are described in terms of response spectra, a new over-damped mode response spectrum is introduced. It follows a similar concept as the conventional response spectrum and is able to describe the peak modal response of the over-damped modes. The mutual interrelationships between the modal displacement response and the modal velocity response as well as the over-damped modal response among each mode are considered in this general modal combination rule. This rule is also applicable to response quantities other than nodal displacements by taking advantage of the unified form presented in Chapter 3. In this study, the rule is referred to as the General-Complete-Quadratic-Combination-3 (GCQC3) rule. In addition, to aid in practical engineering applications, a transformation procedure to construct an over-damped mode response spectrum consistent with the given 5% design response spectrum is established. The adequacy of this transformation procedure is validated.

4.2 Current Directional Combination Rules for Multi-component Excitation

Multi-component ground motions should be considered in seismic analysis and design. Most design codes specify that the contributions from each ground motion component are combined through percentage rules or Square-Root-of-Sum-of-Squares (SRSS) rule. AASHTO (2004) and Caltrans (2004) have accepted the 30% rule to be used in directional combinations, while the SRSS rule and the 40% rule are suggested by other codes and guidelines (Nutt, 1996; MCEER, 2003). The 2003 edition of the International Building Code (IBC, 2003) requires the use of the SRSS rule or 30% rule. Another commonly used rule is the CQC3 rule (Semby and Der Kiureghian, 1985), which considers the correlations between each ground component. Among these combination rules, the choice of the critical seismic input direction is not specified and is left to the designers. These rules are described in the following subsections.

4.2.1 SRSS Rule

The estimate of the peak response R can be calculated by the square-root-of-sum-of-squares rule as:

$$R = \sqrt{R_x^2 + R_y^2 + R_z^2} \quad (4.1)$$

where R_k is the contribution to the response quantity R from the k th component of ground motion ($k = \{x, y, z\}$). The basic assumption of this rule is the response quantities R_x , R_y and R_z are statistically independent.

4.2.2 Percentage Rule

The percentage rule is considered to have originated from the work of Newmark (1975) and Rosenblueth and Contreras (1977). The total response R is approximated by the sum of 100% of the response due to the input in one direction and a certain percentage, α , of the responses to the inputs in the other two directions. As a result, the following three cases must be considered. The combination that gives the largest value is adopted for design.

$$\begin{aligned}
R &= R_x + \alpha R_y + \alpha R_z \\
R &= \alpha R_x + R_y + \alpha R_z \\
R &= \alpha R_x + \alpha R_y + R_z
\end{aligned}
\tag{4.2}$$

where $\alpha = 30\%$ or 40% .

Newmark (1975) used the percentage rule with $\alpha = 40\%$ as an alternative to the SRSS rule. He explained that this method would be slightly conservative for most cases compared to the SRSS rule and would be adequate as its degree of conservatism is relatively small. Rosenblueth and Contreras (1977) suggested $\alpha = 30\%$ for regular structures and $\alpha = 50\%$ for special structures in order to minimize errors. Note that the percentage rules have no theoretical basis.

4.2.3 CQC3 Rule

Semby and Der Kiureghian (1985) proposed the CQC3 combination rule to consider the multi-component excitation effects. The detailed formulation and features of CQC3 are not addressed in this section as it is a special case of the general modal combination rule developed in this study, as shown in Section 4.4.3.

4.3 Ground Motion Model

Basically, earthquake-induced ground motion is described by a vector process consisting of three translational orthogonal components. Penzien and Watabe (1975) have shown that a set of orthogonal axes exist, along which ground motion components can be considered as uncorrelated, and whose orientation remains reasonably stable during the strong ground motion phase. These axes are called the principal axes of the ground motion. It was observed that the major principal axis lies on the horizontal plane and is directed toward the epicenter, the intermediate axis is perpendicular to the major axis within the horizontal plane, and the minor axis is nearly vertical. Thus, based on their study, the transformation, which is a rotation about the vertical axis, between the components along the principal axes, $\ddot{\mathbf{u}}_g(t) = [\ddot{u}_{g1}(t) \quad \ddot{u}_{g2}(t) \quad \ddot{u}_{g3}(t)]^T$, and those along the structure reference axes, $\ddot{\mathbf{u}}'_g(t) = [\ddot{u}'_{gx}(t) \quad \ddot{u}'_{gy}(t) \quad \ddot{u}'_{gz}(t)]^T$, can be expressed as

$$\ddot{\mathbf{u}}'_g(t) = \mathbf{T}\ddot{\mathbf{u}}_g(t) \quad (4.3)$$

\mathbf{T} is the coordinate transformation matrix defined in Chapter 2. The correlation matrix for the components of ground motion along the reference axes of a structure can be written as

$$\mathbf{R}_{\ddot{\mathbf{u}}'_g \ddot{\mathbf{u}}'_g} = E[\ddot{\mathbf{u}}'_g \ddot{\mathbf{u}}'^T_g] = \mathbf{T} E[\ddot{\mathbf{u}}_g \ddot{\mathbf{u}}^T_g] \mathbf{T}^T \quad (4.4)$$

in which

$$E[\ddot{\mathbf{u}}_g(t) \ddot{\mathbf{u}}^T_g(t)] = \begin{bmatrix} E[\ddot{u}_{g1}(t) \ddot{u}_{g1}(t)] & 0 & 0 \\ 0 & E[\ddot{u}_{g2}(t) \ddot{u}_{g2}(t)] & 0 \\ 0 & 0 & E[\ddot{u}_{g3}(t) \ddot{u}_{g3}(t)] \end{bmatrix} \quad (4.5)$$

is a diagonal matrix since the three components of ground motion, along with their respective principal axes, are uncorrelated.

Each element in Equation (4.4), representing the cross correlation between each ground motion component along the structure reference axes, can be written as

$$\begin{aligned} E[\ddot{u}'_{gx}(t) \ddot{u}'_{gx}(t)] &= E[\ddot{u}_{g1}(t) \ddot{u}_{g1}(t)] \cos^2 \theta + E[\ddot{u}_{g2}(t) \ddot{u}_{g2}(t)] \sin^2 \theta \\ E[\ddot{u}'_{gy}(t) \ddot{u}'_{gy}(t)] &= E[\ddot{u}_{g1}(t) \ddot{u}_{g1}(t)] \sin^2 \theta + E[\ddot{u}_{g2}(t) \ddot{u}_{g2}(t)] \cos^2 \theta \\ E[\ddot{u}'_{gx}(t) \ddot{u}'_{gy}(t)] &= \{E[\ddot{u}_{g1}(t) \ddot{u}_{g1}(t)] - E[\ddot{u}_{g2}(t) \ddot{u}_{g2}(t)]\} \sin \theta \cos \theta \\ E[\ddot{u}'_{gz}(t) \ddot{u}'_{gz}(t)] &= E[\ddot{u}_{g3}(t) \ddot{u}_{g3}(t)] \\ E[\ddot{u}'_{gx}(t) \ddot{u}'_{gz}(t)] &= E[\ddot{u}'_{g3}(t) \ddot{u}'_{g1}(t)] = E[\ddot{u}'_{g3}(t) \ddot{u}'_{g2}(t)] = E[\ddot{u}'_{g2}(t) \ddot{u}'_{g3}(t)] = 0 \end{aligned} \quad (4.6)$$

4.4 General Modal Combination Rule for Multi-component Excitation

A general modal combination rule for multidirectional excitation, based on the general modal response history analysis derived in Chapter 3, is formulated in this section to estimate the peak response using the response spectrum. Derivation of the modal combination rule follows the theory of random vibration and Penzien's ground motion model.

4.4.1 Definition of Vector Operation Symbols

Before developing the formulation, it is useful to define a number of vector operators for convenience. They are:

• : Vector multiplication. For example, assuming that \mathbf{a} , \mathbf{b} and \mathbf{c} have the same dimension, $\mathbf{c} = \mathbf{a} \cdot \mathbf{b}$ means that each element in vector \mathbf{c} is the product of the corresponding element in \mathbf{a} and \mathbf{b} .

$\{\}^{1/2}$ or $\sqrt{\{\}}$: Taking the square root of each element in the vector $\{\}$ individually.

$\{\}^2$: Taking the square of the element in the vector $\{\}$ individually.

$\{\}_{\max}$: Representing the peak response of each response history in the vector $\{\}$.

4.4.2 Modal Response to Stationary Excitation

Consider the input ground acceleration vector $\ddot{\mathbf{u}}_g(t)$ as a zero-mean wide-band stationary vector process. Based on the theory of random vibration, the responses of a linear structure subjected to a stationary process vector are also stationary. For the following derivations, it is convenient to revisit the following expressions shown in Chapter 3.

$$q_{ki}(t) = \int_0^t h_i(t-\tau) \ddot{u}_{gk}(\tau) d\tau \quad (4.7)$$

$$q_{ki}^p(t) = \int_0^t h_i^p(t-\tau) \ddot{u}_{gk}(\tau) d\tau \quad (4.8)$$

$$H_i(s = j\omega) = \int_{-\infty}^{+\infty} h_i(t) e^{j\omega t} dt = -\frac{1}{-\omega^2 + j2\xi_i \omega_i \omega + \omega_i^2} \quad (4.9)$$

$$H_{v_i}(s = j\omega) = j\omega H_i(j\omega) = -\frac{j\omega}{-\omega^2 + j2\xi_i \omega_i \omega + \omega_i^2} \quad (4.10)$$

$$H_i^p(s = j\omega) = -\frac{1}{j\omega + \omega_i^p} \quad (4.11)$$

In Equations (4.7) and (4.8), $k = 1, 2, 3$.

4.4.2.1 Displacement-Displacement Covariance

The displacement covariance produced by modes i and j subjected to ground acceleration $\ddot{u}_{gk}(t)$ and $\ddot{u}_{gl}(t)$, respectively, are now examined. The covariance can be written as

$$E[q_{ki}(t)q_{lj}(t)] = \int_0^t \int_0^t h_i(\tau_1)h_j(\tau_2) E[\ddot{u}_{gk}(t-\tau_1)\ddot{u}_{gl}(t-\tau_2)] d\tau_1 d\tau_2 \quad (4.12)$$

in which $k, l = 1, 2, 3$. Knowing that ground excitation $\ddot{u}_{gk}(t)$ or $\ddot{u}_{gl}(t)$ commences from zero at the time instant $t = 0$ (i.e. $\ddot{u}_{gk}(t) = 0$ or $\ddot{u}_{gl}(t) = 0$ when $t \leq 0$), it is reasonable to extend the lower limit of the integration to negative infinity as

$$E[q_{ki}(t)q_{lj}(t)] = \int_{-\infty}^t \int_{-\infty}^t h_i(\tau_1)h_j(\tau_2) E[\ddot{u}_{gk}(t-\tau_1)\ddot{u}_{gl}(t-\tau_2)] d\tau_1 d\tau_2 \quad (4.13)$$

Now, suppose that the all ground motion components are white noise processes with zero mean, described by a constant power spectral density S_0 . It follows that the term $E[\ddot{u}_{gk}(t-\tau_1)\ddot{u}_{gl}(t-\tau_2)]$ becomes (Semby and Der Kiureghian, 1985; Zhou et al., 2004)

$$E[\ddot{u}_{gk}(t-\tau_1)\ddot{u}_{gl}(t-\tau_2)] = \begin{cases} 2\pi S_0 \delta(\tau_1 - \tau_2) & k = l \\ 0 & k \neq l \end{cases} \quad (4.14)$$

where $\delta(\tau)$ is the Dirac function and is defined as follows.

$$\delta(\tau) = \begin{cases} \infty & \tau = 0 \\ 0 & \tau \neq 0 \end{cases} \quad (4.15)$$

and

$$\int_{-\infty}^{+\infty} \delta(\tau) d\tau = 1 \quad (4.16)$$

In light of the inverse of Fourier transform, the Dirac function also can be expressed as

$$\delta(\tau) = \frac{1}{2\pi} \int_{-\infty}^{+\infty} e^{-j\omega\tau} d\omega \quad (4.17)$$

or

$$\delta(\tau_1 - \tau_2) = \frac{1}{2\pi} \int_{-\infty}^{+\infty} e^{-j\omega(\tau_1 - \tau_2)} d\omega \quad (4.18)$$

Substituting Equations (4.14) and (4.18) into Equation (4.13) and setting the upper integral limit to infinity to retain the steady state response, Equation (4.13) becomes

$$E[q_{ki}(\infty)q_{lj}(\infty)] = \begin{cases} S_0 \int_{-\infty}^{+\infty} \left(\int_{-\infty}^{+\infty} h_i(\tau_1) e^{-j\omega\tau_1} d\tau_1 \int_{-\infty}^{+\infty} h_j(\tau_2) e^{j\omega\tau_2} d\tau_2 \right) d\omega & k=l \\ 0 & k \neq l \end{cases} \quad (4.19)$$

Making use of Equation (4.9), Equation (4.19) may be written as

$$R_{ij}^{(kl)DD} = E[q_{ki}(\infty)q_{lj}(\infty)] = \begin{cases} S_0 \int_{-\infty}^{+\infty} H_i(j\omega)H_j(-j\omega)d\omega & k=l \\ 0 & k \neq l \end{cases} \quad (4.20)$$

Define ρ_{ij}^{DD} as

$$\rho_{ij}^{DD} = \frac{\text{Re} \int_{-\infty}^{+\infty} H_i(j\omega)H_j(-j\omega)d\omega}{\sqrt{\int_{-\infty}^{+\infty} H_i(j\omega)H_i(-j\omega)d\omega} \sqrt{\int_{-\infty}^{+\infty} H_j(j\omega)H_j(-j\omega)d\omega}} \quad (4.21)$$

Substituting Equation (4.9) into Equation (4.21) and using contour integration in the complex plane yields

$$\rho_{ij}^{DD} = \frac{8\sqrt{\xi_i\xi_j}(\gamma_{ij}\xi_i + \xi_j)\gamma_{ij}^{3/2}}{(1-\gamma_{ij}^2)^2 + 4\xi_i\xi_j\gamma_{ij}(1+\gamma_{ij}^2) + 4(\xi_i^2 + \xi_j^2)\gamma_{ij}^2}, \quad (\gamma_{ij} = \omega_i/\omega_j, \quad i, j = 1, 2, \dots, N_C) \quad (4.22)$$

is the well-known displacement correlation coefficient originally derived for the CQC rule (Der Kiureghian, 1981). As a result, Equation (4.20) can be written as

$$R_{ij}^{(kl)DD} = \begin{cases} \frac{\pi S_0}{2\omega_i\omega_j\sqrt{\omega_i\omega_j\xi_i\xi_j}} \rho_{ij}^{DD} & k=l \\ 0 & k \neq l \end{cases} \quad (4.23)$$

Let $i = j$ in Equation (4.23), the i th modal displacement variance can be obtained as

$$R_{ii}^{(kl)DD} = \begin{cases} \frac{\pi S_0}{2\xi_i\omega_i^3} & k=l \\ 0 & k \neq l \end{cases} \quad (4.24)$$

Consequently, Equation (4.23) can be simplified as

$$R_{ij}^{(kl)DD} = \begin{cases} \sqrt{R_{ii}^{(kk)DD} R_{jj}^{(ll)DD}} \rho_{ij}^{DD}, & k = l \\ 0 & k \neq l \end{cases} \quad (i, j = 1, 2, \dots, N_C) \quad (4.25)$$

4.4.2.2 Velocity-Velocity Covariance

Following similar procedures as the derivation modal displacement response covariance $R_{ij}^{(kl)DD}$, the modal velocity response covariance $R_{ij}^{(kl)VV}$ can also be derived as (Zhou et al., 2004)

$$\begin{aligned} R_{ij}^{(kl)VV} &= E[\dot{q}_{ki}(\infty)\dot{q}_{lj}(\infty)] \\ &= \begin{cases} S_0 \int_{-\infty}^{+\infty} \omega^2 H_i(j\omega)H_j(-j\omega)d\omega & k = l \\ 0 & k \neq l \end{cases} \\ &= \begin{cases} \frac{\pi S_0}{2\sqrt{\omega_i \omega_j \xi_i \xi_j}} \rho_{ij}^{VV} & k = l \\ 0 & k \neq l \end{cases} \\ &= \begin{cases} \omega_i \omega_j \sqrt{R_{ii}^{(kk)DD} R_{jj}^{(ll)DD}} \rho_{ij}^{VV} & k = l \\ 0 & k \neq l \end{cases}, \quad (i, j = 1, 2, \dots, N_C) \end{aligned} \quad (4.26)$$

where

$$\begin{aligned} \rho_{ij}^{VV} &= \frac{\text{Re} \int_{-\infty}^{\infty} \omega^2 H_i(j\omega)H_j(-j\omega)d\omega}{\sqrt{\int_{-\infty}^{\infty} \omega^2 H_i(j\omega)H_i(-j\omega)d\omega} \sqrt{\int_{-\infty}^{\infty} \omega^2 H_j(j\omega)H_j(-j\omega)d\omega}} \\ &= \frac{8\sqrt{\xi_i \xi_j} (\xi_i + \gamma_{ij} \xi_j) \gamma_{ij}^{3/2}}{(1 - \gamma_{ij}^2)^2 + 4\xi_i \xi_j \gamma_{ij} (1 + \gamma_{ij}^2) + 4(\xi_i^2 + \xi_j^2) \gamma_{ij}^2}, \quad (\gamma_{ij} = \omega_i / \omega_j, \quad i, j = 1, 2, \dots, N_C) \end{aligned} \quad (4.27)$$

is the modal velocity correlation coefficient. A new parameter μ_{ij} is introduced and defined as

$$\mu_{ij} = \frac{\rho_{ij}^{VV}}{\rho_{ij}^{DD}} = \frac{\xi_i + \xi_j \gamma_{ij}}{\xi_j + \xi_i \gamma_{ij}}, \quad (i, j = 1, 2, \dots, N_C) \quad (4.28)$$

The modal velocity covariance $R_{ij}^{(kl)VV}$ can now be written as

$$R_{ij}^{(kl)VV} = \begin{cases} \omega_i \omega_j \mu_{ij} \sqrt{R_{ii}^{(kk)DD} R_{jj}^{(ll)DD}} \rho_{ij}^{DD} & k = l \\ 0 & k \neq l \end{cases}, \quad (i, j = 1, 2, \dots, N_C) \quad (4.29)$$

4.4.2.3 Velocity-Displacement Covariance

Following the same steps as described above, the covariance of response produced by the i th modal velocity and j th modal displacement is found to be (Zhou et al., 2004)

$$\begin{aligned} R_{ij}^{(kl)VD} &= E[\dot{q}_{ki}(\infty)q_{lj}(\infty)] \\ &= \begin{cases} S_0 \int_{-\infty}^{\infty} j\omega H_i(j\omega)H_j(-j\omega)d\omega & k = l \\ 0 & k \neq l \end{cases} \\ &= \begin{cases} \frac{\pi S_0}{2\omega_j \sqrt{\omega_i \omega_j \xi_i \xi_j}} \rho_{ij}^{VD} & k = l \\ 0 & k \neq l \end{cases} \\ &= \begin{cases} \omega_i \sqrt{R_{ii}^{(kk)DD} R_{jj}^{(ll)DD}} \rho_{ij}^{VD} & k = l \\ 0 & k \neq l \end{cases}, \quad (i, j = 1, 2, \dots, N_C) \end{aligned} \quad (4.30)$$

where

$$\begin{aligned} \rho_{ij}^{VD} &= \frac{\text{Re} \int_{-\infty}^{+\infty} j\omega H_i(j\omega)H_j(-j\omega)d\omega}{\sqrt{\int_{-\infty}^{+\infty} \omega^2 H_i(j\omega)H_i(-j\omega)d\omega} \sqrt{\int_{-\infty}^{+\infty} H_j(j\omega)H_j(-j\omega)d\omega}} \\ &= \frac{4\sqrt{\xi_i \xi_j} (1 - \gamma_{ij}^2) \gamma_{ij}^{1/2}}{(1 - \gamma_{ij}^2)^2 + 4\xi_i \xi_j \gamma_{ij} (1 + \gamma_{ij}^2) + 4(\xi_i^2 + \xi_j^2) \gamma_{ij}^2}, \quad (\gamma_{ij} = \omega_i / \omega_j, \quad i, j = 1, 2, \dots, N_C) \end{aligned} \quad (4.31)$$

is the modal velocity-displacement correlation coefficient. Another new parameter ν_{ij} is introduced and defined as

$$v_{ij} = \frac{\rho_{ij}^{\text{VD}}}{\rho_{ij}^{\text{DD}}} = \frac{1 - \gamma_{ij}^2}{2\gamma_{ij}(\xi_j + \xi_i \gamma_{ij})}, \quad (i, j = 1, 2, \dots, N_C) \quad (4.32)$$

Now, Equation (4.30) may be written as

$$R_{ij}^{(kl)\text{VD}} = \begin{cases} \omega_i v_{ij} \sqrt{R_{ii}^{(kk)\text{DD}} R_{jj}^{(ll)\text{DD}}} \rho_{ij}^{\text{DD}} & k = l \\ 0 & k \neq l \end{cases}, \quad (i, j = 1, 2, \dots, N_C) \quad (4.33)$$

Note that when $i = j$, the variance of the modal velocity response $R_{ii}^{(kk)\text{VV}}$ and the covariance of the modal velocity and modal displacement response $R_{ij}^{(kk)\text{VD}}$ becomes

$$R_{ii}^{(kk)\text{VV}} = \frac{\pi S_0}{2\omega_i \xi_i} = \omega_i^2 R_{ii}^{(kk)\text{DD}} \quad (4.34)$$

and
$$R_{ii}^{(kk)\text{VD}} = 0 \quad (4.35)$$

It is clear from Equations (4.34) and (4.35) that for an SDOF system, the velocity variance and displacement variance are related by the squares of its natural circular frequency, and the modal displacement and velocity response are orthogonal with each other under the white noise excitation assumption. It may also be observed from Equations (4.26) and (4.30) that the velocity covariance $R_{ij}^{(kk)\text{VV}}$ and the velocity-displacement covariance $R_{ij}^{(kk)\text{VD}}$ can simply be expressed in terms of the modal displacement variance $R_{ii}^{(kk)\text{DD}}$. They are connected by the two correlation coefficients ρ_{ij}^{VV} and ρ_{ij}^{VD} . The presence of $R_{ij}^{(kl)\text{VV}}$ and $R_{ij}^{(kl)\text{VD}}$ is due to the non-classical damping effect, where vibration phase differences exist among each DOF.

4.4.2.4 Covariance Among Over-damped Modal Responses

To examine the covariance associated with over-damped modes (i.e., over-damped modal response), the over-damped modal response covariance term is considered as follows

$$R_{ij}^{(kl)PP} = E[q_{ki}^p(t)q_{lj}^p(t)]$$

$$= \begin{cases} S_0 \int_{-\infty}^{+\infty} H_i^p(j\omega)H_j^p(-j\omega)d\omega & k=l \\ 0 & k \neq l \end{cases}, \quad (i, j = 1, 2, \dots, N_p) \quad (4.36)$$

Substitution of Equation (4.11) into Equation (4.36) and manipulation with contour integration in complex plane leads to

$$R_{ij}^{(kl)PP} = \begin{cases} \frac{2\pi S_0}{\omega_i^p + \omega_j^p} & k=l \\ 0 & k \neq l \end{cases}, \quad (i, j = 1, 2, \dots, N_p) \quad (4.37)$$

Similarly, considering the over-damped modal response variance by letting $i = j$ leads to

$$R_{ii}^{(kk)PP} = \begin{cases} \frac{\pi S_0}{\omega_i^p} & k=l \\ 0 & k \neq l \end{cases}, \quad (i, j = 1, 2, \dots, N_p) \quad (4.38)$$

Thus, Equation (4.37) can be rewritten as

$$R_{ij}^{(kl)PP} = \begin{cases} \sqrt{R_{ii}^{(kk)PP} R_{jj}^{(ll)PP}} \rho_{ij}^{PP} & k=l \\ 0 & k \neq l \end{cases}, \quad (i, j = 1, 2, \dots, N_p) \quad (4.39)$$

in which

$$\rho_{ij}^{PP} = \frac{\text{Re} \int_{-\infty}^{+\infty} H_i^p(j\omega)H_j^p(-j\omega)d\omega}{\sqrt{\int_{-\infty}^{+\infty} H_i^p(j\omega)H_i^p(-j\omega)d\omega} \sqrt{\int_{-\infty}^{+\infty} H_j^p(j\omega)H_j^p(-j\omega)d\omega}} \quad (4.40)$$

$$= \frac{2\sqrt{\omega_i^p \omega_j^p}}{\omega_i^p + \omega_j^p}, \quad (i, j = 1, 2, \dots, N_p)$$

is a newly derived correlation coefficient that accounts for the relationship between each over-damped modal response.

4.4.2.5 Displacement Over-damped Covariance

Similarly, the modal displacement and over-damped modal response covariance term can be obtained as

$$\begin{aligned}
 R_{ij}^{(kl)DP} &= E[q_{ki}(\infty)q_{kj}^p(\infty)] \\
 &= \begin{cases} S_0 \int_{-\infty}^{+\infty} H_i(j\omega)H_j^p(-j\omega)d\omega & k=l \\ 0 & k \neq l \end{cases} \\
 &= \begin{cases} \frac{2\pi S_0}{\omega_i^2 + 2\xi_i \omega_i \omega_j^p + (\omega_j^p)^2} & k=l \\ 0 & k \neq l \end{cases} \quad (4.41) \\
 &= \begin{cases} \sqrt{R_{ii}^{(kk)DD} R_{jj}^{(ll)PP}} \rho_{ij}^{DP} & k=l \\ 0 & k \neq l \end{cases}, \quad (i=1,2,\dots,N_C, j=1,2,\dots,N_P)
 \end{aligned}$$

where

$$\begin{aligned}
 \rho_{ij}^{DP} &= \frac{\text{Re} \int_{-\infty}^{+\infty} H_i(j\omega)H_j^p(-j\omega)d\omega}{\sqrt{\int_{-\infty}^{+\infty} H_i(j\omega)H_i(-j\omega)d\omega} \sqrt{\int_{-\infty}^{+\infty} H_j^p(j\omega)H_j^p(-j\omega)d\omega}} \\
 &= \frac{2\omega_i \sqrt{2\xi_i \omega_i \omega_j^p}}{\omega_i^2 + 2\xi_i \omega_i \omega_j^p + (\omega_j^p)^2}, \quad (i=1,2,\dots,N_C, j=1,2,\dots,N_P)
 \end{aligned} \quad (4.42)$$

is the correlation coefficient which accounts for the correlation between the modal displacements and the over-damped modal response.

4.4.2.6 Velocity Over-damped Covariance

By analogy, the modal velocity and over-damped modal response covariance term

$E[\dot{q}_{ki}(t)q_{lj}^p(t)]$ will be of the form

$$\begin{aligned}
R_{ij}^{(kl)VP} &= E \left[\dot{q}_{ki}(\infty) q_{lj}^p(\infty) \right] \\
&= \begin{cases} S_0 \int_{-\infty}^{+\infty} H_{Vi}(j\omega) H_j^p(-j\omega) d\omega & k=l \\ 0 & k \neq l \end{cases} \\
&= \begin{cases} \frac{2\pi\omega_j^p S_0}{\omega_i^2 + 2\xi_i \omega_i \omega_j^p + (\omega_j^p)^2} & k=l \\ 0 & k \neq l \end{cases} \\
&= \begin{cases} \sqrt{R_{ii}^{(kk)DD} R_{jj}^{(ll)PP}} \omega_j^p \rho_{ij}^{DP} & k=l \\ 0 & k \neq l \end{cases}, \quad (i=1,2,\dots,N_C, j=1,2,\dots,N_P)
\end{aligned} \tag{4.43}$$

Note that Equations (4.39), (4.41) and (4.43) are new relationships established in this study to consider the presence of the over-damped modes.

4.4.3 Complete Quadratic Combination of Modal Responses

Consider a response $r_0(t)$ which has contributions from all N modes as shown by

$$\begin{aligned}
r_0(t) &= \mathbf{d}^T \mathbf{u}_0(t) \\
&= \sum_{i=1}^{N_C} \left[\mathbf{d}^T \mathbf{A}_{0i} \mathbf{T} \dot{\mathbf{q}}_i(t) + \mathbf{d}^T \mathbf{B}_{0i} \mathbf{T} \mathbf{q}_i(t) \right] + \sum_{i=1}^{N_P} \mathbf{d}^T \mathbf{A}_{0i}^p \mathbf{T} \mathbf{q}_i^p(t)
\end{aligned} \tag{4.44}$$

The corresponding covariance or mean square response of $r_0(t)$, is then given by

$$\begin{aligned}
E \left[r_0^2(t) \right] &= E \left[\mathbf{d}^T \mathbf{u}_0(t) \mathbf{u}_0^T(t) \mathbf{d} \right] \\
&= \mathbf{d}^T \left\{ \begin{aligned} & \sum_{i=1}^{N_C} \sum_{j=1}^{N_C} \left[\mathbf{A}_{0i} \mathbf{T} E \left[\dot{\mathbf{q}}_i(t) \dot{\mathbf{q}}_j^T(t) \right] \mathbf{T}^T \mathbf{A}_{0j}^T + \mathbf{B}_{0i} \mathbf{T} E \left[\mathbf{q}_i(t) \mathbf{q}_j^T(t) \right] \mathbf{T}^T \mathbf{B}_{0j}^T \right. \\ & \left. + \mathbf{A}_{0i} \mathbf{T} E \left[\dot{\mathbf{q}}_i(t) \mathbf{q}_j^T(t) \right] \mathbf{T}^T \mathbf{B}_{0j}^T + \mathbf{B}_{0i} \mathbf{T} E \left[\mathbf{q}_i(t) \dot{\mathbf{q}}_j^T(t) \right] \mathbf{T}^T \mathbf{A}_{0j}^T \right. \\ & + \sum_{i=1}^{N_C} \sum_{j=1}^{N_P} \left[\mathbf{A}_{0i} \mathbf{T} E \left[\dot{\mathbf{q}}_i(t) (\mathbf{q}_j^p)^T(t) \right] \mathbf{T}^T (\mathbf{A}_{0j}^p)^T + \mathbf{A}_{0i}^p \mathbf{T} E \left[\mathbf{q}_i^p(t) \dot{\mathbf{q}}_j(t) \right] \mathbf{T}^T \mathbf{A}_{0j}^T \right. \\ & \left. + \mathbf{B}_{0i} \mathbf{T} E \left[\mathbf{q}_i(t) (\mathbf{q}_j^p)^T(t) \right] \mathbf{T}^T (\mathbf{A}_{0j}^p)^T + \mathbf{A}_{0i}^p \mathbf{T} E \left[\mathbf{q}_i^p(t) \mathbf{q}_j(t) \right] \mathbf{T}^T \mathbf{B}_{0j}^T \right. \\ & \left. + \sum_{i=1}^{N_P} \sum_{j=1}^{N_P} \mathbf{A}_{0i}^p \mathbf{T} E \left[\mathbf{q}_i^p(t) (\mathbf{q}_j^p)^T(t) \right] \mathbf{T}^T (\mathbf{A}_{0j}^p)^T \right. \end{aligned} \right\} \mathbf{d}
\end{aligned} \tag{4.45}$$

Now, considering the modal covariance shown in Equations (4.25), (4.29), (4.33), (4.39), (4.41) and (4.43) into Equation (4.45) leads to a matrix form as

$$\begin{aligned}
E[r_0^2(t)] = & \mathbf{d}^T \left\{ \sum_{i=1}^{N_c} \sum_{j=1}^{N_c} \rho_{ij}^{DD} \mathbf{B}_{0i} \mathbf{T} \sqrt{\mathbf{R}_i^{DD}} \sqrt{\mathbf{R}_j^{DD}} \mathbf{T}^T \mathbf{B}_{0j}^T + \sum_{i=1}^{N_c} \sum_{j=1}^{N_c} \rho_{ij}^{DD} \mu_{ij} \omega_i \omega_j \mathbf{A}_{0i} \mathbf{T} \sqrt{\mathbf{R}_i^{DD}} \sqrt{\mathbf{R}_j^{DD}} \mathbf{T}^T \mathbf{A}_{0j}^T \right. \\
& + \sum_{i=1}^{N_c} \sum_{j=1}^{N_c} \rho_{ij}^{DD} \nu_{ij} \omega_j \mathbf{A}_{0i} \mathbf{T} \sqrt{\mathbf{R}_i^{DD}} \sqrt{\mathbf{R}_j^{DD}} \mathbf{T}^T \mathbf{B}_{0j}^T + \sum_{i=1}^{N_c} \sum_{j=1}^{N_c} \rho_{ij}^{DD} \nu_{ij} \omega_j \mathbf{B}_{0i} \mathbf{T} \sqrt{\mathbf{R}_i^{DD}} \sqrt{\mathbf{R}_j^{DD}} \mathbf{T}^T \mathbf{A}_{0j}^T \\
& + \sum_{i=1}^{N_c} \sum_{j=1}^{N_p} \rho_{ij}^{DP} \omega_j^p \mathbf{A}_{0i} \mathbf{T} \sqrt{\mathbf{R}_i^{DD}} \sqrt{\mathbf{R}_j^{PP}} \mathbf{T}^T (\mathbf{A}_{0j}^P)^T + \sum_{i=1}^{N_c} \sum_{j=1}^{N_p} \rho_{ij}^{DP} \omega_j^p \mathbf{A}_{0j}^P \mathbf{T} \sqrt{\mathbf{R}_j^{PP}} \sqrt{\mathbf{R}_i^{DD}} \mathbf{T}^T \mathbf{A}_{0i}^T \\
& + \sum_{i=1}^{N_c} \sum_{j=1}^{N_p} \rho_{ij}^{DP} \mathbf{B}_{0i} \mathbf{T} \sqrt{\mathbf{R}_i^{DD}} \sqrt{\mathbf{R}_j^{PP}} \mathbf{T}^T (\mathbf{A}_{0j}^P)^T + \sum_{i=1}^{N_c} \sum_{j=1}^{N_p} \rho_{ij}^{DP} \mathbf{A}_{0j}^P \mathbf{T} \sqrt{\mathbf{R}_j^{PP}} \sqrt{\mathbf{R}_i^{DD}} \mathbf{T}^T \mathbf{B}_{0i}^T \\
& \left. + \sum_{i=1}^{N_p} \sum_{j=1}^{N_p} \rho_{ij}^{PP} \mathbf{A}_{0i}^P \mathbf{T} \sqrt{\mathbf{R}_i^{PP}} \sqrt{\mathbf{R}_j^{PP}} \mathbf{T}^T (\mathbf{A}_{0j}^P)^T \right\} \mathbf{d}
\end{aligned} \tag{4.46}$$

In Equation (4.46), $\mathbf{R}_i^{DD} = \text{diag}[R_{ii}^{(kk)DD}]$ and $k = 1, 2, 3$, and $R_{ii}^{(kk)DD}$ is variance of the i th modal displacement response subjected to excitation component k . $\mathbf{R}_i^{PP} = \text{diag}[R_{ii}^{(kk)PP}]$ and $R_{ii}^{(kk)PP}$ is variance of the i th over-damped modal response subjected to excitation component k .

It has been shown in Davenport (1964) and Vanmarcke (1972) that the maximum modal response over a specified duration is proportional to its root mean square, i.e.,

$$\begin{aligned}
|q_i(t)|_{\max} &= S_{ki} = p_i \sqrt{R_{ii}^{(kk)DD}} \\
|q_i(t)|_{\max}^P &= S_{ki}^P = p_i \sqrt{R_{ii}^{(kk)PP}}
\end{aligned} \tag{4.47}$$

in which S_{ki} is the spectral displacement associated with mode i under k th excitation component and S_{ki}^P is the spectral over-damped response associated with the over-damped mode i under k th excitation component. The numerical value of p_i , in general, does not differ greatly in magnitude from mode to mode. Thus, in engineering practice, it is reasonable to assign the same value to p_i for each mode and for the combined responses. This assumption is also assumed to be applicable to the over-damped mode case. Thus, one can express maximum values of modal response through their corresponding response spectral values for the specified excitation component. The diagonal matrices are defined as $\mathbf{S}_i = \text{diag}[S_{ki}]$ and $\mathbf{S}_i^P = \text{diag}[S_{ki}^P]$, $k = 1, 2, 3$, and the

maximum value of the response $|r_0(t)|_{\max}$, denoted as \mathbf{R}_0 , can be expressed as in the following matrix form

$$\begin{aligned}\mathbf{R}_0^2 &= \mathbf{d}^T \mathbf{Z} \mathbf{d} \\ &= \mathbf{d}^T (\mathbf{Z}^{\text{DD}} + \mathbf{Z}^{\text{VV}} + \mathbf{Z}^{\text{VD}} + \mathbf{Z}^{\text{VP}} + \mathbf{Z}^{\text{DP}} + \mathbf{Z}^{\text{PP}}) \mathbf{d}\end{aligned}\quad (4.48)$$

where

$$\mathbf{Z} = \mathbf{Z}^{\text{DD}} + \mathbf{Z}^{\text{VV}} + \mathbf{Z}^{\text{VD}} + \mathbf{Z}^{\text{VP}} + \mathbf{Z}^{\text{DP}} + \mathbf{Z}^{\text{PP}} \quad (4.49)$$

$$\mathbf{Z}^{\text{DD}} = \sum_{i=1}^{N_c} \sum_{j=1}^{N_c} \rho_{ij}^{\text{DD}} \mathbf{B}_{0i} \mathbf{T} \mathbf{S}_i \mathbf{S}_j^T \mathbf{T}^T \mathbf{B}_{0j}^T \quad (4.50)$$

$$\mathbf{Z}^{\text{VV}} = \sum_{i=1}^{N_c} \sum_{j=1}^{N_c} \rho_{ij}^{\text{DD}} \mu_{ij} \omega_i \omega_j \mathbf{A}_{0i} \mathbf{T} \mathbf{S}_i \mathbf{S}_j^T \mathbf{T}^T \mathbf{A}_{0j}^T \quad (4.51)$$

$$\mathbf{Z}^{\text{VD}} = \sum_{i=1}^{N_c} \sum_{j=1}^{N_c} \left[\rho_{ij}^{\text{DD}} v_{ij} \omega_i \mathbf{A}_{0i} \mathbf{T} \mathbf{S}_i \mathbf{S}_j^T \mathbf{T}^T \mathbf{B}_{0j}^T + \rho_{ij}^{\text{DD}} v_{ji} \omega_j \mathbf{B}_{0j} \mathbf{T} \mathbf{S}_j \mathbf{S}_i^T \mathbf{T}^T \mathbf{A}_{0i}^T \right] \quad (4.52)$$

$$\mathbf{Z}^{\text{VP}} = \sum_{i=1}^{N_c} \sum_{j=1}^{N_p} \rho_{ij}^{\text{DP}} \omega_j^p \left[\mathbf{A}_{0i} \mathbf{T} \mathbf{S}_i (\mathbf{S}_j^p)^T \mathbf{T}^T (\mathbf{A}_{0j}^p)^T + \mathbf{A}_{0j}^p \mathbf{T} \mathbf{S}_j^p \mathbf{S}_i^T \mathbf{T}^T \mathbf{A}_{0i}^T \right] \quad (4.53)$$

$$\mathbf{Z}^{\text{DP}} = \sum_{i=1}^{N_c} \sum_{j=1}^{N_p} \rho_{ij}^{\text{DP}} \left[\mathbf{B}_{0i} \mathbf{T} \mathbf{S}_i (\mathbf{S}_j^p)^T \mathbf{T}^T (\mathbf{A}_{0j}^p)^T + \mathbf{A}_{0j}^p \mathbf{T} \mathbf{S}_j^p \mathbf{S}_i^T \mathbf{T}^T \mathbf{B}_{0i}^T \right] \quad (4.54)$$

$$\mathbf{Z}^{\text{PP}} = \sum_{i=1}^{N_p} \sum_{j=1}^{N_p} \rho_{ij}^{\text{PP}} \mathbf{A}_{0i}^p \mathbf{T} \mathbf{S}_i (\mathbf{S}_j^p)^T \mathbf{T}^T (\mathbf{A}_{0j}^p)^T \quad (4.55)$$

Equation (4.48) is referred to as the General Complete Quadratic Combination rule for three-component excitations, denoted as GCQC3. In addition, in order to express the incident angle variable θ explicitly, the transformation matrix \mathbf{T} is considered and $\mathbf{S}_k = \text{diag}[S_{ki}]$, $\mathbf{S}_k^p = \text{diag}[S_{ki}^p]$, $\boldsymbol{\omega} = \text{diag}[\omega_i]$ and $\boldsymbol{\omega}^p = \text{diag}[\omega_i^p]$. $\boldsymbol{\rho}^{\text{DD}} = [\rho_{ij}^{\text{DD}}]$, $\boldsymbol{\rho}^{\text{DP}} = [\rho_{ij}^{\text{DP}}]$, $\boldsymbol{\rho}^{\text{PP}} = [\rho_{ij}^{\text{PP}}]$, $\boldsymbol{\mu} = [\mu_{ij}]$, $\mathbf{v} = [v_{ij}]$, $\mathbf{B}_0^{(k)} = [\mathbf{B}_{0i}^{(k)}]$, $\mathbf{A}_0^{(k)} = [\mathbf{A}_{0i}^{(k)}]$ and $\mathbf{A}_0^{p(k)} = [\mathbf{A}_{0i}^{p(k)}]$. Equation (4.48) is rewritten in a different matrix form as

$$\mathbf{R}_0^2 = |r_0(t)|_{\max}^2 = \mathbf{d}^T (\mathbf{V}_1 + \mathbf{V}_2 \sin^2 \theta + \mathbf{V}_3 \sin \theta \cos \theta) \mathbf{d} = \mathbf{d}^T \mathbf{V} \mathbf{d} \quad (4.56)$$

where

$$\mathbf{V}_1 = \sum_{k=1}^3 \begin{bmatrix} \mathbf{B}_0^{(k)} \mathbf{S}_k \boldsymbol{\rho}^{\text{DD}} \mathbf{S}_k^T (\mathbf{B}_0^{(k)})^T + \mathbf{A}_0^{(k)} \mathbf{S}_k \boldsymbol{\omega} (\boldsymbol{\mu} \bullet \boldsymbol{\rho}^{\text{DD}}) \boldsymbol{\omega}^T \mathbf{S}_k^T (\mathbf{A}_0^{(k)})^T \\ + \mathbf{A}_0^{(k)} \mathbf{S}_k \boldsymbol{\omega} (\mathbf{v} \bullet \boldsymbol{\rho}^{\text{DD}}) \mathbf{S}_k^T (\mathbf{B}_0^{(k)})^T + \mathbf{B}_0^{(k)} \mathbf{S}_k \boldsymbol{\omega} (\mathbf{v} \bullet \boldsymbol{\rho}^{\text{DD}}) \mathbf{S}_k^T (\mathbf{A}_0^{(k)})^T \\ + \mathbf{A}_0^{(k)} \mathbf{S}_k \boldsymbol{\omega}^{\text{P}} \boldsymbol{\rho}^{\text{DP}} (\mathbf{S}_k^{\text{P}})^T (\mathbf{A}_0^{\text{P}(k)})^T + \mathbf{A}_0^{\text{P}(k)} \mathbf{S}_k^{\text{P}} \boldsymbol{\omega}^{\text{P}} \boldsymbol{\rho}^{\text{DP}} \mathbf{S}_k^T (\mathbf{A}_0^{(k)})^T \\ + \mathbf{B}_0^{(k)} \mathbf{S}_k \boldsymbol{\rho}^{\text{DP}} (\mathbf{S}_k^{\text{P}})^T (\mathbf{A}_0^{\text{P}(k)})^T + \mathbf{A}_0^{\text{P}(k)} \mathbf{S}_k^{\text{P}} \boldsymbol{\rho}^{\text{DP}} \mathbf{S}_k^T (\mathbf{B}_0^{(k)})^T \\ + \mathbf{A}_0^{\text{P}(k)} \mathbf{S}_k^{\text{P}} \boldsymbol{\rho}^{\text{PP}} (\mathbf{S}_k^{\text{P}})^T (\mathbf{A}_0^{\text{P}(k)})^T \end{bmatrix} \quad (4.57)$$

$$\mathbf{V}_2 = - \sum_{k=1}^2 \sum_{l=1}^2 (-1)^{k+l} \begin{bmatrix} \mathbf{B}_0^{(k)} \mathbf{S}_l \boldsymbol{\rho}^{\text{DD}} \mathbf{S}_l^T (\mathbf{B}_0^{(k)})^T + \mathbf{A}_0^{(k)} \mathbf{S}_l \boldsymbol{\omega} (\boldsymbol{\mu} \bullet \boldsymbol{\rho}^{\text{DD}}) \boldsymbol{\omega}^T \mathbf{S}_l^T (\mathbf{A}_0^{(k)})^T \\ + \mathbf{A}_0^{(k)} \mathbf{S}_l \boldsymbol{\omega} (\mathbf{v} \bullet \boldsymbol{\rho}^{\text{DD}}) \mathbf{S}_l^T (\mathbf{B}_0^{(k)})^T + \mathbf{B}_0^{(k)} \mathbf{S}_l \boldsymbol{\omega} (\mathbf{v} \bullet \boldsymbol{\rho}^{\text{DD}}) \mathbf{S}_l^T (\mathbf{A}_0^{(k)})^T \\ + \mathbf{A}_0^{(k)} \mathbf{S}_l \boldsymbol{\omega}^{\text{P}} \boldsymbol{\rho}^{\text{DP}} (\mathbf{S}_l^{\text{P}})^T (\mathbf{A}_0^{\text{P}(k)})^T + \mathbf{A}_0^{\text{P}(k)} \mathbf{S}_l^{\text{P}} \boldsymbol{\omega}^{\text{P}} \boldsymbol{\rho}^{\text{DP}} \mathbf{S}_l^T (\mathbf{A}_0^{(k)})^T \\ + \mathbf{B}_0^{(k)} \mathbf{S}_l \boldsymbol{\rho}^{\text{DP}} (\mathbf{S}_l^{\text{P}})^T (\mathbf{A}_0^{\text{P}(k)})^T + \mathbf{A}_0^{\text{P}(k)} \mathbf{S}_l^{\text{P}} \boldsymbol{\rho}^{\text{DP}} \mathbf{S}_l^T (\mathbf{B}_0^{(k)})^T \\ + \mathbf{A}_0^{\text{P}(k)} \mathbf{S}_l^{\text{P}} \boldsymbol{\rho}^{\text{PP}} (\mathbf{S}_l^{\text{P}})^T (\mathbf{A}_0^{\text{P}(k)})^T \end{bmatrix} \quad (4.58)$$

$$\mathbf{V}_3 = - \sum_{k=1}^2 (-1)^k \begin{bmatrix} \mathbf{B}_0^{(1)} \mathbf{S}_k \boldsymbol{\rho}^{\text{DD}} \mathbf{S}_k^T (\mathbf{B}_0^{(2)})^T + \mathbf{B}_0^{(2)} \mathbf{S}_k \boldsymbol{\rho}^{\text{DD}} \mathbf{S}_k^T (\mathbf{B}_0^{(1)})^T \\ + \mathbf{A}_0^{(1)} \mathbf{S}_k \boldsymbol{\omega} (\boldsymbol{\mu} \bullet \boldsymbol{\rho}^{\text{DD}}) \boldsymbol{\omega}^T \mathbf{S}_k^T (\mathbf{A}_0^{(2)})^T + \mathbf{A}_0^{(2)} \mathbf{S}_k \boldsymbol{\omega} (\boldsymbol{\mu} \bullet \boldsymbol{\rho}^{\text{DD}}) \boldsymbol{\omega}^T \mathbf{S}_k^T (\mathbf{A}_0^{(1)})^T \\ + \mathbf{A}_0^{(1)} \mathbf{S}_k \boldsymbol{\omega} (\mathbf{v} \bullet \boldsymbol{\rho}^{\text{DD}}) \mathbf{S}_k^T (\mathbf{B}_0^{(2)})^T + \mathbf{B}_0^{(1)} \mathbf{S}_k \boldsymbol{\omega} (\mathbf{v} \bullet \boldsymbol{\rho}^{\text{DD}}) \mathbf{S}_k^T (\mathbf{A}_0^{(2)})^T \\ + \mathbf{A}_0^{(2)} \mathbf{S}_k \boldsymbol{\omega} (\mathbf{v} \bullet \boldsymbol{\rho}^{\text{DD}}) \mathbf{S}_k^T (\mathbf{B}_0^{(1)})^T + \mathbf{B}_0^{(2)} \mathbf{S}_k \boldsymbol{\omega} (\mathbf{v} \bullet \boldsymbol{\rho}^{\text{DD}}) \mathbf{S}_k^T (\mathbf{A}_0^{(1)})^T \\ + \mathbf{A}_0^{(1)} \mathbf{S}_k \boldsymbol{\omega}^{\text{P}} \boldsymbol{\rho}^{\text{DP}} (\mathbf{S}_k^{\text{P}})^T (\mathbf{A}_0^{\text{P}(2)})^T + \mathbf{A}_0^{\text{P}(1)} \mathbf{S}_k^{\text{P}} \boldsymbol{\omega}^{\text{P}} \boldsymbol{\rho}^{\text{DP}} \mathbf{S}_k^T (\mathbf{A}_0^{(2)})^T \\ + \mathbf{A}_0^{(2)} \mathbf{S}_k \boldsymbol{\omega}^{\text{P}} \boldsymbol{\rho}^{\text{DP}} (\mathbf{S}_k^{\text{P}})^T (\mathbf{A}_0^{\text{P}(1)})^T + \mathbf{A}_0^{\text{P}(2)} \mathbf{S}_k^{\text{P}} \boldsymbol{\omega}^{\text{P}} \boldsymbol{\rho}^{\text{DP}} \mathbf{S}_k^T (\mathbf{A}_0^{(1)})^T \\ + \mathbf{B}_0^{(1)} \mathbf{S}_k \boldsymbol{\rho}^{\text{DP}} (\mathbf{S}_k^{\text{P}})^T (\mathbf{A}_0^{\text{P}(2)})^T + \mathbf{A}_0^{\text{P}(1)} \mathbf{S}_k^{\text{P}} \boldsymbol{\rho}^{\text{DP}} \mathbf{S}_k^T (\mathbf{B}_0^{(2)})^T \\ + \mathbf{B}_0^{(2)} \mathbf{S}_k \boldsymbol{\rho}^{\text{DP}} (\mathbf{S}_k^{\text{P}})^T (\mathbf{A}_0^{\text{P}(1)})^T + \mathbf{A}_0^{\text{P}(2)} \mathbf{S}_k^{\text{P}} \boldsymbol{\rho}^{\text{DP}} \mathbf{S}_k^T (\mathbf{B}_0^{(1)})^T \\ \mathbf{A}_0^{\text{P}(1)} \mathbf{S}_k^{\text{P}} \boldsymbol{\rho}^{\text{PP}} \mathbf{S}_k^T (\mathbf{A}_0^{\text{P}(2)})^T + \mathbf{A}_0^{\text{P}(2)} \mathbf{S}_k^{\text{P}} \boldsymbol{\rho}^{\text{PP}} (\mathbf{S}_k^{\text{P}})^T (\mathbf{A}_0^{\text{P}(1)})^T \end{bmatrix} \quad (4.59)$$

$$\mathbf{V} = \mathbf{V}_1 + \mathbf{V}_2 \sin^2 \theta + \mathbf{V}_3 \sin \theta \cos \theta \quad (4.60)$$

Equation (4.56) can be expanded alternatively as

$$\mathbf{R}_0^2 = (R_{1x}^2 + R_{2y}^2) \cos^2 \theta + (R_{2x}^2 + R_{1y}^2) \sin^2 \theta + 2(R_{1xy} - R_{2xy}) \sin \theta \cos \theta + R_3^2 \quad (4.61)$$

in which

$$\begin{aligned} R_{kx}^2 &= \sum_{i=1}^{N_c} \sum_{j=1}^{N_c} \rho_{ij}^{\text{DD}} \left[\mu_{ij} \omega_i \omega_j A_{0i}^{(1)} A_{0j}^{(1)} + B_{0i}^{(1)} B_{0j}^{(1)} + 2v_{ij} \omega_i A_{0i}^{(1)} B_{0j}^{(1)} \right] S_{ki} S_{kj} \\ &+ 2 \sum_{i=1}^{N_c} \sum_{j=1}^{N_p} \rho_{ij}^{\text{DP}} \left[\omega_j^P A_{0i}^{(1)} A_{0j}^{\text{P}(1)} + B_{0i}^{(1)} A_{0j}^{\text{P}(1)} \right] S_{ki} S_{kj}^{\text{P}} \\ &+ \sum_{i=1}^{N_p} \sum_{j=1}^{N_p} \rho_{ij}^{\text{PP}} A_{0i}^{\text{P}(1)} A_{0j}^{\text{P}(1)} S_{ki}^{\text{P}} S_{kj}^{\text{P}} \end{aligned} \quad (4.62)$$

$$\begin{aligned} R_{ky}^2 &= \sum_{i=1}^{N_c} \sum_{j=1}^{N_c} \rho_{ij}^{\text{DD}} \left[\mu_{ij} \omega_i \omega_j A_{0i}^{(2)} A_{0j}^{(2)} + B_{0i}^{(2)} B_{0j}^{(2)} + 2v_{ij} \omega_i A_{0i}^{(2)} B_{0j}^{(2)} \right] S_{ki} S_{kj} \\ &+ 2 \sum_{i=1}^{N_c} \sum_{j=1}^{N_p} \rho_{ij}^{\text{DP}} \left[\omega_j^P A_{0i}^{(2)} A_{0j}^{\text{P}(2)} + B_{0i}^{(2)} A_{0j}^{\text{P}(2)} \right] S_{ki} S_{kj}^{\text{P}} \\ &+ \sum_{i=1}^{N_p} \sum_{j=1}^{N_p} \rho_{ij}^{\text{PP}} A_{0i}^{\text{P}(2)} A_{0j}^{\text{P}(2)} S_{ki}^{\text{P}} S_{kj}^{\text{P}} \end{aligned} \quad (4.63)$$

$$\begin{aligned} R_{kxy} &= \sum_{i=1}^{N_c} \sum_{j=1}^{N_c} \rho_{ij}^{\text{DD}} \left[\mu_{ij} \omega_i \omega_j A_{0i}^{(1)} A_{0j}^{(2)} + B_{0i}^{(1)} B_{0j}^{(2)} + v_{ij} \omega_i (A_{0i}^{(1)} B_{0j}^{(2)} + A_{0i}^{(2)} B_{0j}^{(1)}) \right] S_{ki} S_{kj} \\ &+ 2 \sum_{i=1}^{N_c} \sum_{j=1}^{N_p} \rho_{ij}^{\text{DP}} \left[\omega_j^P (A_{0i}^{(1)} A_{0j}^{\text{P}(2)} + A_{0i}^{(2)} A_{0j}^{\text{P}(1)}) + B_{0i}^{(1)} A_{0j}^{\text{P}(2)} + B_{0i}^{(2)} A_{0j}^{\text{P}(1)} \right] S_{ki} S_{kj}^{\text{P}} \\ &+ \sum_{i=1}^{N_p} \sum_{j=1}^{N_p} \rho_{ij}^{\text{PP}} A_{0i}^{\text{P}(1)} A_{0j}^{\text{P}(2)} S_{ki}^{\text{P}} S_{kj}^{\text{P}} \end{aligned} \quad (4.64)$$

and

$$\begin{aligned}
R_3^2 = & \sum_{i=1}^{N_c} \sum_{j=1}^{N_c} \rho_{ij}^{DD} \left[\mu_{ij} \omega_i \omega_j A_{0i}^{(3)} A_{0j}^{(3)} + B_{0i}^{(3)} B_{0j}^{(3)} + 2\nu_{ij} \omega_i A_{0i}^{(3)} B_{0j}^{(3)} \right] S_{3i} S_{3j} \\
& + 2 \sum_{i=1}^{N_c} \sum_{j=1}^{N_p} \rho_{ij}^{DP} \left[\omega_j^P A_{0i}^{(3)} A_{0j}^{P(3)} + B_{0i}^{(3)} A_{0j}^{P(3)} \right] S_{3i} S_{3j}^P \\
& + \sum_{i=1}^{N_p} \sum_{j=1}^{N_p} \rho_{ij}^{PP} A_{0i}^{P(3)} A_{0j}^{P(3)} S_{3i}^P S_{3j}^P
\end{aligned} \tag{4.65}$$

R_{kx} and R_{ky} are the peak responses when the spectrum S_{ak} acts along the structure reference axes \mathbf{X} and \mathbf{Y} , respectively. R_{kxy} is a cross term considering the effect of the cross relation between responses R_{kx} and R_{ky} on the total response. The term-by-term expression of Equation (4.61) represented in a tabulated format is given in Table 4.1. In Table 4.1, the sum of Row 1, $\mathbf{d}^T \mathbf{Z}^{DD} \mathbf{d}$, represents the responses contributed from the modal displacements; the sum of Row 2, $\mathbf{d}^T \mathbf{Z}^{VV} \mathbf{d}$, represents the contributions of modal velocities; the sum of Row 3, $\mathbf{d}^T \mathbf{Z}^{VD} \mathbf{d}$, shows the contribution and the effect of the cross relation between modal displacement and modal velocity; the sum of Row 4, $\mathbf{d}^T \mathbf{Z}^{VP} \mathbf{d}$, accounts for the effect of the cross relation between modal velocity and over-damped modal response; the sum of Row 5, $\mathbf{d}^T \mathbf{Z}^{DP} \mathbf{d}$, is used for the influence of the cross relation between modal displacement and over-damped modal response, and the sum of the last row, $\mathbf{d}^T \mathbf{Z}^{PP} \mathbf{d}$, represents the responses contributed from over-damped modal responses. The sum of columns 1 and 4, $(R_{1x}^2 \cos^2 \theta + R_{1y}^2 \sin^2 \theta)$, stands for the response resulting from excitation component 1. The sum of columns 2 and 3, $(R_{2x}^2 \sin^2 \theta + R_{2y}^2 \cos^2 \theta)$, stands for the response resulting from excitation component 2. The sum of column 6, R_3^2 , stands for the response due to excitation component 3. The sum of column 5, $2(R_{1xy} - R_{2xy}) \sin \theta \cos \theta$, is used to account for the cross relation between responses due to excitation components 1 and 2. Thus, it is clear from Table 4.1 that the new GCQC3 not only considers the correlations between modal responses but also the correlations between excitation components.

Table 4.1 Term by term expression of Equation (4.61)

Term	(1)	(2)	(3)	(4)	(5)	1
$\underline{1}$	$\sum_{i=1}^{N_c} \sum_{j=1}^{N_c} \rho_{ij}^{DD} \mathbf{B}_{0i}^{(1)} \mathbf{B}_{0j}^{(1)} S_{1i} S_{1j}$	$\mathbf{B}_{0i}^{(2)} \mathbf{B}_{0j}^{(2)} S_{2i} S_{2j}$	$\mathbf{B}_{0i}^{(1)} \mathbf{B}_{0j}^{(1)} S_{2i} S_{2j}$	$\mathbf{B}_{0i}^{(2)} \mathbf{B}_{0j}^{(2)} S_{1i} S_{1j}$	$\mathbf{B}_{0i}^{(1)} \mathbf{B}_{0j}^{(2)} (S_{1i} S_{1j} - S_{2i} S_{2j})$	$\mathbf{B}_{0i}^{(3)} \mathbf{B}_{0j}^{(3)} S_{3i} S_{3j}$
$\underline{2}$	$\sum_{i=1}^{N_c} \sum_{j=1}^{N_c} \omega_i \omega_j \rho_{ij}^{VV} \mathbf{A}_{0i}^{(1)} \mathbf{A}_{0j}^{(1)} S_{1i} S_{1j}$	$\mathbf{A}_{0i}^{(2)} \mathbf{A}_{0j}^{(2)} S_{2i} S_{2j}$	$\mathbf{A}_{0i}^{(1)} \mathbf{A}_{0j}^{(1)} S_{2i} S_{2j}$	$\mathbf{A}_{0i}^{(2)} \mathbf{A}_{0j}^{(2)} S_{1i} S_{1j}$	$\mathbf{A}_{0i}^{(1)} \mathbf{A}_{0j}^{(2)} (S_{1i} S_{1j} - S_{2i} S_{2j})$	$\mathbf{A}_{0i}^{(3)} \mathbf{A}_{0j}^{(3)} S_{3i} S_{3j}$
$\underline{3}$	$\sum_{i=1}^{N_c} \sum_{j=1}^{N_c} \omega_i \rho_{ij}^{VD} \mathbf{2A}_{0i}^{(1)} \mathbf{B}_{0j}^{(1)} S_{1i} S_{1j}$	$\mathbf{2A}_{0i}^{(2)} \mathbf{B}_{0j}^{(2)} S_{2i} S_{2j}$	$\mathbf{2A}_{0i}^{(1)} \mathbf{B}_{0j}^{(1)} S_{2i} S_{2j}$	$\mathbf{2A}_{0i}^{(2)} \mathbf{B}_{0j}^{(2)} S_{1i} S_{1j}$	$(\mathbf{A}_{0i}^{(1)} \mathbf{B}_{0j}^{(2)} + \mathbf{A}_{0i}^{(2)} \mathbf{B}_{0j}^{(1)}) (S_{1i} S_{1j} - S_{2i} S_{2j})$	$\mathbf{2B}_{0i}^{(3)} \mathbf{B}_{0j}^{(3)} S_{3i} S_{3j}$
$\underline{4}$	$\sum_{i=1}^{N_c} \sum_{j=1}^{N_c} \omega_j^P \rho_{ij}^{DP} \mathbf{2A}_{0i}^{(1)} \mathbf{A}_{0j}^{P(1)} S_{1i} S_{1j}^P$	$\mathbf{2A}_{0i}^{(2)} \mathbf{A}_{0j}^{P(2)} S_{2i} S_{2j}^P$	$\mathbf{2A}_{0i}^{(1)} \mathbf{A}_{0j}^{P(1)} S_{2i} S_{2j}^P$	$\mathbf{2A}_{0i}^{(2)} \mathbf{A}_{0j}^{P(2)} S_{1i} S_{1j}^P$	$(\mathbf{A}_{0i}^{(1)} \mathbf{A}_{0j}^{P(2)} + \mathbf{A}_{0i}^{(2)} \mathbf{A}_{0j}^{P(1)}) (S_{1i} S_{1j}^P - S_{2i} S_{2j}^P)$	$\mathbf{2A}_{0i}^{(3)} \mathbf{A}_{0j}^{P(3)} S_{3i} S_{3j}^P$
$\underline{5}$	$\sum_{i=1}^{N_c} \sum_{j=1}^{N_c} \rho_{ij}^{DP} \mathbf{2B}_{0i}^{(1)} \mathbf{A}_{0j}^{P(1)} S_{1i} S_{1j}^P$	$\mathbf{2B}_{0i}^{(2)} \mathbf{A}_{0j}^{P(2)} S_{2i} S_{2j}^P$	$\mathbf{2B}_{0i}^{(1)} \mathbf{A}_{0j}^{P(1)} S_{2i} S_{2j}^P$	$\mathbf{2B}_{0i}^{(2)} \mathbf{A}_{0j}^{P(2)} S_{1i} S_{1j}^P$	$(\mathbf{B}_{0i}^{(1)} \mathbf{A}_{0j}^{P(2)} + \mathbf{B}_{0i}^{(2)} \mathbf{A}_{0j}^{P(1)}) (S_{1i} S_{1j}^P - S_{2i} S_{2j}^P)$	$\mathbf{2B}_{0i}^{(3)} \mathbf{A}_{0j}^{P(3)} S_{3i} S_{3j}^P$
$\underline{6}$	$\sum_{i=1}^{N_p} \sum_{j=1}^{N_p} \rho_{ij}^{PP} \mathbf{A}_{0i}^{P(1)} \mathbf{A}_{0j}^{P(1)} S_{1i}^P S_{1j}^P$	$\mathbf{A}_{0i}^{P(2)} \mathbf{A}_{0j}^{P(2)} S_{2i}^P S_{2j}^P$	$\mathbf{A}_{0i}^{P(1)} \mathbf{A}_{0j}^{P(1)} S_{2i}^P S_{2j}^P$	$\mathbf{A}_{0i}^{P(2)} \mathbf{A}_{0j}^{P(2)} S_{1i}^P S_{1j}^P$	$\mathbf{A}_{0i}^{P(1)} \mathbf{A}_{0j}^{P(2)} (S_{1i}^P S_{1j}^P - S_{2i}^P S_{2j}^P)$	$\mathbf{A}_{0i}^{P(3)} \mathbf{A}_{0j}^{P(3)} S_{3i}^P S_{3j}^P$
\sum	R_{1x}^2	R_{2y}^2	R_{2x}^2	R_{1y}^2	$R_{1xy} - R_{2xy}$	R_3^2

$k = 1$ and 2

4.4.4 Identical Horizontal Response Spectra

In most design codes, only one response spectrum is specified for a given site while the direction of the ground motion is not specified. Therefore, it is common in practice to assume that the two horizontal orthogonal components have identical spectral shapes but different intensities. This intensity ratio is represented by γ as

$$\gamma = \frac{S_{2i}}{S_{1i}} \quad (0 \leq \gamma \leq 1) \quad (4.66)$$

Based on this assumption, the following relationships can be established: $R_{2y}^2 = \gamma^2 R_{1y}^2$, $R_{2x}^2 = \gamma^2 R_{1x}^2$, and $R_{2xy} = \gamma^2 R_{1xy}$. Using the expressions in Equation (4.61), it is simplified as

$$\mathbf{R}_0^2 = (R_{1x}^2 + \gamma^2 R_{1y}^2) \cos^2 \theta + (\gamma^2 R_{1x}^2 + R_{1y}^2) \sin^2 \theta + 2(1 - \gamma^2) R_{1xy} \sin \theta \cos \theta + R_3^2 \quad (4.67)$$

It can be found that when using identical response spectrum in both horizontal directions, i.e. $\gamma=1$, the response quantity is independent of the incident angle θ and the correlations between excitation components disappear. This finding was also pointed out in a number of studies (Wilson et al., 1995; Lopez and Torres, 1997).

4.4.5 Uniformly Distributed Incident Angle

In most instances, it is reasonable to assume that the seismic incident angle θ is uniformly distributed among $[0, 2\pi]$. Hence, the probability density function of θ , $f(\theta)$, is

$$f(\theta) = \frac{1}{2\pi}, \quad 0 \leq \theta \leq 2\pi \quad (4.68)$$

Thus, the mean value of \mathbf{R}_0^2 , $\bar{\mathbf{R}}_0^2$, can be determined by

$$\bar{\mathbf{R}}_0^2 = \int_0^{2\pi} \mathbf{R}_0^2 f(\theta) d\theta \quad (4.69)$$

If the response \mathbf{R}_0^2 is represented by Equation (4.56), Equation (4.69) becomes

$$\bar{\mathbf{R}}_0^2 = \mathbf{d}^T \left(\mathbf{V}_1 + \frac{1}{2} \mathbf{V}_2 \right) \mathbf{d} \quad (4.70)$$

If Equation (4.61) is used to represent the response \mathbf{R}_0^2 , Equation (4.69) becomes

$$\bar{\mathbf{R}}_0^2 = \frac{1}{2} (R_{1x}^2 + R_{2y}^2 + R_{2x}^2 + R_{1y}^2) + R_3^2 \quad (4.71)$$

Note that the terms, \mathbf{V}_3 and $2(R_{1xy} - R_{2xy})$, which represent the correlation between the excitation components along the structure reference axes, disappear after the integration over θ . When the two horizontal response spectra are related by an intensity ratio γ shown in Equation (4.66), Equation (4.71) is simplified to

$$\bar{\mathbf{R}}_0^2 = \frac{1}{2} (1 + \gamma^2) (R_{1x}^2 + R_{1y}^2) + R_3^2 \quad (4.72)$$

Equation (4.72) is useful in practical applications since only one response spectrum is specified in the design codes, and the principal directions of the seismic input is usually unknown and can be considered as uniformly distributed (Semby and Der Kiureghian, 1985).

4.4.6 GSRSS3

When the frequencies of the contributing modes are well separated, the cross terms in Equation (4.61) are negligible. Equation (4.61) can still be represented as

$$|r_0(t)|_{\max}^2 = (R_{1x}^2 + R_{2y}^2) \cos^2 \theta + (R_{2x}^2 + R_{1y}^2) \sin^2 \theta + 2(R_{1xy} - R_{2xy}) \sin \theta \cos \theta + R_3^2 \quad (4.73)$$

However, R_{kx}^2 , R_{ky}^2 , R_{kxy} and R_3^2 , respectively, now reduce to

$$R_{kx}^2 = \sum_{i=1}^{N_c} \left[\omega_i^2 (A_{0i}^{(1)})^2 + (B_{0i}^{(1)})^2 \right] S_{ki}^2 + \sum_{i=1}^{N_p} (A_{0i}^{P(1)} S_{ki}^P)^2 \quad (4.74)$$

$$R_{ky}^2 = \sum_{i=1}^{N_c} \left[\omega_i^2 (A_{0i}^{(2)})^2 + (B_{0i}^{(2)})^2 \right] S_{ki}^2 + \sum_{i=1}^{N_p} \left(A_{0i}^{P(2)} S_{ki}^P \right)^2 \quad (4.75)$$

$$R_{kxy} = \sum_{i=1}^{N_c} \left[\omega_i^2 A_{0i}^{(1)} A_{0i}^{(2)} + B_{0i}^{(1)} B_{0i}^{(2)} \right] S_{ki}^2 + \sum_{i=1}^{N_p} A_{0i}^{P(1)} A_{0i}^{P(2)} \left(S_{ki}^P \right)^2 \quad (4.76)$$

$$R_3^2 = \sum_{i=1}^{N_c} \left[\omega_i^2 (A_{0i}^{(3)})^2 + (B_{0i}^{(3)})^2 \right] S_{3i}^2 + \sum_{i=1}^{N_p} \left(A_{0i}^{P(3)} S_{3i}^P \right)^2 \quad (4.77)$$

Equation (4.73) combined with Equations (4.74) to (4.77) is referred to as the General Square-Root-Sum-of-Squares rule for three-component excitations (GSRSS3).

4.4.7 Investigation of the Correlation Factors

The correlation coefficients ρ_{ij}^{DD} , ρ_{ij}^{VV} , ρ_{ij}^{VD} , ρ_{ij}^{DP} and ρ_{ij}^{PP} for response to white noise input are presented in Figures 4.1 to 4.5, respectively. Each correlation coefficient was plotted against the ratio ω_i/ω_j for certain representatives of damping. Figure 4.1 (a) compares the ρ_{ij}^{DD} variations for different levels of damping, in which the modal damping ratios of the i th and j th mode are the same; whereas Figure 4.1 (b) compares the ρ_{ij}^{DD} variations when the i th and j th modal damping ratios are not equal. It is observed that ρ_{ij}^{DD} becomes smaller as the two modal frequencies ω_i and ω_j move apart. This is particular true for small damping values. However, the ρ_{ij}^{DD} does not diminish rapidly when one of the modal damping is significantly large. This implies that heavily damped modes may have strong interaction with other modes. Similar results can also be found for the velocity correlation coefficient ρ_{ij}^{VV} shown in Figure 4.2. Figure 4.3 shows the variations of the velocity-displacement correlation coefficient ρ_{ij}^{VD} . It can be seen that the variation of ρ_{ij}^{VD} is quite different from the displacement correlation coefficient ρ_{ij}^{DD} . It has a negative value when the ratio ω_i/ω_j is greater than unity. This negative correlation exists between complex modal displacement and complex modal velocity. When ω_i/ω_j is equal to unity, ρ_{ij}^{VD} is zero. This result is reasonable since the complex modal displacement and velocity belonging to the same mode are independent under the white

noise input assumption. The value of ρ_{ij}^{VD} is significant when ω_i/ω_j is less than unity, indicating that the correlation between modal velocity and displacement should not be neglected. Figure 4.4 shows the variation of ρ_{ij}^{DP} with respect to the ratio $\omega_i/\omega_j^{\text{P}}$. It is found that the values of ρ_{ij}^{DP} are significant, especially at large damping levels. Also, ρ_{ij}^{DP} grows as the ratio $\omega_i/\omega_j^{\text{P}}$ approaches two and decreases slowly beyond that value. Figure 4.5 shows that the variation of ρ_{ij}^{PP} is not related to the damping ratio and remains a significant component across the range of the ratio $\omega_i^{\text{P}}/\omega_j^{\text{P}}$. The results shown in Figures 4.1 to 4.5 suggest that over-damped modes may have strong contributions to the structural responses and should be considered in the combination rule.

4.4.8 Reduction to Classically Under-Damped Systems

A MDOF structure that is a classically under-damped system is considered next. Any of its responses expressed by Equation (4.61) can be simplified as

$$|r_0(t)|_{\text{max}}^2 = (R_{1x}^2 + R_{2y}^2) \cos^2 \theta + (R_{2x}^2 + R_{1y}^2) \sin^2 \theta + 2(R_{1xy} - R_{2xy}) \sin \theta \cos \theta + R_3^2 \quad (4.78)$$

in which

$$R_{kx}^2 = \sum_{i=1}^N \sum_{j=1}^N \rho_{ij}^{\text{DD}} \mathbf{B}_{0i}^{(1)} \mathbf{B}_{0j}^{(1)} S_{ki} S_{kj} \quad (4.79)$$

$$R_{ky}^2 = \sum_{i=1}^N \sum_{j=1}^N \rho_{ij}^{\text{DD}} \mathbf{B}_{0i}^{(2)} \mathbf{B}_{0j}^{(2)} S_{ki} S_{kj} \quad (4.80)$$

$$R_{kxy} = \sum_{i=1}^N \sum_{j=1}^N \rho_{ij}^{\text{DD}} \mathbf{B}_{0i}^{(1)} \mathbf{B}_{0j}^{(2)} S_{ki} S_{kj} \quad (4.81)$$

and

$$R_3^2 = \sum_{i=1}^N \sum_{j=1}^N \rho_{ij}^{\text{DD}} \mathbf{B}_{0i}^{(3)} \mathbf{B}_{0j}^{(3)} S_{3i} S_{3j} \quad (4.82)$$

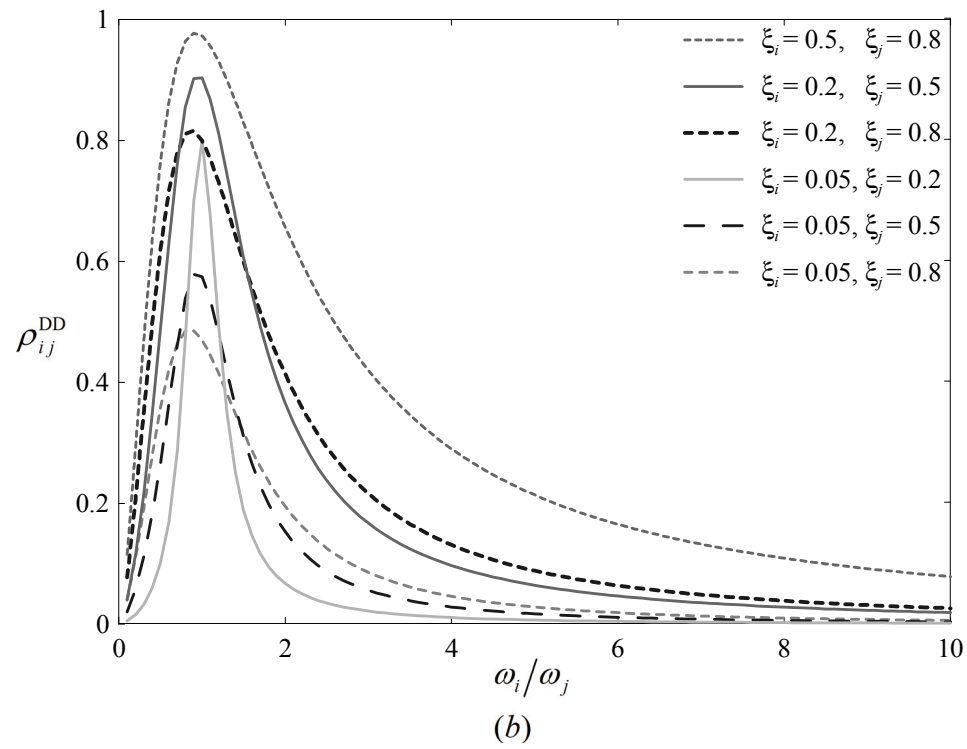
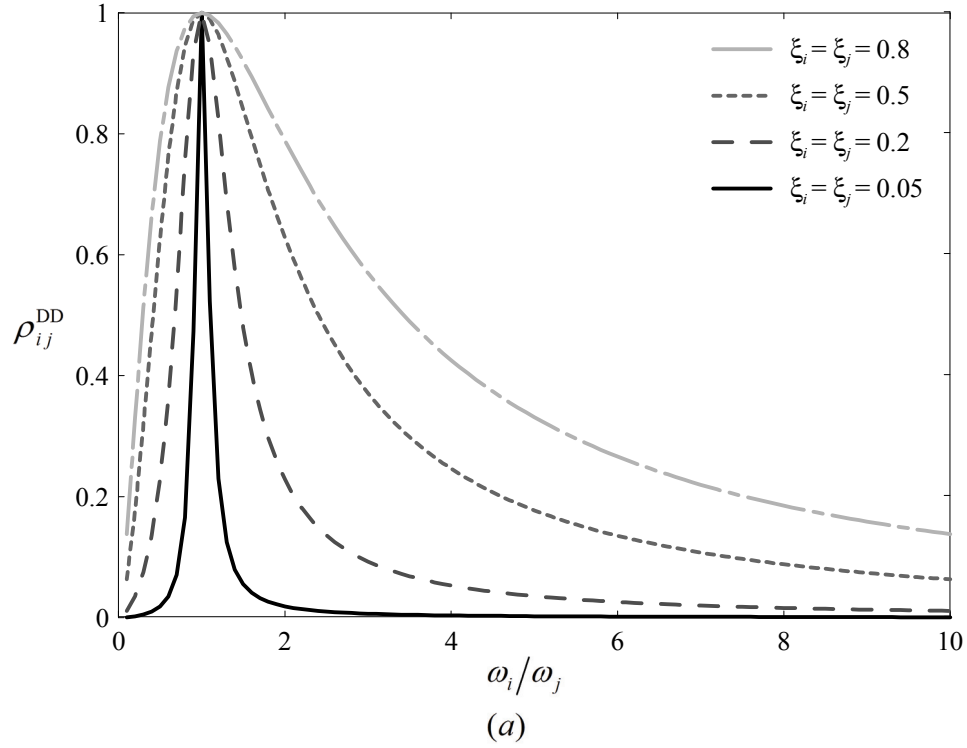


Figure 4.1 Correlation coefficient ρ_{ij}^{DD} for responses to white noise excitations

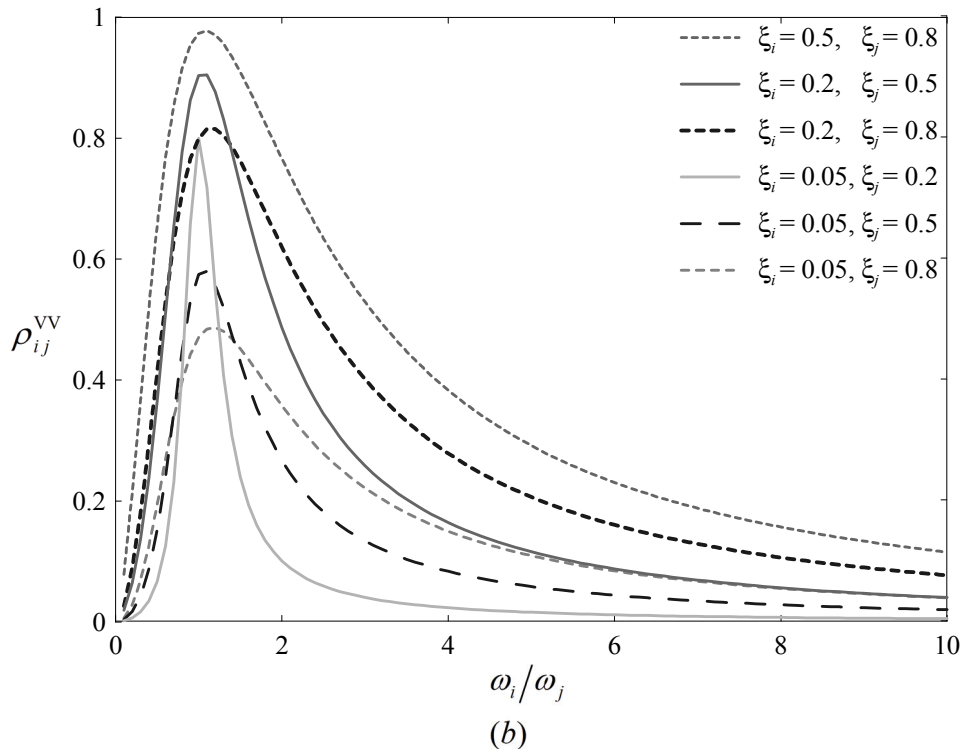
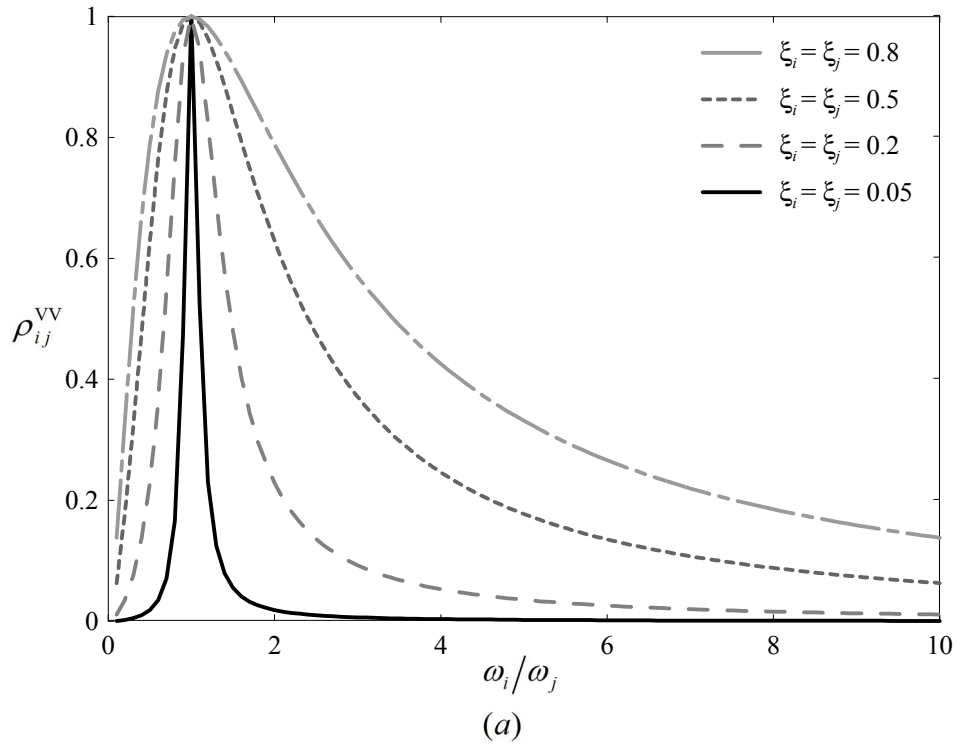


Figure 4.2 Correlation coefficient ρ_{ij}^{VV} for responses to white noise excitations

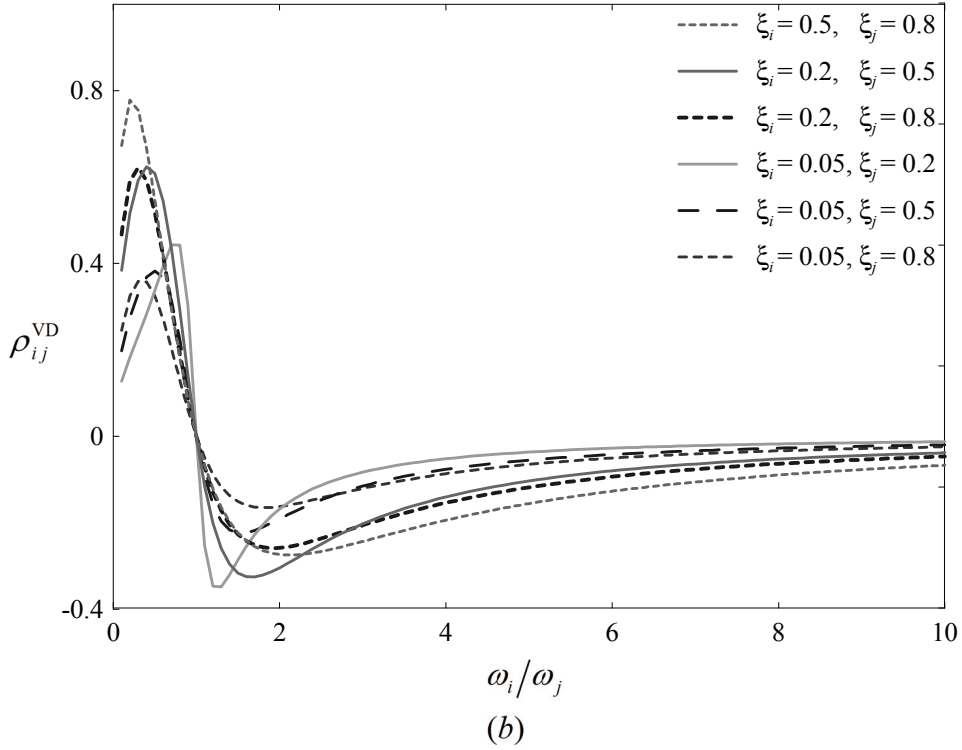
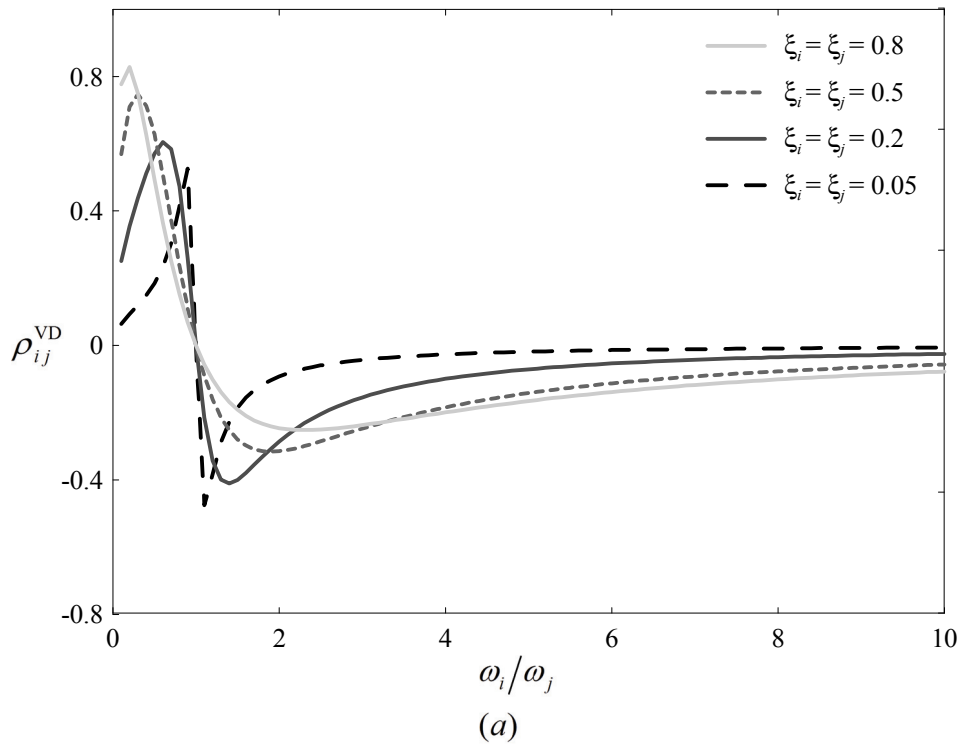


Figure 4.3 Correlation coefficient ρ_{ij}^{VD} for responses to white noise excitations

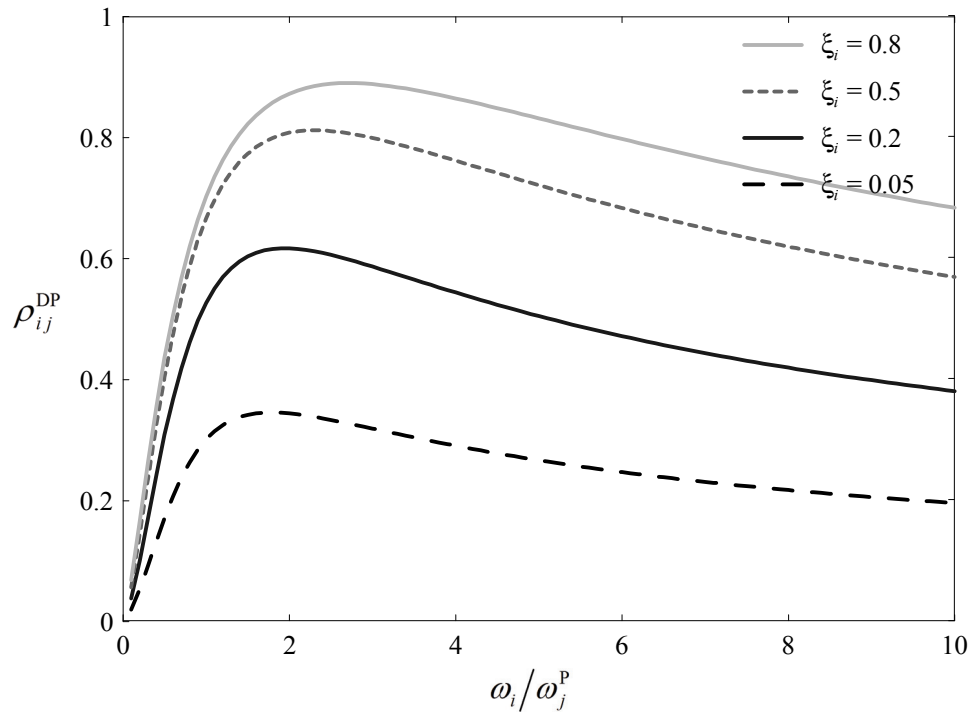


Figure 4.4 Correlation coefficient ρ_{ij}^{DP} for responses to white noise excitations

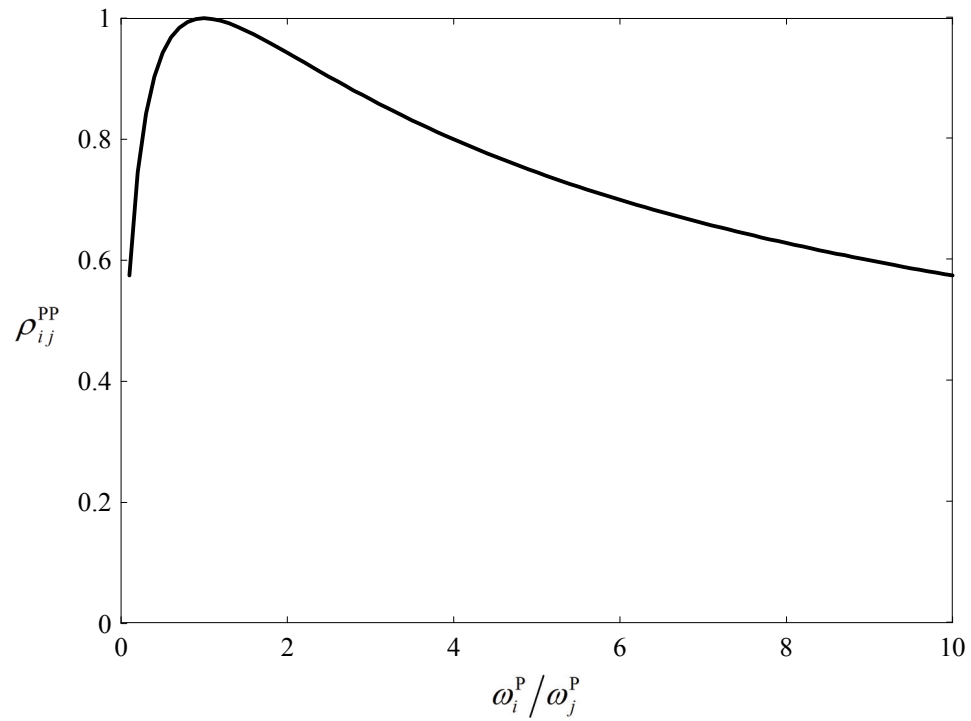


Figure 4.5 Correlation coefficient ρ_{ij}^{PP} for responses to white noise excitations

4.4.8.1 Planar Frame subjected to Single Direction Excitation

When a structure is a two-dimensional frame subjected to a single direction excitation, the peak displacement response vector $|\mathbf{u}(t)|_{\max}$, the peak velocity response vector $|\dot{\mathbf{u}}(t)|_{\max}$ and the peak absolute acceleration vector $|\ddot{\mathbf{u}}_A(t)|_{\max}$ can be estimated by

$$|\mathbf{u}(t)|_{\max} = \sqrt{\sum_{i=1}^N \sum_{j=1}^N \rho_{ij}^{\text{DD}} \boldsymbol{\varphi}_i \cdot \boldsymbol{\varphi}_j \Gamma_i \Gamma_j S_i S_j} \quad (4.83)$$

$$|\dot{\mathbf{u}}(t)|_{\max} = \sqrt{\sum_{i=1}^N \sum_{j=1}^N \mu_{ij} \rho_{ij}^{\text{DD}} \boldsymbol{\varphi}_i \cdot \boldsymbol{\varphi}_j \Gamma_i \Gamma_j \omega_i \omega_j S_i S_j} \quad (4.84)$$

$$|\ddot{\mathbf{u}}_A(t)|_{\max} = \sqrt{\sum_{i=1}^N \sum_{j=1}^N \sigma_{ij} \rho_{ij}^{\text{DD}} \Gamma_i \Gamma_j \boldsymbol{\varphi}_i \cdot \boldsymbol{\varphi}_j \omega_i^2 \omega_j^2 S_i S_j} \quad (4.85)$$

where

$$\begin{aligned} \sigma_{ij} &= 1 + 4\mu_{ij} \xi_i \xi_j + 4\nu_{ij} \xi_i \\ &= \frac{\xi_j \gamma_{ij} + 4\xi_i \xi_j \gamma_{ij} (\xi_i + \xi_j \gamma_{ij}) + \xi_i (2 - \gamma_{ij}^2)}{\gamma_{ij} (\xi_j + \xi_i \gamma_{ij})}, \quad (i, j = 1, 2, \dots, N) \end{aligned} \quad (4.86)$$

$\boldsymbol{\varphi}_i$ is the i th undamped mode shape, $\Gamma_i = \boldsymbol{\varphi}_i^T \mathbf{M} \mathbf{J} / \boldsymbol{\varphi}_i^T \mathbf{M} \boldsymbol{\varphi}_i$ is the i th modal participation factor and S_i is the spectral displacement of mode i . Note that Equation (4.83) coincides with the conventional CQC rule, as expected. Equations (4.84) and (4.85) are newly established formulae to evaluate the peak velocity and peak absolute acceleration of classically damped structures, respectively. As is well known, the pseudo velocity $S_{\text{PV}i}$ and the pseudo acceleration spectra $S_{\text{PA}i}$ associated with the i th mode can be written as $S_{\text{PV}i} = \omega_i S_i$ and $S_{\text{PA}i} = \omega_i^2 S_i$, respectively. Thus, Equations (4.84) and (4.85) may be expressed as

$$|\dot{\mathbf{u}}(t)|_{\max} = \sqrt{\sum_{i=1}^N \sum_{j=1}^N \mu_{ij} \rho_{ij}^{\text{DD}} \boldsymbol{\varphi}_i \cdot \boldsymbol{\varphi}_j \Gamma_i \Gamma_j S_{\text{PV}i} S_{\text{PV}j}} \quad (4.87)$$

$$|\ddot{\mathbf{u}}_A(t)|_{\max} = \sqrt{\sum_{i=1}^N \sum_{j=1}^N \sigma_{ij} \rho_{ij}^{\text{DD}} \boldsymbol{\varphi}_i \cdot \boldsymbol{\varphi}_j \Gamma_i \Gamma_j S_{PAi} S_{PAj}} \quad (4.88)$$

It is seen that, when using the pseudo velocity spectra to estimate the true peak velocity, the results should be modified by the factor μ_{ij} in the combination rule. Also, when using the pseudo acceleration spectra to estimate the true peak absolute acceleration, the results should be modified by the factor σ_{ij} in the combination rule. These important features offer improved estimates on the true relative velocity and true absolute acceleration of classically damped structures and should be very useful in earthquake engineering applications.

4.4.8.2 Under-damped SDOF System

Further, if the system is an under-damped SDOF system, the estimation of the peak absolute acceleration, S_A , can be approximated by customizing Equation (4.88) as

$$S_A = \sqrt{1 + 4\xi^2} S_{PA} \quad (4.89)$$

This formulation provides an efficient and reasonable transformation between the pseudo acceleration and peak absolute acceleration. This relationship was also earlier derived by Song et al. (2007a). The applicability and accuracy of Equation (4.89) was also examined in their study. The result shows that when the damping ratio is less than 40% or so, Equation (4.89) provides excellent estimates.

Furthermore, Equation (4.89) is equivalent to the formula proposed by Tsopelas et al. (1997), which predicts the maximum acceleration based on a given pseudo acceleration. It was developed under the assumption that during the cycle of maximum response, the SDOF system undergoes a harmonic motion with the natural frequency of the SDOF. The equation of this method takes the form of

$$S_A = (f_1 + 2\xi f_2) S_{PA} \quad (4.90)$$

where $f_1 = \cos[\tan^{-1}(2\xi)]$ and $f_2 = \sin[\tan^{-1}(2\xi)]$. The physical meaning of this equation is defined in Tsopelas et al. (1997). If $\theta = \tan^{-1}(2\xi)$, then $f_1 = \cos \theta$, $f_2 = \sin \theta$ and $2\xi = \tan \theta$. The square of $(f_1 + 2\xi f_2)$ is manipulated as follows.

$$\begin{aligned}
 (f_1 + 2\xi f_2)^2 &= (\cos \theta + 2\xi \sin \theta)^2 \\
 &= \cos^2 \theta + 4\xi \cos \theta \sin \theta + 4\xi^2 (1 - \cos^2 \theta) \\
 &= \cos^2 \theta + 2 \tan \theta \cos \theta \sin \theta + 4\xi^2 - \tan^2 \theta \cos^2 \theta \\
 &= \cos^2 \theta + 2 \sin^2 \theta + 4\xi^2 - \sin^2 \theta \\
 &= 1 + 4\xi^2
 \end{aligned} \tag{4.91}$$

Equation (4.91) shows that Equations (4.89) and (4.90) are identical, while Equation (4.89) is easier to use in the engineering applications.

4.5 Over-damped Mode Response Spectrum (Song et al., 2008)

Because the peak over-damped modal responses are not available when performing response spectrum analysis in engineering practice, it is necessary to predict them from the prescribed 5% pseudo-acceleration response spectrum. Thus, a new ‘over-damped mode’ response spectrum is introduced in this study. The over-damped mode response spectrum follows a similar definition as the conventional response spectrum used in earthquake engineering. The objective of the over-damped mode response spectrum is to account for the peak over-damped modal response of structures that have over-damped modes. The interpretation of the over-damped mode response spectrum and an approach that is able to convert a given conventional response spectrum to an over-damped mode response spectrum are described in this section. Validation of the adequacy of the proposed over-damped mode response spectrum conversion approach is also given.

4.5.1 The Concept

Before discussing the over-damped mode response spectrum, it is helpful to briefly review the concept of the conventional response spectrum. Consider a SDOF under-damped system subjected to a ground motion $\ddot{x}_g(t)$. The equation of motion can be written as

$$\ddot{q}(t) + 2\xi\omega_n\dot{q}(t) + \omega_n^2q(t) = -\ddot{x}_g(t) \quad (4.92)$$

where $q(t)$, $\dot{q}(t)$ and $\ddot{q}(t)$ are the relative displacement, velocity and acceleration, respectively; ξ is the damping ratio and ω_n is the natural circular frequency of the SDOF system. The conventional response spectrum is constructed by performing a series of linear response history analysis to a SDOF system under a given ground acceleration $\ddot{x}_g(t)$. The response spectrum is a plot of the peak values of a response quantity as a function of natural vibration period T_n (or corresponding natural circular frequency ω_n). Each plot is for a SDOF system having a fixed damping ratio ξ , and a number of such plots for different values of ξ are included to account for the effect of viscous damping encountered in real structures (Chopra, 2005).

The response of an over-damped mode is characterized by the following linear first order differential equation

$$\dot{q}^p(t) + \omega^p q^p(t) = -\ddot{x}_g(t) \quad (4.93)$$

where $q^p(t)$ is the over-damped modal response and $\dot{q}^p(t)$ is the time derivative of $q^p(t)$, and ω^p is the “over-damped modal natural frequency” (rad/sec) corresponding to the real eigenvalues, solutions of the eigen equation. Similar to the concept of conventional response spectrum, the over-damped mode response spectrum is defined as a plot of the peak over-damped mode responses $q^p(t)$, as a function of the over-damped modal frequency ω^p or the over-damped modal period $T^p = 2\pi/\omega^p$ under a given ground acceleration via Equation (4.93). Unlike the conventional response spectrum, there is only one parameter, ω^p , influencing the response. The procedure to construct the over-damped mode response spectrum is illustrated in Figure 4.6, and it consists of the following three steps: (1) select the ground motion to be considered (as seen in Figure 4.6 (a)); (2) determine the peak over-damped modal responses represented by Equation (4.93) using the selected ground motion for different over-damped modal frequencies (see

Figure 4.6 (b)); and (3) the peak over-damped modal response obtained offers a point on the over-damped mode response spectrum as shown in Figure 4.6 (c).

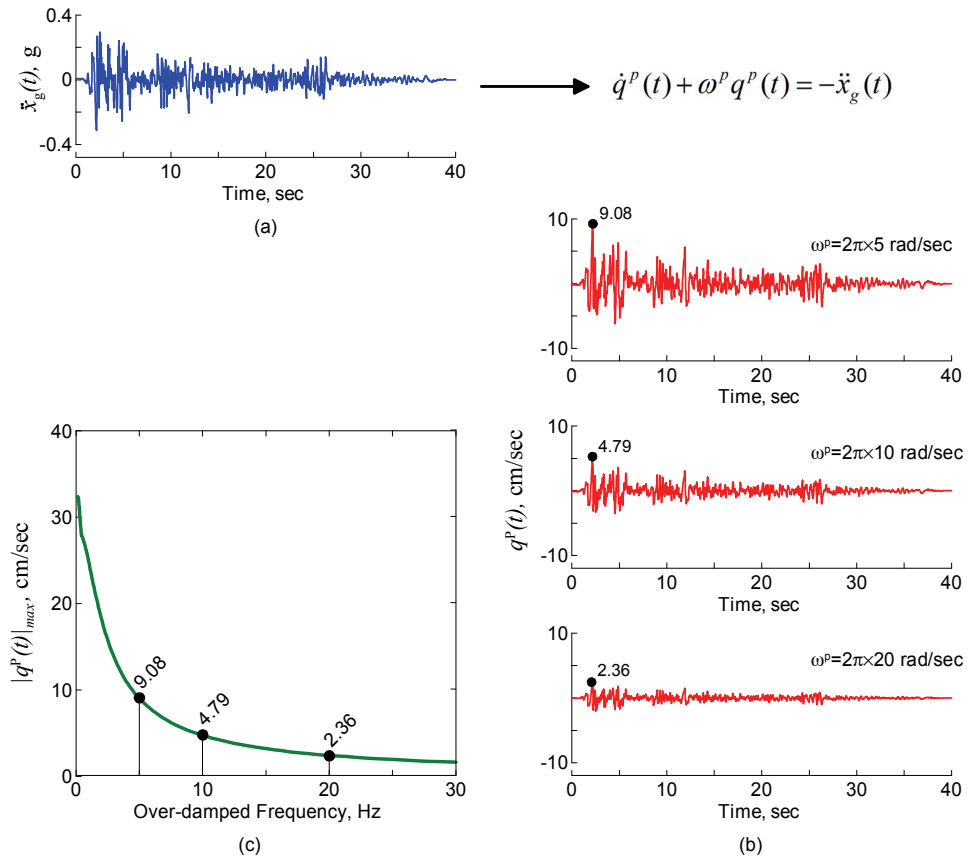


Figure 4.6. Generation of the over-damped mode response spectrum

4.5.2 Construction of Over-damped Mode Response Spectrum Consistent with 5% Displacement Response Spectrum

The construction of the over-damped mode response spectrum relies on the availability of the ground acceleration history. However, when using the response spectrum approach, site response spectrum specified in design provisions is used rather than the ground acceleration histories. Therefore, the over-damped mode response spectrum cannot be directly generated due to the unavailability of ground acceleration records. In this study, an approach based on the theory of random vibration is developed to address this issue, by assuming that the ground excitation can be considered as a wide-banded stationary Gaussian process. In this approach, the input excitation and responses are represented in terms of their respective power spectral density (PSD) functions. For a linear system, the

PSD of a response is the product of the response transmittance function and the PSD of the input process. Further, most structural responses can be characterized by their corresponding response PSD functions. For example, the root mean square (RMS) of a response process is the area under its PSD (Der Kiureghian, 1980). In addition, it has been shown in Davenport (1964) and Vanmarcke (1972) that the peak value of a response process can be related to its root mean square by a proportional factor. From the above considerations, the following procedure is established. First, the ground motion PSD mapped from a given 5% damping displacement spectrum can be established, which is independent of the characteristics of the SDOF systems. Second, this ground motion PSD is used as a base to predict the over-damped mode response spectrum. This proposed approach is based on the work by Song et al. (2007a) to construct the real velocity spectrum from the given 5% response spectrum. The detailed procedures are described in the following subsections.

4.5.2.1 Response Spectrum Consistent PSD $G_{\dot{x}_g}(\omega)$

A reasonable estimate of ground motion PSD, $G_{\dot{x}_g}(\omega)$, consistent with a given 5% displacement spectrum, was proposed by Song et al. (2007a) as follows.

$$G_{\dot{x}_g}(\omega) = \frac{0.1S_d^2(\omega, 5\%)\omega^3}{\alpha^2(\omega, 5\%)\pi} \quad (4.94)$$

where $S_d(\omega, 5\%)$ represents the given 5% displacement response spectrum as a function of ω . $\alpha(\omega, 5\%)$ is a factor that relates the standard deviation or root mean square (RMS) $\sigma(\omega)$ of its response process to its peak response as

$$S_d(\omega, 5\%) = \alpha(\omega, 5\%) \times \sigma(\omega) \quad (4.95)$$

Values of $\alpha(\omega, 5\%)$ determined numerically by using a group of artificial white noise processes can be found in Song et al. (2007a). The applicability of Equation (4.94), along with the white-noise-determined $\alpha(\omega, 5\%)$, has been shown to be appropriate when used to estimate the real spectral velocities (Song et al., 2007a). This response spectrum

consistent PSD $G_{\ddot{x}_g}(\omega)$ will be used to develop the over-damped mode response spectrum described in the next subsection.

4.5.2.2 Procedures

From the over-damped mode equation of motion given by Equation (4.93), it is easy to obtain the over-damped modal frequency response function, $H^p(\omega) = -1/(\omega^p + j\omega)$. Under the wide-band stationary input process assumption, the PSD, G_{q^p} , of the over-damped modal response can be related to ground motion PSD $G_{\ddot{x}_g}(\omega)$ via the frequency response function, $H^p(\omega)$, as

$$G_{q^p} = |H^p(\omega)|^2 \times G_{\ddot{x}_g}(\omega) \quad (4.96)$$

Then, the standard deviation or RMS, σ_{q^p} , of the over-damped modal response may be obtained through

$$\begin{aligned} \sigma_{q^p}^2 &= \int_0^\infty G_{q^p}(\omega) d\omega \\ &= \int_0^\infty |H^p(\omega)|^2 G_{\ddot{x}_g}(\omega) d\omega \end{aligned} \quad (4.97)$$

Further, the peak value of the over-damped modal response $q^p(t)$ can also be related to its RMS σ_{q^p} by a different proportional factor $\eta(\omega^p)$

$$|q^p(t)|_{\max} = \eta(\omega^p) \times \sigma_{q^p}(\omega^p) \quad (4.98)$$

where $\eta(\omega^p)$ is a proportional factor by which the standard deviation must be multiplied to account for the expected peak over-damped modal response. The derivation of $\eta(\omega^p)$ is provided in the following subsection.

4.5.2.3 η Factor Determination

Based on the definition of η , it may be determined numerically by investigating the ratio between peak value and RMS of the response solved from Equation (4.93) while considering the excitation $\ddot{x}_g(t)$ as an artificially generated white noise process for each over-damped modal frequency ω^p of interest. The generated white noise has a duration of eleven seconds and a 0.005 sec time increment. A total of 15,000 response history analyses via Equation (4.93) were performed (corresponding to 150 over-damped modal frequencies ω^p logarithmically spaced between 0.1 Hz and 30 Hz and 100 artificially generated white noise inputs). Mean peak over-damped modal response and its RMS were obtained for each over-damped modal frequency ω^p . The η factor was then determined based on the ratio of these two values. The resulting η factors are tabulated in Table 4.3 while Figure 4.7 shows the plot of η as a function of the over-damped modal frequency ω^p and the over-damped modal period T^p . These η factors are termed as white-noise-determined η factors. Note that η factors are readily available in advance of the construction of the over-damped mode response spectrum and do not favor any ground motion records. Finally, the procedure to construct the over-damped mode response spectrum is illustrated schematically in Figure 4.8.

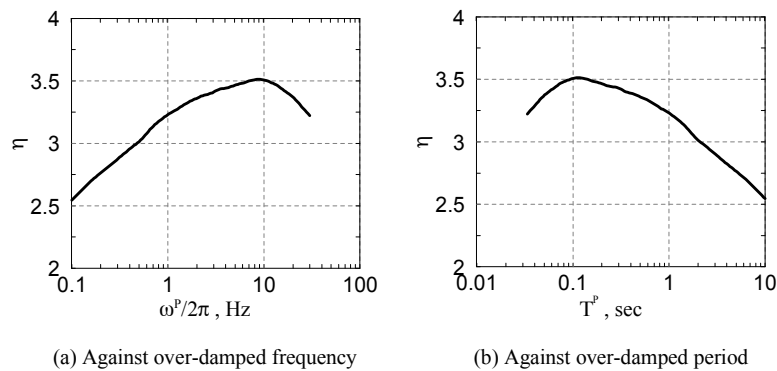


Figure 4.7. Variation of η factor for the over-damped response

Table 4.2. White-noise-determined η factor for over-damped modal response

ω^p	η	ω^p	η	ω^p	η	ω^p	η	ω^p	η	ω^p	η	ω^p	η
0.63	2.55	1.46	2.81	3.39	3.04	7.86	3.28	18.25	3.41	42.36	3.50	98.33	3.43
0.65	2.56	1.52	2.82	3.52	3.05	8.17	3.28	18.96	3.41	44.01	3.50	102.1	3.42
0.68	2.57	1.57	2.83	3.66	3.07	8.49	3.29	19.70	3.42	45.73	3.50	106.1	3.41
0.70	2.59	1.64	2.84	3.80	3.08	8.82	3.30	20.47	3.43	47.51	3.51	110.2	3.41
0.73	2.60	1.70	2.85	3.95	3.10	9.16	3.31	21.27	3.43	49.37	3.51	114.6	3.40
0.76	2.61	1.77	2.86	4.10	3.11	9.52	3.32	22.10	3.44	51.29	3.51	119.0	3.39
0.79	2.62	1.84	2.87	4.26	3.13	9.89	3.32	22.96	3.44	53.29	3.51	123.7	3.38
0.82	2.64	1.91	2.88	4.43	3.14	10.28	3.33	23.85	3.44	55.37	3.51	128.5	3.36
0.85	2.65	1.98	2.89	4.60	3.15	10.68	3.34	24.78	3.44	57.53	3.51	133.5	3.35
0.89	2.66	2.06	2.90	4.78	3.16	11.09	3.34	25.75	3.44	59.78	3.51	138.7	3.34
0.92	2.67	2.14	2.91	4.97	3.17	11.53	3.35	26.76	3.45	62.11	3.51	144.1	3.32
0.96	2.69	2.22	2.92	5.16	3.18	11.98	3.36	27.80	3.45	64.54	3.51	149.8	3.31
0.99	2.70	2.31	2.93	5.36	3.19	12.44	3.36	28.89	3.46	67.05	3.50	155.6	3.29
1.03	2.71	2.40	2.94	5.57	3.20	12.93	3.37	30.01	3.46	69.67	3.50	161.7	3.28
1.07	2.72	2.49	2.95	5.79	3.21	13.43	3.37	31.18	3.47	72.39	3.49	168.0	3.27
1.12	2.73	2.59	2.96	6.01	3.22	13.96	3.38	32.40	3.47	75.22	3.49	174.6	3.25
1.16	2.74	2.69	2.97	6.25	3.23	14.50	3.38	33.67	3.47	78.15	3.48	181.4	3.24
1.20	2.75	2.80	2.99	6.49	3.24	15.07	3.39	34.98	3.48	81.20	3.48	188.5	3.22
1.25	2.76	2.91	2.99	6.74	3.25	15.66	3.39	36.34	3.48	84.37	3.47		
1.30	2.77	3.02	3.00	7.01	3.25	16.27	3.39	37.76	3.48	87.66	3.46		
1.35	2.78	3.14	3.01	7.28	3.26	16.90	3.40	39.24	3.49	91.08	3.45		
1.40	2.79	3.26	3.03	7.56	3.27	17.56	3.40	40.77	3.49	94.64	3.44		

ω^p = over-damped modal frequency (rad/sec)

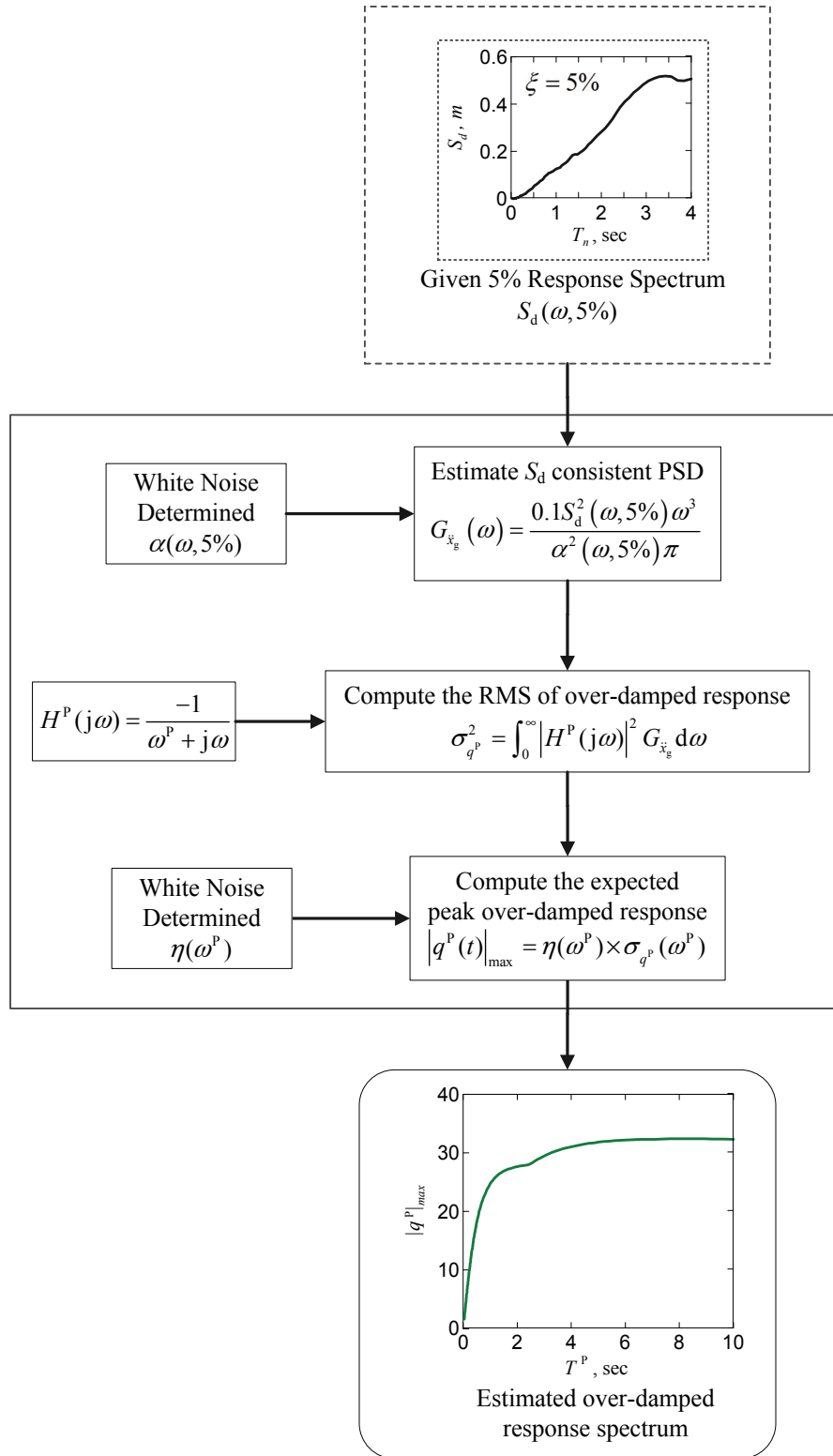


Figure 4.8 Over-damped response spectrum conversion procedures

4.5.3 Validation of the Over-damped Mode Response Spectrum

In order to demonstrate the accuracy and applicability of the proposed approach to convert the given 5% displacement response spectrum to the over-damped mode response spectrum, the exact mean over-damped mode response spectrum and the estimated over-damped mode response spectrum constructed according to the proposed procedures were compared using real earthquake events. Two far-field ground motion ensembles are used in this study. The first, ensemble A, is the ensemble used by Vamvatsikos and Cornell (2004). Detailed information about the records is tabulated in Table 4.3. These records are selected to have large magnitudes of 6.5 to 6.9 and moderate distances from the fault recorded on firm soil. Near-fault data are excluded. The second, ensemble B, is a set containing 50 far-field ground motions used by ATC (2007) to study the earthquake ground motion records scaling method targeted at performance-based design. Detailed information about the records in this ensemble is tabulated in Table 4.4. In the second ensemble, the records are selected based on magnitudes between 6.3 and 7.3, distances from the fault between 21Km to 50Km, and site conditions characterized by soil type C and D. To be consistent with the amount of records used in ensemble A, only the first 20 records from ensemble B are used. In this study, all records are scaled to have PGA equal to 0.4g. Figure 4.9 shows the mean 5% displacement response spectra for both ensembles. The mean exact over-damped mode spectra were constructed by performing a series of response history analysis per over-damped mode equation of motion shown in Equation (4.93) for each record. The over-damped modal period was chosen to be identical to those used in the determination of η . The resulting mean peak over-damped modal response was plotted against the over-damped modal period T^P shown as a solid line in Figure 4.10. The construction of the over-damped modal response follows these proposed procedures. The resulting over-damped mode response spectra converted from the 5% displacement spectra are indicated by the dotted line in Figure 4.10. It is observed that the over-damped mode response spectrum constructed by the proposed procedures is in close agreement with the exact values for both ensembles. This consistency suggests the applicability of the proposed procedures.

Table 4.3 Far-field ground motions used by Vamvatsikos and Cornell (2004)

No	Event	Station	ϕ° ¹
1	Loma Prieta, 1989	Agnews State Hospital	090
2	Imperial Valley, 1979	Plaster City	135
3	Loma Prieta, 1989	Hollister Diff. Array	255
4	Loma Prieta, 1989	Anderson Dam Downstrm	270
5	Loma Prieta, 1989	Coyote Lake Dam Downstrm	285
6	Imperial Valley, 1979	Cucapah	085
7	Loma Prieta, 1989	Sunnyvale Colton Ave	270
8	Imperial Valley, 1979	El Centro Array #13	140
9	Imperial Valley, 1979	Westmoreland Fire Station	090
10	Loma Prieta, 1989	Hollister South & Pine	000
11	Loma Prieta, 1989	Sunnyvale Colton Ave	360
12	Superstition Hills, 1987	Wildlife Liquefaction Array	090
13	Imperial Valley, 1979	Chihuahua	282
14	Imperial Valley, 1979	El Centro Array #13	230
15	Imperial Valley, 1979	Westmoreland Fire Station	180
16	Loma Prieta, 1989	WAHO	000
17	Superstition Hills, 1987	Wildlife Liquefaction Array	360
18	Imperial Valley, 1979	Plaster City	045
19	Loma Prieta, 1989	Hollister Diff. Array	165
20	Loma Prieta, 1989	WAHO	090

1. component

Table 4.4 Far-field ground motions used in ATC-58

Designation	Event	Station	M^1	r^1
FF1, FF2	Cape Mendocino 04/25/92 18:06	89509 Eureka—Myrtle & West	7.1	44.6
FF3, FF4	Cape Mendocino 04/25/92 18:06	89486 Fortuna—Fortuna Blvd	7.1	23.6
FF5, FF6	Coalinga 1983/05/02 23:42	36410 Parkfield—Cholame 3W	6.4	43.9
FF7, FF8	Coalinga 1983/05/02 23:42	36444 Parkfield—Fault Zone 10	6.4	30.4
FF9, FF10	Coalinga 1983/05/02 23:42	36408 Parkfield—Fault Zone 3	6.4	36.4
FF11, FF12	Coalinga 1983/05/02 23:42	36439 Parkfield—Gold Hill 3E	6.4	29.2
FF13, FF14	Imperial Valley 10/15/79 23:16	5052 Plaster City	6.5	31.7
FF15, FF16	Imperial Valley 10/15/79 23:16	724 Niland Fire Station	6.5	35.9
FF17, FF18	Imperial Valley 10/15/79 23:16	6605 Delta	6.5	43.6
FF19, FF20	Imperial Valley 10/15/79 23:16	5066 Coachella Canal #4	6.5	49.3
FF21, FF22	Landers 06/28/92 11:58	22074 Yermo Fire Station	7.3	24.9
FF23, FF24	Landers 06/28/92 11:58	12025 Palm Springs Airport	7.3	37.5
FF25, FF26	Landers 06/28/92 11:58	12149 Desert Hot Springs	7.3	23.2
FF27, FF28	Loma Prieta 10/18/89 00:05	47524 Hollister—South & Pine	6.9	28.8
FF29, FF30	Loma Prieta 10/18/89 00:05	47179 Salinas—John & Work	6.9	32.6
FF31, FF32	Loma Prieta 10/18/89 00:05	1002 APEEL 2—Redwood City	6.9	47.9
FF33, FF34	Northridge 01/17/94 12:31	14368 Downey—Co Maint Bldg	6.7	47.6
FF35, FF36	Northridge 01/17/94 12:31	24271 Lake Hughes #1	6.7	36.3
FF37, FF38	Northridge 01/17/94 12:31	14403 LA—116th St School	6.7	41.9
FF39, FF40	San Fernando 02/09/71 14:00	125 Lake Hughes #1	6.6	25.8
FF41, FF42	San Fernando 02/09/71 14:00	262 Palmdale Fire Station	6.6	25.4
FF43, FF44	San Fernando 02/09/71 14:00	289 Whittier Narrows Dam	6.6	45.1
FF45, FF46	San Fernando 02/09/71 14:00	135 LA—Hollywood Stor Lot	6.6	21.2
FF47, FF48	Superstition Hills (A) 11/24/87 05:14	5210 Wildlife Liquef. Array	6.3	24.7
FF49, FF50	Superstition Hills (B) 11/24/87 13:16	5210 Wildlife Liquef. Array	6.7	24.4

1. M = moment magnitude; r = closest site-to-fault-rupture distance

(Courtesy of Y.N.Huang)

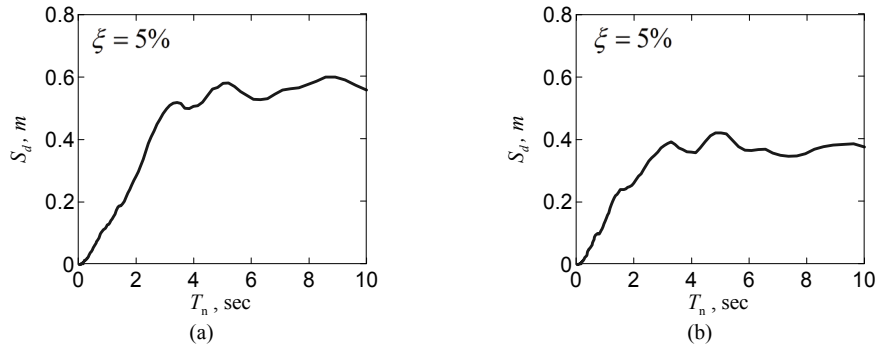


Figure 4.9 Mean 5% damping displacement response spectrum (a) ensemble A (b) ensemble B

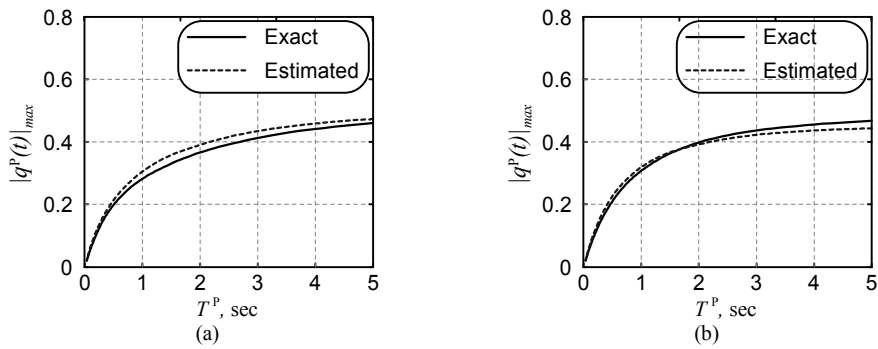


Figure 4.10 Comparisons of exact and estimated over-damped mode response spectrum (a) ensemble A (b) ensemble B

CHAPTER 5

SPATIALLY COMBINED RESPONSES TO MULTI-COMPONENT SEISMIC EXCITATIONS

5.1 Introduction

Spatially combined responses are those whose directions do not coincide with any specified reference axes of a structure. Examples include the peak resultant base shear forces seen in foundation systems and the maximum traveling distance of the isolators in base-isolated structures within the horizontal plane. During an earthquake, the direction and magnitude of the spatially combined responses temporarily fluctuate in a 3-dimensional (3-D) space. For these cases, approaches that can determine the critical responses of the spatially combined responses with a minimum amount of computational effort are desirable. In earthquake engineering, the seismic responses of a structure are determined by either the response history analysis method or the response spectrum method. These two methods have been extended to be suitable for structures with non-classical damping and over-critically damped modes as shown in the previous two chapters. They are ideal for estimating the critical response of a single response quantity specified in a given direction. For spatially combined responses, which are a combination of at most three orthogonal components, relevant methods to determine the critical responses have not yet been addressed. In general, the three orthogonal components contributing to the spatially combined response are correlated and the direction of the critical combination of the responses may not coincide with any given structure reference axes. In addition, during an earthquake, the direction and magnitude of the spatially combined responses fluctuate in the 3-D space as time advances. Traditionally in design practice, the critical response has been calculated by using the square root of the sum of the squares of the individual peak responses along the three orthogonal directions. This approach, in principle, leads to overly conservative results as the responses specified in the three orthogonal directions are unlikely to reach their respective maxima at the same time instant. As a result, it is desirable to develop methods to facilitate the identification of the critical responses of the spatially combined responses in the 3-D physical space

without examining all possible seismic inclinations and all direction vectors that a spatially combined response might take in the space domain.

In this chapter, the approaches using the response history analysis and response spectrum method to determine the critical response of a single response quantity to three-component excitation are first reviewed. These two approaches and their corresponding response expressions are then used to develop a method to account for the spatially combined responses. The development of the response history approach that predicts the critical spatially combined response is identical to the one established by Song et al. (2007b). As shown later, it is instructive to review this procedure as it provides insight into the development of the response spectrum approach and enhances the integrity of this topic. The mathematical formulation for the response spectrum approach follows research previously derived by Gupta and Singh (1977) and Menun and Der Kiureghian (2000), in which an envelope that bounds the response vectors is established. Their work is introduced in Section 5.3.2 by customizing it to spatially combined responses. In addition to the mathematical formulations for the development of the two proposed approaches, the geometrical relationships between the contributing response components and the resulting spatially combined responses varying in the space with time are explained in a graphical manner to provide a physical interpretation of the formulations. It is found that, for the case when the seismic inclination is specified, closed-form solutions to the critical responses are available. For the case when the seismic inclination is not available in advance, the closed-form solutions to find the critical spatially combined response are not available and numerical calculations have to be employed. However, the computational effort needed to find the solutions numerically is much less than examining all possible seismic inclinations and all potential directions along which the responses reach their maxima. The accuracy and application of the response spectrum approach for arbitrarily damped 3-D structures is evaluated in the application example given in Chapter 6.

5.2 Critical Value of Responses Specified in a Given Direction

In this section, the critical response value among all possible seismic inclination angles for responses specified in a given direction are determined, which are often along one of the predefined structure reference axes. The results presented in this section form a basis for the development of the approaches, which are presented in Section 5.3, to determine the critical response values of the spatially combined responses. Two approaches, in terms of response history analysis and response spectrum method, are discussed.

Consider a response quantity r_0 of an arbitrarily damped linear MDOF structure as described in Chapter 3. This response r_0 can be expressed as a linear combination of the nodal displacements, velocities or absolute accelerations, depending upon what types of responses are of interest. It is also seen that the form of any response r_0 is unified regardless of the types of the response quantities by taking advantage of the unified form presented in Chapter 3. The determination of the critical values of a single response expression in terms of the response history analysis and response spectrum method are discussed in Sections 5.2.1 and 5.2.2, respectively.

5.2.1 Excitation Histories as Inputs

When excitation histories are used as input excitations, the response $r_0(t, \theta)$ can be expressed according to Equation (3.142), which is generalized for the case when the seismic direction of the ground motion inclines in the horizontal plane at an angle θ . That is,

$$r_0(t, \theta) = [r_{1x}(t) + r_{2y}(t)] \cos \theta + [r_{1y}(t) - r_{2x}(t)] \sin \theta + r_{3z}(t) \quad (5.1)$$

The definitions of the terms $r_{1x}(t)$, $r_{2y}(t)$, $r_{1y}(t)$ and $r_{2x}(t)$ are given in Section 3.7. The dependence of the response $r_0(t, \theta)$ on θ is shown explicitly in Equation (5.1). The peak response among the entire oscillation process can be easily determined when the seismic incident angle θ is known in advance. However, in general, this angle is uncertain. In such cases, designing a structure with the most critical responses is suggested in order to improve the design safety margin for critical infrastructure. Thus, it is desirable to

develop an approach to determine the critical responses that avoids computations for all possible values of θ .

Next, Equation (5.1) is rewritten for a specific time instant, such as t^* , as

$$\begin{aligned} r_0(t^*) &= r_0^c(t^*) \cos \theta + r_0^s(t^*) \sin \theta + r_{3z}(t^*) \\ &= r_0^{norm}(t^*) \cos(\theta + \phi^*) + r_{3z}(t^*) \end{aligned} \quad (5.2)$$

where

$$r_0^c(t^*) = r_{1x}(t^*) + r_{2y}(t^*) \quad (5.3)$$

$$r_0^s(t^*) = r_{1y}(t^*) - r_{2x}(t^*) \quad (5.4)$$

$$r_0^{norm}(t^*) = \sqrt{[r_0^c(t^*)]^2 + [r_0^s(t^*)]^2} \geq 0 \quad (5.5)$$

and the phase angle ϕ^* can be determined for each time instant by solving

$$\tan \phi^* = \frac{-r_0^s(t^*)}{r_0^c(t^*)} \quad (5.6)$$

It is clear from Equation (5.2) that the variation of the response $r_0(t^*)$ with respect to θ at time instant t^* follows a sinusoidal pattern as shown in Figure 5.1. The bold line in the figure indicates the variation of the term $r_0^{norm}(t^*) \cos(\theta + \phi)$ and the upper dotted line represents the variation of $r_0(t^*)$ with positive $r_{3z}(t^*)$ and the lower dotted line stands for the variation of $r_0(t^*)$ with negative $r_{3z}(t^*)$. As seen in the figure, the maximum value of the response $r_0(t^*, \theta)$, denoted as $r_m(t^*)$, as θ varies from 0^0 to 360^0 can be written as

$$r_m(t^*) = r_0^{norm}(t^*) + |r_{3z}(t^*)| \quad (5.7)$$

It is easy to find that the value of the seismic incident angle resulting in the maximum response, $r_m(t^*)$, at time instant t^* , denoted as θ_{cr}^* , is independent of the response $r_{3z}(t^*)$ and is obtained by solving $\cos(\theta_{cr}^* + \phi^*) = 1$. The result is

$$\theta_{cr}^* = -\phi^* = \tan^{-1} \frac{r_0^s(t^*)}{r_0^c(t^*)} \quad (5.8)$$

By carrying out the steps addressed between Equations (5.2) and (5.8) recursively for each time step, the entire history defining the maximum response at each time step among all incident angles can be established. As a result, the peak value of this history can be easily located, which is the critical value of response $r_0(t, \theta)$.

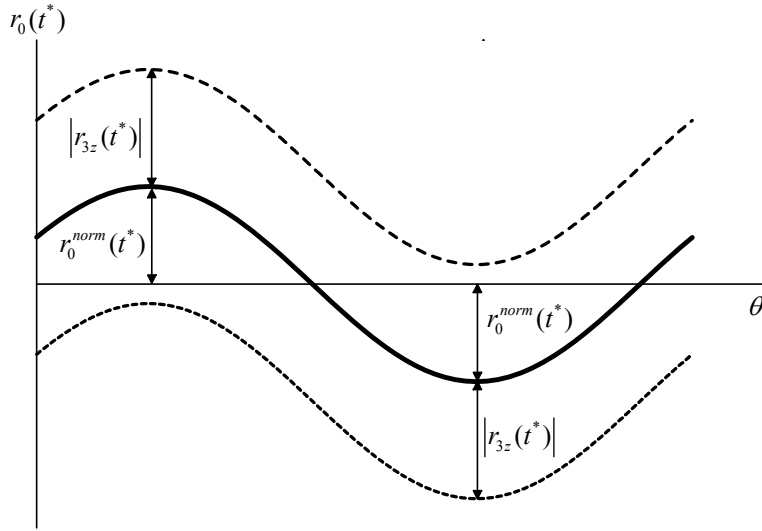


Figure 5.1 Variation of $r_0(t^*)$ at time instant t^* as θ varies

5.2.2 Response Spectra as Inputs

When the seismic excitations are described in terms of the response spectra, the peak response $|r_0(t)|_{\max}^2$ can be determined by Equation (4.56) shown in Chapter 4 as

$$\begin{aligned} R_0^2 &= |r_0(t, \theta)|_{\max}^2 = |\mathbf{d}^T \mathbf{u}_0(t, \theta)|_{\max}^2 \\ &= \mathbf{d}^T \mathbf{V} \mathbf{d} \\ &= \mathbf{d}^T (\mathbf{V}_1 + \mathbf{V}_2 \sin^2 \theta + \mathbf{V}_3 \sin \theta \cos \theta) \mathbf{d} \end{aligned} \quad (5.9)$$

The definitions of \mathbf{d} , \mathbf{V}_1 , \mathbf{V}_2 and \mathbf{V}_3 are given in Section 4.4.3. When the seismic incident angle θ is given in advance, Equation (5.9) is ready to be used to obtain the peak

responses. For the cases in which the θ is not specified, it would be necessary to identify the peak value as θ varies. The value of θ_{cr} that maximizes the response $|r_0(t, \theta)|_{\max}^2$ can be found by solving

$$\frac{d|r_0(t, \theta)|_{\max}^2}{d\theta} = 2\mathbf{d}^T \mathbf{V}_2 \mathbf{d} \sin \theta \cos \theta + \mathbf{d}^T \mathbf{V}_3 \mathbf{d} (\cos^2 \theta - \sin^2 \theta) = 0 \quad (5.10)$$

such that

$$\frac{d^2|r_0(t, \theta)|_{\max}^2}{d\theta^2} = 2\mathbf{d}^T \mathbf{V}_2 \mathbf{d} \cos 2\theta - 2\mathbf{d}^T \mathbf{V}_3 \mathbf{d} \sin 2\theta < 0 \quad (5.11)$$

The solution satisfying both Equations (5.10) and (5.11) is

$$\tan 2\theta_{cr} = -\frac{\mathbf{d}^T \mathbf{V}_3 \mathbf{d}}{\mathbf{d}^T \mathbf{V}_2 \mathbf{d}} \quad (5.12)$$

or

$$\sin 2\theta_{cr} = \frac{\mathbf{d}^T \mathbf{V}_3 \mathbf{d}}{W} \quad \text{and} \quad \cos 2\theta_{cr} = -\frac{\mathbf{d}^T \mathbf{V}_2 \mathbf{d}}{W} \quad (5.13)$$

where

$$W = \left[(\mathbf{d}^T \mathbf{V}_2 \mathbf{d})^2 + (\mathbf{d}^T \mathbf{V}_3 \mathbf{d})^2 \right]^{1/2} \quad (5.14)$$

Note that the critical angle is not influenced by the vertical excitation as the response matrix \mathbf{V}_1 , which contains the responses contributed from the vertical excitation, is not involved in determining the critical angle θ_{cr} as shown in Equation (5.12).

Substituting Equation (5.13) into Equation (5.9) gives

$$R_0^2 = \mathbf{d}^T \left(\mathbf{V}_1 + \frac{\mathbf{V}_2}{2} + \frac{\mathbf{V}_2 \mathbf{d}^T \mathbf{V}_2 \mathbf{d}}{2W} + \frac{\mathbf{V}_3 \mathbf{d}^T \mathbf{V}_3 \mathbf{d}}{2W} \right) \mathbf{d} \quad (5.15)$$

Equation (5.15) defines the most critical response that could happen among all seismic incident angle θ 's. This is an explicit formula which is convenient for design purposes, as it avoids computation of the critical angles (Menun and Der Kiureghian, 2000).

5.3 Critical Value of the Spatially Combined Responses

Figure 5.2 illustrates the concept of the spatially combined responses. It is seen that the nodal displacement or velocity of nodes 1 and 2 in the space domain can be fully described by their three respective orthogonal components. The responses of nodes 1 and 2 varying in the 3-D space are referred to as the spatially combined responses. These types of responses may be important in certain cases related to the design of structures with added dampers. For instance, the relative displacement or velocity between nodes 1 and 2 is a critical response that has to be considered when a damper is inserted between nodes 1 and 2. The approaches described in the previous section are ideal for the determination of the critical values of the responses specified in a given direction (i.e., one of the orthogonal components shown in Figure 5.2). However, due to the complexity of the structures, the most critical responses may not occur along any of the given directions of its reference axes. Furthermore, the direction of the spatially combined response changes temporally over the entire sphere of space. This section presents two approaches on how to determine the most critical responses of the spatially combined responses for seismic inputs described in terms of acceleration histories and response spectra, respectively.

5.3.1 Response History Approach

Let $r_{0x}(t, \theta)$, $r_{0y}(t, \theta)$ and $r_{0z}(t, \theta)$ represent the components of the response at a certain location along a set of structure reference axes **X**, **Y** and **Z**, respectively. They can be expressed in a vector form through Equation (5.2) as follows. Let $\mathbf{r}_0(t, \theta) = [r_{0x}(t, \theta) \quad r_{0y}(t, \theta) \quad r_{0z}(t, \theta)]^T$ denote the spatially combined response consisting of the time-varying responses $r_{0x}(t, \theta)$, $r_{0y}(t, \theta)$ and $r_{0z}(t, \theta)$ at a certain location of the structure. Consequently, the spatially combined response $\mathbf{r}_0(t, \theta)$ can be written in the form of a matrix as

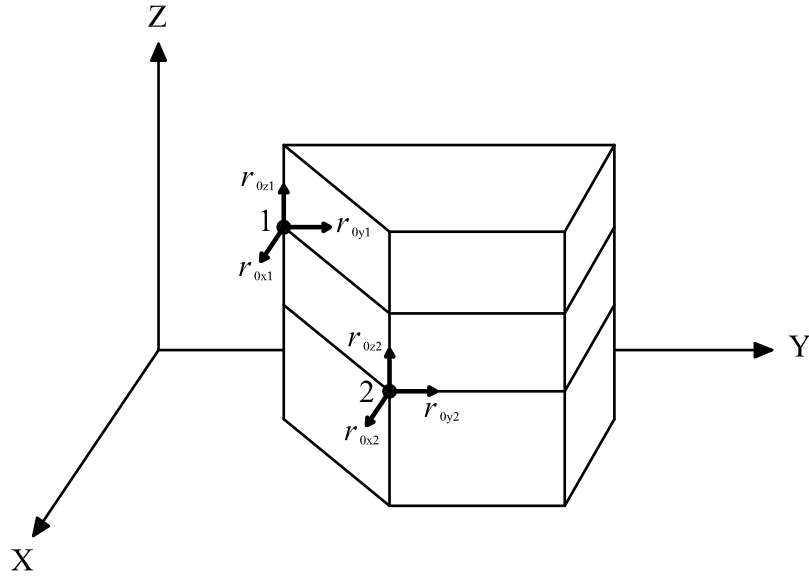


Figure 5.2 Concept of spatially combined responses

$$\mathbf{r}_0(t, \theta) = \begin{Bmatrix} r_{0x}(t, \theta) \\ r_{0y}(t, \theta) \\ r_{0z}(t, \theta) \end{Bmatrix} = \mathbf{L}\Theta \quad (5.16)$$

where $\mathbf{L} = [\mathbf{L}_1 \quad \mathbf{L}_2 \quad \mathbf{L}_3]$ and $\Theta = [\cos \theta \quad \sin \theta \quad 1]^T$. The three elements of \mathbf{L} are $\mathbf{L}_1 = [r_{0x}^c(t) \quad r_{0y}^c(t) \quad r_{0z}^c(t)]^T$, $\mathbf{L}_2 = [r_{0x}^s(t) \quad r_{0y}^s(t) \quad r_{0z}^s(t)]^T$ and $\mathbf{L}_3 = [r_{3z}^{0x}(t) \quad r_{3z}^{0y}(t) \quad r_{3z}^{0z}(t)]^T$. The norm of the spatially combined response $\mathbf{r}_0(t, \theta)$, which is the magnitude of the spatially combined response $\mathbf{r}_0(t, \theta)$, is defined by

$$\|\mathbf{r}_0(t, \theta)\|^2 = \Theta^T \mathbf{L}^T \mathbf{L} \Theta \quad (5.17)$$

The term $\mathbf{L}^T \mathbf{L}$ is defined as the response process matrix. When the seismic inclination angle is specified in advance (i.e., Θ is known), the peak response of the spatially combined response $\mathbf{r}_0(t, \theta)$ can be easily obtained. It is evident that the magnitude of the spatially combined response $\mathbf{r}_0(t, \theta)$ is a function of the seismic incident angle θ . For the

cases where the seismic inclination angle θ is not given, in principle, it is necessary to consider all possible values that θ can take to obtain the most critical response value. In the following, a rapid transformation approach is established to determine the critical response when the seismic inclination angle θ is not known, which requires only a few computations instead of performing response analyses for all possible θ s.

For a certain time instant t^* , Equation (5.17) can be expanded as

$$\|\mathbf{r}_0(t^*, \theta)\|^2 = \begin{bmatrix} \cos \theta & \sin \theta & 1 \end{bmatrix} \begin{bmatrix} l_{11} & l_{12} & l_{13} \\ l_{21} & l_{22} & l_{23} \\ l_{31} & l_{32} & l_{33} \end{bmatrix} \begin{bmatrix} \cos \theta \\ \sin \theta \\ 1 \end{bmatrix} \quad (5.18)$$

where $l_{11} = \mathbf{L}_1^T \mathbf{L}_1$, $l_{22} = \mathbf{L}_2^T \mathbf{L}_2$, $l_{33} = \mathbf{L}_3^T \mathbf{L}_3$, $l_{12} = l_{21} = \mathbf{L}_1^T \mathbf{L}_2$, $l_{13} = l_{31} = \mathbf{L}_1^T \mathbf{L}_3$ and $l_{23} = l_{32} = \mathbf{L}_2^T \mathbf{L}_3$ for the time instant t^* . The value of θ that maximizes the spatially combined response at time instant t^* can be found by solving

$$\frac{d\|\mathbf{r}_0(t^*, \theta)\|^2}{d\theta} = (l_{22} - l_{11}) \sin 2\theta + 2l_{12} \cos 2\theta - 2l_{13} \sin \theta + 2l_{23} \cos \theta = 0 \quad (5.19)$$

Equation (5.19) is a fourth-order polynomial and has no closed-form solution for θ (Song et al., 2007b). Thus, numerical algorithms are required to obtain the solutions. These four roots are then substituted into Equation (5.18) to determine the corresponding responses. The maximum response is the peak response. Repeating this procedure for each time step gives the complete history defining the maximum spatially combined response at each time step. The peak response of the spatially combined response, $\mathbf{r}_0(t, \theta)$ for uncertain θ , can then be determined.

5.3.1.1 Special Case: No Vertical Excitation

When the vertical excitation is not considered, which is commonly assumed in design practice, a convenient closed-form solution for the critical spatially combined responses with uncertain θ can be derived. Under this assumption, the norm of the spatially combined response $\mathbf{r}_0(t^*, \theta)$ shown in Equation (5.18) can be reduced to

$$\|\mathbf{r}_0(t^*, \theta)\|^2 = [\cos \theta \quad \sin \theta] \mathbf{L}^T \mathbf{L} \begin{bmatrix} \cos \theta \\ \sin \theta \end{bmatrix} \quad (5.20)$$

in which the response process matrix $\mathbf{L}^T \mathbf{L}$ is also reduced to

$$\mathbf{L}^T \mathbf{L} = \begin{bmatrix} l_{11} & l_{12} \\ l_{21} & l_{22} \end{bmatrix} \quad (5.21)$$

The value of θ resulting in the maximum $\mathbf{r}_0(t^*, \theta)$ is obtained by solving

$$\frac{d \|\mathbf{r}_0(t^*, \theta)\|^2}{d\theta} = (l_{22} - l_{11}) \sin 2\theta + 2l_{12} \cos 2\theta = 0 \quad (5.22)$$

such that

$$\frac{d^2 \|\mathbf{r}_0(t^*, \theta)\|^2}{d\theta^2} = -2(l_{22} - l_{11}) \cos 2\theta - 4l_{12} \sin 2\theta < 0 \quad (5.23)$$

Substituting the solution satisfying Equations (5.22) and (5.23) into Equation (5.20) gives the critical response. The result is

$$\|\mathbf{r}_0(t^*, \theta)\|_{\max}^2 = \frac{l_{11}(t^*) + l_{22}(t^*)}{2} + \left[\left(\frac{l_{11}(t^*) - l_{22}(t^*)}{2} \right)^2 + l_{12}^2(t^*) \right]^{1/2} \quad (5.24)$$

Equation (5.24) is a closed-form solution defining the critical response for each time step. Furthermore, it is the larger eigenvalue of the response matrix $\mathbf{L}^T \mathbf{L}$. Using Equation (5.24) for each time step generates the maximum response history, from which the most critical one can be easily determined.

5.3.2 Response Spectrum Approach (Menun and Der Kiureghian, 2000)

To determine the peak value of the spatially combined responses as the inputs are described in terms of the response spectra, the spatially combined response $\mathbf{r}_0(t, \theta)$ shown in Equation (5.16) in another form is expressed as

$$\mathbf{r}_0(t, \theta) = \begin{Bmatrix} r_{0x}(t, \theta) \\ r_{0y}(t, \theta) \\ r_{0z}(t, \theta) \end{Bmatrix} = \mathbf{D}^T \mathbf{u}_0(t, \theta) \quad (5.25)$$

where $\mathbf{D} = [\mathbf{d}_x \quad \mathbf{d}_y \quad \mathbf{d}_z]$ is a transformation matrix which transforms the system spatially combined response $\mathbf{u}_0(t, \theta)$ into three individual components at a certain location referenced to axes \mathbf{X} , \mathbf{Y} and \mathbf{Z} , respectively. That is, $r_{0x}(t, \theta) = \mathbf{d}_x^T \mathbf{u}_0(t, \theta)$, $r_{0y}(t, \theta) = \mathbf{d}_y^T \mathbf{u}_0(t, \theta)$ and $r_{0z}(t, \theta) = \mathbf{d}_z^T \mathbf{u}_0(t, \theta)$. To obtain the peak value of the response combined from the three components, the idea is to examine the maximum value of the spatially combined response $\mathbf{r}_0(t, \theta)$ projected on each possible direction in the space domain. Consider the projection of the spatially combined response $\mathbf{r}_0(t, \theta)$ onto a unit vector \mathbf{n} in the 3-D space domain

$$r_{0n}(t, \theta) = \mathbf{n}^T \mathbf{r}_0(t, \theta) = \mathbf{n}^T \mathbf{D}^T \mathbf{u}_0(t, \theta) \quad (5.26)$$

\mathbf{n} consists of three elements $\cos \alpha$, $\cos \beta$ and $\cos \gamma$, in which α , β and γ are the angles between the unit vector \mathbf{n} and the reference axes \mathbf{X} , \mathbf{Y} and \mathbf{Z} , respectively. Note that the magnitude of the unit vector \mathbf{n} is expressed as

$$\|\mathbf{n}\| = \cos^2 \alpha + \cos^2 \beta + \cos^2 \gamma = 1. \quad (5.27)$$

According to Equation (5.9), it is found that the peak value of the projection of the spatially combined response $\mathbf{r}_0(t)$ on the unit vector \mathbf{n} , $R_{0n} = |r_{0n}(t, \theta)|_{\max}$, can be estimated by the response spectrum method as

$$\begin{aligned} R_{0n}^2 &= \mathbf{n}^T \mathbf{D}^T (\mathbf{V}_1 + \mathbf{V}_2 \sin^2 \theta + \mathbf{V}_3 \sin \theta \cos \theta) \mathbf{D} \mathbf{n} \\ &= \mathbf{n}^T \mathbf{D}^T \mathbf{V} \mathbf{D} \mathbf{n} \\ &= \mathbf{n}^T \mathbf{R} \mathbf{n} \end{aligned} \quad (5.28)$$

In Equation (5.28), the following term is introduced

$$\mathbf{R} = \mathbf{D}^T \mathbf{V} \mathbf{D} \quad (5.29)$$

which is defined as the response spectrum-based response matrix for spatially combined response $\mathbf{r}_0(t, \theta)$. It can easily be verified that \mathbf{R} is a 3×3 symmetric matrix, which gives the correlations between the response processes in the spatially combined response $\mathbf{r}_0(t, \theta)$. To determine the peak value of R_{0n} , basically, it is necessary to carry out the calculation for each possible unit vector \mathbf{n} . However, if the seismic incidence θ is known in advance, a convenient method can be found to determine the peak response without carrying out repetitive computations. It is addressed below.

Equation (5.27) indicates that when the unit vector \mathbf{n} varies in the 3-D space domain, it is actually equivalent to a 3-D real vector set with a unit Euclidian norm. The trace of these unit vectors is a unit sphere. Due to this condition, the peak value of R_{0n}^2 can be determined from the eigenvalues of the response matrix \mathbf{R} . Since \mathbf{R} is a 3×3 symmetric matrix, it has three real eigenvalues. Denote the λ_{ii} , $ii = 1, 2, 3$, as the eigenvalues of the \mathbf{R} ; the corresponding unit vectors are \mathbf{n}_{ii} , $ii = 1, 2, 3$. Examining the context of the eigen analysis, the following relationship must hold.

$$\mathbf{R}\mathbf{n}_{ii} = \lambda_{ii}\mathbf{n}_{ii} \quad (5.30)$$

Comparing Equations (5.28) and (5.30), it is found that the peak value of the projection of \mathbf{R} onto \mathbf{n}_{ii} is

$$R_{0n_{ii}}^2 = \mathbf{n}_{ii}^T \mathbf{R} \mathbf{n}_{ii} = \mathbf{n}_{ii}^T \lambda_{ii} \mathbf{n}_{ii} = \lambda_{ii} \quad (5.31)$$

Equation (5.31) shows that the all eigenvalues are non-negative as $R_{0n_{ii}}^2 \geq 0$. Among the three eigenvalues, the largest one gives the peak response of the spatially combined response $\mathbf{r}_0(t, \theta)$ in the 3-D space within the entire vibration duration and its corresponding unit vector is the direction along which the magnitude of the spatially combined response reaches its maximum. Following the preceding procedure, the peak response of the spatially combined response can be easily obtained using the response spectrum method when the seismic incidence is specified in advance.

In the subsequent section, a special case of a two-component spatially combined response is examined in an attempt to provide physical insight into the above formulation in a graphical way, in which a closed-form solution can be found.

5.3.2.1 Special Case: Two-component Spatially Combined Response

Consider the case where the spatially combined response $\mathbf{r}_0(t, \theta)$ only consists of two components. For example,

$$\mathbf{r}_0(t, \theta) = \begin{Bmatrix} r_{0x}(t, \theta) \\ r_{0y}(t, \theta) \end{Bmatrix} = \mathbf{D}^T \mathbf{u}_0(t, \theta) \quad (5.32)$$

in which $\mathbf{D} = [\mathbf{d}_x \quad \mathbf{d}_y]$. In such a case, the direction of the spatially combined response $\mathbf{r}_0(t, \theta)$ is confined to the plane **X-Y**. As a result, the unit vector \mathbf{n} becomes $\mathbf{n} = [\cos \alpha \quad \sin \alpha]^T$, in which the α is the angle formed by axis **X** and vector \mathbf{n} . Figure 5.3 shows the geometrical relationship of the spatially combined response and the unit vector \mathbf{n} . The projection of the spatially combined response $\mathbf{r}_0(t, \theta)$ on the unit vector \mathbf{n} is also shown in Figure 5.3 and can be written as

$$r_{0n}(t, \theta) = \mathbf{n}^T \mathbf{r}_0(t, \theta) = [\cos \alpha \quad \sin \alpha]^T \begin{Bmatrix} r_{0x}(t, \theta) \\ r_{0y}(t, \theta) \end{Bmatrix} \quad (5.33)$$

Note that the magnitude of this projection varies temporally. Based on Equation (5.29), the response spectrum-based response matrix \mathbf{R} reduces to

$$\begin{aligned} \mathbf{R} &= \mathbf{D}^T \mathbf{V} \mathbf{D} \\ &= \begin{bmatrix} \mathbf{d}_x^T \mathbf{V} \mathbf{d}_x & \mathbf{d}_x^T \mathbf{V} \mathbf{d}_y \\ \mathbf{d}_y^T \mathbf{V} \mathbf{d}_x & \mathbf{d}_y^T \mathbf{V} \mathbf{d}_y \end{bmatrix} \end{aligned} \quad (5.34)$$

Note that $\mathbf{d}_x^T \mathbf{V} \mathbf{d}_y = \mathbf{d}_y^T \mathbf{V} \mathbf{d}_x$. As a result, Equation (5.28) can be written as

$$R_{0n}^2 = \mathbf{n}^T \begin{bmatrix} \mathbf{d}_x^T \mathbf{V} \mathbf{d}_x & \mathbf{d}_x^T \mathbf{V} \mathbf{d}_y \\ \mathbf{d}_y^T \mathbf{V} \mathbf{d}_x & \mathbf{d}_y^T \mathbf{V} \mathbf{d}_y \end{bmatrix} \mathbf{n} \quad (5.35)$$

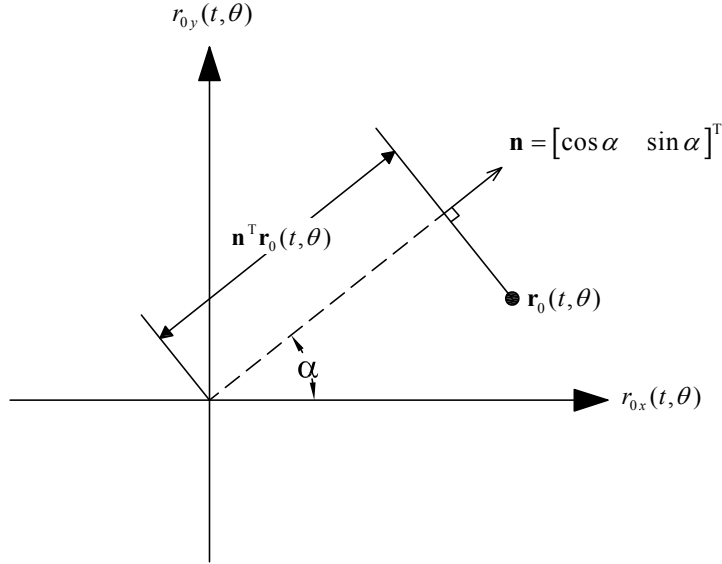


Figure 5.3 Projection of the two-component spatially combined response

Equation (5.35) defines the peak response of the spatially combined response with two components along the projection direction \mathbf{n} . By varying \mathbf{n} , an envelope that bounds the response of the spatially combined response $r_0(t, \theta)$ can be established, and this envelope is in fact an ellipse (Menun and Der Kireghian, 2000). Figure 5.4 illustrates the concept of the generation of the response elliptical bounding envelope for the two-component spatially combined response.

Similar to the spatially combined response with three response components, the most critical case in which the spatially combined response reaches its maximum response can be obtained by finding the eigenvalues of the response spectrum-based matrix \mathbf{R} . There are two eigenvalues of matrix \mathbf{R} . The value of the larger one is denoted as λ_a and can be obtained by

$$\lambda_a = \frac{\mathbf{d}_x^T \mathbf{V} \mathbf{d}_x + \mathbf{d}_y^T \mathbf{V} \mathbf{d}_y}{2} + \left[\left(\frac{\mathbf{d}_x^T \mathbf{V} \mathbf{d}_x - \mathbf{d}_y^T \mathbf{V} \mathbf{d}_y}{2} \right)^2 - (\mathbf{d}_x^T \mathbf{V} \mathbf{d}_y)^2 \right]^{1/2} \quad (5.36)$$

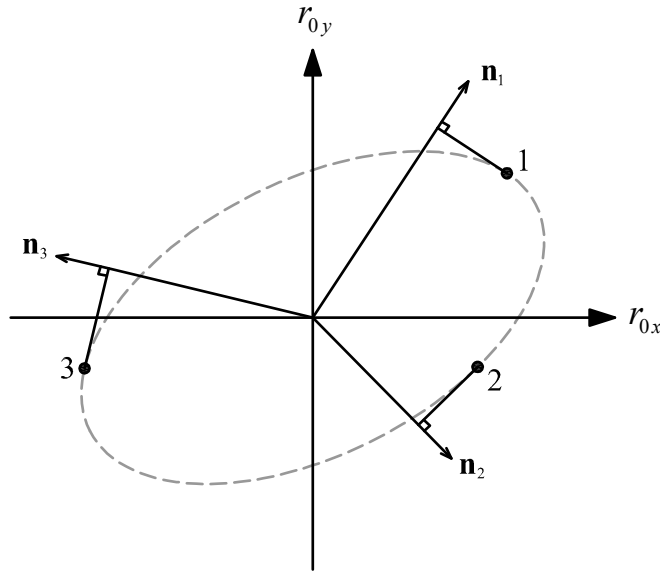


Figure 5.4 Response elliptical envelope for two-component spatially combined response

The square root of the λ_a gives the maximum value of the spatially combined response within the entire duration when the seismic incidence θ is specified.

5.3.2.2 Unknown Seismic Incidence

When θ is unknown, the peak response of the spatially combined response is not only function of \mathbf{n} but also the seismic incidence θ . That is, it is necessary to consider all possible values of θ . For a given direction \mathbf{n} , the value of θ resulting in the maximum value of the magnitude of the spatially combined response can be found by solving (Menun and Der Kiureghian, 2000)

$$\frac{dR_{0n}^2}{d\theta} = \frac{d}{d\theta} \mathbf{n}^T \mathbf{D}^T \mathbf{V} \mathbf{D} \mathbf{n} = \mathbf{n}^T \mathbf{D}^T (\mathbf{V}_2 \sin 2\theta + \mathbf{V}_3 \cos 2\theta) \mathbf{D} \mathbf{n} = 0 \quad (5.37)$$

such that

$$\frac{d^2 R_{0n}^2}{d\theta^2} = \frac{d^2}{d\theta^2} \mathbf{n}^T \mathbf{D}^T \mathbf{V} \mathbf{D} \mathbf{n} = \mathbf{n}^T \mathbf{D}^T (2\mathbf{V}_2 \cos 2\theta - 2\mathbf{V}_3 \sin 2\theta) \mathbf{D} \mathbf{n} < 0 \quad (5.38)$$

As a result, the value of θ should satisfy

$$\sin 2\theta = \frac{\mathbf{n}^T \mathbf{D}^T \mathbf{V}_3 \mathbf{D} \mathbf{n}}{Q} \quad \text{and} \quad \cos 2\theta = \frac{-\mathbf{n}^T \mathbf{D}^T \mathbf{V}_2 \mathbf{D} \mathbf{n}}{Q} \quad (5.39)$$

where

$$Q = \left[\left(\mathbf{n}^T \mathbf{D}^T \mathbf{V}_3 \mathbf{D} \mathbf{n} \right)^2 + \left(\mathbf{n}^T \mathbf{D}^T \mathbf{V}_2 \mathbf{D} \mathbf{n} \right)^2 \right]^{1/2} \quad (5.40)$$

Substituting Equation (5.39) into Equation (5.28), results in

$$R_{0\mathbf{n}}^2 = \mathbf{n}^T \mathbf{R}_F \mathbf{n} \quad (5.41)$$

where

$$\mathbf{R}_F = \mathbf{D}^T \left[\mathbf{V}_1 + \frac{1}{2} \mathbf{V}_2 \left(1 + \frac{\mathbf{n}^T \mathbf{D}^T \mathbf{V}_2 \mathbf{D} \mathbf{n}}{Q} \right) + \frac{1}{2} \mathbf{V}_3 \frac{\mathbf{n}^T \mathbf{D}^T \mathbf{V}_3 \mathbf{D} \mathbf{n}}{Q} \right] \quad (5.42)$$

Equation (5.41) gives the maximum magnitude of the spatially combined response, $\mathbf{r}_0(t)$, along direction \mathbf{n} within all possible seismic incidences. Note that Equations (5.28) and (5.41) are similar. However, the maximum value of $R_{0\mathbf{n}}^2$ among all \mathbf{n} cannot be determined by the eigenvalues of the matrix \mathbf{R}_F since the matrix \mathbf{R}_F is a function of \mathbf{n} . Thus, it would be necessary to examine all possible directions that \mathbf{n} can take to obtain the maximum response when the seismic incidence θ is not specified. However, in engineering practice, it is reasonable to assume that the direction of the responses such as relative deformation or velocity between two nodes is the direction formed by two nodes as the dimension of the responses is small compared to the dimension of the structure. In such cases, the direction of the unit vector \mathbf{n} is known in advance. As a result, the peak response can be determined by the larger eigenvalue of the response matrix \mathbf{R}_F .

CHAPTER 6

APPLICATION EXAMPLE

6.1 Introduction

In Chapters 3 and 4, seismic response analysis approaches for 3-D arbitrarily damped linear structures using both the ground motion history and the response spectrum as the input excitations through modal analysis are given. In this chapter, the applications of these two methods are demonstrated and the accuracy of the GCQC3 rule developed in Chapter 4 is assessed by comparing the results to the “exact” results obtained by the response history analyses for an example 3-D multistory building with added linear viscous dampers. Also, the effects of using the classical damping assumption and ignoring the over-damped modes in the analysis results are examined. The accuracy of the response spectrum method developed in Chapter 5 to predict the peak response of a spatially combined response is also evaluated by comparing the response envelopes of the floor accelerations obtained by the developed method to those obtained by the response history analyses. First, the configurations of the example building frame and the ground motions considered are described, followed by an evaluation of the two analysis procedures. Note that the procedure developed in Chapter 4 for the response spectrum method is based on random vibration theory and assumes that the peak proportional factors are involved. The ground motion is assumed to have a strong stationary phase with broad frequency content and a duration several times longer than the fundamental period of the structure. These assumptions will affect the accuracy of the response spectrum method when dealing with real earthquakes. The comparison of the estimated and exact responses is made within a statistical framework. Further, in order to evaluate the errors caused by the combination rule itself and the classical damping assumption, the estimated modal maximum responses are replaced by the exact modal maxima. These exact modal maxima and exact peak responses are determined by the response history analysis.

6.2 Description of the Example Building

A mid-rise 6-story asymmetric steel building is considered in the following analyses.

Figure 6.1 shows a typical floor plan of the building. The seismic resistance system consists of four special steel moment frames, denoted as Frames 1, 2, 3 and 4, respectively, located on the perimeter of the building as indicated by the bold lines in Figure 6.1. In accordance with engineering practice, the corner columns are not considered in the seismic resistance moment frames. Each of the floors is assumed to be rigid and has three degrees-of-freedom: two horizontal translational (along **X**-axis and **Y**-axis) and one rotational (about **Z**-axis). Therefore, a total of 18 degrees-of-freedom will be considered in constructing the equations of motion of this example building. The eccentricity, caused by the asymmetric configuration, and the rotational degrees-of-freedom are used to consider the coupling effects among the two orthogonal horizontal directions. Frames 2, 3 and 4 are adopted from “Example No.5: frame 6S-75” in Ramirez et al. (2000), which is designed to meet the 1997 *NEHRP Recommended Provisions for Seismic Regular for New Buildings and other Structures* (FEMA, 1997), assuming that the building will be enhanced by viscous dampers and is located at a site with a design spectrum characterized by parameters $S_{D1} = 0.6$, $S_{DS} = 1.0$ and $T_S = 0.6$ sec per NEHRP (1997). As a result, Frames 2, 3 and 4 are three-bay special moment frames. In order to meet the dimension along the Frame 1 direction, the above three-bay frame is expanded to be a five-bay frame while the sections of the additional beams and columns remain unchanged. All frame beams and columns are oriented such that the strong axes are perpendicular to the plane of the frame. Each frame is equipped with linear viscous dampers to improve the seismic performance of the building. Frame 1 has no damper in the first floor in order to provide open space. The rest of the stories are equipped with linear viscous dampers. Frames 2 and 3 have three linear viscous dampers concentrated in the first story, respectively. Frame 4 has linear viscous dampers installed from the first to the fourth story. This damper distribution is selected because it is representative of damper distributions that are commonly encountered when performing damper configuration optimization. This damper distribution results in a highly non-classically damped structure with certain over-critically damped modes. The inherent damping ratios of this building are assumed to be 2% for all modes.

In summary, the beam and column sizes and configurations as well as the damper properties for Frames 1 to 4 are shown in Figures 6.2 to 6.5, respectively. The reactive masses of each story are listed in Table 6.1.

Using the mass, stiffness and damping matrices, the modal properties of this building are determined by eigenvalue analysis programmed in MATLAB by using both the forced classical damping assumption and the state space approach.

Table 6.2 summarizes the modal periods and damping ratios. The data listed in this table are sorted in an ascending order according to the modal period. Table 6.2 shows that there are 14 over-damped modes, marked in bold face. It is observed that the damping ratios obtained by the forced classical damping assumption are significantly different from those exact damping ratios determined from the state space approach. In particular, using the forced damping assumption overestimates the damping ratios and the presence of the over-damped modes are not identified correctly.

Table 6.1 Reactive mass of the example building

Story	Reactive mass (Kg)
1	380,750
2	380,750
3	380,750
4	380,750
5	380,750
6	205,740

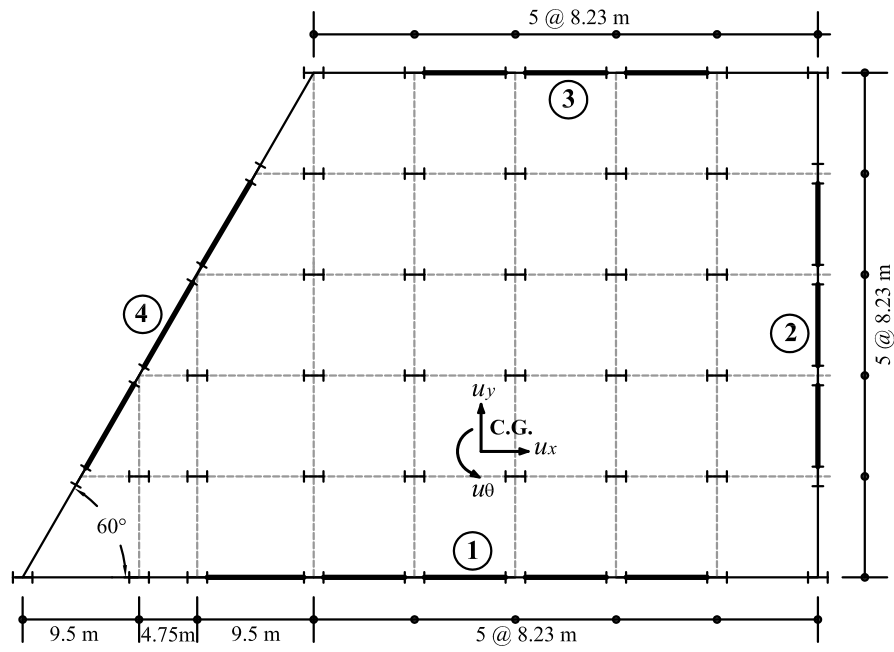


Figure 6.1 Planar view of the example six-story steel moment frame building

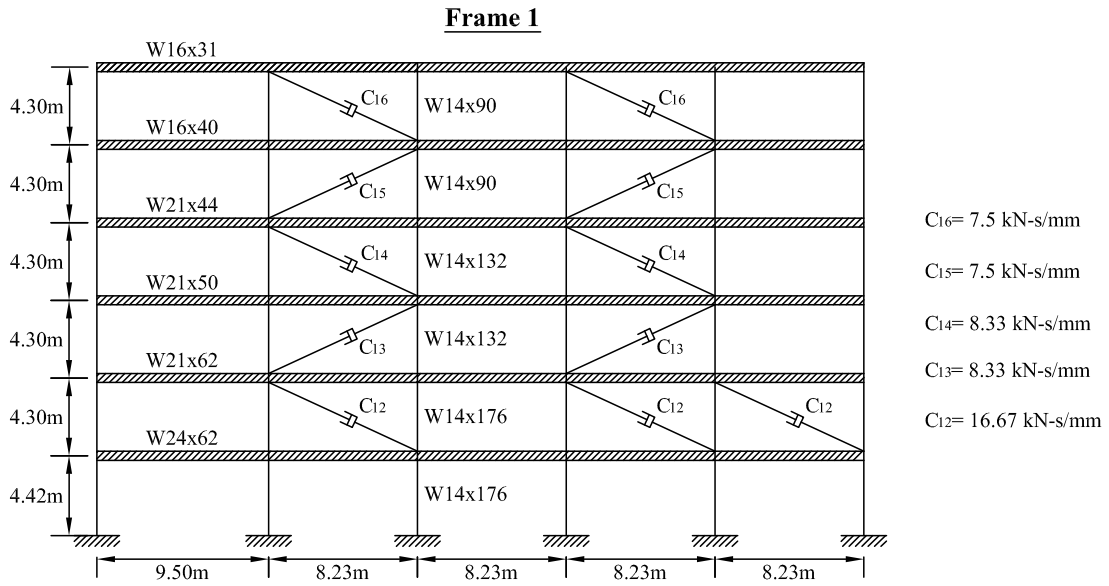


Figure 6.2 Details of Frame 1 of the example building

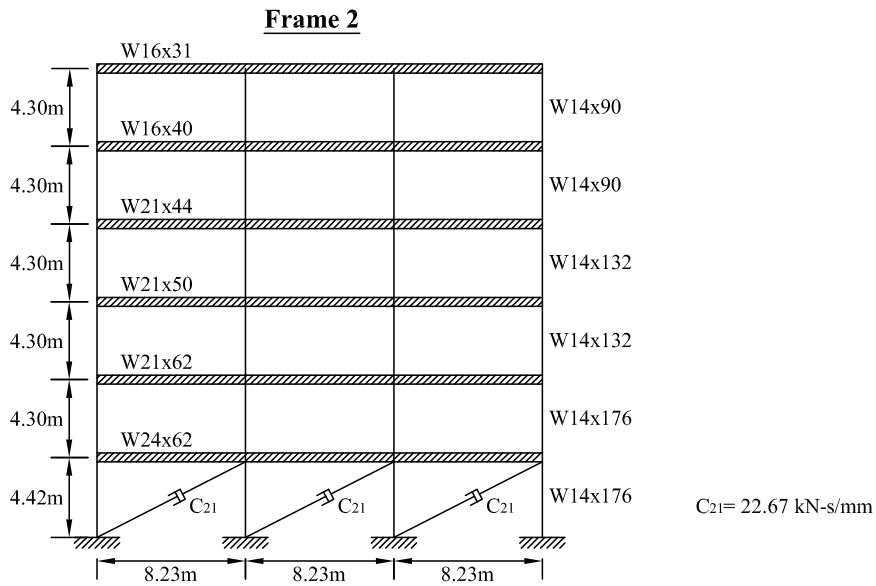


Figure 6.3 Details of Frame 2 of the example building

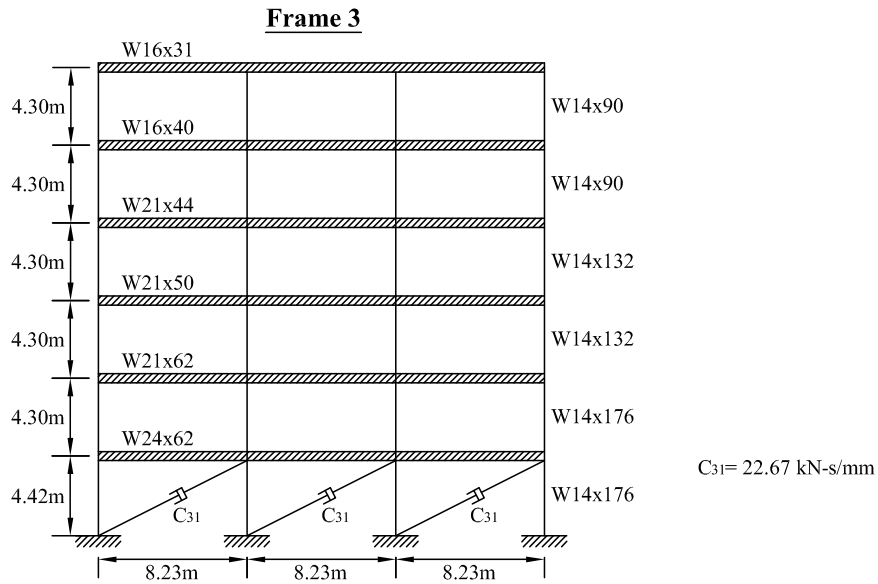


Figure 6.4 Details of Frame 3 of the example building

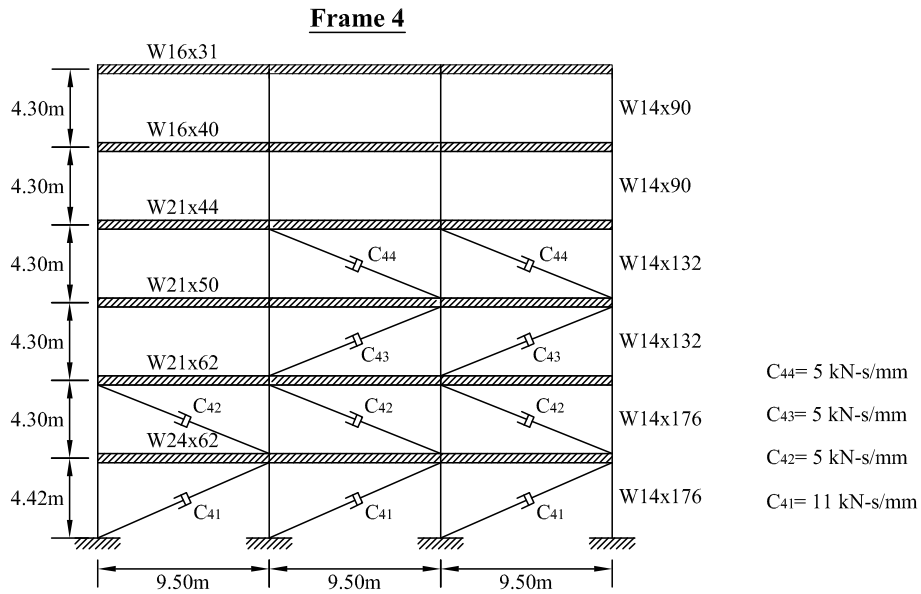


Figure 6.5 Details of Frame 4 of the example building

Table 6.2. Modal periods and damping ratio of the example building

Mode	Period (sec) ^{1,2,3}			Damping ratio (%)		
	Undamped frame	Damped frame		Undamped frame	Damped frame	
		Exact	CDA		Exact	CDA
1	2.33	3.17	2.36	2	NA	17.68
2	1.23	2.20	1.31	2	13.65	34.24
3	0.89	1.88	0.98	2	NA	41.02
4	0.89	1.13	0.99	2	12.48	44.33
5	0.57	1.04	0.74	2	NA	63.81
6	0.47	0.78	0.81	2	34.30	81.17
7	0.45	0.77	0.49	2	17.99	42.09
8	0.38	0.74	0.51	2	NA	67.15
9	0.34	0.60	NA	2	NA	NA
10	0.31	0.50	NA	2	41.69	NA
11	0.30	0.46	NA	2	NA	NA
12	0.24	0.42	0.29	2	NA	56.02
13	0.22	0.41	NA	2	7.92	NA
14	0.20	0.39	NA	2	10.51	NA
15	0.17	0.32	NA	2	12.40	NA
16	0.16	0.28	NA	2	97.11	NA
17	0.15	0.26	NA	2	8.42	NA
18	0.12	0.22	NA	2	2.43	NA
19	NA	0.22	NA	NA	NA	NA
20	NA	0.10	NA	NA	NA	NA
21	NA	0.07	NA	NA	NA	NA
22	NA	0.05	NA	NA	NA	NA
23	NA	0.04	NA	NA	NA	NA
24	NA	0.03	NA	NA	NA	NA
25	NA	0.02	NA	NA	NA	NA

1. NA=Not Available

2. Exact=2N dimensional eigenvalue analysis

3. CDA= Classical damping assumption

6.3 Ground Motion Records

The ground motion ensemble B (referred to Table 4.4) used in Section 4.3.5 to verify the accuracy of the transformed over-damped mode response spectrum is used. It consists of 25 pairs of far-field ground motion. For each of these pairs of records, the odd component is applied along the X-axis while the even component is applied along the Y-axis to conduct the response analysis. The vertical components of the ground motions are not

included in the analyses. For response spectrum analysis, in addition to the excitations applied along the two orthogonal reference axes X and Y, a number of selected orientations of the principal axes of the ground motion, defined by the angle θ ranging from 0 to 2π , are considered to study the effect of the seismic incidences. In this study, all odd records are scaled to have Peak Ground Acceleration (PGA) equal to 0.4g and the even records are scaled to have PGA with 0.3g. Mean peak responses resulting from these 25 pairs of ground motions are presented for comparison.

6.4 Modal Response History Analysis

The application of the proposed general modal response history analysis presented in Chapter 3 is demonstrated in this section, including an investigation of the effects of using the forced classical damping assumption and the response contributions from the over-damped modes. The following three approaches are used to compare the analytical assumptions from the viewpoint of structural responses:

- (1) Using the general modal response history analysis shown in Equation (3.60). This set is referred to as “Exact”;
- (2) Using the forced classical damping assumption while excluding the over-damped modes. This set is referred to as “CDA” (Classical Damping Assumption);
- (3) Ignoring the contribution of the over-damped modes in the analysis, i.e., considering the first two terms in Equation (3.60) only. This set is referred to as “EOM” (Exclude Over-damped Mode).

6.4.1 Responses of Each Story

Peak responses of each story, i.e., referenced to the 18 DOFs of the example building, are obtained for each ground motion pair based on the above three analytical approaches. Their mean values are presented in Table 6.3, 6.4 and 6.5 for peak displacement, peak velocity and peak total acceleration, respectively. The mean results obtained from the first approach are considered to be the “exact” results. The data listed in Table 6.3, 6.4 and 6.5 are also plotted in Figure 6.6, 6.7 and 6.8, accordingly for comparisons. In these three figures, the vertical axis is the result of the mean responses from the response history analysis and the horizontal axis represents the mean responses calculated by the

three approaches. The diagonal line in each figure serves as a reference line. The symbols located below the reference line are conservative results whereas those above it are underestimated. It is apparent that the results from the first approach lie on the reference line since the results from this approach are considered to be the “exact” solutions. Figure 6.9 presents the estimation errors arising from the forced classical damping assumption and ignoring the over-damped modes.

Table 6.3 Results of mean peak displacement responses of defined degree-of-freedoms of the example building using ground motion records as inputs

Level of story	Response quantities								
	Displacement along X-axis (mm) ^{1,2,3}			Displacement along Y-axis (mm)			Rotation about Z-axis (10 ⁻³ rad)		
	Exact	CDA	EOM	Exact	CDA	EOM	Exact	CDA	EOM
1	17	14	15	12	17	11	0.32	0.03	0.40
2	30	26	26	33	31	30	0.30	0.06	0.32
3	52	42	49	66	50	63	0.31	0.09	0.32
4	70	55	67	94	64	92	0.32	0.12	0.32
5	88	68	85	126	77	123	0.51	0.16	0.50
6	95	72	93	139	81	136	0.71	0.17	0.70

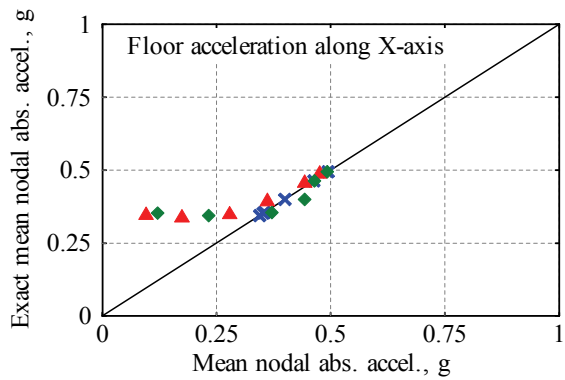
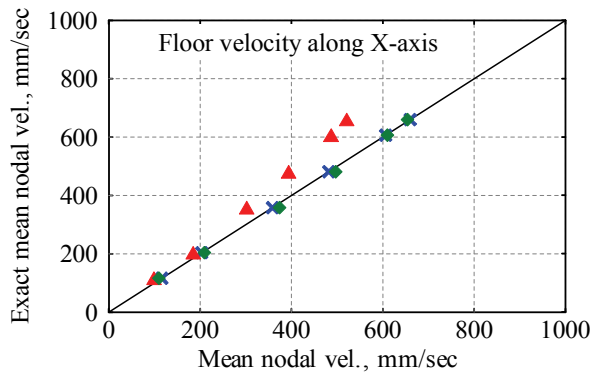
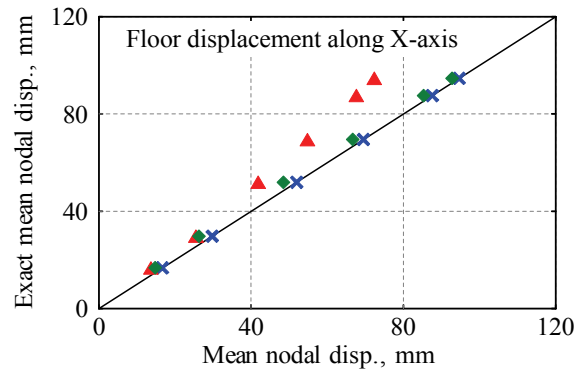
Table 6.4 Results of mean peak velocity responses of defined degree-of-freedoms of the example building using ground motion records as inputs

Level of story	Response quantities								
	Velocity along X-axis (mm/sec) ^{1,2,3}			Velocity along Y-axis (mm/sec)			Rotational Velocity about Z-axis (10 ⁻³ rad/sec)		
	Exact	CDA	EOM	Exact	CDA	EOM	Exact	CDA	EOM
1	116	99	110	63	105	70	2.18	0.11	2.34
2	204	185	210	222	192	226	2.05	0.18	2.04
3	358	302	374	433	303	436	2.32	0.31	2.35
4	482	394	497	579	382	587	1.98	0.42	2.00
5	606	487	610	748	454	755	2.75	0.56	2.77
6	660	521	654	844	485	849	4.37	0.62	4.43

Table 6.5 Results of mean peak total acceleration responses of defined degree-of-freedoms of the example building using ground motion records as inputs

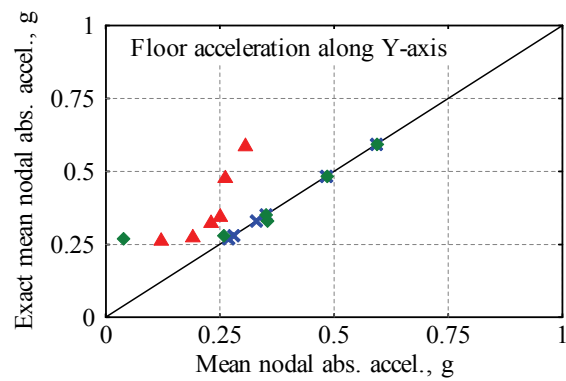
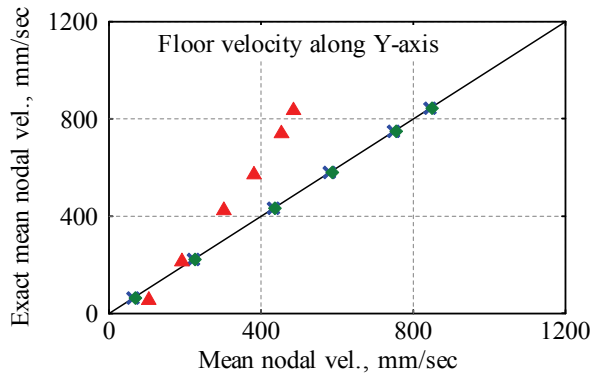
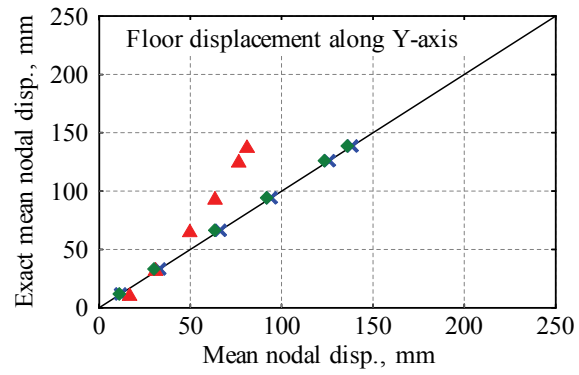
Level of story	Response quantities								
	Total acceleration along X-axis (g) ^{1,2,3}			Total acceleration along Y-axis (g)			Rotational acceleration about Z-axis (rad/sec ²)		
	Exact	CDA	EOM	Exact	CDA	EOM	Exact	CDA	EOM
1	0.35	0.10	0.12	0.27	0.12	0.04	0.025	0.001	0.026
2	0.34	0.17	0.23	0.28	0.19	0.26	0.021	0.001	0.022
3	0.36	0.28	0.37	0.33	0.23	0.35	0.022	0.002	0.022
4	0.40	0.36	0.44	0.35	0.25	0.35	0.021	0.002	0.021
5	0.46	0.44	0.46	0.48	0.26	0.48	0.020	0.003	0.020
6	0.49	0.48	0.49	0.59	0.31	0.59	0.037	0.004	0.036

1. Exact=General modal analysis including effects of over-damped modes
2. CDA= Classical damping assumption while over-damped modes excluded
3. EOM= General modal analysis excluding over-damped modes



- × × × Exact mean values
- ▲ ▲ ▲ Classical damping assumption
- ◆ ◆ ◆ Ignore over-damped modes

Figure 6.6 Comparisons of story responses along X-axis by response history analysis



- × × × Exact mean values
- ▲ ▲ ▲ Classical damping assumption
- ◆ ◆ ◆ Ignore over-damped modes

Figure 6.7 Comparisons of story responses along Y-axis by response history analysis

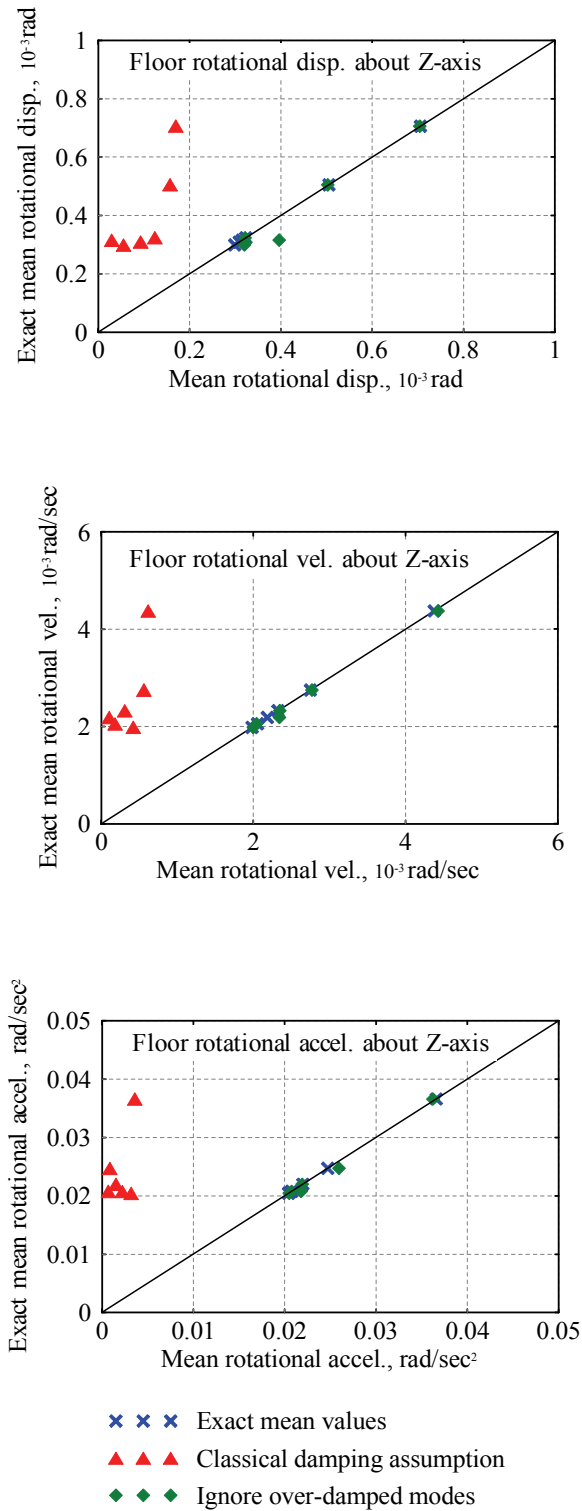


Figure 6.8 Comparisons of story responses about Z-axis by response history analysis

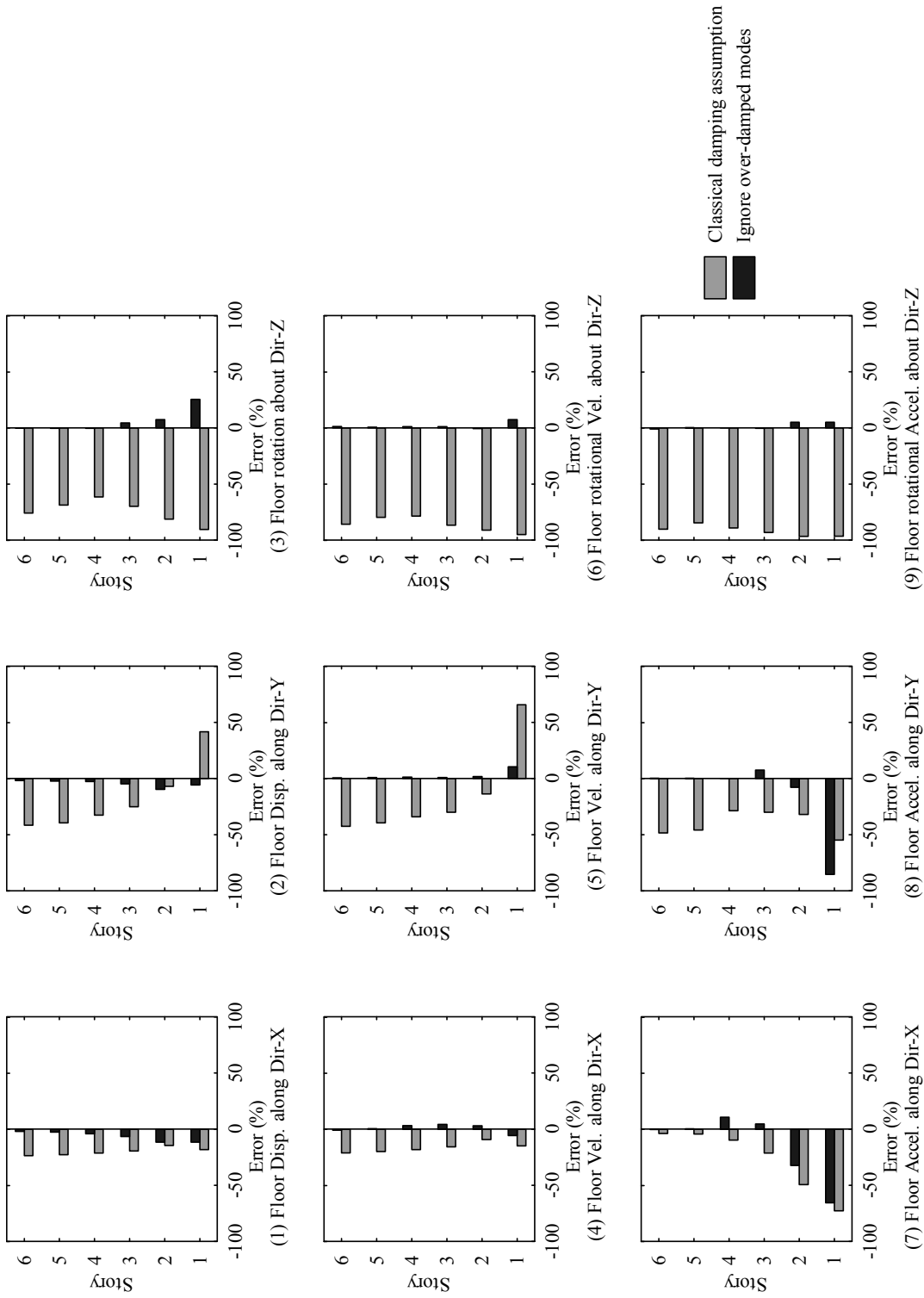


Figure 6.9 Estimation errors of the story responses by response history analysis

6.4.2 Responses of Each Frame

Response estimates of each frame based on the three approaches are presented in Table 6.6 to Table 6.9. Four response quantities are included in the tables, which are (a) peak interstory drift; (b) peak interstory velocity; (c) story shear force at the time of maximum interstory drift; and (d) maximum story shear force (which includes the damping force as appropriate). Figure 6.10 to Figure 6.13 compare the results obtained from these three approaches for the four response quantities. The associated estimation errors resulting from the forced classical damping assumption and ignoring the over-damped modes are presented in Figure 6.14 to 6.17.

6.4.3 Discussion

By evaluating Table 6.3 to 6.9 and Figure 6.6 to 6.17, it is found that using the forced classical damping assumption results in inaccurate seismic response estimates for all the responses considered. Most results determined from the forced classical damping assumption are underestimated. This phenomenon becomes more significant for floor acceleration responses. For certain response quantities, the error can be more than 100%. The source of the errors can be attributed to inaccurate calculation of the modal damping ratios and modal periods determined under the classical damping assumption. It is also found that the effect of the over-damped modes is not significant in the response calculations for this example. The exception is that the floor accelerations in the lower stories are considerably underestimated. This may result in errors in seismic demand estimates of nonstructural components.

From the above comparisons, it may be concluded that the over-damped modes should be considered in order to obtain more accurate structural response estimates. This is particular true for floor accelerations. Further, using the forced classical damping assumption may lead to large inaccuracies when a structure is heavily non-classically damped and has over-critically damped modes.

Table 6.6. Results of mean peak responses of frame 1 of the example building using ground motion records as inputs

Level of story	Response quantities											
	Story drift (mm)		Interstory velocity (mm/sec)			Story Shear at Max. Drift (KN)			Max. Story Shear (KN)			
	Exact	CDA	EOM	Exact	CDA	EOM	Exact	CDA	EOM	Exact	CDA	EOM
1	22	14	22	155	100	150	4131	2546	4074	4131	2546	4074
2	12	12	11	78	86	91	2450	2374	2253	4377	4608	4395
3	21	16	21	147	116	160	2661	2072	2639	3447	2771	3535
4	16	13	17	124	92	122	2047	1624	2115	2753	2178	2802
5	14	13	15	107	93	100	1169	1060	1211	1882	1686	1801
6	6	5	6	50	37	48	480	393	522	846	636	803

Table 6.7. Results of mean peak responses of frame 2 of the example building using ground motion records as inputs

Level of story	Response quantities											
	Story drift (mm)		Interstory velocity (mm/sec)			Story Shear at Max. Drift (KN)			Max. Story Shear (KN)			
	Exact	CDA	EOM	Exact	CDA	EOM	Exact	CDA	EOM	Exact	CDA	EOM
1	11	17	11	58	106	68	1225	1889	1232	3768	6569	3967
2	26	14	26	201	87	206	3098	1723	3135	3098	1723	3135
3	38	19	38	262	112	262	2878	1452	2895	2878	1452	2895
4	32	14	33	228	83	229	2487	1081	2497	2487	1081	2497
5	40	14	40	308	85	309	1981	678	1983	1981	678	1983
6	17	5	17	150	49	150	831	271	832	831	271	832

1. Exact=General modal analysis including effects of over-damped modes
2. CDA= Classical damping assumption while over-damped modes excluded
3. EOM= General modal analysis excluding over-damped modes

Table 6.8. Results of mean peak responses of frame 3 of the example building using ground motion records as inputs

Level of story	Response quantities											
	Story drift (mm)		Interstory velocity (mm/sec)			Story Shear at Max. Drift (KN)			Max. Story Shear (KN)			
	Exact	CDA	EOM	Exact	CDA	EOM	Exact	CDA	EOM	Exact	CDA	EOM
1	11	14	7	76	98	69	1219	1517	827	4864	6098	4225
2	15	12	14	116	86	131	1860	1433	1736	1860	1433	1736
3	25	17	25	186	119	190	1880	1274	1904	1880	1274	1904
4	21	13	21	156	95	157	1596	1009	1615	1596	1009	1615
5	27	13	27	202	97	197	1348	667	1365	1348	667	1365
6	12	5	12	110	38	108	622	248	624	622	248	624

Table 6.9. Results of mean peak responses of frame 4 of the example building using ground motion records as inputs

Level of story	Response quantities											
	Story drift (mm)		Interstory velocity (mm/sec)			Story Shear at Max. Drift (KN)			Max. Story Shear (KN)			
	Exact	CDA	EOM	Exact	CDA	EOM	Exact	CDA	EOM	Exact	CDA	EOM
1	14	14	15	82	90	95	1504	1505	1686	2796	3034	2847
2	18	12	18	125	77	133	2159	1400	2216	2791	1748	2906
3	24	16	25	164	105	162	1847	1214	1895	2388	1542	2423
4	20	12	20	134	81	137	1504	934	1515	1920	1188	1944
5	32	12	33	288	86	287	1620	605	1629	1620	605	1629
6	15	5	15	168	41	167	763	234	765	763	234	765

1. Exact=General modal analysis including effects of over-damped modes
2. CDA= Classical damping assumption while over-damped modes excluded
3. EOM= General modal analysis excluding over-damped modes

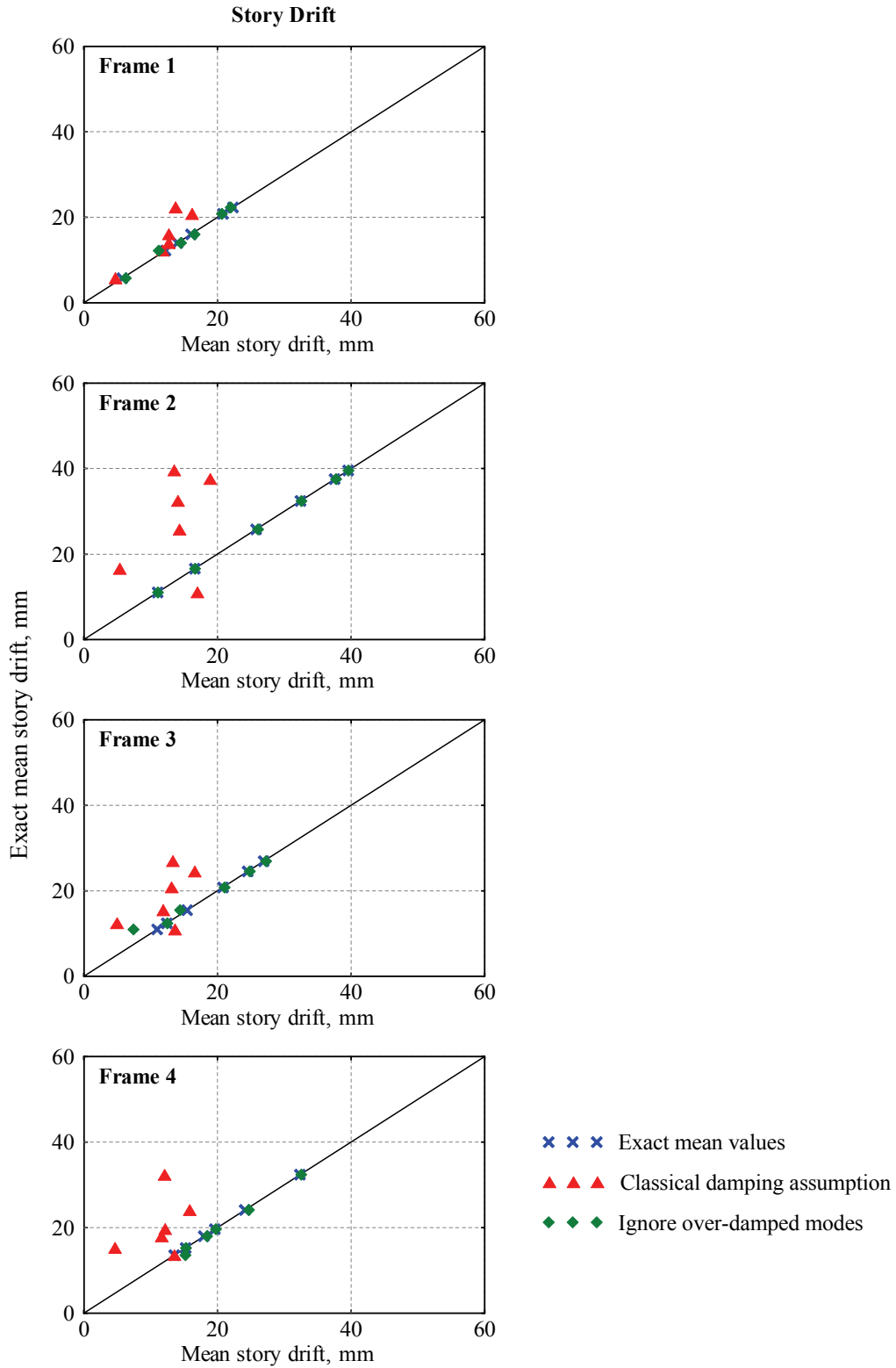


Figure 6.10 Comparisons of interstory drifts per frame by response history analysis

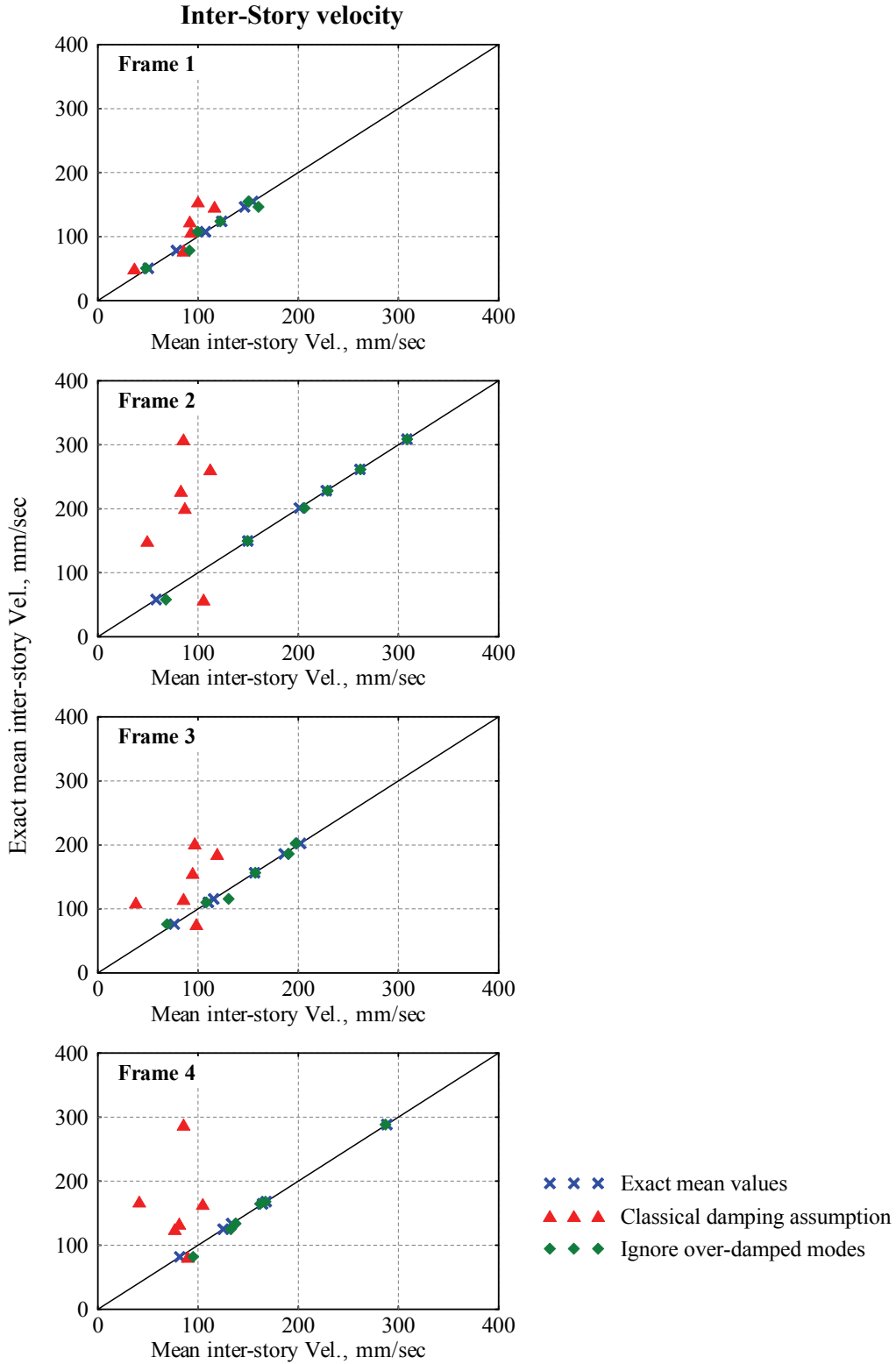


Figure 6.11 Comparisons of interstory velocities per frame by response history analysis

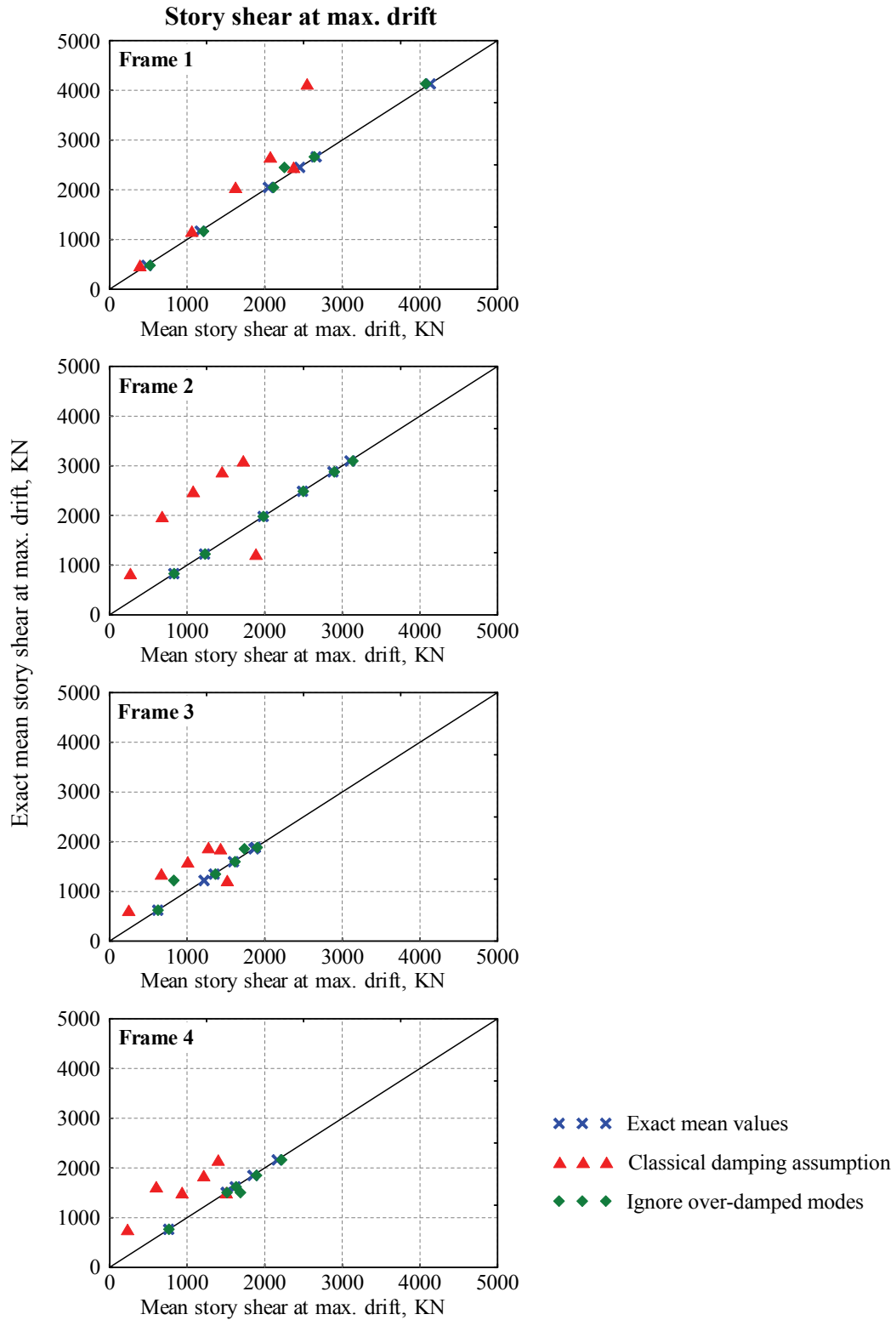


Figure 6.12 Comparisons of story shear forces at max. drifts per frame by response history analysis

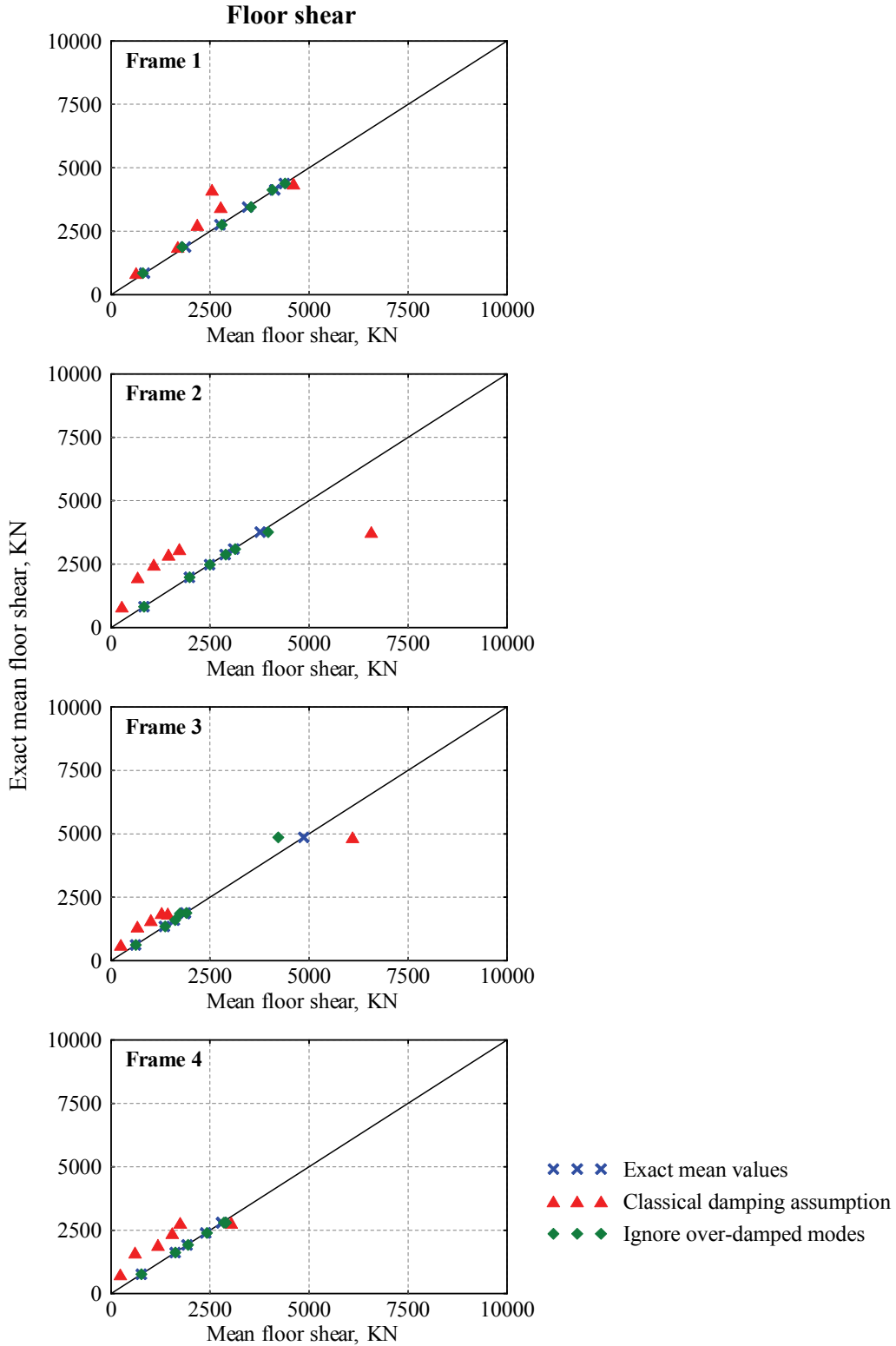
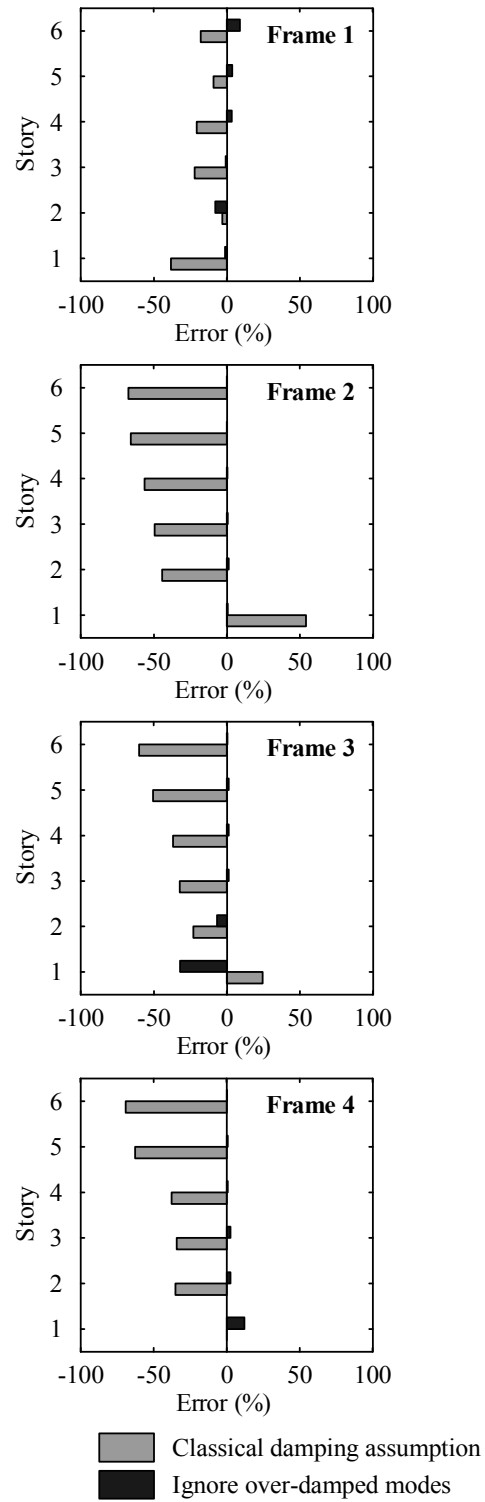
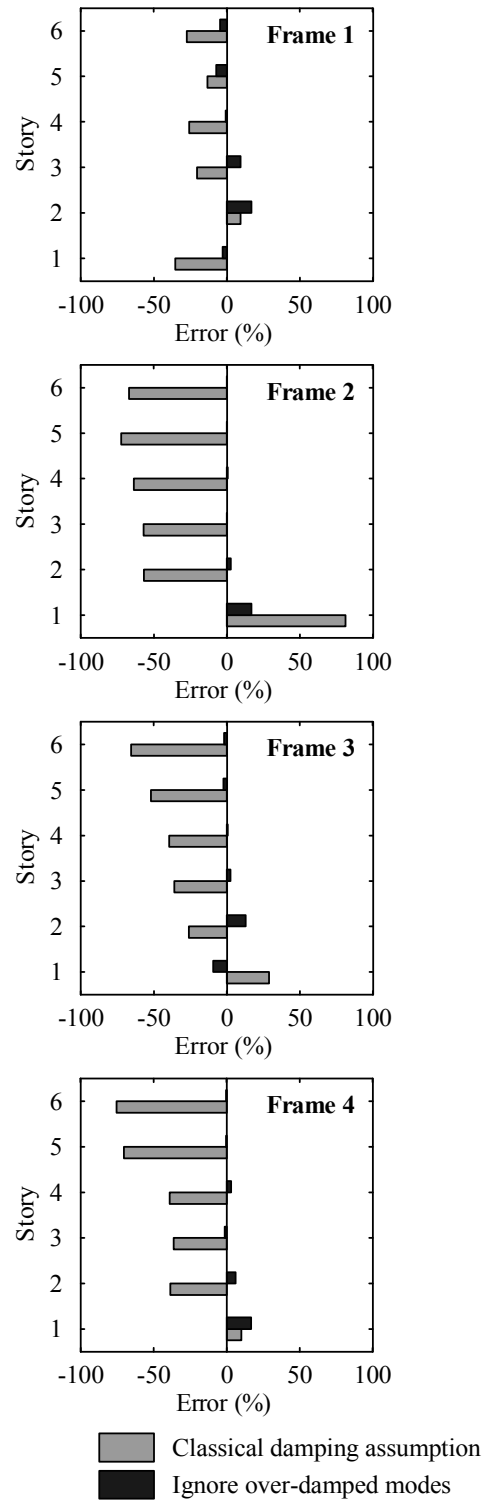


Figure 6.13 Comparisons of maximum story shear forces per frame by response history analysis



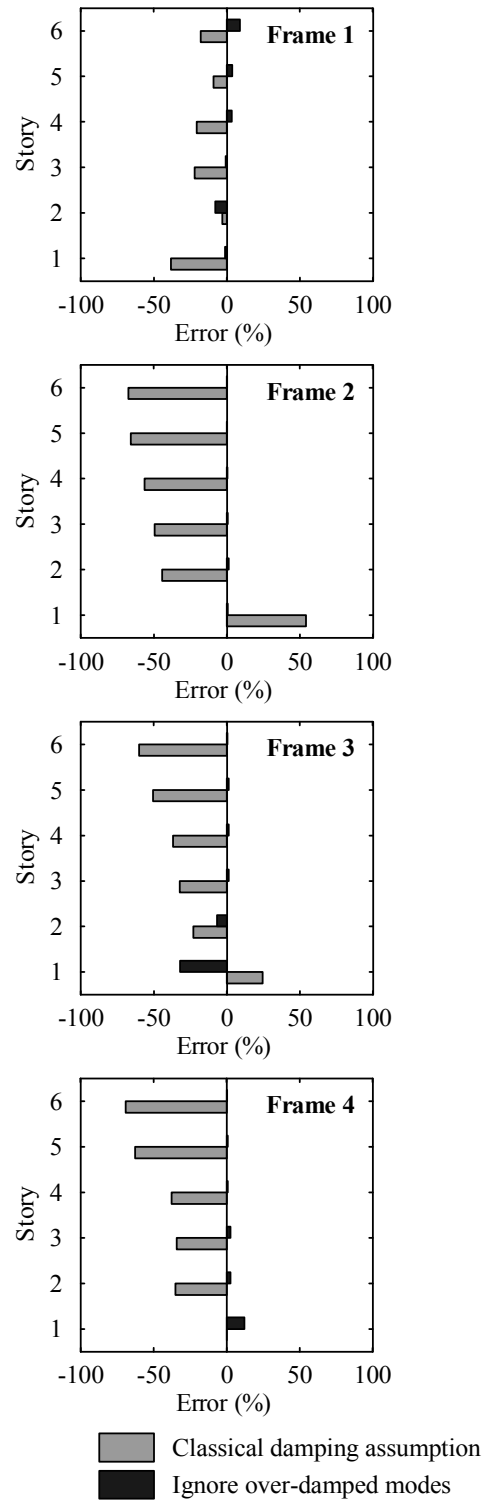
Story Drift

Figure 6.14 Estimation errors of the story drift per frame by response history analysis



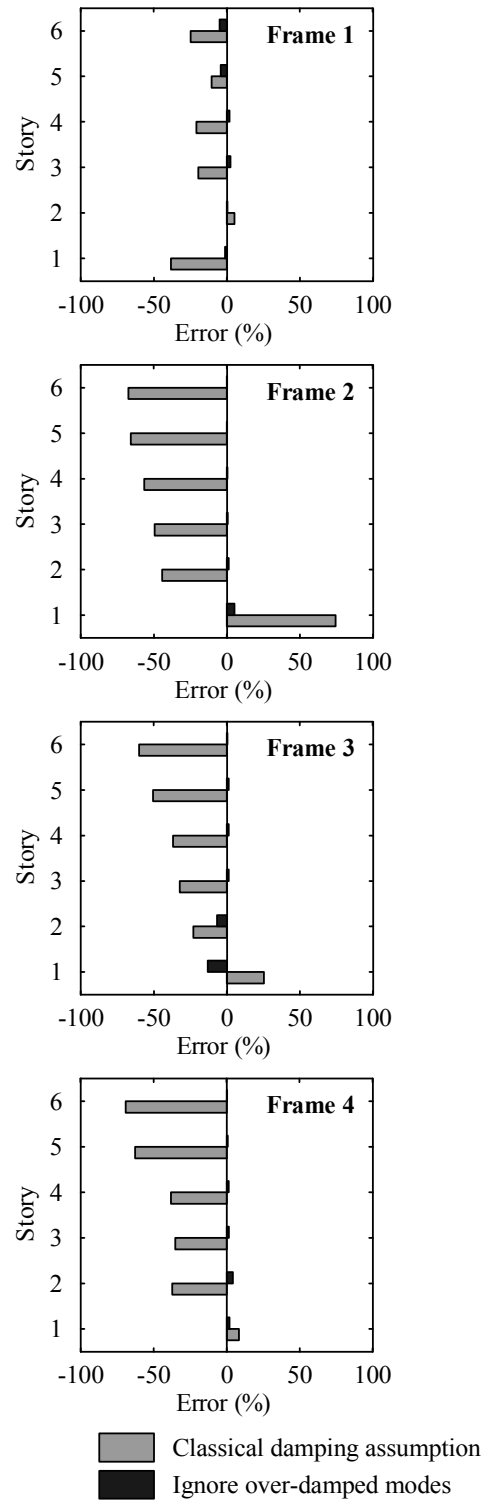
Inter Story Velocity

Figure 6.15 Estimation errors of the inter story velocity per frame by response history analysis



Story Shear at max. Drift

Figure 6.16 Estimation errors of the story shear force at max. inter story drift per frame by response history analysis



Floor Shear

Figure 6.17 Estimation errors of the maximum story shear force per frame by response history analysis

6.5 Response Spectrum Analysis

In this section, the accuracy and applicability of the generalized response spectrum method, i.e., the GCQC3 combination rule, are assessed. As in the modal response history analyses, the effect of assuming forced classical damping and ignoring the over-damped modes are also examined. The mean response history results are considered to be the exact results and are used to examine the accuracy of the GCQC3 rule. As a result, three sets of results are obtained and compared with the exact results. These three sets of analysis approaches are described as follows:

- (4) Results of the first set are obtained based on the newly developed GCQC3 rule, defined by Equations (4.48), (4.56) or (4.61). The state space approach is used to derive the mode shapes, modal periods and modal damping ratios. These modal properties are then used to generate the correlation coefficients and peak modal responses required in the GCQC3 rule. The contributions from the over-damped modes are considered when they are present.
- (5) Results of the second set are based on the modal properties obtained under the forced classical damping assumption. Similar to the GCQC3 rule, these properties are used to generate the data required in the modal combination rule. The over-damped modes are not considered. This method is often used for the design and analysis of structures with added damping devices. This rule is referred to as the forced CDA (forced Classical Damping Assumption).
- (6) Results of the third set are identical to the GCQC3 rule except that it does not consider the over-damped modes in the modal combination process. This consideration is aimed to examine the effects of the over-damped modes on the response estimates. This rule is referred to as the EOM (Exclude Over-damped Modes).

In addition, the effect of the seismic incidence θ and the correlation between the two orthogonal ground motion components on the response estimates are also investigated. The procedure proposed in Chapter 5 is also evaluated by examining the floor acceleration estimates to determine if they can be used to predict the peak value of a spatially combined response using the response spectrum method.

6.5.1 Responses of Each Story

In evaluating the results obtained from these three rules, only those from the case with seismic incidence $\theta = 0$ are presented for comparison. This is because the purpose of the comparison is to examine the accuracy of the GCQC3 rule itself and the effect of classical damping assumption as well as the influence of the over-damped modes.

Peak responses of each story obtained by the three rules are listed in Table 6.10 to 6.12. Their respective “exact” solutions, obtained from the mean response history analyses, are also included. Figure 6.18 to 6.20 compare the results obtained by these three rules to the exact results. It is apparent that CDA underestimates the response values for all response quantities while GCQC3 significantly reduces the scatter of the data along the diagonal reference line and provides excellent estimates. The associated estimation errors are presented in Figure 6.21.

6.5.2 Responses of Each Seismic Frame

Similar to the evaluation of the responses of each story, only the results of seismic incidence $\theta = 0$ are presented for comparisons. As noted earlier, the peak modal responses required in each modal combination rule were obtained by performing the response history analysis using the respective modal properties. The response estimates obtained using the three rules along with their corresponding exact solutions are tabulated in Table 6.13 to 6.16 for the four frames, respectively. The response quantities included are the same as those considered in Section 6.4.2. A comparison of the results obtained from the three rules to the exact results are presented in Figure 6.22 to 6.25 for the four response quantities, respectively. Figure 6.26 to 6.29 show the associated estimation errors.

Table 6.10 Results of mean peak displacement responses of defined degree-of-freedom of the example building using response spectra as inputs

Level of story	Displacement along X-axis (mm)			Displacement along Y-axis (mm)			Rotation about Z-axis (10^{-3} rad)				
	Exact	GCQC3	CDA EOM	Exact	GCQC3	CDA EOM	Exact	GCQC3	CDA EOM		
1	17	16	14	12	13	18	10	0.32	0.33	0.03	0.40
2	30	29	26	33	35	33	31	0.30	0.28	0.05	0.31
3	52	51	47	66	70	52	66	0.31	0.27	0.08	0.28
4	70	68	65	94	97	66	94	0.32	0.27	0.11	0.27
5	88	84	82	126	126	79	124	0.51	0.44	0.13	0.44
6	95	91	89	139	139	84	136	0.71	0.60	0.14	0.60

Table 6.11 Results of mean peak velocity responses of defined degree-of-freedom of the example building using response spectra as inputs

Level of story	Velocity along X-axis (mm/sec)			Velocity along Y-axis (mm/sec)			Rotational velocity about Z-axis (10^{-3} rad/sec)				
	Exact	GCQC3	CDA EOM	Exact	GCQC3	CDA EOM	Exact	GCQC3	CDA EOM		
1	116	116	112	63	63	106	69	2.18	2.26	0.10	2.38
2	204	207	214	222	222	186	223	2.05	1.82	0.14	1.83
3	358	354	368	433	412	278	414	2.32	1.99	0.23	2.01
4	482	462	476	579	549	348	554	1.98	1.81	0.33	1.81
5	606	561	563	748	717	411	721	2.75	2.44	0.45	2.47
6	660	599	593	844	798	425	801	4.37	3.80	0.50	3.84

Table 6.12 Results of mean peak total acceleration responses of defined degree-of-freedom of the example building using response spectra as inputs

Level of story	Total acceleration along X-axis (g)			Total acceleration along Y-axis (g)			Total rotational acceleration about Z-axis (rad/sec ²)					
	Exact	GCQC3	CDA	EOM	Exact	GCQC3	CDA	EOM	Exact	GCQC3	CDA	EOM
1	0.35	0.32	0.10	0.13	0.27	0.27	0.14	0.04	0.0247	0.0284	0.0009	0.0274
2	0.34	0.35	0.17	0.24	0.31	0.28	0.21	0.29	0.0208	0.0210	0.0008	0.0209
3	0.36	0.38	0.27	0.38	0.35	0.33	0.25	0.37	0.0220	0.0212	0.0013	0.0216
4	0.40	0.40	0.34	0.43	0.36	0.35	0.26	0.36	0.0207	0.0207	0.0020	0.0215
5	0.46	0.43	0.41	0.43	0.44	0.48	0.26	0.45	0.0204	0.0184	0.0028	0.0185
6	0.49	0.45	0.43	0.46	0.54	0.59	0.31	0.55	0.0366	0.0316	0.0032	0.0318

1. Exact=Modal response analysis including effects of over-damped modes
2. GCQC3=General complete quadratic combination rule including over-damped modes
3. CDA= Classical damping assumption while over-damped modes excluded
4. EOM= General modal analysis excluding over-damped modes

Table 6.13. Results of mean peak responses of frame 1 of the example building using response spectra as inputs

Response Quantity	Story	Frame 1			
		Exact	GCQC3	CDA	EOM
Story Drift (mm)	1	22	22	14	22
	2	12	13	12	11
	3	21	20	16	20
	4	16	15	13	16
	5	14	14	12	14
	6	6	5	4	6
Interstory Velocity (mm/sec)	1	155	156	94	153
	2	78	76	79	87
	3	147	138	106	150
	4	124	110	83	107
	5	107	100	83	96
	6	50	47	34	50
Story Shear at Max. Drift (KN)	1	4131	4043	2561	4012
	2	2450	2516	2381	2135
	3	2661	2567	2067	2538
	4	2047	1935	1604	2018
	5	1169	1127	1037	1175
	6	480	452	375	490
Max. General Story Shear (KN)	1	4131	4043	2561	4012
	2	4377	4193	4231	4228
	3	3447	3280	2592	3347
	4	2753	2527	2023	2561
	5	1882	1738	1517	1703
	6	846	769	583	775

1. Exact=Modal response analysis including effects of over-damped modes
2. GCQC3=General complete quadratic combination rule including over-damped modes
3. CDA= Classical damping assumption while over-damped modes excluded
4. EOM= General modal analysis excluding over-damped modes

Table 6.14. Results of mean peak responses of frame 2 of the example building using response spectra as inputs

Response Quantity	Story	Frame 2			
		Exact	GCQC3	CDA	EOM
Story Drift (mm)	1	11	12	18	11
	2	26	27	15	27
	3	38	38	19	38
	4	32	32	14	32
	5	40	37	14	37
	6	17	15	5	15
Interstory Velocity (mm/sec)	1	58	63	106	70
	2	201	203	80	205
	3	262	241	96	241
	4	228	207	75	209
	5	308	277	80	277
	6	150	130	60	130
Story Shear at Max. Drift (KN)	1	1225	1368	1974	1218
	2	3098	3222	1792	3259
	3	2878	2933	1493	2950
	4	2487	2476	1100	2485
	5	1981	1846	677	1851
	6	831	746	248	748
Max. General Story Shear (KN)	1	3768	4019	6689	4132
	2	3098	3222	1792	3259
	3	2878	2933	1493	2950
	4	2487	2476	1100	2485
	5	1981	1846	677	1851
	6	831	746	248	748

1. Exact=Modal response analysis including effects of over-damped modes
2. GCQC3=General complete quadratic combination rule including over-damped modes
3. CDA= Classical damping assumption while over-damped modes excluded
4. EOM= General modal analysis excluding over-damped modes

Table 6.15. Results of mean peak responses of frame 3 of the example building using response spectra as inputs

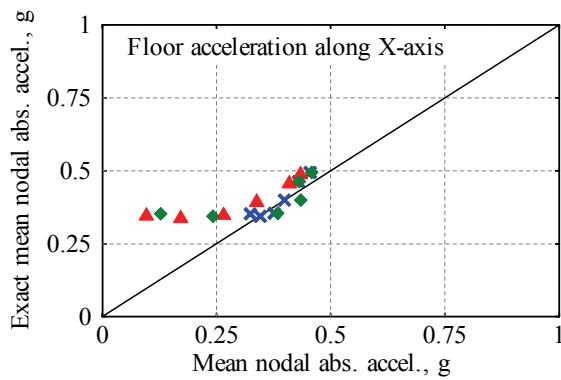
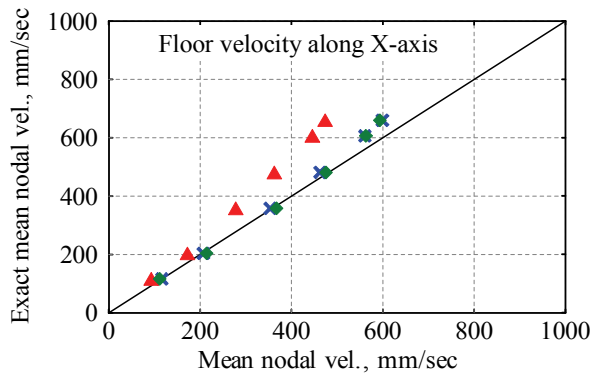
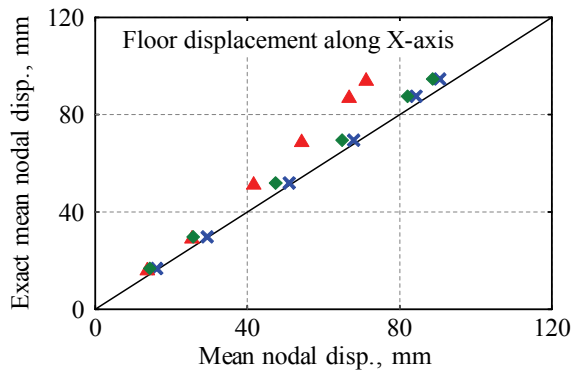
Response Quantity	Story	Frame 3			
		Exact	GCQC3	CDA	EOM
Story Drift (mm)	1	11	11	13	7
	2	15	15	12	14
	3	25	24	16	24
	4	21	20	13	20
	5	27	24	13	25
	6	12	11	5	11
Interstory Velocity (mm/sec)	1	76	74	92	70
	2	116	123	79	137
	3	186	174	109	177
	4	156	142	86	141
	5	202	177	87	174
	6	110	95	35	96
Story Shear at Max. Drift (KN)	1	1219	1178	1497	755
	2	1860	1826	1408	1703
	3	1880	1843	1244	1864
	4	1596	1545	978	1569
	5	1348	1208	638	1230
	6	622	540	233	550
Max. General Story Shear (KN)	1	4864	4629	5745	4191
	2	1860	1826	1408	1703
	3	1880	1843	1244	1864
	4	1596	1545	978	1569
	5	1348	1208	638	1230
	6	622	540	233	550

1. Exact=Modal response analysis including effects of over-damped modes
2. GCQC3=General complete quadratic combination rule including over-damped modes
3. CDA= Classical damping assumption while over-damped modes excluded
4. EOM= General modal analysis excluding over-damped modes

Table 6.16. Results of mean peak responses of frame 4 of the example building using response spectra as inputs

Response Quantity	Story	Frame 4			
		Exact	GCQC3	CDA	EOM
Story Drift (mm)	1	14	14	14	15
	2	18	19	12	19
	3	24	25	17	26
	4	20	20	13	20
	5	32	29	13	29
	6	15	14	5	14
Interstory Velocity (mm/sec)	1	82	82	90	94
	2	125	141	75	149
	3	164	170	101	165
	4	134	128	80	132
	5	288	254	85	254
	6	168	158	50	158
Story Shear at Max. Drift (KN)	1	1504	1599	1581	1661
	2	2159	2244	1473	2309
	3	1847	1897	1283	1970
	4	1504	1516	991	1516
	5	1620	1461	641	1471
	6	763	703	239	705
Max. General Story Shear (KN)	1	2796	2883	3074	2901
	2	2791	2924	1776	3037
	3	2388	2422	1561	2452
	4	1920	1895	1217	1914
	5	1620	1461	641	1471
	6	763	703	239	705

1. Exact=Modal response analysis including effects of over-damped modes
2. GCQC3=General complete quadratic combination rule including over-damped modes
3. CDA= Classical damping assumption while over-damped modes excluded
4. EOM= General modal analysis excluding over-damped modes



- × × × GCQC3
- ▲ ▲ ▲ CDA
- ◆ ◆ ◆ EOM

Figure 6.18 Comparisons of story responses along X-axis by response spectrum method

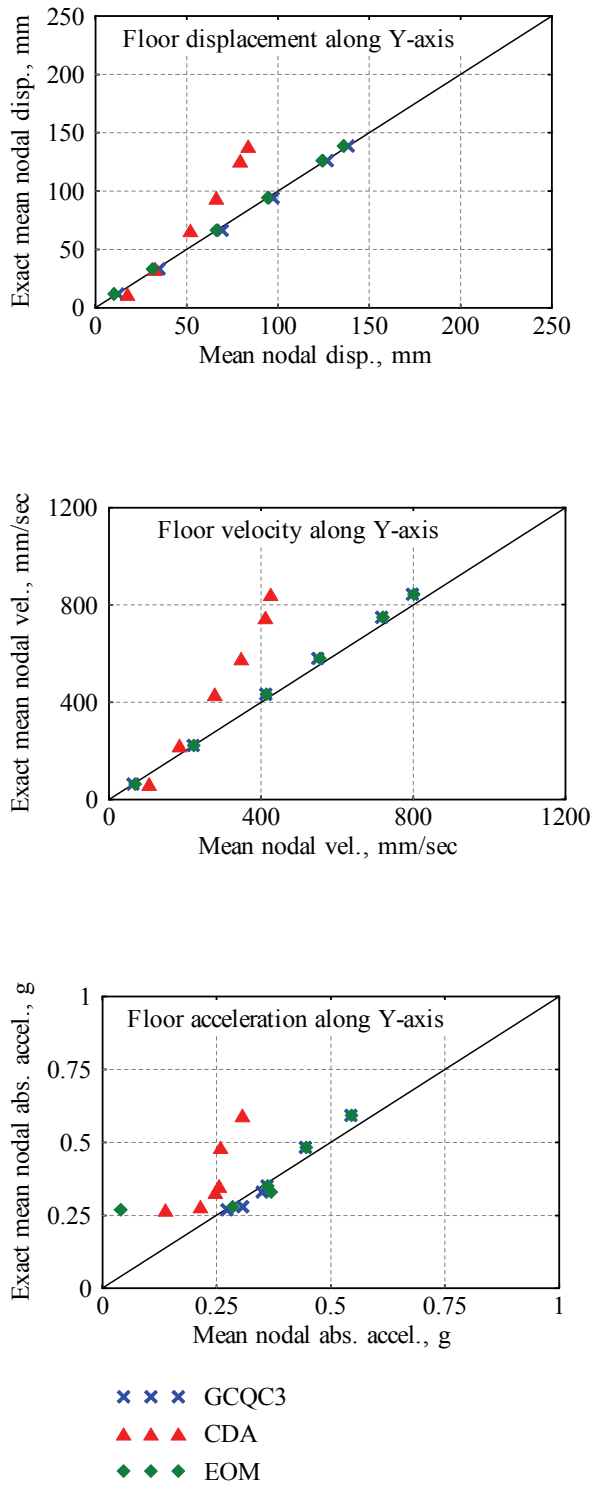


Figure 6.19 Comparisons of story responses along Y-axis by response spectrum method

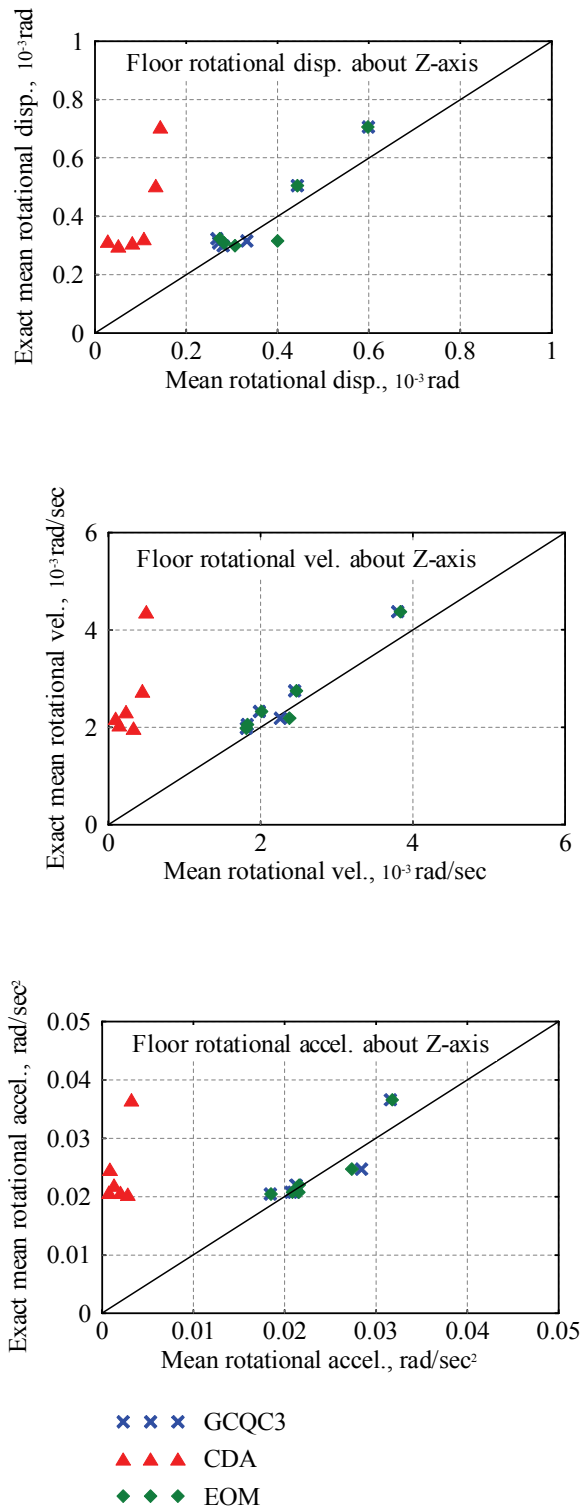


Figure 6.20 Comparisons of story responses about Z-axis by response spectrum method

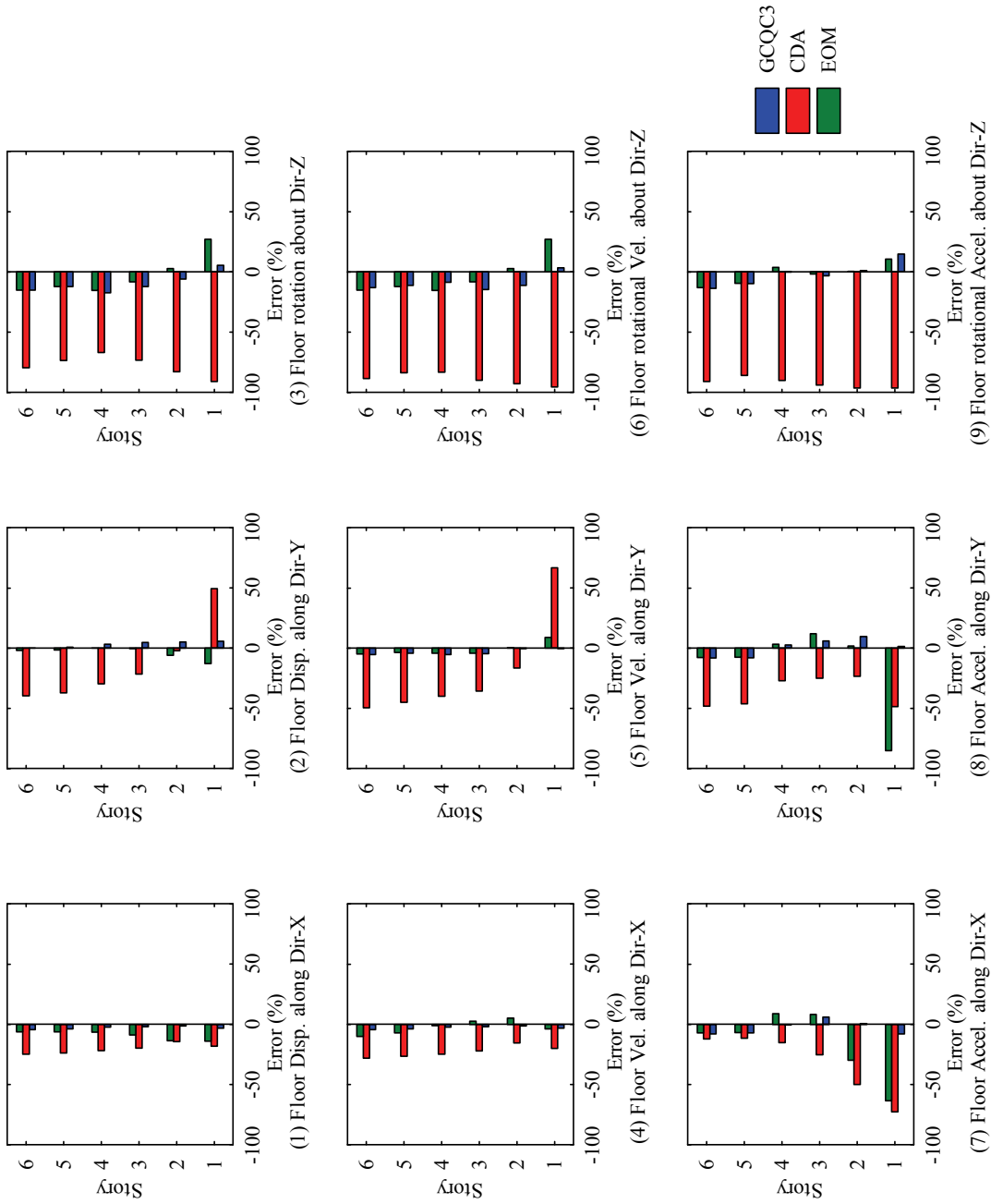


Figure 6.21 Estimation errors of the story responses by response spectrum method

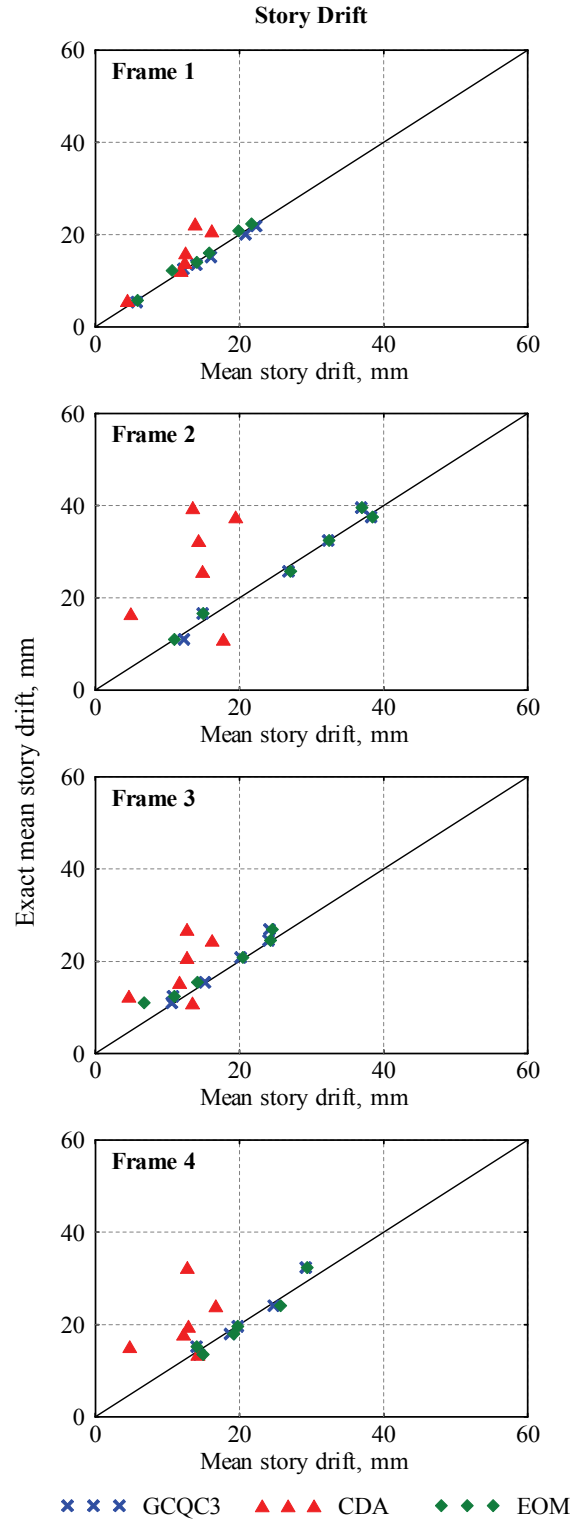


Figure 6.22 Comparisons of interstory drifts per frame by response spectrum method

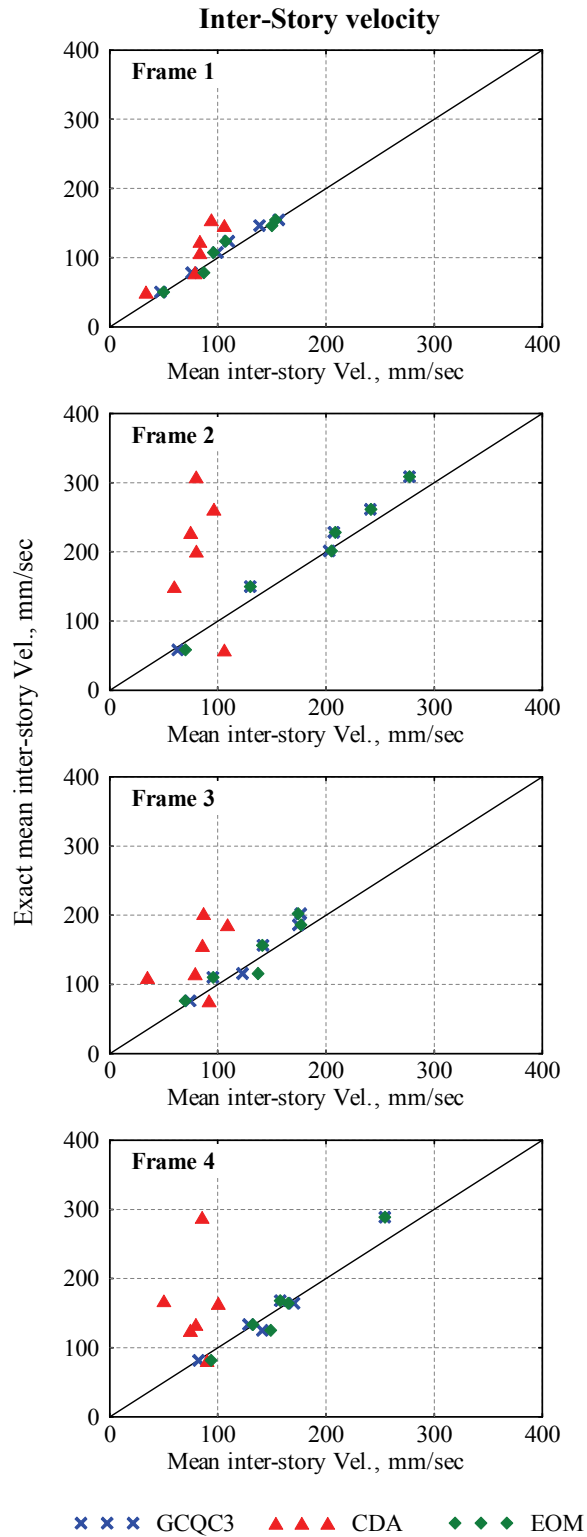


Figure 6.23 Comparisons of interstory velocities per frame by response spectrum method

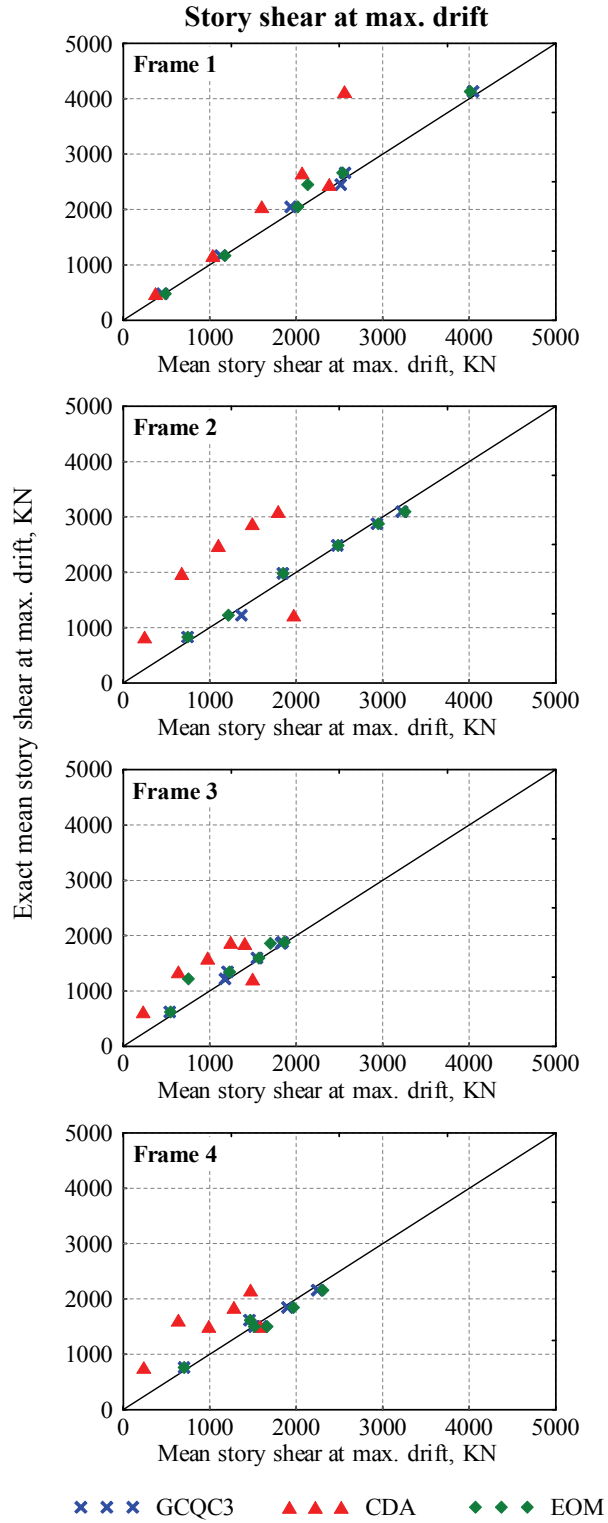


Figure 6.24 Comparisons of story shear forces at max. drifts per frame by response spectrum method

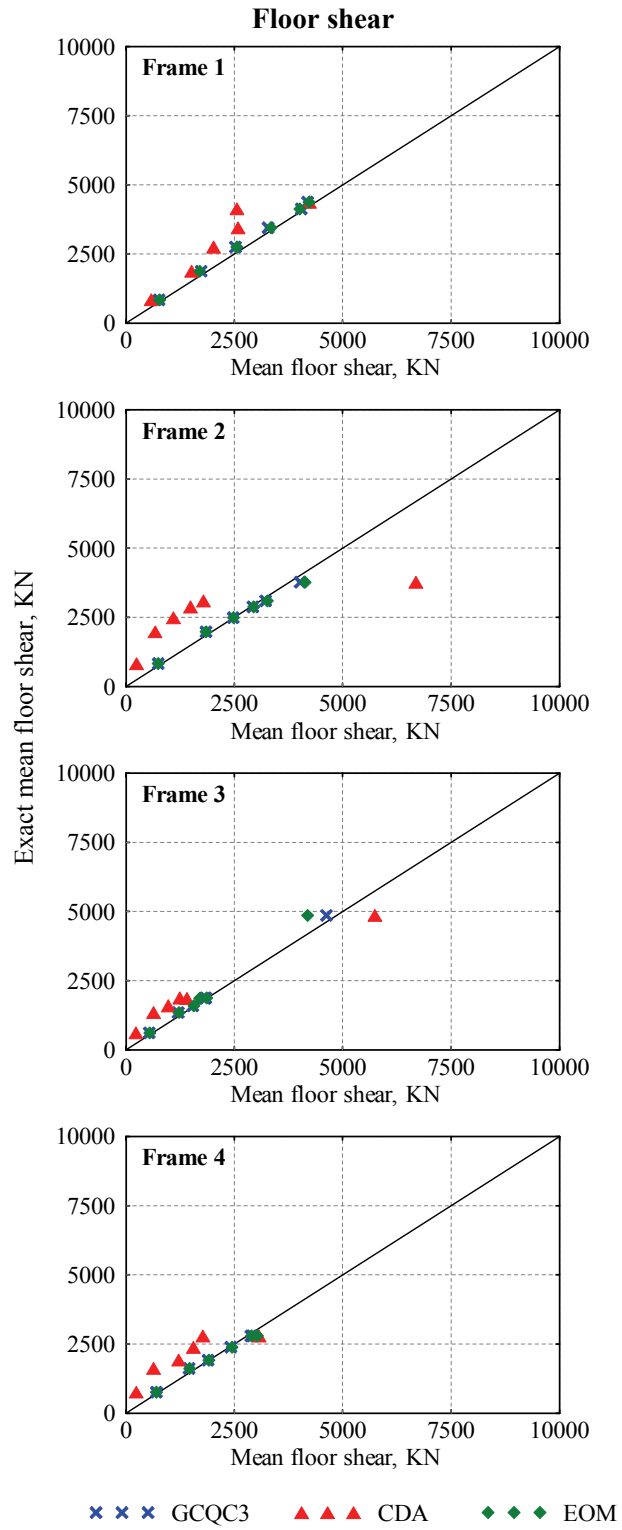


Figure 6.25 Comparisons of maximum story shear forces per frame by response spectrum method

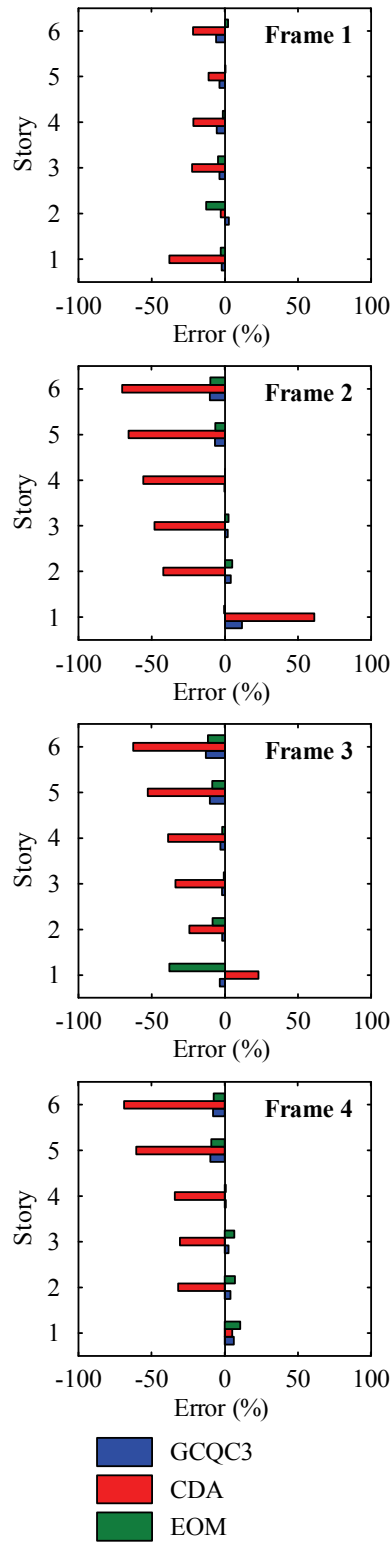


Figure 6.26 Estimation errors of the story drift per frame by response spectrum method

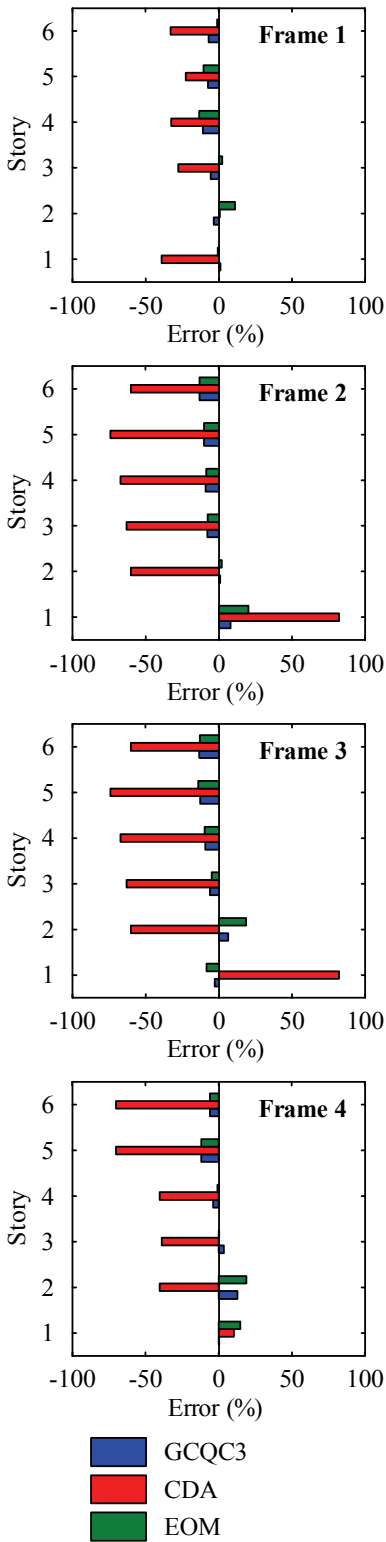


Figure 6.27 Estimation errors of the inter story velocity per frame by response spectrum method

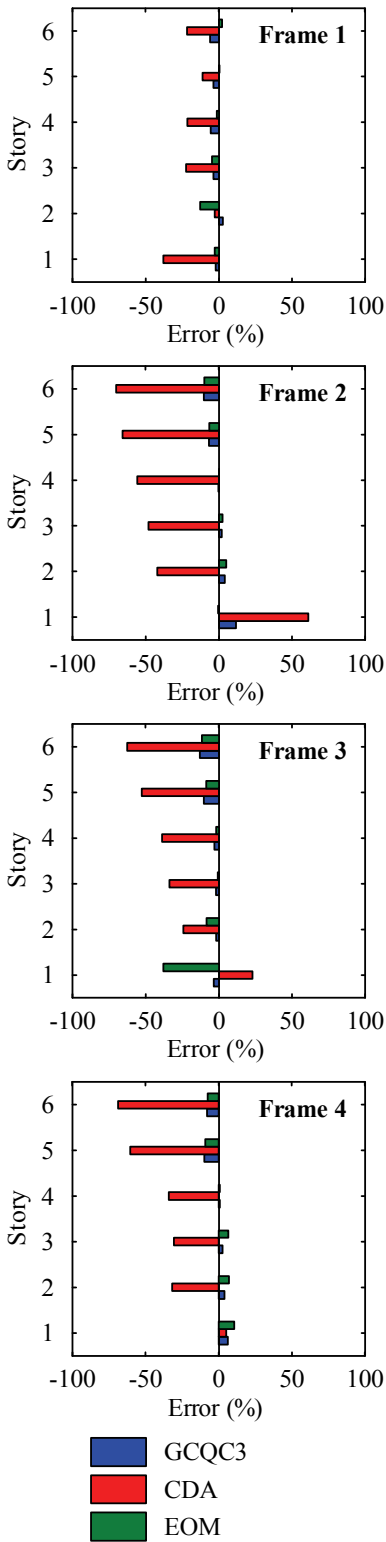


Figure 6.28 Estimation errors of the story shear force at max. inter story drift per frame by response spectrum method

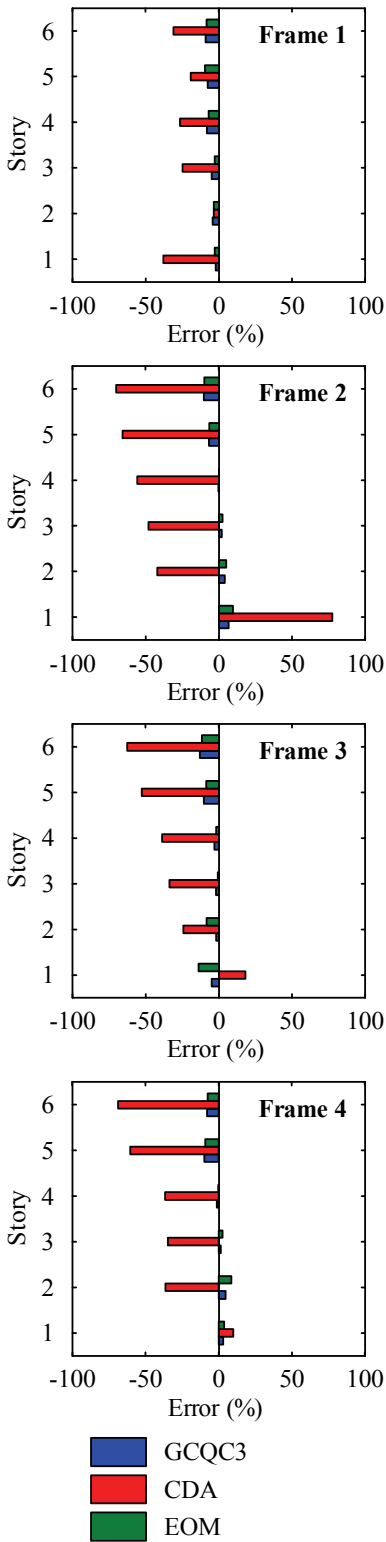


Figure 6.29 Estimation errors of the maximum story shear force per frame by response spectrum method

6.5.3 Discussion

By comparing all the response estimates obtained from the three approaches, it is shown that the GCQC3 rule provides excellent estimates for all response quantities overall. However, using the classical damping assumption (CDA) considerably underestimates the peak responses. The errors for some response quantities can be larger than 100%. Similar to the observation made in the response history analysis, the EOM is not able to predict the floor acceleration accurately as shown in Figure 6.18 and 6.19.

In general, these results show that the GCQC3 rule, which considers the over-damped modes, can estimate the peak response accurately. It is found that the peak floor accelerations are significantly affected by the over-damped modes. The responses estimated by using the forced classical damping assumption deviate substantially from the exact values. Most of the responses were underestimated. This is understandable because the modal properties calculated by the forced classical damping assumption are significantly different from the exact values computed by the state space approach. This implies that the utility of the forced classical damping assumption should be further examined in the design and analysis of structures with added damping devices, especially for complex and irregular structures.

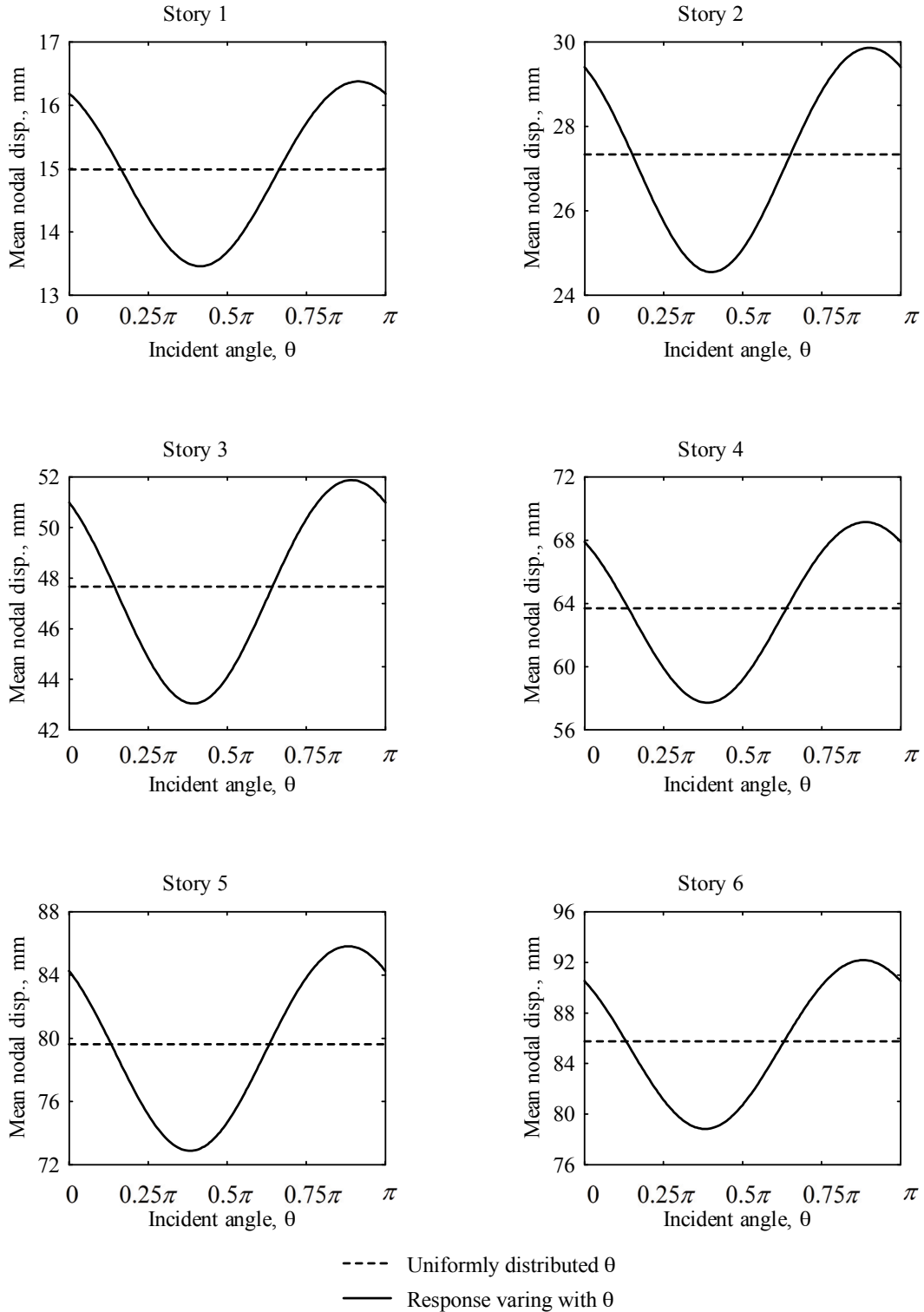
6.5.4 Effect of Seismic Incidence

In most cases, the seismic incident angle, i.e., the direction of the principal axes of the ground motion, remains unknown in the design process. It is clear from Equation (4.61) that the calculated peak responses of the structure change when the incident angle changes. To be conservative, the structure should be designed using the most critical value. In the following, the variations of seismic responses with respect to the seismic incident angle are examined. The peak displacement, velocity and total acceleration responses for each story are plotted against incident angle θ in Figure 6.30 to 6.38. Note that the value of θ that causes the most critical response depends on the response quantities being considered. In other words, the values will not be the same for all response quantities. Therefore, using the critical values in the design causes tremendous calculations for design engineers and is therefore not preferred. Also, the design will not be economical in a statistical sense. To consider this issue, it is reasonable to assume that

the incident angle θ is uniformly distributed among 0 to 2π and, as a result, the response can be calculated by Equation (4.71). The responses shown in Figure 6.30 to Figure 6.38 using a uniform distribution of θ are indicated by the dashed lines. One of the advantages of using the uniformly distributed θ is that the effect between the ground motion components disappears.

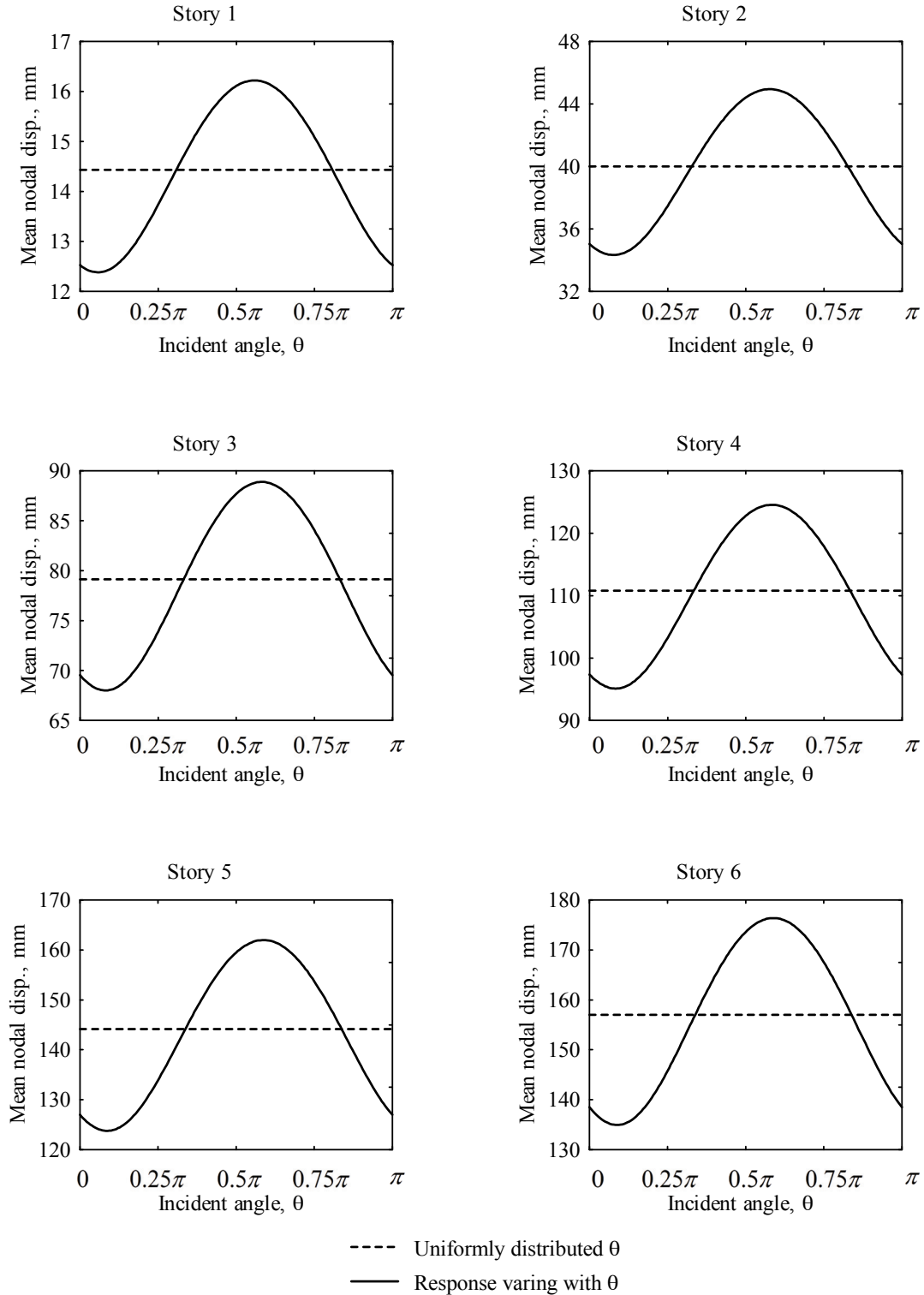
6.5.5 Peak Floor Acceleration Bounding Envelope

In this section, the accuracy of the procedure to predict the peak response of a spatially combined response developed in Chapter 5 is evaluated. The floor accelerations at each story are examined. Figure 6.39 compares the response envelopes according to the procedure proposed in Section 5.3.2.1 to the response envelopes simulated from the response history analyses. From Figure 6.39, excellent agreement between these two response envelopes can be observed, suggesting the adequacy of the proposed procedure.



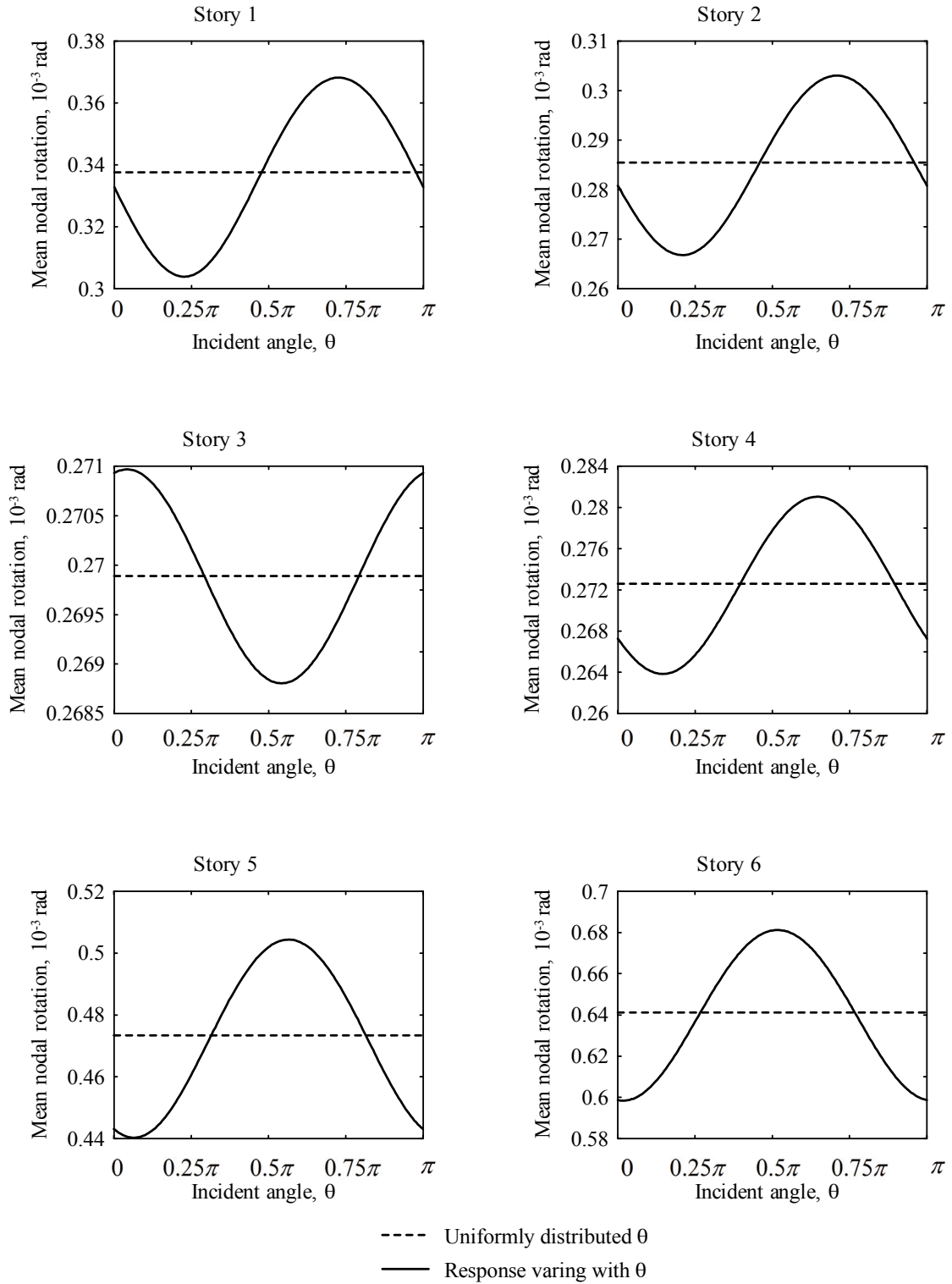
Displacement along X-Direction

Figure 6.30 Story displacement response variation along X-axis with respect to θ



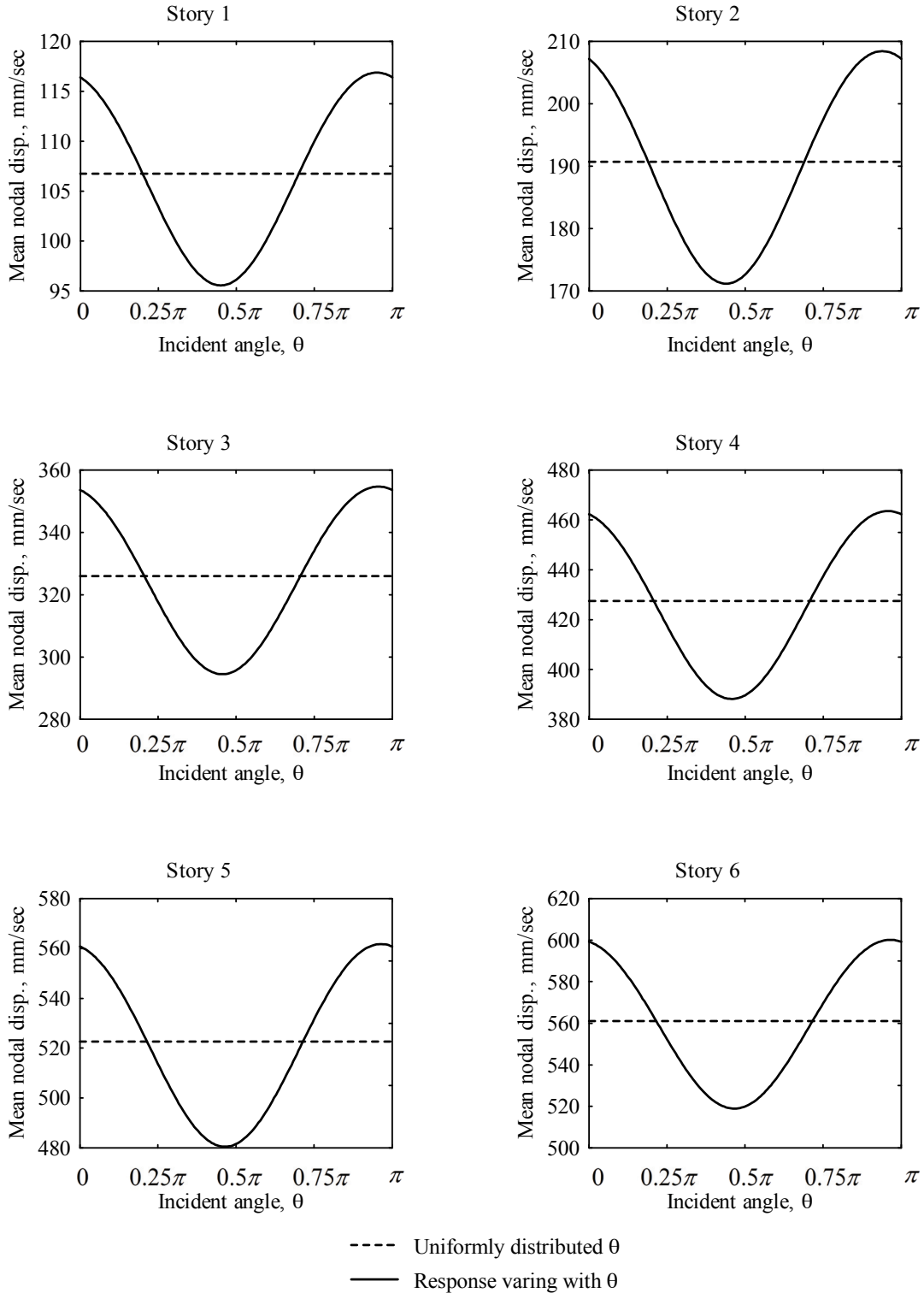
Displacement along Y-Direction

Figure 6.31 Story displacement response variation along Y-axis with respect to θ



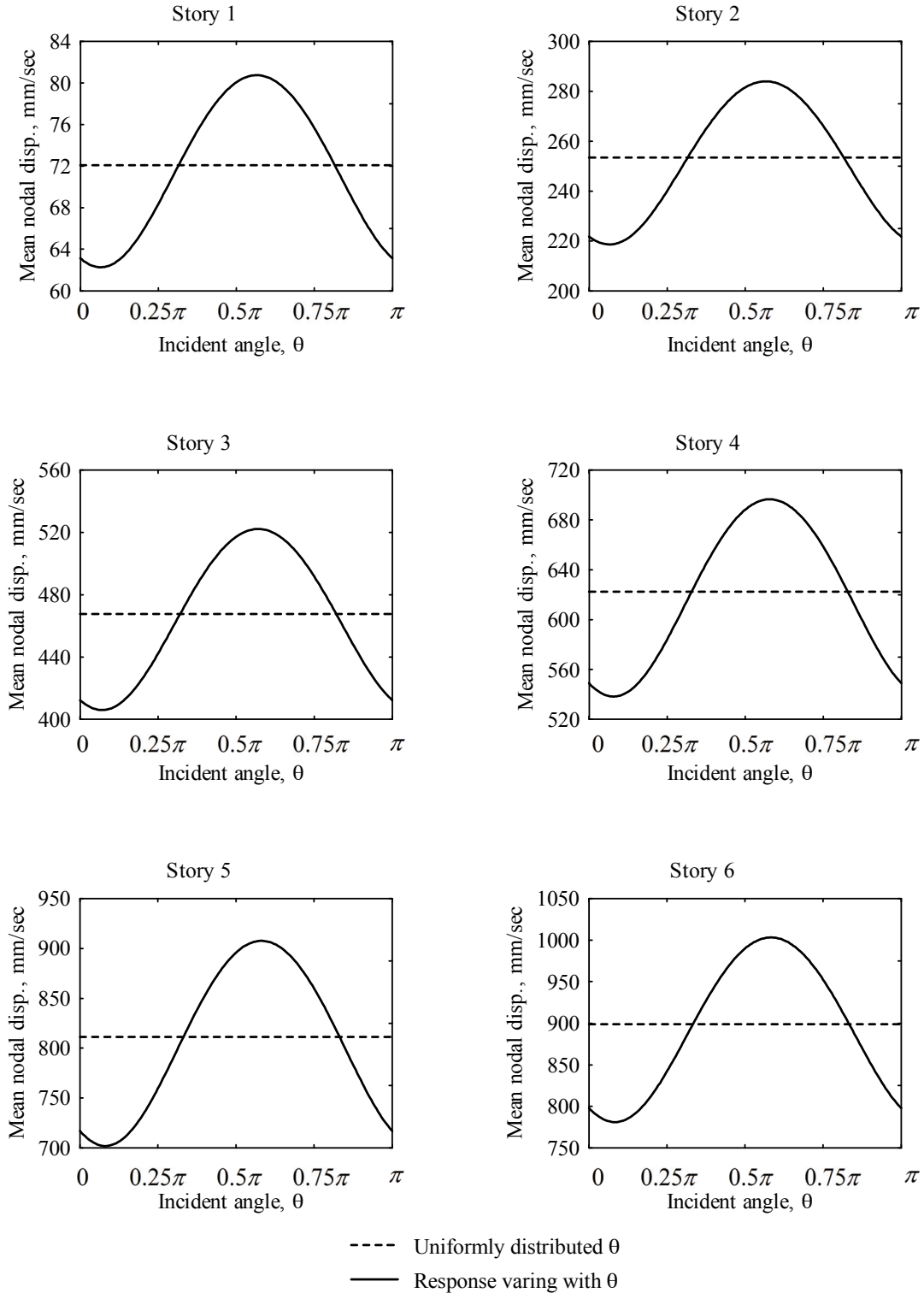
Rotation about Z-Direction

Figure 6.32 Story displacement response variation about Z-axis with respect to θ



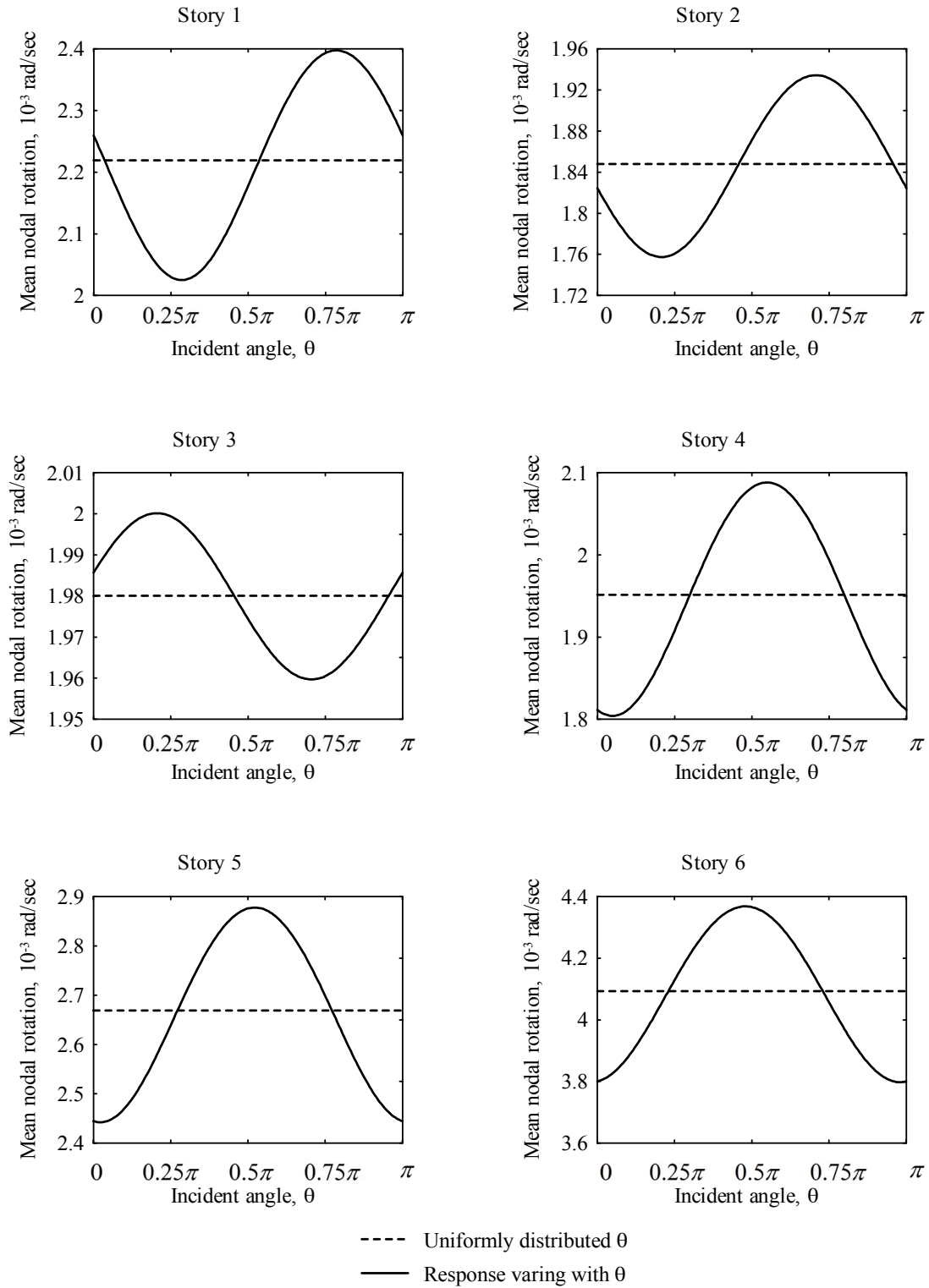
Velocity along X-Direction

Figure 6.33 Story velocity response variation along X-axis with respect to θ



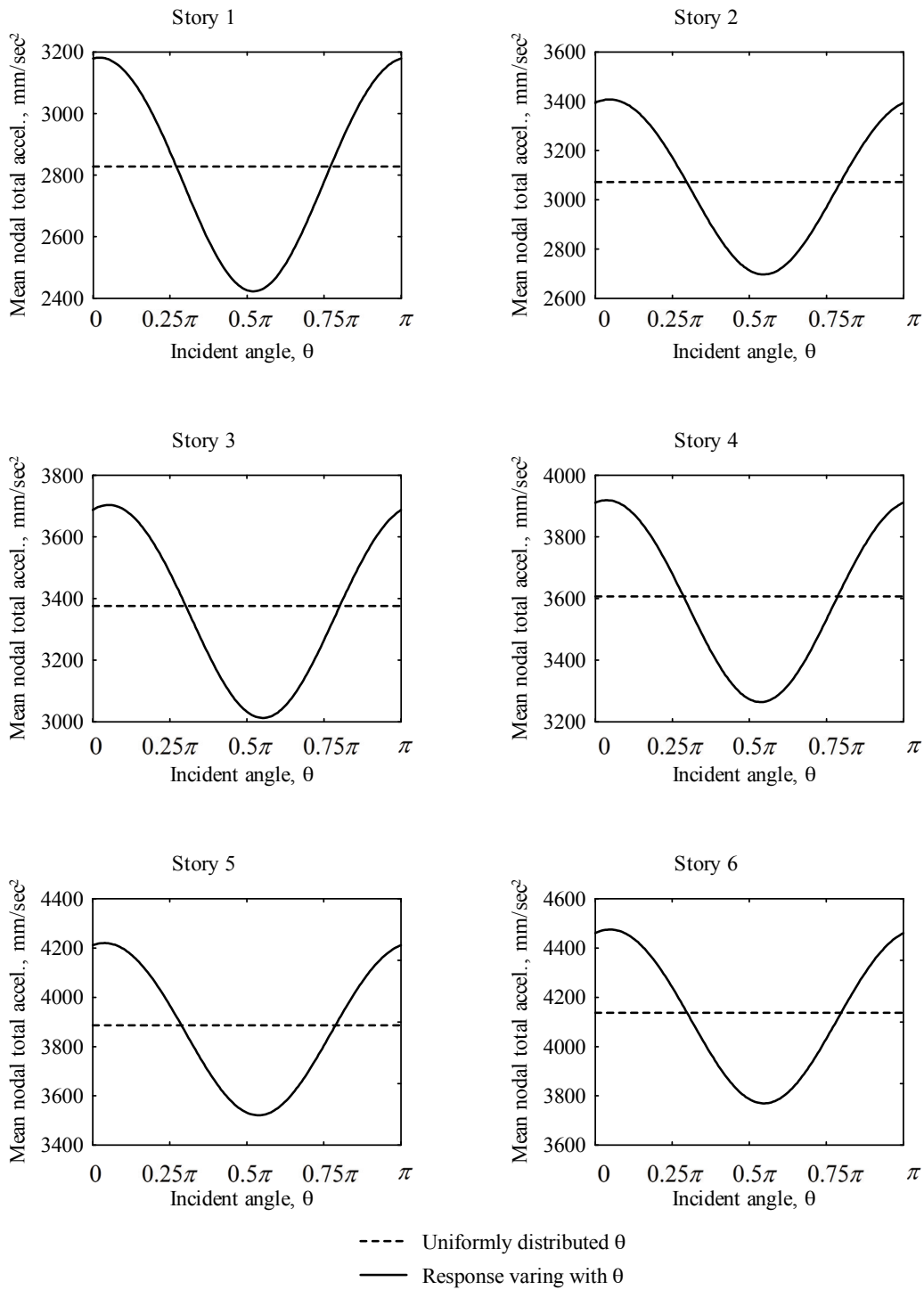
Velocity along Y-Direction

Figure 6.34 Story velocity response variation along Y-axis with respect to θ



Rotational Velocity about Z-Direction

Figure 6.35 Story velocity response variation about Z-axis with respect to θ



Total Accel. along X-Direction

Figure 6.36 Story total acceleration response variation along X-axis with respect to θ

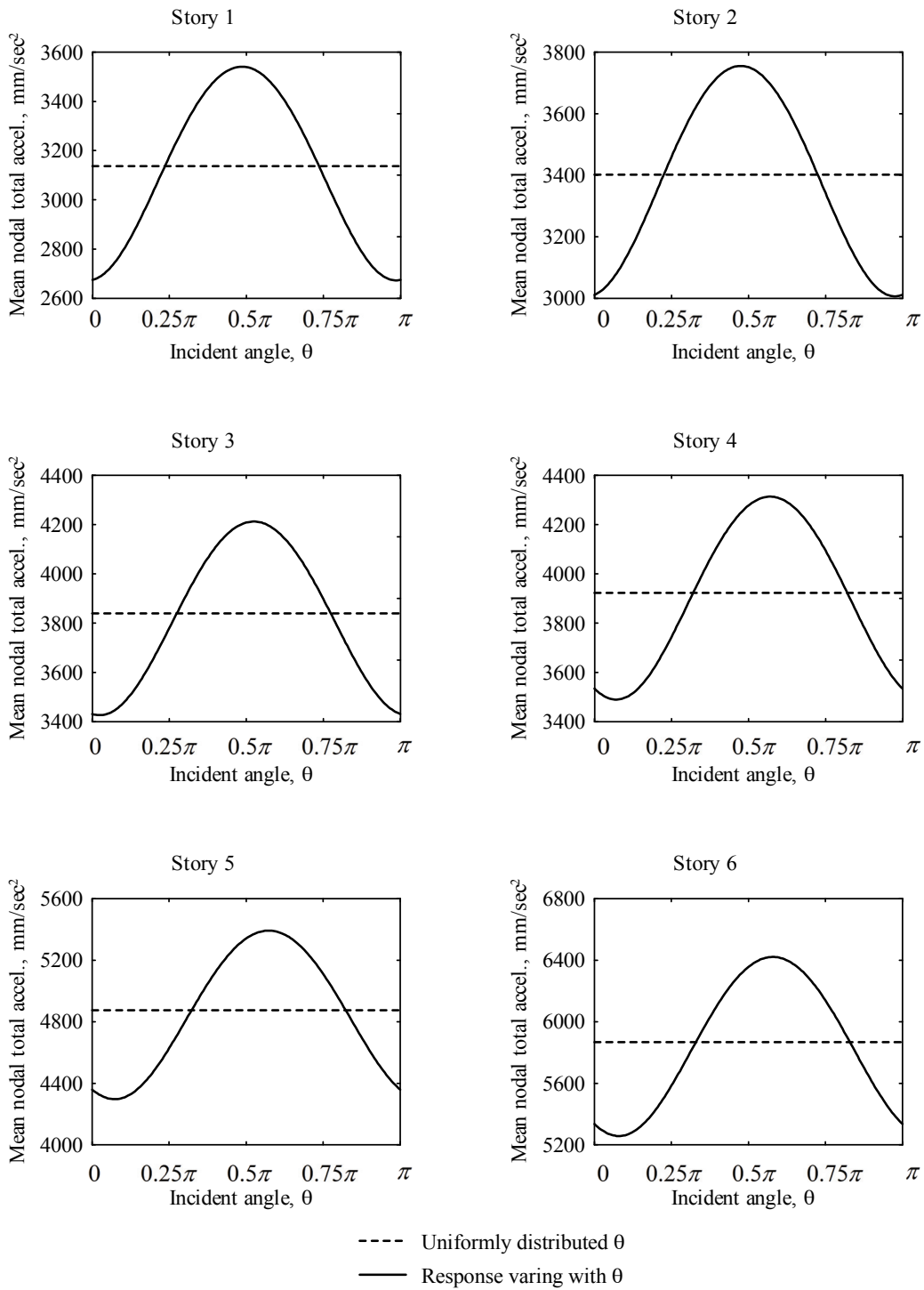
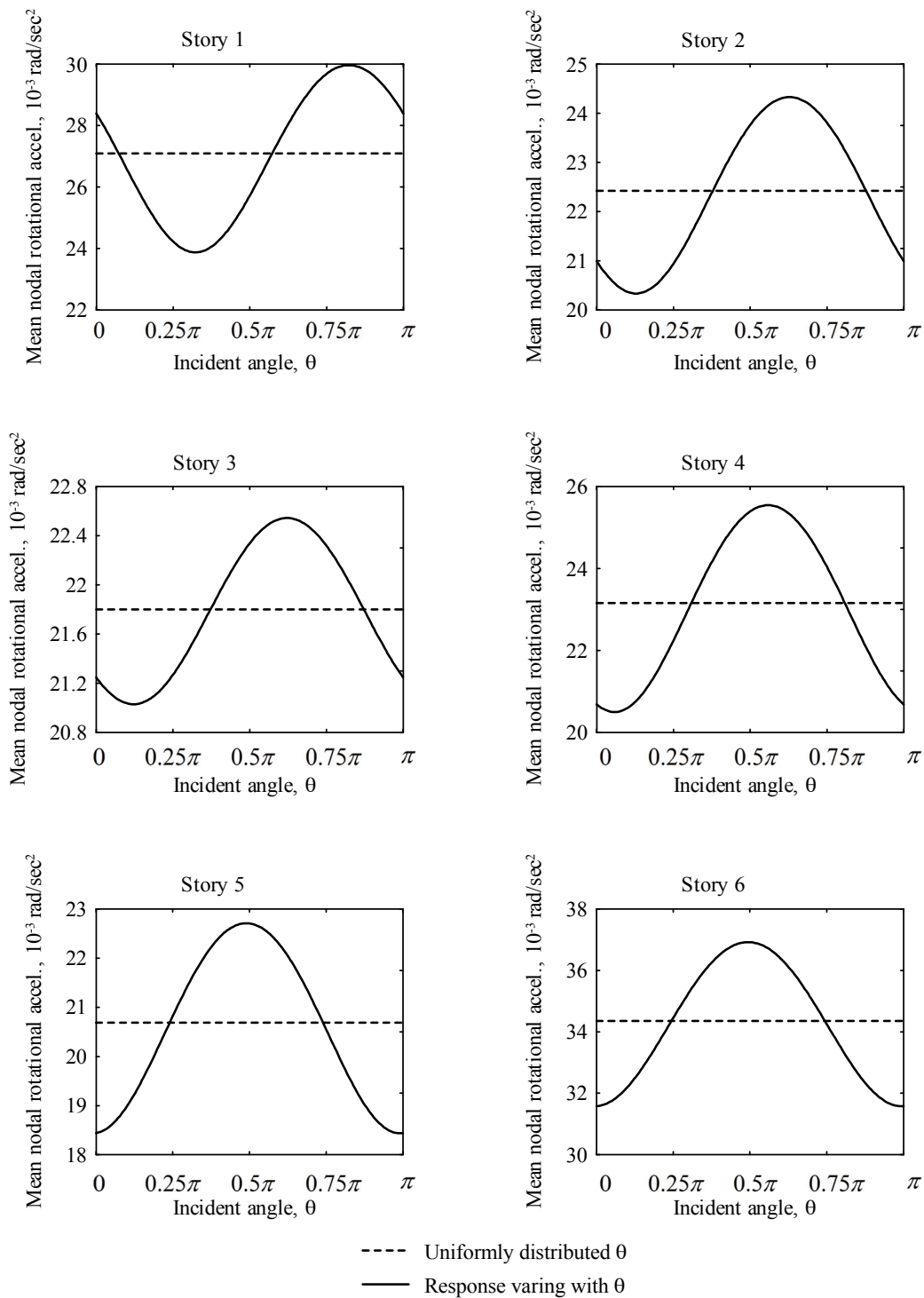


Figure 6.37 Story total acceleration y response variation along Y-axis with respect to θ



Rotational Accel. about Z-Direction

Figure 6.38 Story total acceleration response variation about Z-axis with respect to θ

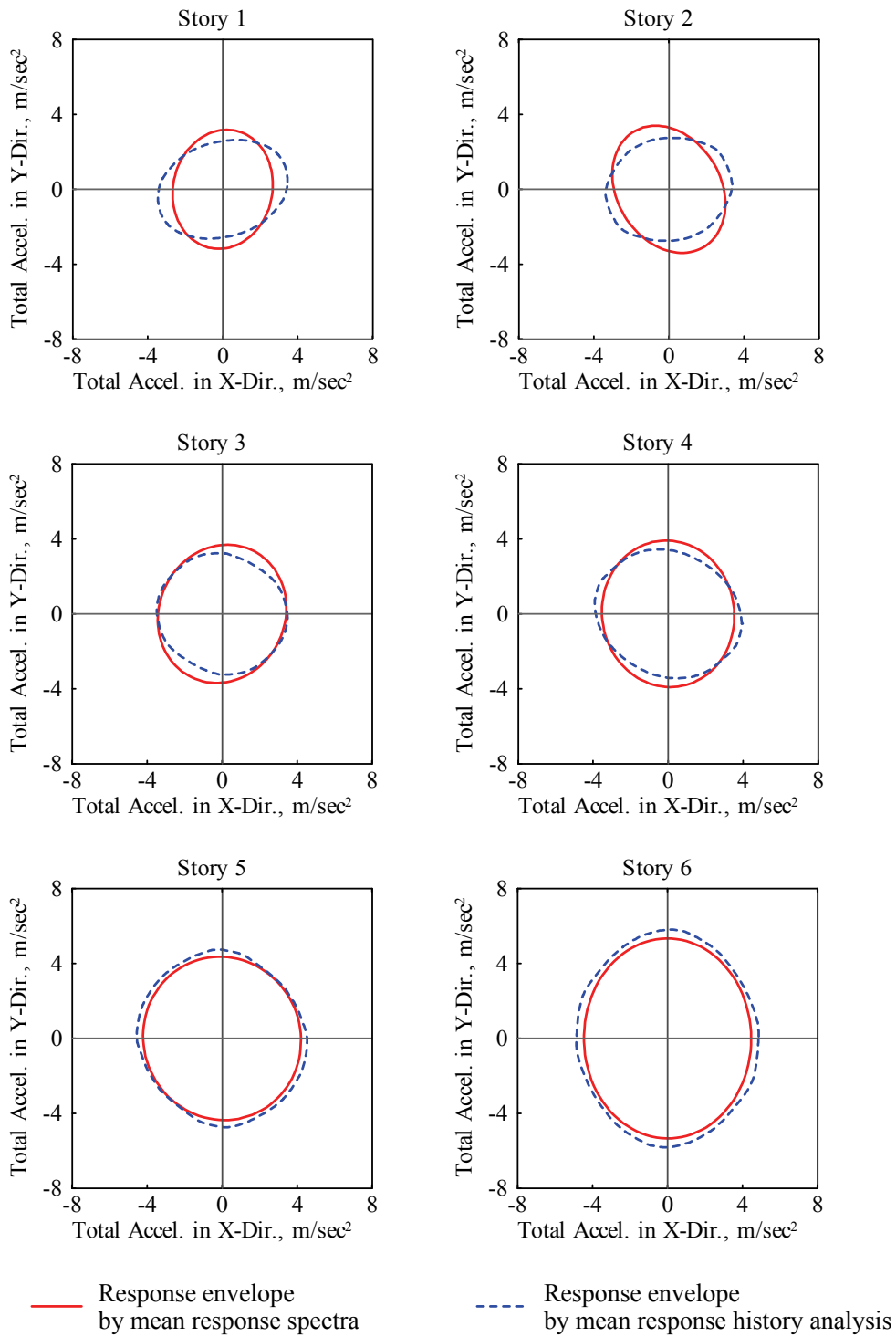


Figure 6.39 Comparison of the response envelopes for the example building

CHAPTER 7

SUMMARY, CONCLUSIONS AND FUTURE RESEARCH

7.1 Summary

Large, unusual and complex structures with earthquake response control devices may exhibit highly non-classical damping and may develop over-damped modes. This phenomenon can be further magnified under multi-directional seismic loadings. However, there is a gap in current knowledge about how to properly handle these uncertainties. This study is aimed at dealing with these issues using a modal analysis approach.

In this study, a general modal response history analysis method is developed first. This method extends complex modal analysis to structures with over-damped modes. A unified form that is able to express most response quantities of a given system, including velocities and absolute accelerations, is established. This unified form is obtained by several modal properties found in this study. Also, on the basis of the general modal response history analysis and the fundamental concept of stationary random process as well as the existence of the principal axes of ground motions, two general modal combination rules for the response spectrum method are formulated to deal with the non-classical damping and over-critically damped modes. This first rule is referred to as the ‘General-Complete-Quadratic-Combination-3’ (GCQC3) rule in this study while the second is the ‘General Square-Root-of-Sum-of Squares-3 (GSRSS3), in which the modal correlations are ignored. Further, an over-damped mode response spectrum is introduced to account for the peak modal responses of the over-damped modes. In addition to the displacement correlation coefficient given in the conventional CQC3 rule, new correlation coefficients to account for the cross correlations between modal displacement, modal velocity and the over-damped modal responses are also provided. The applicability of the general modal response history analysis method is demonstrated by a numerical example. Also, the errors in structural response estimations arising from the classical damping assumption are identified, and the effect of the over-damped modes on certain response quantities is observed. The accuracy of the GCQC3 rule is also evaluated through the example by comparing it to the mean response history results. This GCQC3

rule retains the conceptual simplicity of the CQC rule and offers an efficient and accurate estimation of the peak responses of structures with added damping devices. To enable the new rule to be applicable in earthquake engineering practice, a conversion procedure to construct an over-damped mode response spectrum compatible with the given 5% standard design response spectrum is established. Its accuracy is also validated. This ensures the applicability of the GCQC3 rule in engineering practice. An example evaluation shows that MDOF systems with added dampers should be modeled as non-classically damped systems and the over-damped modes should be included in the analysis to achieve more reliable estimates. In addition, a general real-valued modal coordinate transformation matrix which can decouple the equations of motion of arbitrarily damped structures is found during the process of theoretical formulation. A rigorous proof of the modal decoupling process by using this general modal coordinate transformation is given.

7.2 Conclusions

In this report, a comprehensive modal analysis approach for seismically excited arbitrarily damped 3-D structures is developed. The following key conclusions can be drawn from the theoretical formulation work:

- (1) The over-damped modes are allowed in the formulation. Their real eigenvalues and eigenvectors are treated individually instead of grouped into pairs.
- (2) Equation of motion of arbitrarily damped structures can be decoupled in a physical space using the general modal coordinate transformation matrix established in this study.
- (3) Through the formulation presented in this study, the 3-D coupling and orthogonal effect as well as the non-synchronization motions between DOFs and the over-damped modes can be quantified and explained both mathematically and physically.
- (4) Complex algebra operations are only required when solving the eigenvalue problems.

- (5) A unified form is available to express most response quantities in the modal analysis approach. This unified form only requires three sets of modal responses $\mathbf{q}_i(t)$, $\dot{\mathbf{q}}_i(t)$ and $\mathbf{q}_i^p(t)$.
- (6) The GCQC3 and GSRSS3 modal combination rules are applicable to estimate the velocity-related and absolute acceleration-related response quantities due to the establishment of the unified form. For example, the absolute acceleration of a single-degree-of-freedom system can be approximated more accurately by this rule instead of using the corresponding pseudo values.
- (7) A conversion procedure to construct an over-damped mode response spectrum compatible with the 5% design response spectrum is established to enable the GCQC3/GSRSS3 rule to be applicable for use in earthquake engineering practice.
- (8) From the example demonstration, it is found that the over-damped modes may have significant influence on the absolute acceleration-related response quantities. In general, the responses are under estimated if the over-damped modes are not properly considered.

7.3 Future Research

The formulation and application in this study are limited to linear systems. Further research should be performed to consider the inelastic behavior of a system. It is believed that the analysis procedure along with the use of equivalent linear approaches may be a reasonable approach for nonlinear analysis of systems with added dampers.

Possible future research work and topics are:

- (1) Development of a computer software system which incorporates all the proposed procedures to handle the effect of non-classical damping and the over-damped modes when the modal analysis approach is employed.

- (2) Principles of modal truncation of large scale arbitrarily damped systems/structures should be established to minimize the computation effort without losing the estimation accuracy.
- (3) Research the nonlinear behavior of structures that are supplemented with nonlinear damping devices and subjected to 3-D earthquake excitations. Based the results of such research, a linear equivalent MDOF model that can more accurately represent 3-D nonlinear structures may be developed. With this equivalent method, new design principles and guidelines based on the linear modal analysis approach for the structure-damper system may be established.
- (4) The effectiveness of supplemental dampers installed in real structures has not been demonstrated under large, very strong earthquakes, particularly when the structure experiences large deformation. Therefore, full scale experiments on structures with supplemental dampers should be conducted to validate the theory and observe the behavior of structure-damper systems that are subjected to large nonlinear deformations.
- (5) Develop design principles, methods and technology transfer materials, especially based on “equivalent linear approaches,” for structural engineers to aid in the design of supplemental damping.

CHAPTER 8

REFERENCES

- AASHTO. (2004). *AASHTO LRFD bridge design specifications*, Washington, DC.
- American Society of Civil Engineers (ASCE). (2006). *Minimum Design Loads for Buildings and Other Structures*, ASCE/SEI 7-05, ASCE, Reston, VA.
- Applied Technology Council (ATC). (2007). *Guidelines for seismic performance assessment of buildings. ATC-58 35% Draft*, Applied Technology Council, Redwood City, CA.
- Building Seismic Safety Council (BSSC). (2003). *NEHRP Recommended Provisions for Seismic Regulation for New Buildings and Other Structures, 2003 Edition*, Report No. FEMA 450, Federal Emergency Management Agency, Washington, DC.
- California Department of Transportation (Caltrans). (2004). *Seismic design criteria*, Sacramento, CA.
- Caughey, T.K. and O’Kelly, M.E.J. (1965). “Classical normal modes in damped linear dynamic systems,” *Journal of Applied Mechanics, ASME*, 32, 583-588.
- Chopra, A.K. (2001). *Dynamics of Structures: Theory and Applications to Earthquake Engineering* (Second Edition), Prentice-Hall: Englewood Cliffs, NJ.
- Chopra, A.K. (2005). *Earthquake dynamics of structures, A Primer*. EERI MNO-11, Oakland, CA.
- Clough, R.W. and Mojtahedi, S. (1976). “Earthquake response analysis considering non-proportional damping,” *Earthquake Engineering and Structural Dynamics*, 4, 489-496.
- Clough, R.W. and Penzien, J. (1993). *Dynamics of Structures*, Second Edition, McGraw-Hill, New York, NY.
- Davenport, A.G. (1964). “Note on the distribution of the largest value of a random function with application to gust loading,” *Proceedings, Institution of Civil Engineers*, 28, 187-196.

- Der Kiureghian, A. (1980). "Structural response to stationary excitation," *Journal of the Engineering Mechanics Division, ASCE*, 106, 1195-1213.
- Der Kiureghian, A. (1981). "A response spectrum method for random vibration analysis of MDF systems," *Earthquake Engineering and Structural Dynamics*, 9, 419-435.
- Der Kiureghian, A., Sackman, J. L. and Nour-Omid, B. (1983). "Dynamic Analysis of Light Equipment in Structures: Response to Stochastic Input," *Journal of Engineering Mechanics, ASCE*, Vol. 109, pp. 90-95.
- Federal Emergency Management Agency (FEMA). (1997). *NEHRP Recommended provisions for seismic regulations for new buildings and other structures*, 1997 edition, FEMA-302, Washington DC.
- Foss, F.K. (1958). "Co-ordinates which uncouple the linear dynamic systems," *Journal of Applied Mechanics, ASME*, 24, 361-364.
- Gupta, A. K. and Jaw, J.-W. (1986). "Response spectrum method for nonclassically damped systems," *Nuclear Engineering and Design*, 91, 161-169.
- Gupta, A. K. and Singh, M. P. (1977). "Design of Column Sections Subjected to Three Components of Earthquake," *Nuclear Engineering and Design*, 41, 129-133.
- Hanson, R.D. and Soong T.T. (2001). *Seismic design with supplemental energy dissipation devices*, EERI, MNO-8, Oakland, CA.
- Hart, G.C. and Wong, K. (1999). *Structural Dynamics for Structural Engineers*, Wiley & Sons, Inc., New York, NY.
- Hernandez, J. J. and Lopez, O. A. (2002). "Response to three-component seismic motion of arbitrary direction," *Earthquake Engineering and Structural Dynamics*, 31, 55-77.
- Igusa, T., Der Kiureghian, A. and Sackman, J.L. (1984). "Modal decomposition method for stationary response of non-classically damped systems," *Earthquake Engineering and Structural Dynamics*, 12, 121-136.
- Inman, D.J. and Andry, Jr. A.N. (1980). "Some results on the nature of eigenvalues of discrete damped linear systems," *Journal of Applied Mechanics, ASME*, 47, 927-930.

- International Code Council, (2003). “2003 International Building Code,” ICBO, Whittier, CA.
- Iwan, W. D. and Gates, N. C. (1979a). The effective period and damping of a class of hysteretic structures,” *Earthquake Engineering and Structural Dynamics*, 7(3), 199-211.
- Iwan, W. D. and Gates, N. C. (1979b). “Estimating earthquake response of simple hysteretic structures,” *J. of Engineering Mechanics Division*, 105(EM3), 391-405.
- Lee, G. C. and Liang, Z. (1998). “On cross effects of seismic responses of structures,” *Engineering Structures*, 20, 503-509.
- Lopez, O. and Torres, R. (1997). “The Critical Angle of Seismic Incidence and the Maximum Structural Response,” *Earthquake Engineering and Structural Dynamics*, 26, 881-894.
- Maldonado, G.O. and Singh, M.P. (1991). “An improved response spectrum method for calculating seismic design response. Part 2: Non-classically damped structures,” *Earthquake Engineering and Structural Dynamics*, 20(7): 637-649.
- MCEER. (2003). *MCEER/ATC-49 Recommended LRFD guidelines for the seismic design of highway bridges*, University at Buffalo, Buffalo, NY.
- Menun, C. and Der Kiureghian, A. (2000). “Envelopes for Seismic Response Vectors I: Theory,” *Journal of Structural Engineering*, ASCE, 126(4), 467-473.
- Newmark, N. M. (1975). “Seismic design criteria for structures and facilities, trans-Alaska pipeline systems,” *Proceedings of the US National Conference Earthquake Engineering*. EERI, 94-103.
- Nutt, R. V. (1996). “ATC-32: Provisional recommendations for the seismic design of bridges,” *The Fourth Caltrans Seismic Workshop*, Caltrans, Sacramento, CA.
- Penzien, J. and Watabe, M. (1975). “Characteristics of 3-Dimensional earthquake ground motions,” *Earthquake Engineering Structural Dynamics*, 3:365-373.
- Ramirez, O. M., Constantinou, M. C., Kircher, C. A., Whittaker, A. S., Johnson, M. W., Gomez, J. D. and Chrysostomou, C. Z. (2000). *Development and evaluation of*

simplified procedures for analysis and design of buildings with passive energy dissipation systems, Technical Report MCEER-00-0010 Revision 1, MCEER, University at Buffalo, Buffalo, NY.

Rosenblueth, E. (1951). *A basis for aseismic design*. Ph.D. Thesis, University of Illinois, Urbana, USA.

Rosenblueth, E, and Contreras, H. (1977). "Approximate design for multi-component earthquake," *Journal of Engineering Mechanics*, 103, 895-911.

Semby, W and Der Kiureghian, A. (1985). "Modal Combination Rules for Multicomponent Earthquake Excitation," *Earthquake Engineering Structural Dynamics*, 13:1-12.

Singh, M.P. (1980). "Seismic response by SRSS for nonproportional damping," *Journal of the Engineering Mechanics Division, ASCE*, 106(6), 1405-1419.

Singh, M. P. and Chu, S. L. (1976). "Stochastic Considerations in Seismic Analysis of Structures," *Earthquake Engineering and Structural Dynamics*, Vol. 4, pp. 295-307.

Singh, M.P. and Ghafory-Ashtiany, M. (1986). "Modal time-history analysis of non-classically damped structures for seismic motions," *Earthquake Engineering and Structural Dynamics*, 1986, 14, 133-146.

Sinha, R. and Igusa, T. (1995). "CQC and SRSS methods for non-classically damped structures," *Earthquake Engineering and Structural Dynamics*, 24, 615-619.

Song, J., Chu, Y.-L., Liang, Z. and Lee, G. C. (2007a). "Estimation of peak relative velocity and peak absolute acceleration of linear SDOF systems," *Earthquake Engineering and Engineering Vibration*, 6(1), 1-10.

Song, J, Liang, Z., Chu, Y.-L. and Lee, G.C. (2007b) "Peak Earthquake Response of Structures under Multi-Component Excitations," *Earthquake Engineering and Engineering Vibration*, 6(4), 1-14.

Song, J., Chu, Y.-L., Liang, Z. and Lee, G. C. (2008). *Modal Analysis of Generally Damped Linear Structures subjected to Seismic Excitations*, Technical Report MCEER-08-0005, MCEER, University at Buffalo, Buffalo, NY.

- Soong, T. T. and Dargush, G F. (1997). *Passive energy dissipation systems in structural engineering*, John Wiley & Sons, New York, USA.
- Soong, T. T. and Spencer, B. F. (2002). "Supplementary energy dissipation: state-of-the-art and state-of-the-practice," *Engineering Structures*, 24, 243-259.
- Takewaki, I. (2004). "Frequency domain modal analysis of earthquake input energy to highly damped passive control structures," *Earthquake Engineering and Structural Dynamics*, 33, 575-590.
- Tsopelas, P., Constantinou, M. C., Kircher, C. A. and Whittaker, A. S. (1997). *Evaluation of simplified methods of analysis for yielding structures*, Technical Report NCEER-97-0012, National Center for Earthquake Engineering Research, University at Buffalo, Buffalo, NY.
- Vamvatsikos, D. and Cornell, C.A. (2004). "Applied Incremental dynamic analysis," *Earthquake Spectra*, 20(2), 523-553.
- Vanmarcke, E.H. (1972). "Properties of spectral moments with applications to random vibration," *Journal of the Engineering Mechanics Division*, ASCE, 98, 425-446.
- Veletsos, A.S. and Ventura, C.E. (1986). "Modal analysis of non-classically damped linear systems," *Earthquake Engineering and Structural Dynamics*, 14, 217-243.
- Ventura, C.E. (1985). *Dynamic analysis of nonclassically damped systems*, Ph.D. Thesis, Rice University, Houston, Texas.
- Villaverde, R. (1988). "Rosenblueth's modal combination rule for systems with non-classical damping," *Earthquake Engineering and Structural Dynamics*, 16, 315-328.
- Villaverde, R. and Newmark, N. M. (1980). "Seismic Response of Light Attachments to Buildings," *Structural Research Series*, No. 469, University of Illinois, Urbana.
- Warburton, G.B. and Soni, S.R. (1977). "Errors in response calculations of non-classically damped structures," *Earthquake Engineering and Structural Dynamics*, 5, 365-376.
- Wilson, E.L. (2004). *Static & Dynamic Analysis of Structures* (Fourth Edition), Computers and Structures, Inc., Berkeley, CA.

- Wilson, E.L., Suharwardy, I. and Habibullah, A. (1995). "A Clarification of the Orthogonal Effects in a Three-Dimensional Seismic Analysis," *Earthquake Spectra*, 11(4), 659-666.
- Yang, J.N., Sarkani, S. and Long, F.X. (1987). *Modal Analysis of Nonclassically Damped Structural Systems Using Canonical Transformation*, Technical Report NCEER-87-0019, National Center for Earthquake Engineering Research, University at Buffalo, Buffalo, NY.
- Yang, J.N., Sarkani, S. and Long, F.X. (1988). *A Response Spectrum Approach for Analysis of Nonclassically Damped Structures*, Technical Report NCEER-88-0020, National Center for Earthquake Engineering Research, University at Buffalo, Buffalo, NY.
- Zhou, X.Y., Yu, R. and Dong, D. (2004). "Complex mode superposition algorithm for seismic responses of non-classically damped linear MDOF system," *Journal of Earthquake Engineering*, 8(4), 597-641.

MCEER Technical Reports

MCEER publishes technical reports on a variety of subjects written by authors funded through MCEER. These reports are available from both MCEER Publications and the National Technical Information Service (NTIS). Requests for reports should be directed to MCEER Publications, MCEER, University at Buffalo, State University of New York, Red Jacket Quadrangle, Buffalo, New York 14261. Reports can also be requested through NTIS, 5285 Port Royal Road, Springfield, Virginia 22161. NTIS accession numbers are shown in parenthesis, if available.

- NCEER-87-0001 "First-Year Program in Research, Education and Technology Transfer," 3/5/87, (PB88-134275, A04, MF-A01).
- NCEER-87-0002 "Experimental Evaluation of Instantaneous Optimal Algorithms for Structural Control," by R.C. Lin, T.T. Soong and A.M. Reinhorn, 4/20/87, (PB88-134341, A04, MF-A01).
- NCEER-87-0003 "Experimentation Using the Earthquake Simulation Facilities at University at Buffalo," by A.M. Reinhorn and R.L. Ketter, to be published.
- NCEER-87-0004 "The System Characteristics and Performance of a Shaking Table," by J.S. Hwang, K.C. Chang and G.C. Lee, 6/1/87, (PB88-134259, A03, MF-A01). This report is available only through NTIS (see address given above).
- NCEER-87-0005 "A Finite Element Formulation for Nonlinear Viscoplastic Material Using a Q Model," by O. Gyebe and G. Dasgupta, 11/2/87, (PB88-213764, A08, MF-A01).
- NCEER-87-0006 "Symbolic Manipulation Program (SMP) - Algebraic Codes for Two and Three Dimensional Finite Element Formulations," by X. Lee and G. Dasgupta, 11/9/87, (PB88-218522, A05, MF-A01).
- NCEER-87-0007 "Instantaneous Optimal Control Laws for Tall Buildings Under Seismic Excitations," by J.N. Yang, A. Akbarpour and P. Ghaemmaghami, 6/10/87, (PB88-134333, A06, MF-A01). This report is only available through NTIS (see address given above).
- NCEER-87-0008 "IDARC: Inelastic Damage Analysis of Reinforced Concrete Frame - Shear-Wall Structures," by Y.J. Park, A.M. Reinhorn and S.K. Kunnath, 7/20/87, (PB88-134325, A09, MF-A01). This report is only available through NTIS (see address given above).
- NCEER-87-0009 "Liquefaction Potential for New York State: A Preliminary Report on Sites in Manhattan and Buffalo," by M. Budhu, V. Vijayakumar, R.F. Giese and L. Baumgras, 8/31/87, (PB88-163704, A03, MF-A01). This report is available only through NTIS (see address given above).
- NCEER-87-0010 "Vertical and Torsional Vibration of Foundations in Inhomogeneous Media," by A.S. Veletsos and K.W. Dotson, 6/1/87, (PB88-134291, A03, MF-A01). This report is only available through NTIS (see address given above).
- NCEER-87-0011 "Seismic Probabilistic Risk Assessment and Seismic Margins Studies for Nuclear Power Plants," by Howard H.M. Hwang, 6/15/87, (PB88-134267, A03, MF-A01). This report is only available through NTIS (see address given above).
- NCEER-87-0012 "Parametric Studies of Frequency Response of Secondary Systems Under Ground-Acceleration Excitations," by Y. Yong and Y.K. Lin, 6/10/87, (PB88-134309, A03, MF-A01). This report is only available through NTIS (see address given above).
- NCEER-87-0013 "Frequency Response of Secondary Systems Under Seismic Excitation," by J.A. HoLung, J. Cai and Y.K. Lin, 7/31/87, (PB88-134317, A05, MF-A01). This report is only available through NTIS (see address given above).
- NCEER-87-0014 "Modelling Earthquake Ground Motions in Seismically Active Regions Using Parametric Time Series Methods," by G.W. Ellis and A.S. Cakmak, 8/25/87, (PB88-134283, A08, MF-A01). This report is only available through NTIS (see address given above).
- NCEER-87-0015 "Detection and Assessment of Seismic Structural Damage," by E. DiPasquale and A.S. Cakmak, 8/25/87, (PB88-163712, A05, MF-A01). This report is only available through NTIS (see address given above).

- NCEER-87-0016 "Pipeline Experiment at Parkfield, California," by J. Isenberg and E. Richardson, 9/15/87, (PB88-163720, A03, MF-A01). This report is available only through NTIS (see address given above).
- NCEER-87-0017 "Digital Simulation of Seismic Ground Motion," by M. Shinozuka, G. Deodatis and T. Harada, 8/31/87, (PB88-155197, A04, MF-A01). This report is available only through NTIS (see address given above).
- NCEER-87-0018 "Practical Considerations for Structural Control: System Uncertainty, System Time Delay and Truncation of Small Control Forces," J.N. Yang and A. Akbarpour, 8/10/87, (PB88-163738, A08, MF-A01). This report is only available through NTIS (see address given above).
- NCEER-87-0019 "Modal Analysis of Nonclassically Damped Structural Systems Using Canonical Transformation," by J.N. Yang, S. Sarkani and F.X. Long, 9/27/87, (PB88-187851, A04, MF-A01).
- NCEER-87-0020 "A Nonstationary Solution in Random Vibration Theory," by J.R. Red-Horse and P.D. Spanos, 11/3/87, (PB88-163746, A03, MF-A01).
- NCEER-87-0021 "Horizontal Impedances for Radially Inhomogeneous Viscoelastic Soil Layers," by A.S. Veletsos and K.W. Dotson, 10/15/87, (PB88-150859, A04, MF-A01).
- NCEER-87-0022 "Seismic Damage Assessment of Reinforced Concrete Members," by Y.S. Chung, C. Meyer and M. Shinozuka, 10/9/87, (PB88-150867, A05, MF-A01). This report is available only through NTIS (see address given above).
- NCEER-87-0023 "Active Structural Control in Civil Engineering," by T.T. Soong, 11/11/87, (PB88-187778, A03, MF-A01).
- NCEER-87-0024 "Vertical and Torsional Impedances for Radially Inhomogeneous Viscoelastic Soil Layers," by K.W. Dotson and A.S. Veletsos, 12/87, (PB88-187786, A03, MF-A01).
- NCEER-87-0025 "Proceedings from the Symposium on Seismic Hazards, Ground Motions, Soil-Liquefaction and Engineering Practice in Eastern North America," October 20-22, 1987, edited by K.H. Jacob, 12/87, (PB88-188115, A23, MF-A01). This report is available only through NTIS (see address given above).
- NCEER-87-0026 "Report on the Whittier-Narrows, California, Earthquake of October 1, 1987," by J. Pantelic and A. Reinhorn, 11/87, (PB88-187752, A03, MF-A01). This report is available only through NTIS (see address given above).
- NCEER-87-0027 "Design of a Modular Program for Transient Nonlinear Analysis of Large 3-D Building Structures," by S. Srivastav and J.F. Abel, 12/30/87, (PB88-187950, A05, MF-A01). This report is only available through NTIS (see address given above).
- NCEER-87-0028 "Second-Year Program in Research, Education and Technology Transfer," 3/8/88, (PB88-219480, A04, MF-A01).
- NCEER-88-0001 "Workshop on Seismic Computer Analysis and Design of Buildings With Interactive Graphics," by W. McGuire, J.F. Abel and C.H. Conley, 1/18/88, (PB88-187760, A03, MF-A01). This report is only available through NTIS (see address given above).
- NCEER-88-0002 "Optimal Control of Nonlinear Flexible Structures," by J.N. Yang, F.X. Long and D. Wong, 1/22/88, (PB88-213772, A06, MF-A01).
- NCEER-88-0003 "Substructuring Techniques in the Time Domain for Primary-Secondary Structural Systems," by G.D. Manolis and G. Juhn, 2/10/88, (PB88-213780, A04, MF-A01).
- NCEER-88-0004 "Iterative Seismic Analysis of Primary-Secondary Systems," by A. Singhal, L.D. Lutes and P.D. Spanos, 2/23/88, (PB88-213798, A04, MF-A01).
- NCEER-88-0005 "Stochastic Finite Element Expansion for Random Media," by P.D. Spanos and R. Ghanem, 3/14/88, (PB88-213806, A03, MF-A01).

- NCEER-88-0006 "Combining Structural Optimization and Structural Control," by F.Y. Cheng and C.P. Pantelides, 1/10/88, (PB88-213814, A05, MF-A01).
- NCEER-88-0007 "Seismic Performance Assessment of Code-Designed Structures," by H.H-M. Hwang, J-W. Jaw and H-J. Shau, 3/20/88, (PB88-219423, A04, MF-A01). This report is only available through NTIS (see address given above).
- NCEER-88-0008 "Reliability Analysis of Code-Designed Structures Under Natural Hazards," by H.H-M. Hwang, H. Ushiba and M. Shinozuka, 2/29/88, (PB88-229471, A07, MF-A01). This report is only available through NTIS (see address given above).
- NCEER-88-0009 "Seismic Fragility Analysis of Shear Wall Structures," by J-W Jaw and H.H-M. Hwang, 4/30/88, (PB89-102867, A04, MF-A01).
- NCEER-88-0010 "Base Isolation of a Multi-Story Building Under a Harmonic Ground Motion - A Comparison of Performances of Various Systems," by F-G Fan, G. Ahmadi and I.G. Tadjbakhsh, 5/18/88, (PB89-122238, A06, MF-A01). This report is only available through NTIS (see address given above).
- NCEER-88-0011 "Seismic Floor Response Spectra for a Combined System by Green's Functions," by F.M. Lavelle, L.A. Bergman and P.D. Spanos, 5/1/88, (PB89-102875, A03, MF-A01).
- NCEER-88-0012 "A New Solution Technique for Randomly Excited Hysteretic Structures," by G.Q. Cai and Y.K. Lin, 5/16/88, (PB89-102883, A03, MF-A01).
- NCEER-88-0013 "A Study of Radiation Damping and Soil-Structure Interaction Effects in the Centrifuge," by K. Weissman, supervised by J.H. Prevost, 5/24/88, (PB89-144703, A06, MF-A01).
- NCEER-88-0014 "Parameter Identification and Implementation of a Kinematic Plasticity Model for Frictional Soils," by J.H. Prevost and D.V. Griffiths, to be published.
- NCEER-88-0015 "Two- and Three- Dimensional Dynamic Finite Element Analyses of the Long Valley Dam," by D.V. Griffiths and J.H. Prevost, 6/17/88, (PB89-144711, A04, MF-A01).
- NCEER-88-0016 "Damage Assessment of Reinforced Concrete Structures in Eastern United States," by A.M. Reinhorn, M.J. Seidel, S.K. Kunnath and Y.J. Park, 6/15/88, (PB89-122220, A04, MF-A01). This report is only available through NTIS (see address given above).
- NCEER-88-0017 "Dynamic Compliance of Vertically Loaded Strip Foundations in Multilayered Viscoelastic Soils," by S. Ahmad and A.S.M. Israil, 6/17/88, (PB89-102891, A04, MF-A01).
- NCEER-88-0018 "An Experimental Study of Seismic Structural Response With Added Viscoelastic Dampers," by R.C. Lin, Z. Liang, T.T. Soong and R.H. Zhang, 6/30/88, (PB89-122212, A05, MF-A01). This report is available only through NTIS (see address given above).
- NCEER-88-0019 "Experimental Investigation of Primary - Secondary System Interaction," by G.D. Manolis, G. Juhn and A.M. Reinhorn, 5/27/88, (PB89-122204, A04, MF-A01).
- NCEER-88-0020 "A Response Spectrum Approach For Analysis of Nonclassically Damped Structures," by J.N. Yang, S. Sarkani and F.X. Long, 4/22/88, (PB89-102909, A04, MF-A01).
- NCEER-88-0021 "Seismic Interaction of Structures and Soils: Stochastic Approach," by A.S. Veletsos and A.M. Prasad, 7/21/88, (PB89-122196, A04, MF-A01). This report is only available through NTIS (see address given above).
- NCEER-88-0022 "Identification of the Serviceability Limit State and Detection of Seismic Structural Damage," by E. DiPasquale and A.S. Cakmak, 6/15/88, (PB89-122188, A05, MF-A01). This report is available only through NTIS (see address given above).
- NCEER-88-0023 "Multi-Hazard Risk Analysis: Case of a Simple Offshore Structure," by B.K. Bhartia and E.H. Vanmarcke, 7/21/88, (PB89-145213, A05, MF-A01).

- NCEER-88-0024 "Automated Seismic Design of Reinforced Concrete Buildings," by Y.S. Chung, C. Meyer and M. Shinozuka, 7/5/88, (PB89-122170, A06, MF-A01). This report is available only through NTIS (see address given above).
- NCEER-88-0025 "Experimental Study of Active Control of MDOF Structures Under Seismic Excitations," by L.L. Chung, R.C. Lin, T.T. Soong and A.M. Reinhorn, 7/10/88, (PB89-122600, A04, MF-A01).
- NCEER-88-0026 "Earthquake Simulation Tests of a Low-Rise Metal Structure," by J.S. Hwang, K.C. Chang, G.C. Lee and R.L. Ketter, 8/1/88, (PB89-102917, A04, MF-A01).
- NCEER-88-0027 "Systems Study of Urban Response and Reconstruction Due to Catastrophic Earthquakes," by F. Kozin and H.K. Zhou, 9/22/88, (PB90-162348, A04, MF-A01).
- NCEER-88-0028 "Seismic Fragility Analysis of Plane Frame Structures," by H.H-M. Hwang and Y.K. Low, 7/31/88, (PB89-131445, A06, MF-A01).
- NCEER-88-0029 "Response Analysis of Stochastic Structures," by A. Kardara, C. Bucher and M. Shinozuka, 9/22/88, (PB89-174429, A04, MF-A01).
- NCEER-88-0030 "Nonnormal Accelerations Due to Yielding in a Primary Structure," by D.C.K. Chen and L.D. Lutes, 9/19/88, (PB89-131437, A04, MF-A01).
- NCEER-88-0031 "Design Approaches for Soil-Structure Interaction," by A.S. Veletsos, A.M. Prasad and Y. Tang, 12/30/88, (PB89-174437, A03, MF-A01). This report is available only through NTIS (see address given above).
- NCEER-88-0032 "A Re-evaluation of Design Spectra for Seismic Damage Control," by C.J. Turkstra and A.G. Tallin, 11/7/88, (PB89-145221, A05, MF-A01).
- NCEER-88-0033 "The Behavior and Design of Noncontact Lap Splices Subjected to Repeated Inelastic Tensile Loading," by V.E. Sagan, P. Gergely and R.N. White, 12/8/88, (PB89-163737, A08, MF-A01).
- NCEER-88-0034 "Seismic Response of Pile Foundations," by S.M. Mamoon, P.K. Banerjee and S. Ahmad, 11/1/88, (PB89-145239, A04, MF-A01).
- NCEER-88-0035 "Modeling of R/C Building Structures With Flexible Floor Diaphragms (IDARC2)," by A.M. Reinhorn, S.K. Kunnath and N. Panahshahi, 9/7/88, (PB89-207153, A07, MF-A01).
- NCEER-88-0036 "Solution of the Dam-Reservoir Interaction Problem Using a Combination of FEM, BEM with Particular Integrals, Modal Analysis, and Substructuring," by C-S. Tsai, G.C. Lee and R.L. Ketter, 12/31/88, (PB89-207146, A04, MF-A01).
- NCEER-88-0037 "Optimal Placement of Actuators for Structural Control," by F.Y. Cheng and C.P. Pantelides, 8/15/88, (PB89-162846, A05, MF-A01).
- NCEER-88-0038 "Teflon Bearings in Aseismic Base Isolation: Experimental Studies and Mathematical Modeling," by A. Mokha, M.C. Constantinou and A.M. Reinhorn, 12/5/88, (PB89-218457, A10, MF-A01). This report is available only through NTIS (see address given above).
- NCEER-88-0039 "Seismic Behavior of Flat Slab High-Rise Buildings in the New York City Area," by P. Weidlinger and M. Ettouney, 10/15/88, (PB90-145681, A04, MF-A01).
- NCEER-88-0040 "Evaluation of the Earthquake Resistance of Existing Buildings in New York City," by P. Weidlinger and M. Ettouney, 10/15/88, to be published.
- NCEER-88-0041 "Small-Scale Modeling Techniques for Reinforced Concrete Structures Subjected to Seismic Loads," by W. Kim, A. El-Attar and R.N. White, 11/22/88, (PB89-189625, A05, MF-A01).
- NCEER-88-0042 "Modeling Strong Ground Motion from Multiple Event Earthquakes," by G.W. Ellis and A.S. Cakmak, 10/15/88, (PB89-174445, A03, MF-A01).

- NCEER-88-0043 "Nonstationary Models of Seismic Ground Acceleration," by M. Grigoriu, S.E. Ruiz and E. Rosenblueth, 7/15/88, (PB89-189617, A04, MF-A01).
- NCEER-88-0044 "SARCF User's Guide: Seismic Analysis of Reinforced Concrete Frames," by Y.S. Chung, C. Meyer and M. Shinozuka, 11/9/88, (PB89-174452, A08, MF-A01).
- NCEER-88-0045 "First Expert Panel Meeting on Disaster Research and Planning," edited by J. Pantelic and J. Stoyke, 9/15/88, (PB89-174460, A05, MF-A01).
- NCEER-88-0046 "Preliminary Studies of the Effect of Degrading Infill Walls on the Nonlinear Seismic Response of Steel Frames," by C.Z. Chrysostomou, P. Gergely and J.F. Abel, 12/19/88, (PB89-208383, A05, MF-A01).
- NCEER-88-0047 "Reinforced Concrete Frame Component Testing Facility - Design, Construction, Instrumentation and Operation," by S.P. Pessiki, C. Conley, T. Bond, P. Gergely and R.N. White, 12/16/88, (PB89-174478, A04, MF-A01).
- NCEER-89-0001 "Effects of Protective Cushion and Soil Compliancy on the Response of Equipment Within a Seismically Excited Building," by J.A. HoLung, 2/16/89, (PB89-207179, A04, MF-A01).
- NCEER-89-0002 "Statistical Evaluation of Response Modification Factors for Reinforced Concrete Structures," by H.H-M. Hwang and J-W. Jaw, 2/17/89, (PB89-207187, A05, MF-A01).
- NCEER-89-0003 "Hysteretic Columns Under Random Excitation," by G-Q. Cai and Y.K. Lin, 1/9/89, (PB89-196513, A03, MF-A01).
- NCEER-89-0004 "Experimental Study of 'Elephant Foot Bulge' Instability of Thin-Walled Metal Tanks," by Z-H. Jia and R.L. Ketter, 2/22/89, (PB89-207195, A03, MF-A01).
- NCEER-89-0005 "Experiment on Performance of Buried Pipelines Across San Andreas Fault," by J. Isenberg, E. Richardson and T.D. O'Rourke, 3/10/89, (PB89-218440, A04, MF-A01). This report is available only through NTIS (see address given above).
- NCEER-89-0006 "A Knowledge-Based Approach to Structural Design of Earthquake-Resistant Buildings," by M. Subramani, P. Gergely, C.H. Conley, J.F. Abel and A.H. Zaghaw, 1/15/89, (PB89-218465, A06, MF-A01).
- NCEER-89-0007 "Liquefaction Hazards and Their Effects on Buried Pipelines," by T.D. O'Rourke and P.A. Lane, 2/1/89, (PB89-218481, A09, MF-A01).
- NCEER-89-0008 "Fundamentals of System Identification in Structural Dynamics," by H. Imai, C-B. Yun, O. Maruyama and M. Shinozuka, 1/26/89, (PB89-207211, A04, MF-A01).
- NCEER-89-0009 "Effects of the 1985 Michoacan Earthquake on Water Systems and Other Buried Lifelines in Mexico," by A.G. Ayala and M.J. O'Rourke, 3/8/89, (PB89-207229, A06, MF-A01).
- NCEER-89-R010 "NCEER Bibliography of Earthquake Education Materials," by K.E.K. Ross, Second Revision, 9/1/89, (PB90-125352, A05, MF-A01). This report is replaced by NCEER-92-0018.
- NCEER-89-0011 "Inelastic Three-Dimensional Response Analysis of Reinforced Concrete Building Structures (IDARC-3D), Part I - Modeling," by S.K. Kunnath and A.M. Reinhorn, 4/17/89, (PB90-114612, A07, MF-A01). This report is available only through NTIS (see address given above).
- NCEER-89-0012 "Recommended Modifications to ATC-14," by C.D. Poland and J.O. Malley, 4/12/89, (PB90-108648, A15, MF-A01).
- NCEER-89-0013 "Repair and Strengthening of Beam-to-Column Connections Subjected to Earthquake Loading," by M. Corazao and A.J. Durrani, 2/28/89, (PB90-109885, A06, MF-A01).
- NCEER-89-0014 "Program EXKAL2 for Identification of Structural Dynamic Systems," by O. Maruyama, C-B. Yun, M. Hoshiya and M. Shinozuka, 5/19/89, (PB90-109877, A09, MF-A01).

- NCEER-89-0015 "Response of Frames With Bolted Semi-Rigid Connections, Part I - Experimental Study and Analytical Predictions," by P.J. DiCorso, A.M. Reinhorn, J.R. Dickerson, J.B. Radzinski and W.L. Harper, 6/1/89, to be published.
- NCEER-89-0016 "ARMA Monte Carlo Simulation in Probabilistic Structural Analysis," by P.D. Spanos and M.P. Mignolet, 7/10/89, (PB90-109893, A03, MF-A01).
- NCEER-89-P017 "Preliminary Proceedings from the Conference on Disaster Preparedness - The Place of Earthquake Education in Our Schools," Edited by K.E.K. Ross, 6/23/89, (PB90-108606, A03, MF-A01).
- NCEER-89-0017 "Proceedings from the Conference on Disaster Preparedness - The Place of Earthquake Education in Our Schools," Edited by K.E.K. Ross, 12/31/89, (PB90-207895, A012, MF-A02). This report is available only through NTIS (see address given above).
- NCEER-89-0018 "Multidimensional Models of Hysteretic Material Behavior for Vibration Analysis of Shape Memory Energy Absorbing Devices, by E.J. Graesser and F.A. Cozzarelli, 6/7/89, (PB90-164146, A04, MF-A01).
- NCEER-89-0019 "Nonlinear Dynamic Analysis of Three-Dimensional Base Isolated Structures (3D-BASIS)," by S. Nagarajaiah, A.M. Reinhorn and M.C. Constantinou, 8/3/89, (PB90-161936, A06, MF-A01). This report has been replaced by NCEER-93-0011.
- NCEER-89-0020 "Structural Control Considering Time-Rate of Control Forces and Control Rate Constraints," by F.Y. Cheng and C.P. Pantelides, 8/3/89, (PB90-120445, A04, MF-A01).
- NCEER-89-0021 "Subsurface Conditions of Memphis and Shelby County," by K.W. Ng, T-S. Chang and H-H.M. Hwang, 7/26/89, (PB90-120437, A03, MF-A01).
- NCEER-89-0022 "Seismic Wave Propagation Effects on Straight Jointed Buried Pipelines," by K. Elhmadi and M.J. O'Rourke, 8/24/89, (PB90-162322, A10, MF-A02).
- NCEER-89-0023 "Workshop on Serviceability Analysis of Water Delivery Systems," edited by M. Grigoriu, 3/6/89, (PB90-127424, A03, MF-A01).
- NCEER-89-0024 "Shaking Table Study of a 1/5 Scale Steel Frame Composed of Tapered Members," by K.C. Chang, J.S. Hwang and G.C. Lee, 9/18/89, (PB90-160169, A04, MF-A01).
- NCEER-89-0025 "DYNA1D: A Computer Program for Nonlinear Seismic Site Response Analysis - Technical Documentation," by Jean H. Prevost, 9/14/89, (PB90-161944, A07, MF-A01). This report is available only through NTIS (see address given above).
- NCEER-89-0026 "1:4 Scale Model Studies of Active Tendon Systems and Active Mass Dampers for Aseismic Protection," by A.M. Reinhorn, T.T. Soong, R.C. Lin, Y.P. Yang, Y. Fukao, H. Abe and M. Nakai, 9/15/89, (PB90-173246, A10, MF-A02). This report is available only through NTIS (see address given above).
- NCEER-89-0027 "Scattering of Waves by Inclusions in a Nonhomogeneous Elastic Half Space Solved by Boundary Element Methods," by P.K. Hadley, A. Askar and A.S. Cakmak, 6/15/89, (PB90-145699, A07, MF-A01).
- NCEER-89-0028 "Statistical Evaluation of Deflection Amplification Factors for Reinforced Concrete Structures," by H.H.M. Hwang, J-W. Jaw and A.L. Ch'ng, 8/31/89, (PB90-164633, A05, MF-A01).
- NCEER-89-0029 "Bedrock Accelerations in Memphis Area Due to Large New Madrid Earthquakes," by H.H.M. Hwang, C.H.S. Chen and G. Yu, 11/7/89, (PB90-162330, A04, MF-A01).
- NCEER-89-0030 "Seismic Behavior and Response Sensitivity of Secondary Structural Systems," by Y.Q. Chen and T.T. Soong, 10/23/89, (PB90-164658, A08, MF-A01).
- NCEER-89-0031 "Random Vibration and Reliability Analysis of Primary-Secondary Structural Systems," by Y. Ibrahim, M. Grigoriu and T.T. Soong, 11/10/89, (PB90-161951, A04, MF-A01).

- NCEER-89-0032 "Proceedings from the Second U.S. - Japan Workshop on Liquefaction, Large Ground Deformation and Their Effects on Lifelines, September 26-29, 1989," Edited by T.D. O'Rourke and M. Hamada, 12/1/89, (PB90-209388, A22, MF-A03).
- NCEER-89-0033 "Deterministic Model for Seismic Damage Evaluation of Reinforced Concrete Structures," by J.M. Bracci, A.M. Reinhorn, J.B. Mander and S.K. Kunnath, 9/27/89, (PB91-108803, A06, MF-A01).
- NCEER-89-0034 "On the Relation Between Local and Global Damage Indices," by E. DiPasquale and A.S. Cakmak, 8/15/89, (PB90-173865, A05, MF-A01).
- NCEER-89-0035 "Cyclic Undrained Behavior of Nonplastic and Low Plasticity Silts," by A.J. Walker and H.E. Stewart, 7/26/89, (PB90-183518, A10, MF-A01).
- NCEER-89-0036 "Liquefaction Potential of Surficial Deposits in the City of Buffalo, New York," by M. Budhu, R. Giese and L. Baumgrass, 1/17/89, (PB90-208455, A04, MF-A01).
- NCEER-89-0037 "A Deterministic Assessment of Effects of Ground Motion Incoherence," by A.S. Veletsos and Y. Tang, 7/15/89, (PB90-164294, A03, MF-A01).
- NCEER-89-0038 "Workshop on Ground Motion Parameters for Seismic Hazard Mapping," July 17-18, 1989, edited by R.V. Whitman, 12/1/89, (PB90-173923, A04, MF-A01).
- NCEER-89-0039 "Seismic Effects on Elevated Transit Lines of the New York City Transit Authority," by C.J. Costantino, C.A. Miller and E. Heymsfield, 12/26/89, (PB90-207887, A06, MF-A01).
- NCEER-89-0040 "Centrifugal Modeling of Dynamic Soil-Structure Interaction," by K. Weissman, Supervised by J.H. Prevost, 5/10/89, (PB90-207879, A07, MF-A01).
- NCEER-89-0041 "Linearized Identification of Buildings With Cores for Seismic Vulnerability Assessment," by I-K. Ho and A.E. Aktan, 11/1/89, (PB90-251943, A07, MF-A01).
- NCEER-90-0001 "Geotechnical and Lifeline Aspects of the October 17, 1989 Loma Prieta Earthquake in San Francisco," by T.D. O'Rourke, H.E. Stewart, F.T. Blackburn and T.S. Dickerman, 1/90, (PB90-208596, A05, MF-A01).
- NCEER-90-0002 "Nonnormal Secondary Response Due to Yielding in a Primary Structure," by D.C.K. Chen and L.D. Lutes, 2/28/90, (PB90-251976, A07, MF-A01).
- NCEER-90-0003 "Earthquake Education Materials for Grades K-12," by K.E.K. Ross, 4/16/90, (PB91-251984, A05, MF-A05). This report has been replaced by NCEER-92-0018.
- NCEER-90-0004 "Catalog of Strong Motion Stations in Eastern North America," by R.W. Busby, 4/3/90, (PB90-251984, A05, MF-A01).
- NCEER-90-0005 "NCEER Strong-Motion Data Base: A User Manual for the GeoBase Release (Version 1.0 for the Sun3)," by P. Friberg and K. Jacob, 3/31/90 (PB90-258062, A04, MF-A01).
- NCEER-90-0006 "Seismic Hazard Along a Crude Oil Pipeline in the Event of an 1811-1812 Type New Madrid Earthquake," by H.H.M. Hwang and C-H.S. Chen, 4/16/90, (PB90-258054, A04, MF-A01).
- NCEER-90-0007 "Site-Specific Response Spectra for Memphis Sheahan Pumping Station," by H.H.M. Hwang and C.S. Lee, 5/15/90, (PB91-108811, A05, MF-A01).
- NCEER-90-0008 "Pilot Study on Seismic Vulnerability of Crude Oil Transmission Systems," by T. Ariman, R. Dobry, M. Grigoriu, F. Kozin, M. O'Rourke, T. O'Rourke and M. Shinozuka, 5/25/90, (PB91-108837, A06, MF-A01).
- NCEER-90-0009 "A Program to Generate Site Dependent Time Histories: EQGEN," by G.W. Ellis, M. Srinivasan and A.S. Cakmak, 1/30/90, (PB91-108829, A04, MF-A01).
- NCEER-90-0010 "Active Isolation for Seismic Protection of Operating Rooms," by M.E. Talbott, Supervised by M. Shinozuka, 6/8/9, (PB91-110205, A05, MF-A01).

- NCEER-90-0011 "Program LINEARID for Identification of Linear Structural Dynamic Systems," by C-B. Yun and M. Shinozuka, 6/25/90, (PB91-110312, A08, MF-A01).
- NCEER-90-0012 "Two-Dimensional Two-Phase Elasto-Plastic Seismic Response of Earth Dams," by A.N. Yiagos, Supervised by J.H. Prevost, 6/20/90, (PB91-110197, A13, MF-A02).
- NCEER-90-0013 "Secondary Systems in Base-Isolated Structures: Experimental Investigation, Stochastic Response and Stochastic Sensitivity," by G.D. Manolis, G. Juhn, M.C. Constantinou and A.M. Reinhorn, 7/1/90, (PB91-110320, A08, MF-A01).
- NCEER-90-0014 "Seismic Behavior of Lightly-Reinforced Concrete Column and Beam-Column Joint Details," by S.P. Pessiki, C.H. Conley, P. Gergely and R.N. White, 8/22/90, (PB91-108795, A11, MF-A02).
- NCEER-90-0015 "Two Hybrid Control Systems for Building Structures Under Strong Earthquakes," by J.N. Yang and A. Daniellians, 6/29/90, (PB91-125393, A04, MF-A01).
- NCEER-90-0016 "Instantaneous Optimal Control with Acceleration and Velocity Feedback," by J.N. Yang and Z. Li, 6/29/90, (PB91-125401, A03, MF-A01).
- NCEER-90-0017 "Reconnaissance Report on the Northern Iran Earthquake of June 21, 1990," by M. Mehrain, 10/4/90, (PB91-125377, A03, MF-A01).
- NCEER-90-0018 "Evaluation of Liquefaction Potential in Memphis and Shelby County," by T.S. Chang, P.S. Tang, C.S. Lee and H. Hwang, 8/10/90, (PB91-125427, A09, MF-A01).
- NCEER-90-0019 "Experimental and Analytical Study of a Combined Sliding Disc Bearing and Helical Steel Spring Isolation System," by M.C. Constantinou, A.S. Mokha and A.M. Reinhorn, 10/4/90, (PB91-125385, A06, MF-A01). This report is available only through NTIS (see address given above).
- NCEER-90-0020 "Experimental Study and Analytical Prediction of Earthquake Response of a Sliding Isolation System with a Spherical Surface," by A.S. Mokha, M.C. Constantinou and A.M. Reinhorn, 10/11/90, (PB91-125419, A05, MF-A01).
- NCEER-90-0021 "Dynamic Interaction Factors for Floating Pile Groups," by G. Gazetas, K. Fan, A. Kaynia and E. Kausel, 9/10/90, (PB91-170381, A05, MF-A01).
- NCEER-90-0022 "Evaluation of Seismic Damage Indices for Reinforced Concrete Structures," by S. Rodriguez-Gomez and A.S. Cakmak, 9/30/90, PB91-171322, A06, MF-A01).
- NCEER-90-0023 "Study of Site Response at a Selected Memphis Site," by H. Desai, S. Ahmad, E.S. Gazetas and M.R. Oh, 10/11/90, (PB91-196857, A03, MF-A01).
- NCEER-90-0024 "A User's Guide to Strongmo: Version 1.0 of NCEER's Strong-Motion Data Access Tool for PCs and Terminals," by P.A. Friberg and C.A.T. Susch, 11/15/90, (PB91-171272, A03, MF-A01).
- NCEER-90-0025 "A Three-Dimensional Analytical Study of Spatial Variability of Seismic Ground Motions," by L-L. Hong and A.H.-S. Ang, 10/30/90, (PB91-170399, A09, MF-A01).
- NCEER-90-0026 "MUMOID User's Guide - A Program for the Identification of Modal Parameters," by S. Rodriguez-Gomez and E. DiPasquale, 9/30/90, (PB91-171298, A04, MF-A01).
- NCEER-90-0027 "SARCF-II User's Guide - Seismic Analysis of Reinforced Concrete Frames," by S. Rodriguez-Gomez, Y.S. Chung and C. Meyer, 9/30/90, (PB91-171280, A05, MF-A01).
- NCEER-90-0028 "Viscous Dampers: Testing, Modeling and Application in Vibration and Seismic Isolation," by N. Makris and M.C. Constantinou, 12/20/90 (PB91-190561, A06, MF-A01).
- NCEER-90-0029 "Soil Effects on Earthquake Ground Motions in the Memphis Area," by H. Hwang, C.S. Lee, K.W. Ng and T.S. Chang, 8/2/90, (PB91-190751, A05, MF-A01).

- NCEER-91-0001 "Proceedings from the Third Japan-U.S. Workshop on Earthquake Resistant Design of Lifeline Facilities and Countermeasures for Soil Liquefaction, December 17-19, 1990," edited by T.D. O'Rourke and M. Hamada, 2/1/91, (PB91-179259, A99, MF-A04).
- NCEER-91-0002 "Physical Space Solutions of Non-Proportionally Damped Systems," by M. Tong, Z. Liang and G.C. Lee, 1/15/91, (PB91-179242, A04, MF-A01).
- NCEER-91-0003 "Seismic Response of Single Piles and Pile Groups," by K. Fan and G. Gazetas, 1/10/91, (PB92-174994, A04, MF-A01).
- NCEER-91-0004 "Damping of Structures: Part 1 - Theory of Complex Damping," by Z. Liang and G. Lee, 10/10/91, (PB92-197235, A12, MF-A03).
- NCEER-91-0005 "3D-BASIS - Nonlinear Dynamic Analysis of Three Dimensional Base Isolated Structures: Part II," by S. Nagarajaiah, A.M. Reinhorn and M.C. Constantinou, 2/28/91, (PB91-190553, A07, MF-A01). This report has been replaced by NCEER-93-0011.
- NCEER-91-0006 "A Multidimensional Hysteretic Model for Plasticity Deforming Metals in Energy Absorbing Devices," by E.J. Graesser and F.A. Cozzarelli, 4/9/91, (PB92-108364, A04, MF-A01).
- NCEER-91-0007 "A Framework for Customizable Knowledge-Based Expert Systems with an Application to a KBES for Evaluating the Seismic Resistance of Existing Buildings," by E.G. Ibarra-Anaya and S.J. Fenves, 4/9/91, (PB91-210930, A08, MF-A01).
- NCEER-91-0008 "Nonlinear Analysis of Steel Frames with Semi-Rigid Connections Using the Capacity Spectrum Method," by G.G. Deierlein, S-H. Hsieh, Y-J. Shen and J.F. Abel, 7/2/91, (PB92-113828, A05, MF-A01).
- NCEER-91-0009 "Earthquake Education Materials for Grades K-12," by K.E.K. Ross, 4/30/91, (PB91-212142, A06, MF-A01). This report has been replaced by NCEER-92-0018.
- NCEER-91-0010 "Phase Wave Velocities and Displacement Phase Differences in a Harmonically Oscillating Pile," by N. Makris and G. Gazetas, 7/8/91, (PB92-108356, A04, MF-A01).
- NCEER-91-0011 "Dynamic Characteristics of a Full-Size Five-Story Steel Structure and a 2/5 Scale Model," by K.C. Chang, G.C. Yao, G.C. Lee, D.S. Hao and Y.C. Yeh, 7/2/91, (PB93-116648, A06, MF-A02).
- NCEER-91-0012 "Seismic Response of a 2/5 Scale Steel Structure with Added Viscoelastic Dampers," by K.C. Chang, T.T. Soong, S-T. Oh and M.L. Lai, 5/17/91, (PB92-110816, A05, MF-A01).
- NCEER-91-0013 "Earthquake Response of Retaining Walls; Full-Scale Testing and Computational Modeling," by S. Alampalli and A-W.M. Elgamal, 6/20/91, to be published.
- NCEER-91-0014 "3D-BASIS-M: Nonlinear Dynamic Analysis of Multiple Building Base Isolated Structures," by P.C. Tsopelas, S. Nagarajaiah, M.C. Constantinou and A.M. Reinhorn, 5/28/91, (PB92-113885, A09, MF-A02).
- NCEER-91-0015 "Evaluation of SEAOC Design Requirements for Sliding Isolated Structures," by D. Theodossiou and M.C. Constantinou, 6/10/91, (PB92-114602, A11, MF-A03).
- NCEER-91-0016 "Closed-Loop Modal Testing of a 27-Story Reinforced Concrete Flat Plate-Core Building," by H.R. Somaprasad, T. Toksoy, H. Yoshiyuki and A.E. Aktan, 7/15/91, (PB92-129980, A07, MF-A02).
- NCEER-91-0017 "Shake Table Test of a 1/6 Scale Two-Story Lightly Reinforced Concrete Building," by A.G. El-Attar, R.N. White and P. Gergely, 2/28/91, (PB92-222447, A06, MF-A02).
- NCEER-91-0018 "Shake Table Test of a 1/8 Scale Three-Story Lightly Reinforced Concrete Building," by A.G. El-Attar, R.N. White and P. Gergely, 2/28/91, (PB93-116630, A08, MF-A02).
- NCEER-91-0019 "Transfer Functions for Rigid Rectangular Foundations," by A.S. Veletsos, A.M. Prasad and W.H. Wu, 7/31/91, to be published.

- NCEER-91-0020 "Hybrid Control of Seismic-Excited Nonlinear and Inelastic Structural Systems," by J.N. Yang, Z. Li and A. Daniellians, 8/1/91, (PB92-143171, A06, MF-A02).
- NCEER-91-0021 "The NCEER-91 Earthquake Catalog: Improved Intensity-Based Magnitudes and Recurrence Relations for U.S. Earthquakes East of New Madrid," by L. Seeber and J.G. Armbruster, 8/28/91, (PB92-176742, A06, MF-A02).
- NCEER-91-0022 "Proceedings from the Implementation of Earthquake Planning and Education in Schools: The Need for Change - The Roles of the Changemakers," by K.E.K. Ross and F. Winslow, 7/23/91, (PB92-129998, A12, MF-A03).
- NCEER-91-0023 "A Study of Reliability-Based Criteria for Seismic Design of Reinforced Concrete Frame Buildings," by H.H.M. Hwang and H-M. Hsu, 8/10/91, (PB92-140235, A09, MF-A02).
- NCEER-91-0024 "Experimental Verification of a Number of Structural System Identification Algorithms," by R.G. Ghanem, H. Gavin and M. Shinozuka, 9/18/91, (PB92-176577, A18, MF-A04).
- NCEER-91-0025 "Probabilistic Evaluation of Liquefaction Potential," by H.H.M. Hwang and C.S. Lee," 11/25/91, (PB92-143429, A05, MF-A01).
- NCEER-91-0026 "Instantaneous Optimal Control for Linear, Nonlinear and Hysteretic Structures - Stable Controllers," by J.N. Yang and Z. Li, 11/15/91, (PB92-163807, A04, MF-A01).
- NCEER-91-0027 "Experimental and Theoretical Study of a Sliding Isolation System for Bridges," by M.C. Constantinou, A. Kartoum, A.M. Reinhorn and P. Bradford, 11/15/91, (PB92-176973, A10, MF-A03).
- NCEER-92-0001 "Case Studies of Liquefaction and Lifeline Performance During Past Earthquakes, Volume 1: Japanese Case Studies," Edited by M. Hamada and T. O'Rourke, 2/17/92, (PB92-197243, A18, MF-A04).
- NCEER-92-0002 "Case Studies of Liquefaction and Lifeline Performance During Past Earthquakes, Volume 2: United States Case Studies," Edited by T. O'Rourke and M. Hamada, 2/17/92, (PB92-197250, A20, MF-A04).
- NCEER-92-0003 "Issues in Earthquake Education," Edited by K. Ross, 2/3/92, (PB92-222389, A07, MF-A02).
- NCEER-92-0004 "Proceedings from the First U.S. - Japan Workshop on Earthquake Protective Systems for Bridges," Edited by I.G. Buckle, 2/4/92, (PB94-142239, A99, MF-A06).
- NCEER-92-0005 "Seismic Ground Motion from a Haskell-Type Source in a Multiple-Layered Half-Space," A.P. Theoharis, G. Deodatis and M. Shinozuka, 1/2/92, to be published.
- NCEER-92-0006 "Proceedings from the Site Effects Workshop," Edited by R. Whitman, 2/29/92, (PB92-197201, A04, MF-A01).
- NCEER-92-0007 "Engineering Evaluation of Permanent Ground Deformations Due to Seismically-Induced Liquefaction," by M.H. Baziar, R. Dobry and A-W.M. Elgamel, 3/24/92, (PB92-222421, A13, MF-A03).
- NCEER-92-0008 "A Procedure for the Seismic Evaluation of Buildings in the Central and Eastern United States," by C.D. Poland and J.O. Malley, 4/2/92, (PB92-222439, A20, MF-A04).
- NCEER-92-0009 "Experimental and Analytical Study of a Hybrid Isolation System Using Friction Controllable Sliding Bearings," by M.Q. Feng, S. Fujii and M. Shinozuka, 5/15/92, (PB93-150282, A06, MF-A02).
- NCEER-92-0010 "Seismic Resistance of Slab-Column Connections in Existing Non-Ductile Flat-Plate Buildings," by A.J. Durrani and Y. Du, 5/18/92, (PB93-116812, A06, MF-A02).
- NCEER-92-0011 "The Hysteretic and Dynamic Behavior of Brick Masonry Walls Upgraded by Ferrocement Coatings Under Cyclic Loading and Strong Simulated Ground Motion," by H. Lee and S.P. Prawel, 5/11/92, to be published.
- NCEER-92-0012 "Study of Wire Rope Systems for Seismic Protection of Equipment in Buildings," by G.F. Demetriades, M.C. Constantinou and A.M. Reinhorn, 5/20/92, (PB93-116655, A08, MF-A02).

- NCEER-92-0013 "Shape Memory Structural Dampers: Material Properties, Design and Seismic Testing," by P.R. Witting and F.A. Cozzarelli, 5/26/92, (PB93-116663, A05, MF-A01).
- NCEER-92-0014 "Longitudinal Permanent Ground Deformation Effects on Buried Continuous Pipelines," by M.J. O'Rourke, and C. Nordberg, 6/15/92, (PB93-116671, A08, MF-A02).
- NCEER-92-0015 "A Simulation Method for Stationary Gaussian Random Functions Based on the Sampling Theorem," by M. Grigoriu and S. Balopoulou, 6/11/92, (PB93-127496, A05, MF-A01).
- NCEER-92-0016 "Gravity-Load-Designed Reinforced Concrete Buildings: Seismic Evaluation of Existing Construction and Detailing Strategies for Improved Seismic Resistance," by G.W. Hoffmann, S.K. Kunnath, A.M. Reinhorn and J.B. Mander, 7/15/92, (PB94-142007, A08, MF-A02).
- NCEER-92-0017 "Observations on Water System and Pipeline Performance in the Limón Area of Costa Rica Due to the April 22, 1991 Earthquake," by M. O'Rourke and D. Ballantyne, 6/30/92, (PB93-126811, A06, MF-A02).
- NCEER-92-0018 "Fourth Edition of Earthquake Education Materials for Grades K-12," Edited by K.E.K. Ross, 8/10/92, (PB93-114023, A07, MF-A02).
- NCEER-92-0019 "Proceedings from the Fourth Japan-U.S. Workshop on Earthquake Resistant Design of Lifeline Facilities and Countermeasures for Soil Liquefaction," Edited by M. Hamada and T.D. O'Rourke, 8/12/92, (PB93-163939, A99, MF-E11).
- NCEER-92-0020 "Active Bracing System: A Full Scale Implementation of Active Control," by A.M. Reinhorn, T.T. Soong, R.C. Lin, M.A. Riley, Y.P. Wang, S. Aizawa and M. Higashino, 8/14/92, (PB93-127512, A06, MF-A02).
- NCEER-92-0021 "Empirical Analysis of Horizontal Ground Displacement Generated by Liquefaction-Induced Lateral Spreads," by S.F. Bartlett and T.L. Youd, 8/17/92, (PB93-188241, A06, MF-A02).
- NCEER-92-0022 "IDARC Version 3.0: Inelastic Damage Analysis of Reinforced Concrete Structures," by S.K. Kunnath, A.M. Reinhorn and R.F. Lobo, 8/31/92, (PB93-227502, A07, MF-A02).
- NCEER-92-0023 "A Semi-Empirical Analysis of Strong-Motion Peaks in Terms of Seismic Source, Propagation Path and Local Site Conditions, by M. Kamiyama, M.J. O'Rourke and R. Flores-Berrones, 9/9/92, (PB93-150266, A08, MF-A02).
- NCEER-92-0024 "Seismic Behavior of Reinforced Concrete Frame Structures with Nonductile Details, Part I: Summary of Experimental Findings of Full Scale Beam-Column Joint Tests," by A. Beres, R.N. White and P. Gergely, 9/30/92, (PB93-227783, A05, MF-A01).
- NCEER-92-0025 "Experimental Results of Repaired and Retrofitted Beam-Column Joint Tests in Lightly Reinforced Concrete Frame Buildings," by A. Beres, S. El-Borgi, R.N. White and P. Gergely, 10/29/92, (PB93-227791, A05, MF-A01).
- NCEER-92-0026 "A Generalization of Optimal Control Theory: Linear and Nonlinear Structures," by J.N. Yang, Z. Li and S. Vongchavalitkul, 11/2/92, (PB93-188621, A05, MF-A01).
- NCEER-92-0027 "Seismic Resistance of Reinforced Concrete Frame Structures Designed Only for Gravity Loads: Part I - Design and Properties of a One-Third Scale Model Structure," by J.M. Bracci, A.M. Reinhorn and J.B. Mander, 12/1/92, (PB94-104502, A08, MF-A02).
- NCEER-92-0028 "Seismic Resistance of Reinforced Concrete Frame Structures Designed Only for Gravity Loads: Part II - Experimental Performance of Subassemblages," by L.E. Aycaardi, J.B. Mander and A.M. Reinhorn, 12/1/92, (PB94-104510, A08, MF-A02).
- NCEER-92-0029 "Seismic Resistance of Reinforced Concrete Frame Structures Designed Only for Gravity Loads: Part III - Experimental Performance and Analytical Study of a Structural Model," by J.M. Bracci, A.M. Reinhorn and J.B. Mander, 12/1/92, (PB93-227528, A09, MF-A01).

- NCEER-92-0030 "Evaluation of Seismic Retrofit of Reinforced Concrete Frame Structures: Part I - Experimental Performance of Retrofitted Subassemblages," by D. Choudhuri, J.B. Mander and A.M. Reinhorn, 12/8/92, (PB93-198307, A07, MF-A02).
- NCEER-92-0031 "Evaluation of Seismic Retrofit of Reinforced Concrete Frame Structures: Part II - Experimental Performance and Analytical Study of a Retrofitted Structural Model," by J.M. Bracci, A.M. Reinhorn and J.B. Mander, 12/8/92, (PB93-198315, A09, MF-A03).
- NCEER-92-0032 "Experimental and Analytical Investigation of Seismic Response of Structures with Supplemental Fluid Viscous Dampers," by M.C. Constantinou and M.D. Symans, 12/21/92, (PB93-191435, A10, MF-A03). This report is available only through NTIS (see address given above).
- NCEER-92-0033 "Reconnaissance Report on the Cairo, Egypt Earthquake of October 12, 1992," by M. Khater, 12/23/92, (PB93-188621, A03, MF-A01).
- NCEER-92-0034 "Low-Level Dynamic Characteristics of Four Tall Flat-Plate Buildings in New York City," by H. Gavin, S. Yuan, J. Grossman, E. Pekelis and K. Jacob, 12/28/92, (PB93-188217, A07, MF-A02).
- NCEER-93-0001 "An Experimental Study on the Seismic Performance of Brick-Infilled Steel Frames With and Without Retrofit," by J.B. Mander, B. Nair, K. Wojtkowski and J. Ma, 1/29/93, (PB93-227510, A07, MF-A02).
- NCEER-93-0002 "Social Accounting for Disaster Preparedness and Recovery Planning," by S. Cole, E. Pantoja and V. Razak, 2/22/93, (PB94-142114, A12, MF-A03).
- NCEER-93-0003 "Assessment of 1991 NEHRP Provisions for Nonstructural Components and Recommended Revisions," by T.T. Soong, G. Chen, Z. Wu, R-H. Zhang and M. Grigoriu, 3/1/93, (PB93-188639, A06, MF-A02).
- NCEER-93-0004 "Evaluation of Static and Response Spectrum Analysis Procedures of SEAOC/UBC for Seismic Isolated Structures," by C.W. Winters and M.C. Constantinou, 3/23/93, (PB93-198299, A10, MF-A03).
- NCEER-93-0005 "Earthquakes in the Northeast - Are We Ignoring the Hazard? A Workshop on Earthquake Science and Safety for Educators," edited by K.E.K. Ross, 4/2/93, (PB94-103066, A09, MF-A02).
- NCEER-93-0006 "Inelastic Response of Reinforced Concrete Structures with Viscoelastic Braces," by R.F. Lobo, J.M. Bracci, K.L. Shen, A.M. Reinhorn and T.T. Soong, 4/5/93, (PB93-227486, A05, MF-A02).
- NCEER-93-0007 "Seismic Testing of Installation Methods for Computers and Data Processing Equipment," by K. Kosar, T.T. Soong, K.L. Shen, J.A. HoLung and Y.K. Lin, 4/12/93, (PB93-198299, A07, MF-A02).
- NCEER-93-0008 "Retrofit of Reinforced Concrete Frames Using Added Dampers," by A. Reinhorn, M. Constantinou and C. Li, to be published.
- NCEER-93-0009 "Seismic Behavior and Design Guidelines for Steel Frame Structures with Added Viscoelastic Dampers," by K.C. Chang, M.L. Lai, T.T. Soong, D.S. Hao and Y.C. Yeh, 5/1/93, (PB94-141959, A07, MF-A02).
- NCEER-93-0010 "Seismic Performance of Shear-Critical Reinforced Concrete Bridge Piers," by J.B. Mander, S.M. Waheed, M.T.A. Chaudhary and S.S. Chen, 5/12/93, (PB93-227494, A08, MF-A02).
- NCEER-93-0011 "3D-BASIS-TABS: Computer Program for Nonlinear Dynamic Analysis of Three Dimensional Base Isolated Structures," by S. Nagarajaiah, C. Li, A.M. Reinhorn and M.C. Constantinou, 8/2/93, (PB94-141819, A09, MF-A02).
- NCEER-93-0012 "Effects of Hydrocarbon Spills from an Oil Pipeline Break on Ground Water," by O.J. Helweg and H.H.M. Hwang, 8/3/93, (PB94-141942, A06, MF-A02).
- NCEER-93-0013 "Simplified Procedures for Seismic Design of Nonstructural Components and Assessment of Current Code Provisions," by M.P. Singh, L.E. Suarez, E.E. Matheu and G.O. Maldonado, 8/4/93, (PB94-141827, A09, MF-A02).
- NCEER-93-0014 "An Energy Approach to Seismic Analysis and Design of Secondary Systems," by G. Chen and T.T. Soong, 8/6/93, (PB94-142767, A11, MF-A03).

- NCEER-93-0015 "Proceedings from School Sites: Becoming Prepared for Earthquakes - Commemorating the Third Anniversary of the Loma Prieta Earthquake," Edited by F.E. Winslow and K.E.K. Ross, 8/16/93, (PB94-154275, A16, MF-A02).
- NCEER-93-0016 "Reconnaissance Report of Damage to Historic Monuments in Cairo, Egypt Following the October 12, 1992 Dahshur Earthquake," by D. Sykora, D. Look, G. Croci, E. Karaesmen and E. Karaesmen, 8/19/93, (PB94-142221, A08, MF-A02).
- NCEER-93-0017 "The Island of Guam Earthquake of August 8, 1993," by S.W. Swan and S.K. Harris, 9/30/93, (PB94-141843, A04, MF-A01).
- NCEER-93-0018 "Engineering Aspects of the October 12, 1992 Egyptian Earthquake," by A.W. Elgamal, M. Amer, K. Adalier and A. Abul-Fadl, 10/7/93, (PB94-141983, A05, MF-A01).
- NCEER-93-0019 "Development of an Earthquake Motion Simulator and its Application in Dynamic Centrifuge Testing," by I. Krstelj, Supervised by J.H. Prevost, 10/23/93, (PB94-181773, A-10, MF-A03).
- NCEER-93-0020 "NCEER-Taisei Corporation Research Program on Sliding Seismic Isolation Systems for Bridges: Experimental and Analytical Study of a Friction Pendulum System (FPS)," by M.C. Constantinou, P. Tsopelas, Y-S. Kim and S. Okamoto, 11/1/93, (PB94-142775, A08, MF-A02).
- NCEER-93-0021 "Finite Element Modeling of Elastomeric Seismic Isolation Bearings," by L.J. Billings, Supervised by R. Shepherd, 11/8/93, to be published.
- NCEER-93-0022 "Seismic Vulnerability of Equipment in Critical Facilities: Life-Safety and Operational Consequences," by K. Porter, G.S. Johnson, M.M. Zadeh, C. Scawthorn and S. Eder, 11/24/93, (PB94-181765, A16, MF-A03).
- NCEER-93-0023 "Hokkaido Nansei-oki, Japan Earthquake of July 12, 1993, by P.I. Yanev and C.R. Scawthorn, 12/23/93, (PB94-181500, A07, MF-A01).
- NCEER-94-0001 "An Evaluation of Seismic Serviceability of Water Supply Networks with Application to the San Francisco Auxiliary Water Supply System," by I. Markov, Supervised by M. Grigoriu and T. O'Rourke, 1/21/94, (PB94-204013, A07, MF-A02).
- NCEER-94-0002 "NCEER-Taisei Corporation Research Program on Sliding Seismic Isolation Systems for Bridges: Experimental and Analytical Study of Systems Consisting of Sliding Bearings, Rubber Restoring Force Devices and Fluid Dampers," Volumes I and II, by P. Tsopelas, S. Okamoto, M.C. Constantinou, D. Ozaki and S. Fujii, 2/4/94, (PB94-181740, A09, MF-A02 and PB94-181757, A12, MF-A03).
- NCEER-94-0003 "A Markov Model for Local and Global Damage Indices in Seismic Analysis," by S. Rahman and M. Grigoriu, 2/18/94, (PB94-206000, A12, MF-A03).
- NCEER-94-0004 "Proceedings from the NCEER Workshop on Seismic Response of Masonry Infills," edited by D.P. Abrams, 3/1/94, (PB94-180783, A07, MF-A02).
- NCEER-94-0005 "The Northridge, California Earthquake of January 17, 1994: General Reconnaissance Report," edited by J.D. Goltz, 3/11/94, (PB94-193943, A10, MF-A03).
- NCEER-94-0006 "Seismic Energy Based Fatigue Damage Analysis of Bridge Columns: Part I - Evaluation of Seismic Capacity," by G.A. Chang and J.B. Mander, 3/14/94, (PB94-219185, A11, MF-A03).
- NCEER-94-0007 "Seismic Isolation of Multi-Story Frame Structures Using Spherical Sliding Isolation Systems," by T.M. Al-Hussaini, V.A. Zayas and M.C. Constantinou, 3/17/94, (PB94-193745, A09, MF-A02).
- NCEER-94-0008 "The Northridge, California Earthquake of January 17, 1994: Performance of Highway Bridges," edited by I.G. Buckle, 3/24/94, (PB94-193851, A06, MF-A02).
- NCEER-94-0009 "Proceedings of the Third U.S.-Japan Workshop on Earthquake Protective Systems for Bridges," edited by I.G. Buckle and I. Friedland, 3/31/94, (PB94-195815, A99, MF-A06).

- NCEER-94-0010 "3D-BASIS-ME: Computer Program for Nonlinear Dynamic Analysis of Seismically Isolated Single and Multiple Structures and Liquid Storage Tanks," by P.C. Tsopelas, M.C. Constantinou and A.M. Reinhorn, 4/12/94, (PB94-204922, A09, MF-A02).
- NCEER-94-0011 "The Northridge, California Earthquake of January 17, 1994: Performance of Gas Transmission Pipelines," by T.D. O'Rourke and M.C. Palmer, 5/16/94, (PB94-204989, A05, MF-A01).
- NCEER-94-0012 "Feasibility Study of Replacement Procedures and Earthquake Performance Related to Gas Transmission Pipelines," by T.D. O'Rourke and M.C. Palmer, 5/25/94, (PB94-206638, A09, MF-A02).
- NCEER-94-0013 "Seismic Energy Based Fatigue Damage Analysis of Bridge Columns: Part II - Evaluation of Seismic Demand," by G.A. Chang and J.B. Mander, 6/1/94, (PB95-18106, A08, MF-A02).
- NCEER-94-0014 "NCEER-Taisei Corporation Research Program on Sliding Seismic Isolation Systems for Bridges: Experimental and Analytical Study of a System Consisting of Sliding Bearings and Fluid Restoring Force/Damping Devices," by P. Tsopelas and M.C. Constantinou, 6/13/94, (PB94-219144, A10, MF-A03).
- NCEER-94-0015 "Generation of Hazard-Consistent Fragility Curves for Seismic Loss Estimation Studies," by H. Hwang and J-R. Huo, 6/14/94, (PB95-181996, A09, MF-A02).
- NCEER-94-0016 "Seismic Study of Building Frames with Added Energy-Absorbing Devices," by W.S. Pong, C.S. Tsai and G.C. Lee, 6/20/94, (PB94-219136, A10, A03).
- NCEER-94-0017 "Sliding Mode Control for Seismic-Excited Linear and Nonlinear Civil Engineering Structures," by J. Yang, J. Wu, A. Agrawal and Z. Li, 6/21/94, (PB95-138483, A06, MF-A02).
- NCEER-94-0018 "3D-BASIS-TABS Version 2.0: Computer Program for Nonlinear Dynamic Analysis of Three Dimensional Base Isolated Structures," by A.M. Reinhorn, S. Nagarajaiah, M.C. Constantinou, P. Tsopelas and R. Li, 6/22/94, (PB95-182176, A08, MF-A02).
- NCEER-94-0019 "Proceedings of the International Workshop on Civil Infrastructure Systems: Application of Intelligent Systems and Advanced Materials on Bridge Systems," Edited by G.C. Lee and K.C. Chang, 7/18/94, (PB95-252474, A20, MF-A04).
- NCEER-94-0020 "Study of Seismic Isolation Systems for Computer Floors," by V. Lambrou and M.C. Constantinou, 7/19/94, (PB95-138533, A10, MF-A03).
- NCEER-94-0021 "Proceedings of the U.S.-Italian Workshop on Guidelines for Seismic Evaluation and Rehabilitation of Unreinforced Masonry Buildings," Edited by D.P. Abrams and G.M. Calvi, 7/20/94, (PB95-138749, A13, MF-A03).
- NCEER-94-0022 "NCEER-Taisei Corporation Research Program on Sliding Seismic Isolation Systems for Bridges: Experimental and Analytical Study of a System Consisting of Lubricated PTFE Sliding Bearings and Mild Steel Dampers," by P. Tsopelas and M.C. Constantinou, 7/22/94, (PB95-182184, A08, MF-A02).
- NCEER-94-0023 "Development of Reliability-Based Design Criteria for Buildings Under Seismic Load," by Y.K. Wen, H. Hwang and M. Shinozuka, 8/1/94, (PB95-211934, A08, MF-A02).
- NCEER-94-0024 "Experimental Verification of Acceleration Feedback Control Strategies for an Active Tendon System," by S.J. Dyke, B.F. Spencer, Jr., P. Quast, M.K. Sain, D.C. Kaspari, Jr. and T.T. Soong, 8/29/94, (PB95-212320, A05, MF-A01).
- NCEER-94-0025 "Seismic Retrofitting Manual for Highway Bridges," Edited by I.G. Buckle and I.F. Friedland, published by the Federal Highway Administration (PB95-212676, A15, MF-A03).
- NCEER-94-0026 "Proceedings from the Fifth U.S.-Japan Workshop on Earthquake Resistant Design of Lifeline Facilities and Countermeasures Against Soil Liquefaction," Edited by T.D. O'Rourke and M. Hamada, 11/7/94, (PB95-220802, A99, MF-E08).

- NCEER-95-0001 “Experimental and Analytical Investigation of Seismic Retrofit of Structures with Supplemental Damping: Part 1 - Fluid Viscous Damping Devices,” by A.M. Reinhorn, C. Li and M.C. Constantinou, 1/3/95, (PB95-266599, A09, MF-A02).
- NCEER-95-0002 “Experimental and Analytical Study of Low-Cycle Fatigue Behavior of Semi-Rigid Top-And-Seat Angle Connections,” by G. Pekcan, J.B. Mander and S.S. Chen, 1/5/95, (PB95-220042, A07, MF-A02).
- NCEER-95-0003 “NCEER-ATC Joint Study on Fragility of Buildings,” by T. Anagnos, C. Rojahn and A.S. Kiremidjian, 1/20/95, (PB95-220026, A06, MF-A02).
- NCEER-95-0004 “Nonlinear Control Algorithms for Peak Response Reduction,” by Z. Wu, T.T. Soong, V. Gattulli and R.C. Lin, 2/16/95, (PB95-220349, A05, MF-A01).
- NCEER-95-0005 “Pipeline Replacement Feasibility Study: A Methodology for Minimizing Seismic and Corrosion Risks to Underground Natural Gas Pipelines,” by R.T. Eguchi, H.A. Seligson and D.G. Honegger, 3/2/95, (PB95-252326, A06, MF-A02).
- NCEER-95-0006 “Evaluation of Seismic Performance of an 11-Story Frame Building During the 1994 Northridge Earthquake,” by F. Naeim, R. DiSulio, K. Benuska, A. Reinhorn and C. Li, to be published.
- NCEER-95-0007 “Prioritization of Bridges for Seismic Retrofitting,” by N. Basöz and A.S. Kiremidjian, 4/24/95, (PB95-252300, A08, MF-A02).
- NCEER-95-0008 “Method for Developing Motion Damage Relationships for Reinforced Concrete Frames,” by A. Singhal and A.S. Kiremidjian, 5/11/95, (PB95-266607, A06, MF-A02).
- NCEER-95-0009 “Experimental and Analytical Investigation of Seismic Retrofit of Structures with Supplemental Damping: Part II - Friction Devices,” by C. Li and A.M. Reinhorn, 7/6/95, (PB96-128087, A11, MF-A03).
- NCEER-95-0010 “Experimental Performance and Analytical Study of a Non-Ductile Reinforced Concrete Frame Structure Retrofitted with Elastomeric Spring Dampers,” by G. Pekcan, J.B. Mander and S.S. Chen, 7/14/95, (PB96-137161, A08, MF-A02).
- NCEER-95-0011 “Development and Experimental Study of Semi-Active Fluid Damping Devices for Seismic Protection of Structures,” by M.D. Symans and M.C. Constantinou, 8/3/95, (PB96-136940, A23, MF-A04).
- NCEER-95-0012 “Real-Time Structural Parameter Modification (RSPM): Development of Innervated Structures,” by Z. Liang, M. Tong and G.C. Lee, 4/11/95, (PB96-137153, A06, MF-A01).
- NCEER-95-0013 “Experimental and Analytical Investigation of Seismic Retrofit of Structures with Supplemental Damping: Part III - Viscous Damping Walls,” by A.M. Reinhorn and C. Li, 10/1/95, (PB96-176409, A11, MF-A03).
- NCEER-95-0014 “Seismic Fragility Analysis of Equipment and Structures in a Memphis Electric Substation,” by J-R. Huo and H.H.M. Hwang, 8/10/95, (PB96-128087, A09, MF-A02).
- NCEER-95-0015 “The Hanshin-Awaji Earthquake of January 17, 1995: Performance of Lifelines,” Edited by M. Shinozuka, 11/3/95, (PB96-176383, A15, MF-A03).
- NCEER-95-0016 “Highway Culvert Performance During Earthquakes,” by T.L. Youd and C.J. Beckman, available as NCEER-96-0015.
- NCEER-95-0017 “The Hanshin-Awaji Earthquake of January 17, 1995: Performance of Highway Bridges,” Edited by I.G. Buckle, 12/1/95, to be published.
- NCEER-95-0018 “Modeling of Masonry Infill Panels for Structural Analysis,” by A.M. Reinhorn, A. Madan, R.E. Valles, Y. Reichmann and J.B. Mander, 12/8/95, (PB97-110886, MF-A01, A06).
- NCEER-95-0019 “Optimal Polynomial Control for Linear and Nonlinear Structures,” by A.K. Agrawal and J.N. Yang, 12/11/95, (PB96-168737, A07, MF-A02).

- NCEER-95-0020 "Retrofit of Non-Ductile Reinforced Concrete Frames Using Friction Dampers," by R.S. Rao, P. Gergely and R.N. White, 12/22/95, (PB97-133508, A10, MF-A02).
- NCEER-95-0021 "Parametric Results for Seismic Response of Pile-Supported Bridge Bents," by G. Mylonakis, A. Nikolaou and G. Gazetas, 12/22/95, (PB97-100242, A12, MF-A03).
- NCEER-95-0022 "Kinematic Bending Moments in Seismically Stressed Piles," by A. Nikolaou, G. Mylonakis and G. Gazetas, 12/23/95, (PB97-113914, MF-A03, A13).
- NCEER-96-0001 "Dynamic Response of Unreinforced Masonry Buildings with Flexible Diaphragms," by A.C. Costley and D.P. Abrams, 10/10/96, (PB97-133573, MF-A03, A15).
- NCEER-96-0002 "State of the Art Review: Foundations and Retaining Structures," by I. Po Lam, to be published.
- NCEER-96-0003 "Ductility of Rectangular Reinforced Concrete Bridge Columns with Moderate Confinement," by N. Wehbe, M. Saiidi, D. Sanders and B. Douglas, 11/7/96, (PB97-133557, A06, MF-A02).
- NCEER-96-0004 "Proceedings of the Long-Span Bridge Seismic Research Workshop," edited by I.G. Buckle and I.M. Friedland, to be published.
- NCEER-96-0005 "Establish Representative Pier Types for Comprehensive Study: Eastern United States," by J. Kulicki and Z. Prucz, 5/28/96, (PB98-119217, A07, MF-A02).
- NCEER-96-0006 "Establish Representative Pier Types for Comprehensive Study: Western United States," by R. Imbsen, R.A. Schamber and T.A. Osterkamp, 5/28/96, (PB98-118607, A07, MF-A02).
- NCEER-96-0007 "Nonlinear Control Techniques for Dynamical Systems with Uncertain Parameters," by R.G. Ghanem and M.I. Bujakov, 5/27/96, (PB97-100259, A17, MF-A03).
- NCEER-96-0008 "Seismic Evaluation of a 30-Year Old Non-Ductile Highway Bridge Pier and Its Retrofit," by J.B. Mander, B. Mahmoodzadegan, S. Bhadra and S.S. Chen, 5/31/96, (PB97-110902, MF-A03, A10).
- NCEER-96-0009 "Seismic Performance of a Model Reinforced Concrete Bridge Pier Before and After Retrofit," by J.B. Mander, J.H. Kim and C.A. Ligozio, 5/31/96, (PB97-110910, MF-A02, A10).
- NCEER-96-0010 "IDARC2D Version 4.0: A Computer Program for the Inelastic Damage Analysis of Buildings," by R.E. Valles, A.M. Reinhorn, S.K. Kunnath, C. Li and A. Madan, 6/3/96, (PB97-100234, A17, MF-A03).
- NCEER-96-0011 "Estimation of the Economic Impact of Multiple Lifeline Disruption: Memphis Light, Gas and Water Division Case Study," by S.E. Chang, H.A. Seligson and R.T. Eguchi, 8/16/96, (PB97-133490, A11, MF-A03).
- NCEER-96-0012 "Proceedings from the Sixth Japan-U.S. Workshop on Earthquake Resistant Design of Lifeline Facilities and Countermeasures Against Soil Liquefaction, Edited by M. Hamada and T. O'Rourke, 9/11/96, (PB97-133581, A99, MF-A06).
- NCEER-96-0013 "Chemical Hazards, Mitigation and Preparedness in Areas of High Seismic Risk: A Methodology for Estimating the Risk of Post-Earthquake Hazardous Materials Release," by H.A. Seligson, R.T. Eguchi, K.J. Tierney and K. Richmond, 11/7/96, (PB97-133565, MF-A02, A08).
- NCEER-96-0014 "Response of Steel Bridge Bearings to Reversed Cyclic Loading," by J.B. Mander, D-K. Kim, S.S. Chen and G.J. Premus, 11/13/96, (PB97-140735, A12, MF-A03).
- NCEER-96-0015 "Highway Culvert Performance During Past Earthquakes," by T.L. Youd and C.J. Beckman, 11/25/96, (PB97-133532, A06, MF-A01).
- NCEER-97-0001 "Evaluation, Prevention and Mitigation of Pounding Effects in Building Structures," by R.E. Valles and A.M. Reinhorn, 2/20/97, (PB97-159552, A14, MF-A03).
- NCEER-97-0002 "Seismic Design Criteria for Bridges and Other Highway Structures," by C. Rojahn, R. Mayes, D.G. Anderson, J. Clark, J.H. Hom, R.V. Nutt and M.J. O'Rourke, 4/30/97, (PB97-194658, A06, MF-A03).

- NCEER-97-0003 "Proceedings of the U.S.-Italian Workshop on Seismic Evaluation and Retrofit," Edited by D.P. Abrams and G.M. Calvi, 3/19/97, (PB97-194666, A13, MF-A03).
- NCEER-97-0004 "Investigation of Seismic Response of Buildings with Linear and Nonlinear Fluid Viscous Dampers," by A.A. Seleemah and M.C. Constantinou, 5/21/97, (PB98-109002, A15, MF-A03).
- NCEER-97-0005 "Proceedings of the Workshop on Earthquake Engineering Frontiers in Transportation Facilities," edited by G.C. Lee and I.M. Friedland, 8/29/97, (PB98-128911, A25, MR-A04).
- NCEER-97-0006 "Cumulative Seismic Damage of Reinforced Concrete Bridge Piers," by S.K. Kunnath, A. El-Bahy, A. Taylor and W. Stone, 9/2/97, (PB98-108814, A11, MF-A03).
- NCEER-97-0007 "Structural Details to Accommodate Seismic Movements of Highway Bridges and Retaining Walls," by R.A. Imbsen, R.A. Schamber, E. Thorkildsen, A. Kartoum, B.T. Martin, T.N. Rosser and J.M. Kulicki, 9/3/97, (PB98-108996, A09, MF-A02).
- NCEER-97-0008 "A Method for Earthquake Motion-Damage Relationships with Application to Reinforced Concrete Frames," by A. Singhal and A.S. Kiremidjian, 9/10/97, (PB98-108988, A13, MF-A03).
- NCEER-97-0009 "Seismic Analysis and Design of Bridge Abutments Considering Sliding and Rotation," by K. Fishman and R. Richards, Jr., 9/15/97, (PB98-108897, A06, MF-A02).
- NCEER-97-0010 "Proceedings of the FHWA/NCEER Workshop on the National Representation of Seismic Ground Motion for New and Existing Highway Facilities," edited by I.M. Friedland, M.S. Power and R.L. Mayes, 9/22/97, (PB98-128903, A21, MF-A04).
- NCEER-97-0011 "Seismic Analysis for Design or Retrofit of Gravity Bridge Abutments," by K.L. Fishman, R. Richards, Jr. and R.C. Divito, 10/2/97, (PB98-128937, A08, MF-A02).
- NCEER-97-0012 "Evaluation of Simplified Methods of Analysis for Yielding Structures," by P. Tsopelas, M.C. Constantinou, C.A. Kircher and A.S. Whittaker, 10/31/97, (PB98-128929, A10, MF-A03).
- NCEER-97-0013 "Seismic Design of Bridge Columns Based on Control and Repairability of Damage," by C-T. Cheng and J.B. Mander, 12/8/97, (PB98-144249, A11, MF-A03).
- NCEER-97-0014 "Seismic Resistance of Bridge Piers Based on Damage Avoidance Design," by J.B. Mander and C-T. Cheng, 12/10/97, (PB98-144223, A09, MF-A02).
- NCEER-97-0015 "Seismic Response of Nominally Symmetric Systems with Strength Uncertainty," by S. Balopoulou and M. Grigoriu, 12/23/97, (PB98-153422, A11, MF-A03).
- NCEER-97-0016 "Evaluation of Seismic Retrofit Methods for Reinforced Concrete Bridge Columns," by T.J. Wipf, F.W. Klaiber and F.M. Russo, 12/28/97, (PB98-144215, A12, MF-A03).
- NCEER-97-0017 "Seismic Fragility of Existing Conventional Reinforced Concrete Highway Bridges," by C.L. Mullen and A.S. Cakmak, 12/30/97, (PB98-153406, A08, MF-A02).
- NCEER-97-0018 "Loss Assessment of Memphis Buildings," edited by D.P. Abrams and M. Shinozuka, 12/31/97, (PB98-144231, A13, MF-A03).
- NCEER-97-0019 "Seismic Evaluation of Frames with Infill Walls Using Quasi-static Experiments," by K.M. Mosalam, R.N. White and P. Gergely, 12/31/97, (PB98-153455, A07, MF-A02).
- NCEER-97-0020 "Seismic Evaluation of Frames with Infill Walls Using Pseudo-dynamic Experiments," by K.M. Mosalam, R.N. White and P. Gergely, 12/31/97, (PB98-153430, A07, MF-A02).
- NCEER-97-0021 "Computational Strategies for Frames with Infill Walls: Discrete and Smeared Crack Analyses and Seismic Fragility," by K.M. Mosalam, R.N. White and P. Gergely, 12/31/97, (PB98-153414, A10, MF-A02).

- NCEER-97-0022 "Proceedings of the NCEER Workshop on Evaluation of Liquefaction Resistance of Soils," edited by T.L. Youd and I.M. Idriss, 12/31/97, (PB98-155617, A15, MF-A03).
- MCEER-98-0001 "Extraction of Nonlinear Hysteretic Properties of Seismically Isolated Bridges from Quick-Release Field Tests," by Q. Chen, B.M. Douglas, E.M. Maragakis and I.G. Buckle, 5/26/98, (PB99-118838, A06, MF-A01).
- MCEER-98-0002 "Methodologies for Evaluating the Importance of Highway Bridges," by A. Thomas, S. Eshenaur and J. Kulicki, 5/29/98, (PB99-118846, A10, MF-A02).
- MCEER-98-0003 "Capacity Design of Bridge Piers and the Analysis of Overstrength," by J.B. Mander, A. Dutta and P. Goel, 6/1/98, (PB99-118853, A09, MF-A02).
- MCEER-98-0004 "Evaluation of Bridge Damage Data from the Loma Prieta and Northridge, California Earthquakes," by N. Basoz and A. Kiremidjian, 6/2/98, (PB99-118861, A15, MF-A03).
- MCEER-98-0005 "Screening Guide for Rapid Assessment of Liquefaction Hazard at Highway Bridge Sites," by T. L. Youd, 6/16/98, (PB99-118879, A06, not available on microfiche).
- MCEER-98-0006 "Structural Steel and Steel/Concrete Interface Details for Bridges," by P. Ritchie, N. Kauh and J. Kulicki, 7/13/98, (PB99-118945, A06, MF-A01).
- MCEER-98-0007 "Capacity Design and Fatigue Analysis of Confined Concrete Columns," by A. Dutta and J.B. Mander, 7/14/98, (PB99-118960, A14, MF-A03).
- MCEER-98-0008 "Proceedings of the Workshop on Performance Criteria for Telecommunication Services Under Earthquake Conditions," edited by A.J. Schiff, 7/15/98, (PB99-118952, A08, MF-A02).
- MCEER-98-0009 "Fatigue Analysis of Unconfined Concrete Columns," by J.B. Mander, A. Dutta and J.H. Kim, 9/12/98, (PB99-123655, A10, MF-A02).
- MCEER-98-0010 "Centrifuge Modeling of Cyclic Lateral Response of Pile-Cap Systems and Seat-Type Abutments in Dry Sands," by A.D. Gadre and R. Dobry, 10/2/98, (PB99-123606, A13, MF-A03).
- MCEER-98-0011 "IDARC-BRIDGE: A Computational Platform for Seismic Damage Assessment of Bridge Structures," by A.M. Reinhorn, V. Simeonov, G. Mylonakis and Y. Reichman, 10/2/98, (PB99-162919, A15, MF-A03).
- MCEER-98-0012 "Experimental Investigation of the Dynamic Response of Two Bridges Before and After Retrofitting with Elastomeric Bearings," by D.A. Wendichansky, S.S. Chen and J.B. Mander, 10/2/98, (PB99-162927, A15, MF-A03).
- MCEER-98-0013 "Design Procedures for Hinge Restrainers and Hinge Sear Width for Multiple-Frame Bridges," by R. Des Roches and G.L. Fenves, 11/3/98, (PB99-140477, A13, MF-A03).
- MCEER-98-0014 "Response Modification Factors for Seismically Isolated Bridges," by M.C. Constantinou and J.K. Quarshie, 11/3/98, (PB99-140485, A14, MF-A03).
- MCEER-98-0015 "Proceedings of the U.S.-Italy Workshop on Seismic Protective Systems for Bridges," edited by I.M. Friedland and M.C. Constantinou, 11/3/98, (PB2000-101711, A22, MF-A04).
- MCEER-98-0016 "Appropriate Seismic Reliability for Critical Equipment Systems: Recommendations Based on Regional Analysis of Financial and Life Loss," by K. Porter, C. Scawthorn, C. Taylor and N. Blais, 11/10/98, (PB99-157265, A08, MF-A02).
- MCEER-98-0017 "Proceedings of the U.S. Japan Joint Seminar on Civil Infrastructure Systems Research," edited by M. Shinozuka and A. Rose, 11/12/98, (PB99-156713, A16, MF-A03).
- MCEER-98-0018 "Modeling of Pile Footings and Drilled Shafts for Seismic Design," by I. PoLam, M. Kapuskar and D. Chaudhuri, 12/21/98, (PB99-157257, A09, MF-A02).

- MCEER-99-0001 "Seismic Evaluation of a Masonry Infilled Reinforced Concrete Frame by Pseudodynamic Testing," by S.G. Buonopane and R.N. White, 2/16/99, (PB99-162851, A09, MF-A02).
- MCEER-99-0002 "Response History Analysis of Structures with Seismic Isolation and Energy Dissipation Systems: Verification Examples for Program SAP2000," by J. Scheller and M.C. Constantinou, 2/22/99, (PB99-162869, A08, MF-A02).
- MCEER-99-0003 "Experimental Study on the Seismic Design and Retrofit of Bridge Columns Including Axial Load Effects," by A. Dutta, T. Kokorina and J.B. Mander, 2/22/99, (PB99-162877, A09, MF-A02).
- MCEER-99-0004 "Experimental Study of Bridge Elastomeric and Other Isolation and Energy Dissipation Systems with Emphasis on Uplift Prevention and High Velocity Near-source Seismic Excitation," by A. Kasalanati and M. C. Constantinou, 2/26/99, (PB99-162885, A12, MF-A03).
- MCEER-99-0005 "Truss Modeling of Reinforced Concrete Shear-flexure Behavior," by J.H. Kim and J.B. Mander, 3/8/99, (PB99-163693, A12, MF-A03).
- MCEER-99-0006 "Experimental Investigation and Computational Modeling of Seismic Response of a 1:4 Scale Model Steel Structure with a Load Balancing Supplemental Damping System," by G. Pekcan, J.B. Mander and S.S. Chen, 4/2/99, (PB99-162893, A11, MF-A03).
- MCEER-99-0007 "Effect of Vertical Ground Motions on the Structural Response of Highway Bridges," by M.R. Button, C.J. Cronin and R.L. Mayes, 4/10/99, (PB2000-101411, A10, MF-A03).
- MCEER-99-0008 "Seismic Reliability Assessment of Critical Facilities: A Handbook, Supporting Documentation, and Model Code Provisions," by G.S. Johnson, R.E. Sheppard, M.D. Quilici, S.J. Eder and C.R. Scawthorn, 4/12/99, (PB2000-101701, A18, MF-A04).
- MCEER-99-0009 "Impact Assessment of Selected MCEER Highway Project Research on the Seismic Design of Highway Structures," by C. Rojahn, R. Mayes, D.G. Anderson, J.H. Clark, D'Appolonia Engineering, S. Gloyd and R.V. Nutt, 4/14/99, (PB99-162901, A10, MF-A02).
- MCEER-99-0010 "Site Factors and Site Categories in Seismic Codes," by R. Dobry, R. Ramos and M.S. Power, 7/19/99, (PB2000-101705, A08, MF-A02).
- MCEER-99-0011 "Restraint Design Procedures for Multi-Span Simply-Supported Bridges," by M.J. Randall, M. Saiidi, E. Maragakis and T. Isakovic, 7/20/99, (PB2000-101702, A10, MF-A02).
- MCEER-99-0012 "Property Modification Factors for Seismic Isolation Bearings," by M.C. Constantinou, P. Tsopelas, A. Kasalanati and E. Wolff, 7/20/99, (PB2000-103387, A11, MF-A03).
- MCEER-99-0013 "Critical Seismic Issues for Existing Steel Bridges," by P. Ritchie, N. Kauh and J. Kulicki, 7/20/99, (PB2000-101697, A09, MF-A02).
- MCEER-99-0014 "Nonstructural Damage Database," by A. Kao, T.T. Soong and A. Vender, 7/24/99, (PB2000-101407, A06, MF-A01).
- MCEER-99-0015 "Guide to Remedial Measures for Liquefaction Mitigation at Existing Highway Bridge Sites," by H.G. Cooke and J. K. Mitchell, 7/26/99, (PB2000-101703, A11, MF-A03).
- MCEER-99-0016 "Proceedings of the MCEER Workshop on Ground Motion Methodologies for the Eastern United States," edited by N. Abrahamson and A. Becker, 8/11/99, (PB2000-103385, A07, MF-A02).
- MCEER-99-0017 "Quindío, Colombia Earthquake of January 25, 1999: Reconnaissance Report," by A.P. Asfura and P.J. Flores, 10/4/99, (PB2000-106893, A06, MF-A01).
- MCEER-99-0018 "Hysteretic Models for Cyclic Behavior of Deteriorating Inelastic Structures," by M.V. Sivaselvan and A.M. Reinhorn, 11/5/99, (PB2000-103386, A08, MF-A02).

- MCEER-99-0019 "Proceedings of the 7th U.S.- Japan Workshop on Earthquake Resistant Design of Lifeline Facilities and Countermeasures Against Soil Liquefaction," edited by T.D. O'Rourke, J.P. Bardet and M. Hamada, 11/19/99, (PB2000-103354, A99, MF-A06).
- MCEER-99-0020 "Development of Measurement Capability for Micro-Vibration Evaluations with Application to Chip Fabrication Facilities," by G.C. Lee, Z. Liang, J.W. Song, J.D. Shen and W.C. Liu, 12/1/99, (PB2000-105993, A08, MF-A02).
- MCEER-99-0021 "Design and Retrofit Methodology for Building Structures with Supplemental Energy Dissipating Systems," by G. Pekcan, J.B. Mander and S.S. Chen, 12/31/99, (PB2000-105994, A11, MF-A03).
- MCEER-00-0001 "The Marmara, Turkey Earthquake of August 17, 1999: Reconnaissance Report," edited by C. Scawthorn; with major contributions by M. Bruneau, R. Eguchi, T. Holzer, G. Johnson, J. Mander, J. Mitchell, W. Mitchell, A. Papageorgiou, C. Scaethorn, and G. Webb, 3/23/00, (PB2000-106200, A11, MF-A03).
- MCEER-00-0002 "Proceedings of the MCEER Workshop for Seismic Hazard Mitigation of Health Care Facilities," edited by G.C. Lee, M. Ettouney, M. Grigoriu, J. Hauer and J. Nigg, 3/29/00, (PB2000-106892, A08, MF-A02).
- MCEER-00-0003 "The Chi-Chi, Taiwan Earthquake of September 21, 1999: Reconnaissance Report," edited by G.C. Lee and C.H. Loh, with major contributions by G.C. Lee, M. Bruneau, I.G. Buckle, S.E. Chang, P.J. Flores, T.D. O'Rourke, M. Shinozuka, T.T. Soong, C-H. Loh, K-C. Chang, Z-J. Chen, J-S. Hwang, M-L. Lin, G-Y. Liu, K-C. Tsai, G.C. Yao and C-L. Yen, 4/30/00, (PB2001-100980, A10, MF-A02).
- MCEER-00-0004 "Seismic Retrofit of End-Sway Frames of Steel Deck-Truss Bridges with a Supplemental Tendon System: Experimental and Analytical Investigation," by G. Pekcan, J.B. Mander and S.S. Chen, 7/1/00, (PB2001-100982, A10, MF-A02).
- MCEER-00-0005 "Sliding Fragility of Unrestrained Equipment in Critical Facilities," by W.H. Chong and T.T. Soong, 7/5/00, (PB2001-100983, A08, MF-A02).
- MCEER-00-0006 "Seismic Response of Reinforced Concrete Bridge Pier Walls in the Weak Direction," by N. Abo-Shadi, M. Saiidi and D. Sanders, 7/17/00, (PB2001-100981, A17, MF-A03).
- MCEER-00-0007 "Low-Cycle Fatigue Behavior of Longitudinal Reinforcement in Reinforced Concrete Bridge Columns," by J. Brown and S.K. Kunnath, 7/23/00, (PB2001-104392, A08, MF-A02).
- MCEER-00-0008 "Soil Structure Interaction of Bridges for Seismic Analysis," I. PoLam and H. Law, 9/25/00, (PB2001-105397, A08, MF-A02).
- MCEER-00-0009 "Proceedings of the First MCEER Workshop on Mitigation of Earthquake Disaster by Advanced Technologies (MEDAT-1), edited by M. Shinozuka, D.J. Inman and T.D. O'Rourke, 11/10/00, (PB2001-105399, A14, MF-A03).
- MCEER-00-0010 "Development and Evaluation of Simplified Procedures for Analysis and Design of Buildings with Passive Energy Dissipation Systems, Revision 01," by O.M. Ramirez, M.C. Constantinou, C.A. Kircher, A.S. Whittaker, M.W. Johnson, J.D. Gomez and C. Chrysostomou, 11/16/01, (PB2001-105523, A23, MF-A04).
- MCEER-00-0011 "Dynamic Soil-Foundation-Structure Interaction Analyses of Large Caissons," by C-Y. Chang, C-M. Mok, Z-L. Wang, R. Settgast, F. Waggoner, M.A. Ketchum, H.M. Gonnermann and C-C. Chin, 12/30/00, (PB2001-104373, A07, MF-A02).
- MCEER-00-0012 "Experimental Evaluation of Seismic Performance of Bridge Restrainers," by A.G. Vlassis, E.M. Maragakis and M. Saiid Saiidi, 12/30/00, (PB2001-104354, A09, MF-A02).
- MCEER-00-0013 "Effect of Spatial Variation of Ground Motion on Highway Structures," by M. Shinozuka, V. Saxena and G. Deodatis, 12/31/00, (PB2001-108755, A13, MF-A03).
- MCEER-00-0014 "A Risk-Based Methodology for Assessing the Seismic Performance of Highway Systems," by S.D. Werner, C.E. Taylor, J.E. Moore, II, J.S. Walton and S. Cho, 12/31/00, (PB2001-108756, A14, MF-A03).

- MCEER-01-0001 "Experimental Investigation of P-Delta Effects to Collapse During Earthquakes," by D. Vian and M. Bruneau, 6/25/01, (PB2002-100534, A17, MF-A03).
- MCEER-01-0002 "Proceedings of the Second MCEER Workshop on Mitigation of Earthquake Disaster by Advanced Technologies (MEDAT-2)," edited by M. Bruneau and D.J. Inman, 7/23/01, (PB2002-100434, A16, MF-A03).
- MCEER-01-0003 "Sensitivity Analysis of Dynamic Systems Subjected to Seismic Loads," by C. Roth and M. Grigoriu, 9/18/01, (PB2003-100884, A12, MF-A03).
- MCEER-01-0004 "Overcoming Obstacles to Implementing Earthquake Hazard Mitigation Policies: Stage 1 Report," by D.J. Alesch and W.J. Petak, 12/17/01, (PB2002-107949, A07, MF-A02).
- MCEER-01-0005 "Updating Real-Time Earthquake Loss Estimates: Methods, Problems and Insights," by C.E. Taylor, S.E. Chang and R.T. Eguchi, 12/17/01, (PB2002-107948, A05, MF-A01).
- MCEER-01-0006 "Experimental Investigation and Retrofit of Steel Pile Foundations and Pile Bents Under Cyclic Lateral Loadings," by A. Shama, J. Mander, B. Blabac and S. Chen, 12/31/01, (PB2002-107950, A13, MF-A03).
- MCEER-02-0001 "Assessment of Performance of Bolu Viaduct in the 1999 Duzce Earthquake in Turkey" by P.C. Roussis, M.C. Constantinou, M. Erdik, E. Durukal and M. Dicleli, 5/8/02, (PB2003-100883, A08, MF-A02).
- MCEER-02-0002 "Seismic Behavior of Rail Counterweight Systems of Elevators in Buildings," by M.P. Singh, Rildova and L.E. Suarez, 5/27/02. (PB2003-100882, A11, MF-A03).
- MCEER-02-0003 "Development of Analysis and Design Procedures for Spread Footings," by G. Mylonakis, G. Gazetas, S. Nikolaou and A. Chauncey, 10/02/02, (PB2004-101636, A13, MF-A03, CD-A13).
- MCEER-02-0004 "Bare-Earth Algorithms for Use with SAR and LIDAR Digital Elevation Models," by C.K. Huyck, R.T. Eguchi and B. Houshmand, 10/16/02, (PB2004-101637, A07, CD-A07).
- MCEER-02-0005 "Review of Energy Dissipation of Compression Members in Concentrically Braced Frames," by K.Lee and M. Bruneau, 10/18/02, (PB2004-101638, A10, CD-A10).
- MCEER-03-0001 "Experimental Investigation of Light-Gauge Steel Plate Shear Walls for the Seismic Retrofit of Buildings" by J. Berman and M. Bruneau, 5/2/03, (PB2004-101622, A10, MF-A03, CD-A10).
- MCEER-03-0002 "Statistical Analysis of Fragility Curves," by M. Shinozuka, M.Q. Feng, H. Kim, T. Uzawa and T. Ueda, 6/16/03, (PB2004-101849, A09, CD-A09).
- MCEER-03-0003 "Proceedings of the Eighth U.S.-Japan Workshop on Earthquake Resistant Design of Lifeline Facilities and Countermeasures Against Liquefaction," edited by M. Hamada, J.P. Bardet and T.D. O'Rourke, 6/30/03, (PB2004-104386, A99, CD-A99).
- MCEER-03-0004 "Proceedings of the PRC-US Workshop on Seismic Analysis and Design of Special Bridges," edited by L.C. Fan and G.C. Lee, 7/15/03, (PB2004-104387, A14, CD-A14).
- MCEER-03-0005 "Urban Disaster Recovery: A Framework and Simulation Model," by S.B. Miles and S.E. Chang, 7/25/03, (PB2004-104388, A07, CD-A07).
- MCEER-03-0006 "Behavior of Underground Piping Joints Due to Static and Dynamic Loading," by R.D. Meis, M. Maragakis and R. Siddharthan, 11/17/03, (PB2005-102194, A13, MF-A03, CD-A00).
- MCEER-04-0001 "Experimental Study of Seismic Isolation Systems with Emphasis on Secondary System Response and Verification of Accuracy of Dynamic Response History Analysis Methods," by E. Wolff and M. Constantinou, 1/16/04 (PB2005-102195, A99, MF-E08, CD-A00).
- MCEER-04-0002 "Tension, Compression and Cyclic Testing of Engineered Cementitious Composite Materials," by K. Kesner and S.L. Billington, 3/1/04, (PB2005-102196, A08, CD-A08).


- MCEER-04-0003 "Cyclic Testing of Braces Laterally Restrained by Steel Studs to Enhance Performance During Earthquakes," by O.C. Celik, J.W. Berman and M. Bruneau, 3/16/04, (PB2005-102197, A13, MF-A03, CD-A00).
- MCEER-04-0004 "Methodologies for Post Earthquake Building Damage Detection Using SAR and Optical Remote Sensing: Application to the August 17, 1999 Marmara, Turkey Earthquake," by C.K. Huyck, B.J. Adams, S. Cho, R.T. Eguchi, B. Mansouri and B. Houshmand, 6/15/04, (PB2005-104888, A10, CD-A00).
- MCEER-04-0005 "Nonlinear Structural Analysis Towards Collapse Simulation: A Dynamical Systems Approach," by M.V. Sivaselvan and A.M. Reinhorn, 6/16/04, (PB2005-104889, A11, MF-A03, CD-A00).
- MCEER-04-0006 "Proceedings of the Second PRC-US Workshop on Seismic Analysis and Design of Special Bridges," edited by G.C. Lee and L.C. Fan, 6/25/04, (PB2005-104890, A16, CD-A00).
- MCEER-04-0007 "Seismic Vulnerability Evaluation of Axially Loaded Steel Built-up Laced Members," by K. Lee and M. Bruneau, 6/30/04, (PB2005-104891, A16, CD-A00).
- MCEER-04-0008 "Evaluation of Accuracy of Simplified Methods of Analysis and Design of Buildings with Damping Systems for Near-Fault and for Soft-Soil Seismic Motions," by E.A. Pavlou and M.C. Constantinou, 8/16/04, (PB2005-104892, A08, MF-A02, CD-A00).
- MCEER-04-0009 "Assessment of Geotechnical Issues in Acute Care Facilities in California," by M. Lew, T.D. O'Rourke, R. Dobry and M. Koch, 9/15/04, (PB2005-104893, A08, CD-A00).
- MCEER-04-0010 "Scissor-Jack-Damper Energy Dissipation System," by A.N. Sigaher-Boyle and M.C. Constantinou, 12/1/04 (PB2005-108221).
- MCEER-04-0011 "Seismic Retrofit of Bridge Steel Truss Piers Using a Controlled Rocking Approach," by M. Pollino and M. Bruneau, 12/20/04 (PB2006-105795).
- MCEER-05-0001 "Experimental and Analytical Studies of Structures Seismically Isolated with an Uplift-Restraint Isolation System," by P.C. Roussis and M.C. Constantinou, 1/10/05 (PB2005-108222).
- MCEER-05-0002 "A Versatile Experimentation Model for Study of Structures Near Collapse Applied to Seismic Evaluation of Irregular Structures," by D. Kusumastuti, A.M. Reinhorn and A. Rutenberg, 3/31/05 (PB2006-101523).
- MCEER-05-0003 "Proceedings of the Third PRC-US Workshop on Seismic Analysis and Design of Special Bridges," edited by L.C. Fan and G.C. Lee, 4/20/05, (PB2006-105796).
- MCEER-05-0004 "Approaches for the Seismic Retrofit of Braced Steel Bridge Piers and Proof-of-Concept Testing of an Eccentrically Braced Frame with Tubular Link," by J.W. Berman and M. Bruneau, 4/21/05 (PB2006-101524).
- MCEER-05-0005 "Simulation of Strong Ground Motions for Seismic Fragility Evaluation of Nonstructural Components in Hospitals," by A. Wanitkorkul and A. Filiatrault, 5/26/05 (PB2006-500027).
- MCEER-05-0006 "Seismic Safety in California Hospitals: Assessing an Attempt to Accelerate the Replacement or Seismic Retrofit of Older Hospital Facilities," by D.J. Alesch, L.A. Arendt and W.J. Petak, 6/6/05 (PB2006-105794).
- MCEER-05-0007 "Development of Seismic Strengthening and Retrofit Strategies for Critical Facilities Using Engineered Cementitious Composite Materials," by K. Kesner and S.L. Billington, 8/29/05 (PB2006-111701).
- MCEER-05-0008 "Experimental and Analytical Studies of Base Isolation Systems for Seismic Protection of Power Transformers," by N. Murota, M.Q. Feng and G-Y. Liu, 9/30/05 (PB2006-111702).
- MCEER-05-0009 "3D-BASIS-ME-MB: Computer Program for Nonlinear Dynamic Analysis of Seismically Isolated Structures," by P.C. Tsopelas, P.C. Roussis, M.C. Constantinou, R. Buchanan and A.M. Reinhorn, 10/3/05 (PB2006-111703).
- MCEER-05-0010 "Steel Plate Shear Walls for Seismic Design and Retrofit of Building Structures," by D. Vian and M. Bruneau, 12/15/05 (PB2006-111704).

- MCEER-05-0011 "The Performance-Based Design Paradigm," by M.J. Astrella and A. Whittaker, 12/15/05 (PB2006-111705).
- MCEER-06-0001 "Seismic Fragility of Suspended Ceiling Systems," H. Badillo-Almaraz, A.S. Whittaker, A.M. Reinhorn and G.P. Cimellaro, 2/4/06 (PB2006-111706).
- MCEER-06-0002 "Multi-Dimensional Fragility of Structures," by G.P. Cimellaro, A.M. Reinhorn and M. Bruneau, 3/1/06 (PB2007-106974, A09, MF-A02, CD A00).
- MCEER-06-0003 "Built-Up Shear Links as Energy Dissipators for Seismic Protection of Bridges," by P. Dusicka, A.M. Itani and I.G. Buckle, 3/15/06 (PB2006-111708).
- MCEER-06-0004 "Analytical Investigation of the Structural Fuse Concept," by R.E. Vargas and M. Bruneau, 3/16/06 (PB2006-111709).
- MCEER-06-0005 "Experimental Investigation of the Structural Fuse Concept," by R.E. Vargas and M. Bruneau, 3/17/06 (PB2006-111710).
- MCEER-06-0006 "Further Development of Tubular Eccentrically Braced Frame Links for the Seismic Retrofit of Braced Steel Truss Bridge Piers," by J.W. Berman and M. Bruneau, 3/27/06 (PB2007-105147).
- MCEER-06-0007 "REDARS Validation Report," by S. Cho, C.K. Huyck, S. Ghosh and R.T. Eguchi, 8/8/06 (PB2007-106983).
- MCEER-06-0008 "Review of Current NDE Technologies for Post-Earthquake Assessment of Retrofitted Bridge Columns," by J.W. Song, Z. Liang and G.C. Lee, 8/21/06 (PB2007-106984).
- MCEER-06-0009 "Liquefaction Remediation in Silty Soils Using Dynamic Compaction and Stone Columns," by S. Thevanayagam, G.R. Martin, R. Nashed, T. Shenthan, T. Kanagalingam and N. Ecemis, 8/28/06 (PB2007-106985).
- MCEER-06-0010 "Conceptual Design and Experimental Investigation of Polymer Matrix Composite Infill Panels for Seismic Retrofitting," by W. Jung, M. Chiewanichakorn and A.J. Aref, 9/21/06 (PB2007-106986).
- MCEER-06-0011 "A Study of the Coupled Horizontal-Vertical Behavior of Elastomeric and Lead-Rubber Seismic Isolation Bearings," by G.P. Warn and A.S. Whittaker, 9/22/06 (PB2007-108679).
- MCEER-06-0012 "Proceedings of the Fourth PRC-US Workshop on Seismic Analysis and Design of Special Bridges: Advancing Bridge Technologies in Research, Design, Construction and Preservation," Edited by L.C. Fan, G.C. Lee and L. Ziang, 10/12/06 (PB2007-109042).
- MCEER-06-0013 "Cyclic Response and Low Cycle Fatigue Characteristics of Plate Steels," by P. Dusicka, A.M. Itani and I.G. Buckle, 11/1/06 (PB2007-106987).
- MCEER-06-0014 "Proceedings of the Second US-Taiwan Bridge Engineering Workshop," edited by W.P. Yen, J. Shen, J-Y. Chen and M. Wang, 11/15/06 (PB2008-500041).
- MCEER-06-0015 "User Manual and Technical Documentation for the REDARSTM Import Wizard," by S. Cho, S. Ghosh, C.K. Huyck and S.D. Werner, 11/30/06 (PB2007-114766).
- MCEER-06-0016 "Hazard Mitigation Strategy and Monitoring Technologies for Urban and Infrastructure Public Buildings: Proceedings of the China-US Workshops," edited by X.Y. Zhou, A.L. Zhang, G.C. Lee and M. Tong, 12/12/06 (PB2008-500018).
- MCEER-07-0001 "Static and Kinetic Coefficients of Friction for Rigid Blocks," by C. Kafali, S. Fathali, M. Grigoriu and A.S. Whittaker, 3/20/07 (PB2007-114767).
- MCEER-07-0002 "Hazard Mitigation Investment Decision Making: Organizational Response to Legislative Mandate," by L.A. Arendt, D.J. Alesch and W.J. Petak, 4/9/07 (PB2007-114768).
- MCEER-07-0003 "Seismic Behavior of Bidirectional-Resistant Ductile End Diaphragms with Unbonded Braces in Straight or Skewed Steel Bridges," by O. Celik and M. Bruneau, 4/11/07 (PB2008-105141).

- MCEER-07-0004 “Modeling Pile Behavior in Large Pile Groups Under Lateral Loading,” by A.M. Dodds and G.R. Martin, 4/16/07(PB2008-105142).
- MCEER-07-0005 “Experimental Investigation of Blast Performance of Seismically Resistant Concrete-Filled Steel Tube Bridge Piers,” by S. Fujikura, M. Bruneau and D. Lopez-Garcia, 4/20/07 (PB2008-105143).
- MCEER-07-0006 “Seismic Analysis of Conventional and Isolated Liquefied Natural Gas Tanks Using Mechanical Analogs,” by I.P. Christovasilis and A.S. Whittaker, 5/1/07.
- MCEER-07-0007 “Experimental Seismic Performance Evaluation of Isolation/Restraint Systems for Mechanical Equipment – Part 1: Heavy Equipment Study,” by S. Fathali and A. Filiatrault, 6/6/07 (PB2008-105144).
- MCEER-07-0008 “Seismic Vulnerability of Timber Bridges and Timber Substructures,” by A.A. Sharma, J.B. Mander, I.M. Friedland and D.R. Allicock, 6/7/07 (PB2008-105145).
- MCEER-07-0009 “Experimental and Analytical Study of the XY-Friction Pendulum (XY-FP) Bearing for Bridge Applications,” by C.C. Marin-Artieda, A.S. Whittaker and M.C. Constantinou, 6/7/07 (PB2008-105191).
- MCEER-07-0010 “Proceedings of the PRC-US Earthquake Engineering Forum for Young Researchers,” Edited by G.C. Lee and X.Z. Qi, 6/8/07 (PB2008-500058).
- MCEER-07-0011 “Design Recommendations for Perforated Steel Plate Shear Walls,” by R. Purba and M. Bruneau, 6/18/07, (PB2008-105192).
- MCEER-07-0012 “Performance of Seismic Isolation Hardware Under Service and Seismic Loading,” by M.C. Constantinou, A.S. Whittaker, Y. Kalpakidis, D.M. Fenz and G.P. Warn, 8/27/07, (PB2008-105193).
- MCEER-07-0013 “Experimental Evaluation of the Seismic Performance of Hospital Piping Subassemblies,” by E.R. Goodwin, E. Maragakis and A.M. Itani, 9/4/07, (PB2008-105194).
- MCEER-07-0014 “A Simulation Model of Urban Disaster Recovery and Resilience: Implementation for the 1994 Northridge Earthquake,” by S. Miles and S.E. Chang, 9/7/07, (PB2008-106426).
- MCEER-07-0015 “Statistical and Mechanistic Fragility Analysis of Concrete Bridges,” by M. Shinozuka, S. Banerjee and S-H. Kim, 9/10/07, (PB2008-106427).
- MCEER-07-0016 “Three-Dimensional Modeling of Inelastic Buckling in Frame Structures,” by M. Schachter and AM. Reinhorn, 9/13/07, (PB2008-108125).
- MCEER-07-0017 “Modeling of Seismic Wave Scattering on Pile Groups and Caissons,” by I. Po Lam, H. Law and C.T. Yang, 9/17/07 (PB2008-108150).
- MCEER-07-0018 “Bridge Foundations: Modeling Large Pile Groups and Caissons for Seismic Design,” by I. Po Lam, H. Law and G.R. Martin (Coordinating Author), 12/1/07 (PB2008-111190).
- MCEER-07-0019 “Principles and Performance of Roller Seismic Isolation Bearings for Highway Bridges,” by G.C. Lee, Y.C. Ou, Z. Liang, T.C. Niu and J. Song, 12/10/07 (PB2009-110466).
- MCEER-07-0020 “Centrifuge Modeling of Permeability and Pinning Reinforcement Effects on Pile Response to Lateral Spreading,” by L.L Gonzalez-Lagos, T. Abdoun and R. Dobry, 12/10/07 (PB2008-111191).
- MCEER-07-0021 “Damage to the Highway System from the Pisco, Perú Earthquake of August 15, 2007,” by J.S. O’Connor, L. Mesa and M. Nykamp, 12/10/07, (PB2008-108126).
- MCEER-07-0022 “Experimental Seismic Performance Evaluation of Isolation/Restraint Systems for Mechanical Equipment – Part 2: Light Equipment Study,” by S. Fathali and A. Filiatrault, 12/13/07 (PB2008-111192).
- MCEER-07-0023 “Fragility Considerations in Highway Bridge Design,” by M. Shinozuka, S. Banerjee and S.H. Kim, 12/14/07 (PB2008-111193).


- MCEER-07-0024 “Performance Estimates for Seismically Isolated Bridges,” by G.P. Warn and A.S. Whittaker, 12/30/07 (PB2008-112230).
- MCEER-08-0001 “Seismic Performance of Steel Girder Bridge Superstructures with Conventional Cross Frames,” by L.P. Carden, A.M. Itani and I.G. Buckle, 1/7/08, (PB2008-112231).
- MCEER-08-0002 “Seismic Performance of Steel Girder Bridge Superstructures with Ductile End Cross Frames with Seismic Isolators,” by L.P. Carden, A.M. Itani and I.G. Buckle, 1/7/08 (PB2008-112232).
- MCEER-08-0003 “Analytical and Experimental Investigation of a Controlled Rocking Approach for Seismic Protection of Bridge Steel Truss Piers,” by M. Pollino and M. Bruneau, 1/21/08 (PB2008-112233).
- MCEER-08-0004 “Linking Lifeline Infrastructure Performance and Community Disaster Resilience: Models and Multi-Stakeholder Processes,” by S.E. Chang, C. Pasion, K. Tatebe and R. Ahmad, 3/3/08 (PB2008-112234).
- MCEER-08-0005 “Modal Analysis of Generally Damped Linear Structures Subjected to Seismic Excitations,” by J. Song, Y-L. Chu, Z. Liang and G.C. Lee, 3/4/08 (PB2009-102311).
- MCEER-08-0006 “System Performance Under Multi-Hazard Environments,” by C. Kafali and M. Grigoriu, 3/4/08 (PB2008-112235).
- MCEER-08-0007 “Mechanical Behavior of Multi-Spherical Sliding Bearings,” by D.M. Fenz and M.C. Constantinou, 3/6/08 (PB2008-112236).
- MCEER-08-0008 “Post-Earthquake Restoration of the Los Angeles Water Supply System,” by T.H.P. Tabucchi and R.A. Davidson, 3/7/08 (PB2008-112237).
- MCEER-08-0009 “Fragility Analysis of Water Supply Systems,” by A. Jacobson and M. Grigoriu, 3/10/08 (PB2009-105545).
- MCEER-08-0010 “Experimental Investigation of Full-Scale Two-Story Steel Plate Shear Walls with Reduced Beam Section Connections,” by B. Qu, M. Bruneau, C-H. Lin and K-C. Tsai, 3/17/08 (PB2009-106368).
- MCEER-08-0011 “Seismic Evaluation and Rehabilitation of Critical Components of Electrical Power Systems,” S. Ersoy, B. Feizi, A. Ashrafi and M. Ala Saadeghvaziri, 3/17/08 (PB2009-105546).
- MCEER-08-0012 “Seismic Behavior and Design of Boundary Frame Members of Steel Plate Shear Walls,” by B. Qu and M. Bruneau, 4/26/08 . (PB2009-106744).
- MCEER-08-0013 “Development and Appraisal of a Numerical Cyclic Loading Protocol for Quantifying Building System Performance,” by A. Filiatrault, A. Wanitkorkul and M. Constantinou, 4/27/08 (PB2009-107906).
- MCEER-08-0014 “Structural and Nonstructural Earthquake Design: The Challenge of Integrating Specialty Areas in Designing Complex, Critical Facilities,” by W.J. Petak and D.J. Alesch, 4/30/08 (PB2009-107907).
- MCEER-08-0015 “Seismic Performance Evaluation of Water Systems,” by Y. Wang and T.D. O’Rourke, 5/5/08 (PB2009-107908).
- MCEER-08-0016 “Seismic Response Modeling of Water Supply Systems,” by P. Shi and T.D. O’Rourke, 5/5/08 (PB2009-107910).
- MCEER-08-0017 “Numerical and Experimental Studies of Self-Centering Post-Tensioned Steel Frames,” by D. Wang and A. Filiatrault, 5/12/08 (PB2009-110479).
- MCEER-08-0018 “Development, Implementation and Verification of Dynamic Analysis Models for Multi-Spherical Sliding Bearings,” by D.M. Fenz and M.C. Constantinou, 8/15/08 (PB2009-107911).
- MCEER-08-0019 “Performance Assessment of Conventional and Base Isolated Nuclear Power Plants for Earthquake Blast Loadings,” by Y.N. Huang, A.S. Whittaker and N. Luco, 10/28/08 (PB2009-107912).
- MCEER-08-0020 “Remote Sensing for Resilient Multi-Hazard Disaster Response – Volume I: Introduction to Damage Assessment Methodologies,” by B.J. Adams and R.T. Eguchi, 11/17/08.

- MCEER-08-0021 “Remote Sensing for Resilient Multi-Hazard Disaster Response – Volume II: Counting the Number of Collapsed Buildings Using an Object-Oriented Analysis: Case Study of the 2003 Bam Earthquake,” by L. Gusella, C.K. Huyck and B.J. Adams, 11/17/08.
- MCEER-08-0022 “Remote Sensing for Resilient Multi-Hazard Disaster Response – Volume III: Multi-Sensor Image Fusion Techniques for Robust Neighborhood-Scale Urban Damage Assessment,” by B.J. Adams and A. McMillan, 11/17/08.
- MCEER-08-0023 “Remote Sensing for Resilient Multi-Hazard Disaster Response – Volume IV: A Study of Multi-Temporal and Multi-Resolution SAR Imagery for Post-Katrina Flood Monitoring in New Orleans,” by A. McMillan, J.G. Morley, B.J. Adams and S. Chesworth, 11/17/08.
- MCEER-08-0024 “Remote Sensing for Resilient Multi-Hazard Disaster Response – Volume V: Integration of Remote Sensing Imagery and VIEWS™ Field Data for Post-Hurricane Charley Building Damage Assessment,” by J.A. Womble, K. Mehta and B.J. Adams, 11/17/08.
- MCEER-08-0025 “Building Inventory Compilation for Disaster Management: Application of Remote Sensing and Statistical Modeling,” by P. Sarabandi, A.S. Kiremidjian, R.T. Eguchi and B. J. Adams, 11/20/08 (PB2009-110484).
- MCEER-08-0026 “New Experimental Capabilities and Loading Protocols for Seismic Qualification and Fragility Assessment of Nonstructural Systems,” by R. Retamales, G. Mosqueda, A. Filiatrault and A. Reinhorn, 11/24/08 (PB2009-110485).
- MCEER-08-0027 “Effects of Heating and Load History on the Behavior of Lead-Rubber Bearings,” by I.V. Kalpakidis and M.C. Constantinou, 12/1/08.
- MCEER-08-0028 “Experimental and Analytical Investigation of Blast Performance of Seismically Resistant Bridge Piers,” by S.Fujikura and M. Bruneau, 12/8/08.
- MCEER-08-0029 “Evolutionary Methodology for Aseismic Decision Support,” by Y. Hu and G. Dargush, 12/15/08.
- MCEER-08-0030 “Development of a Steel Plate Shear Wall Bridge Pier System Conceived from a Multi-Hazard Perspective,” by D. Keller and M. Bruneau, 12/19/08.
- MCEER-09-0001 “Modal Analysis of Arbitrarily Damped Three-Dimensional Linear Structures Subjected to Seismic Excitations,” by Y.L. Chu, J. Song and G.C. Lee, 1/31/09.



EARTHQUAKE ENGINEERING TO EXTREME EVENTS

University at Buffalo, The State University of New York
Red Jacket Quadrangle ■ Buffalo, New York 14261
Phone: (716) 645-3391 ■ Fax: (716) 645-3399
E-mail: mceer@buffalo.edu ■ WWW Site <http://mceer.buffalo.edu>



University at Buffalo *The State University of New York*

ISSN 1520-295X